Spatial variability
of the snow cover and its effect
on avalanche formation

Dissertation
zur Erlangung des Doktorgrades der Naturwissenschaften
im Department Geowissenschaften
der Universität Hamburg

Sascha Bellaire

geboren in

Lippstadt

Hamburg

2010

Als Dissertation angenommen vom Department Geowissenschaften der Universität Hamburg

Auf Grund der Gutachten von Prof. Dr. Dirk Gajewski
und Dr. Jürg Schweizer

Hamburg, den 23. Juni 2010

Prof. Dr. Jürgen Oßenbrügge
Leiter des Departments für Geowissenschaften

Contents

Abstract

Avalanches threaten humans. About 250 person die in snow avalanches each year. Avalanches affect roads, railways, ski resorts and buildings located in mountainous terrain. Prerequisites for a dry-snow slab avalanche are a weak layer below slab layers. This study focused on the formation of skier-triggered dry snow slab avalanches.

Failure initiation within the weak layer and fracture propagation are key processes for avalanche formation. It is believed that spatial variations of weak and slab layer properties affect fracture initiation and fracture propagation propensity. The length scale, or range, of these variations is of particular importance for the avalanche formation process. Previous studies have quantified the spatial variability of snow cover properties at different scales. However, none of these studies was able to relate the variation of snow cover properties to snow slope stability.

To quantify spatial variations of snow cover properties at the slope scale, spatially distributed measurements have been carried out on 23 slopes above treeline near Davos, Switzerland. Seventeen of these slopes were analyzed, six had to be discarded due to data quality problems. The SnowMicroPen (SMP), a constant speed penetrometer, was used for high resolution resistance probing in a partly randomized grid pattern. In addition, manual snow cover observations, stability tests and manual snow profiles were performed. In total, 1058 SMP profiles, 340 compression tests and 17 manual snow profiles were analyzed.

Previous studies were not able to relate spatial variations of snow cover properties to snow slope stability, because of the insufficient number of point stability information at the slope scale. Therefore, the SMP resistance signal was analyzed to derive snow stability. The proposed stability algorithm was developed by comparing 71 SMP force-distance profiles to the corresponding manual profiles including stability tests. The algorithm identifies a set of four potentially weak layers by taking into account changes in structure and rupture strength of micro-structural elements that make up snow layers as derived from the SMP signal. In 90% of the cases one of the four potentially weak layers proposed by the algorithm coincided with the failure layer observed in the stability test. To select the critical layer out of the four potential weaknesses proved to be more difficult. With a fully automatic picking of the critical layer, an agreement with the failure layer observed

in the stability test was reached in 58% of the cases. To derive a stability classification, weak layer as well as slab properties were analyzed. These predictor variables allow the SMP signal to be classified into two stability classes of $poor$ and $fair-to-good$ with an accuracy of about 75% (cross-validated) when compared to observed stability. The SMP in combination with the proposed algorithm shows high potential for providing snow cover stability information with high resolution in time and space.

The spatial variation of weak layer and slab properties were characterized using non-spatial as well as spatial statistics and results were related to slope stability. These layer properties were the penetration resistance, the maximum penetration resistance, the layer thickness and a structural parameter derived from the SMP signal. The investigated weak layers were spatially continuous, i.e. were identified in almost all SMP signals, and the properties showed more spatial variations than slab layers suggesting that the slab layers are the most relevant factor for avalanche formation. Spatial slope scale trends of slab layer properties explained most of these variations suggesting the importance of meteorological conditions during and after deposition as a driving agent for spatial variability. Varying weak layer properties were found to be positively correlated with varying slab layer properties showing the influence of the slab layer on the weak layer properties.

Grids with low median compression test scores showed less variation than grids of intermediate or high compression test scores. The variation of the layer properties was positively correlated with the variation of the compression test scores. In other words, stability increased with increasing variation.

The geostatistical analysis revealed that in most cases no range (or correlation length) could be determined neither for the slab layers nor for the weak layers. However, the slab layers tended to show more often spatial structure, i.e. a range, than the corresponding weak layers. Weak layers showed generally less variance than the slab layers. A certain range could not be related to slope stability and therefore the effect of length scale on slope stability remains unknown for the time being. Though some trends are apparent, firm conclusions on the dependence of slope stability on spatial variations were not possible due to limited range of snow conditions in the dataset, and the fact that the definition of slope stability remains elusive.

Nevertheless, based on the limited dataset a hypothetical concept was introduced. Spatial variations of weak layer and slab layer properties are only relevant if the variations at the slope scale are around the threshold of rather stable to rather unstable conditions. As this hypothetical concept can not be supported with observations, it should be considered as preliminary.

Acknowledgements

Acknowledgements, I don't really know how to start. So I probably start to tell you where I am right now. I am sitting in an aircraft 10363 m above ground on my way to Calgary, Canada. At the moment we are crossing Iceland heading to south Greenland. I can see Iceland and will hopefully see the Greenland icecap. I will start my new job in Calgary under the supervision of Dr. Bruce Jamieson tomorrow. That means, I will still work at the field of snow and avalanche research the next years.

This would not have been possible without the help of many people. I cannot list all people here who provided help, guidance and any other imaginable support. I am deeply grateful for all your help.

However, I would like to start to thank my parents and therefore I have to switch to German. Ich danke meinen Eltern Mechthild Bellaire und Franz-Josef Bellaire für ihre unermüdliche Unterstützung in all den Jahren. Ich hoffe ich habe euch nicht enttäuscht und ein wenig stolz gemacht.

Prof. Dr. Hartmut Grassl told me to visit the SLF during a ski touring trip close to Davos, Switzerland. After this visit I started my master thesis at SLF and one could probably say this was the initiation of all this. Thanks for this great idea.

Dr. Jürg Schweizer is the person I have to acknowledge for the last 5 great years. He accepted me as a master student supervised me and gave me the chance to work with him as a Ph.D student. I could not really describe how grateful I am. A friend told me once "Sascha, you have the best job ever!", he was and is still absolutely right. So Jürg thanks for giving me the chance to make my dream come true, for all the support you gave me, and for being there when I needed guidance not only on the way down from fieldwork. Thanks for all your help!

Prof. Dr. Dirk Gajewski accepted me as a Ph.D student. For that trust in me, being a climbing partner and friend I am deeply grateful. Hopefully there is more time for a common "de-acceleration" in future.

Thanks Alec van Herwijnen for sharing the office, answering my questions and helping to get this thesis ready. Thanks Alec for your help and great backcountry and "indoor"

recreation.

This thesis would not have been possible without the help of numerous persons helping with the data acquisition, and of course just being there to listen to my problems and answering questions. Therefore, I would like to thank, Charles Fierz, Nora Helbig, Kalle Kronholm, Michael Lehning, Henning Löwe, Christoph Mitterer, Christine Pielmeier, Ingrid Reiweger, Ben Reuter, Hansueli Rhyner, Michael Schirmer, Martin Schneebeli, Michaela Teich, as well as Kurt Winkler. Many thanks to Prof. Dr. Martin Claussen and Prof. Dr. Jürgen Böhner who are beside Prof. Dr. Hartmut Grassl, Prof. Dr. Dirk Gajewski and Dr. Jürg Schweizer part of the committee. Thanks for being interested in this topic.

Finally, I would like to thank one person who gave me support and made my life easier during hard times. Thanks, Kerstin!

Introduction

A snow avalanche is a rapid down-slope movement of snow, triggered naturally or artificially (e.g. by humans). Estimates suggest that worldwide each year about 250 people die due to snow avalanches (Schweizer, 2004). Avalanches affect ski resorts, roads, railways, buildings, and other infrastructure located in mountainous terrain, causing monetary damage and loss of life. Avalanche fatalities during recreational activities can be reduced by forecasting as well as education on safe traveling in avalanche terrain. Avalanche forecasting is based on snow cover stability observations, meteorological observations and weather forecasts. Forecasting of avalanche hazard has to be done for large areas (several 100 km^2) where snow cover observations are infrequent. Therefore, forecasting the release probability of a single slope is not possible - at least not presently. The main reason for this is that the exact state of the mountain snow cover is not known.

The varying meteorological conditions, such as wind and radiation, influence the formation of the seasonal alpine snow cover. Understanding the relevant physical processes affecting a seasonal mountain snow cover allows one to forecast its state. In the following the main properties of snow on the ground and processes acting on a seasonal alpine snow cover are summarized. The concept of avalanche formation and recent findings on spatial snow cover variations are presented.

1.1 Snow cover

Snow crystals are formed in clouds through water vapor deposition on condensation nuclei. During this process the crystals grow into typically hexagonal unique structures. These single structures are complex on their own and a system, i.e. snow on the ground, consisting of these unique structures becomes highly complex.

Newly fallen snow which was not affected by wind has typically densities (ρ_{snow}) below

100 kg m^{-3} (McClung and Schaerer, 2006). The ratio ρ_{snow}/ρ_{ice} is a measure of porosity. New snow with a density of 50 kg m^{-3} has a porosity of 95% ($\rho_{ice} = 917$ kg m^{-3}). That means only 5% ice exists within one cubic meter of snow of this density. Firn, with a density of about 550 kg m^{-3}, is defined as the last stage of snow densification. Densification is due to the weight of the snow. Large overburden pressure and high air temperature favour densification.

The seasonal snow cover on the ground is layered with distinct upper and lower boundaries. Layering is mainly caused by varying snow deposition. Meteorological processes affect directly the exposed snow surface. Short wave radiation or positive air temperature, might cause melt-freeze crusts and snow can be eroded and deposited by wind. The snow layer thickness can range from a few millimeter to decimeters.

### 1.1.1 Metamorphism and snow types

Metamorphism within the snow cover is driven by water vapor transport which is a direct consequence of temperature gradients within the snow cover. Geothermal heat and the low thermal conductivity of ice cause a temperature of about 0 $°C$ at the base of the snow cover. The upper part of the snow cover, on the other hand, is subjected to diurnal temperature fluctuations. Temperature gradients exists always within the snow cover. The water vapor leaves one crystal and condenses on a neighboring crystal. This upward motion of water vapor increases with increasing temperature gradient, depends on the pore space and determines the shape of the crystal.

Once snow is deposited on the ground it undergoes metamorphic processes (Figure 1.1). New snow crystals are most prone to changes due to their dendritic structure. The vapor pressure is larger over convex surfaces than it is over concave surfaces. That means, the branches of a new snow crystal will start to sublimate since the surrounding air is typically not super-saturated. Dendritic snow crystals tend to reach the shape of a sphere, i.e. a rounded particle, because this is the minimum surface-to-volume ratio. As described above depending on the amount of available water vapor, the intensity of the temperature gradient and the size of the pore space different grain shapes are formed. Typically rounded crystals are formed if temperature gradients below 10 Cm^{-1} exist within the snow cover (equilibrium growth). Temperature gradients larger than 10 C m^{-1} form faceted crystals (Akitaya, 1974).

Snow types (Colbeck et al. (1990); Fierz et al. (2009)) can be grouped into either persistent or non-persistent snow types (Jamieson and Johnston, 1998, 2001). New snow (PP), decomposed and fragmented precipitation particles (DF) and small rounded grains (RG) belong to the group of non-persistent snow types (Figure 1.1). Faceted crystals (FC) and depth hoar (DH) belong to the group of persistent grain types (Figure 1.2). A special form of faceted crystals are rounded facets (FCxr). These crystals show rounded edges as well as sharp edges. The size of snow grains range typically from fractions of

millimeters to centimeters. Surface hoar (SH) is formed on top of the snow surface during clear, humid and calm nights (Figure 1.3). The snow surface is cooled by radiative heat transport while humid air condenses at the snow surface. Wind reduces the size or even hinders surface hoar growth. Surface hoar crystals can reach sizes of a few centimeters.

Snow is a sintered material and is therefore bonded. Bonds between grains are a result of water vapor transport through the pore space and molecular motion at the surface. The strength of a layer depends on the bonding of the individual grains. Layers consisting of persistent grain types (e.g. depth hoar) form fewer bonds per unit volume than layers of non-persistent grain types (e.g. small rounded grains). Layers of poorly bonded grain types are weaker in shear than in compression (Akitaya, 1974). Bond growth is fastest for new snow, high temperatures and large load. Bonding is of particular importance for the avalanche formation process.
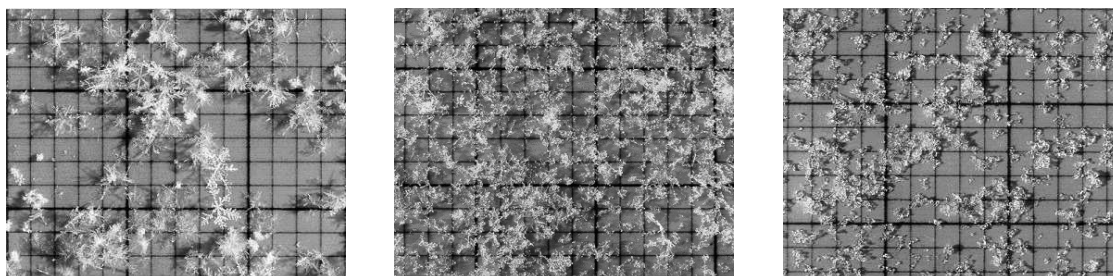
Figure 1.1: Non-persistent snow crystals on a 2 mm grid. New snow (left), decomposed and fragmented precipitation particles (mid) and small rounded grains (right).(Photo: SLF archive).
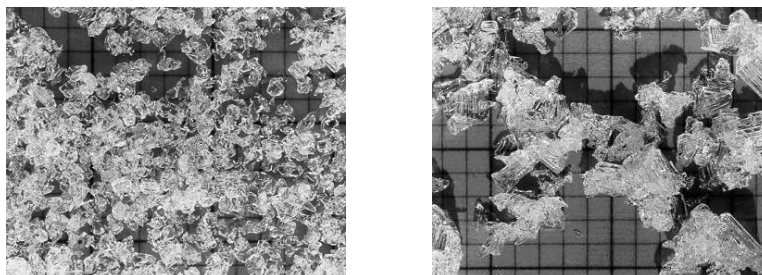
Figure 1.2: Persistent snow crystals on a 2 mm grid. Faceted crystals (left), depth hoar (right). (Photo: SLF archive).

Figure 1.3: Surface hoar crystals on top of the snow surface.

1.1.2 Observation and measurement methods

Manual observations

When analyzing the snow cover a manual snow profile is commonly observed. The snow layering is recorded including layer thickness, snow type, grain size and hardness of the layers. These point observations are time consuming and somewhat subjective, but are still the most relevant information on the snow cover stratigraphy used by avalanche forecasters.

A manual snow profile is often supplemented by stability tests. Stability tests are used for mainly two reasons: to find potential weak layers and to qualify their strength. Various field tests have been used by practitioners as well as by researchers. The two most common tests are the rutschblock (RB) (Föhn, 1987) and the compression test (CT) (Jamieson, 1999). For these two tests, snow columns of different size (RB: 2 m x 1.5 m, CT: 30 cm x 30 cm) are isolated from the snow cover and are subsequently loaded from the top (see Methods section for more details). The observed release type (RB) and the fracture character (CT) provide additional stability information. Winkler and Schweizer (2009) compared different stability tests. They found that stability tests performed adjacent to each other revealed the same failure layer in only about 60% of the cases and pointed out the challenge of automatically detecting potential failure layers within a snow cover. Furthermore, they argued that the compression test typically underestimates stability.

Birkeland and Chabot (2006) analyzed stability tests performed on slopes rated as unstable. They found that if only one test is considered for slope stability classification the slope can still be rated as stable in about 10% of the cases. They, as others before (Jamieson and Johnston (1993); Schweizer et al. (2008b)), proposed to perform a second observation at a representative site about ten meters apart from the first test and choosing the test with the lowest score.

SnowMicroPen

Schneebeli and Johnson (1998) developed the SnowMicroPen (SMP), a digital penetrometer to enable quick snowpack resistance probing. The method requires no digging and provides objective high resolution penetration resistance data. Johnson and Schneebeli (1999) introduced a micro-structural model to derive snow properties from the signal. Recently, Marshall and Johnson (2009) improved this micro-structural model. Their model was not available during this study and could therefore not be used.

Snow cover stability information is crucial for avalanche warning services as well as for backcountry recreationists. This information is typically derived from manual snow cover observations and stability tests. Pielmeier and Marshall (2009) related point stability (as estimated with the rutschblock) to layer properties derived from the SMP calculated with the improved micro-structural model. They found the micro-structural strength of the a priori defined weak layer (see Methods section) to be the most reliable predictor of stability (84% total accuracy, predicting stable and unstable). Compared to earlier studies (e.g. Pielmeier and Schweizer (2007)) the classification accuracy found by Pielmeier and Marshall (2009) was higher, suggesting that the improved micro-structural model allows better signal interpretation.

Previous SMP studies analyzed properties of specific weak layers, such as layers of buried surface hoar, in space and time using various statistical methods (Lutz et al. (2007); Schweizer and Kronholm (2007); Kronholm et al. (2004); Birkeland et al. (2004a)). Satyawali et al. (2009) related the mean, the standard deviation and the coefficient of variation of the SMP penetration resistance to the major grain types. With the help of some additional expert rules they suggested a preliminary method to relate the SMP signal to grain types.

Common practice when analyzing SMP signals is a visual inspection of the signal. If no obvious errors, e.g. signal drift, are identified, the layer of interest is defined manually and the properties are calculated. Lutz et al. (2007) used moving window statistics as a refinement of manual weak layer detection. Floyer and Jamieson (2008) and van Herwijnen et al. (2009) used various signal processing methods to identify known weak layers, i.e previously identified by stability tests, in penetrometer signals. Additionally, Floyer and Jamieson (2008) suggested a conceptual framework for automatic detection of weak layers.

Bellaire et al. (2009) introduced an algorithm which automatically detects weak layers and estimates stability (see Methods section for more details). This algorithm shows promising potential for an automatic weak layer detection and a direct stability estimation. The method needs more improvements, but weak layer detection in manual snow cover observations seems similarly difficult (Schweizer and Jamieson, 2007). In addition, Schweizer and Jamieson (2007) related manually observed failure layer properties to observed instability and developed a threshold sum approach to classify failure layers based on structural properties. When they used the method for failure layer detection, i.e. identifying the principal weakness in a given snow stratigraphy, the accuracy was only 53% - exemplifying the difficulty of failure layer detection. Bellaire et al. (2009) found an accuracy of 60% to detect a weak layer automatically within a SMP signal.

1.2 Avalanche formation

Prerequisites for the release of a dry-snow slab avalanche (Figure 1.4) are a weak layer below one or more slab layers. Figure 1.5 illustrates the two required processes for a slab avalanche release. First, a fracture needs to be initiated within the weak layer or at a weak interface. Second, the failure has to grow until it reaches a critical length assumed to be larger than 1 m and smaller than 10 m (Schweizer et al., 2003). Beyond this critical length the fracture becomes self-propagating, the slab might detach and an avalanche releases. As a matter of fact the critical length is unknown, but is assumed to be < 10 m (Schweizer et al., 2008b) - and probably on the order of the slab thickness.

Figure 1.6 shows a schematic of a slab avalanche. The energy required for fracture propagation has to be lower or equal to the available energy supplied by the slab layers. The slab layers consist of well-bonded snow with densities of about 200 kg m^{-3}, i.e. the slab layers are cohesive enough to form a block of snow. The typical thickness of slab layers is about 0.5 m (McClung and Schaerer, 2006). van Herwijnen and Jamieson (2007b) argued that hard slab layers impede failure initiation by skiers, but pointed out that they favor fracture propagation. This was supported by numerical simulations performed by Habermann et al. (2008). Dry-snow slab avalanches can be triggered by continuous loading during snowfall as well as by localized rapid near-surface loading by, for example, skiers. Layers deeper than 1 m are rarely skier-triggered (Schweizer et al., 2003).

Weak layers underneath the slab typically consist of poorly bonded snow such as depth hoar, surface hoar or faceted crystals. These large (in size) persistent grain types form fewer bonds per unit volume. It is assumed that, the amount of bonds is much more important in terms of failure growth and fracture propagation than the size of the bonds. A critical weak layer has to favor fracture initiation as well as fracture propagation. However, without cohesive slab layers an avalanche release is unlikely. For example, fracture initiation within a layer of surface hoar below a 50 cm slab layer of low density

snow (new snow) might be possible, but will not propagate. The same critical weak layer below a well-bonded cohesive slab might favor fracture initiation because the additional stress induced by a skier is better applied to the weak layer and more energy is available for fracture propagation.

Once a fracture propagates and the slab becomes detached a crown fracture (Figure 1.6) is formed by a dynamic tension fracture usually slope perpendicular. The fractures at the sides, or avalanche flanks, are formed by the downward motion of the slab layers. The Stauchwall (not shown in Figure 1.6) is the bottom boundary of the slab caused by a shear fracture. The stauchwall may be difficult to identify after an avalanche release, because the slab overruns the stauchwall. The fracture is assumed to appear at the same time as the fractures at the sides just before the slab moves downhill (McClung and Schaerer, 2006). The bed surface is the surface on which the avalanche slides downhill. This can either be a harder snow layer below the weak layer, like visible in Figure 1.4 and illustrated in Figure 1.6, or the avalanche can slide directly on the ground.

In general, fracture initiation requires a smaller area, e.g. area below skies, whereas the fracture growth and propagation requires larger areas of low weak layer strength. van Herwijnen and Jamieson (2005) showed that a fracture below a skier can be large enough to propagate. In addition, they pointed out the importance of slab layers for fracture propagation. In other words, a weak layer cannot be triggered without a slab and on the other hand, there is no avalanche without a weak layer. That means dry-snow slab avalanche release depends on weak layer and slab layer properties, and their interaction.

1.3 Spatial variability of the snow cover

As described above avalanche formation is strongly influenced by weak layer and slab layer properties. The snow cover is exposed to varying meteorological conditions such as wind and radiation. In addition, the snow cover is also subjected to internal metamorphic processes forced by meteorological conditions. These varying conditions and the snow cover underlying ground (e.g blocks), are driving agents for spatial variability of the snow cover.

This study distinguish between spatial variability of the weak layer and the slab layer properties. A weak layer is often formed at the snow surface (e.g. surface hoar, near surface faceting). The weak layer formation can be assumed to be spatially rather uniform. Wind during and after a snow storm affects the slab layering due to irregular deposition or erosion. If irregular deposition occurs, different temperature gradients are established

Figure 1.4: Dry-snow slab avalanche. 25 February 2009, Steintälli, Davos, Switzerland
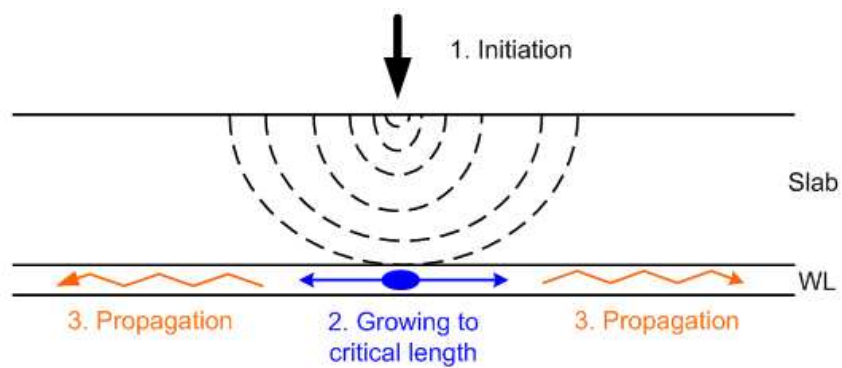
Figure 1.5: Schematic of the required processes for a slab avalanche release. First, a fracture needs to be initiated, e.g. by a skier. Second, the failure growth until it reaches a critical length and third the fracture propagates until the slab becomes detached.
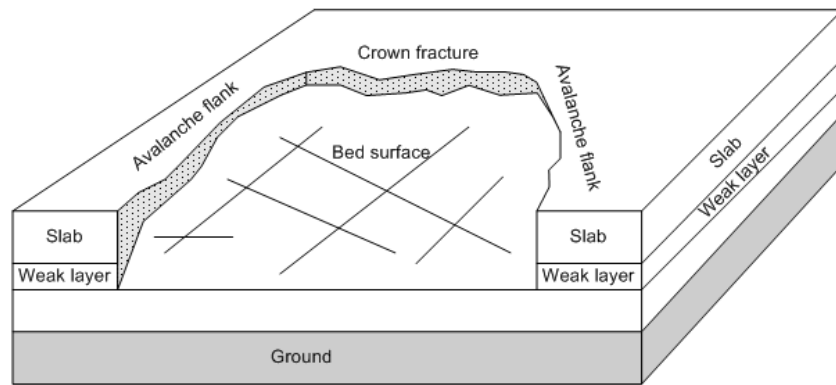
Figure 1.6: Schematic of a dry-snow slab avalanche.

affecting the metamorphic processes acting on the weak layer as well as on the slab layer properties.

Before the most relevant studies on spatial variability of the snow cover are discussed the term "spatial variability" needs to be defined. The term spatial variability is used in this study to describe variations of snow cover properties at the slope scale. To capture spatial variations of snow cover properties measurements need to be spatially distributed. If measurements are correlated and a correlation length exists the investigated snow cover property shows a spatial structure, i.e. a clustering. The scale of this structure is of particular importance, since it is believed to be related to failure initiation and propagation.

Various sampling methods have been used throughout the years to quantify spatial variability. These methods include point stability tests like the rutschblock (Föhn, 1987) or compression test Jamieson (1999). Weak layer properties were measured using shear frames (Jamieson and Johnston, 2001) and high resolution penetrometers (Schneebeli and Johnson, 1998). Slopes of different size in different terrain located in different snow climates were tested.

During the last years various studies on spatial variability have been carried out. Recently, Schweizer et al. (2008b) reviewed spatial variability studies at different scales. These studies investigated the variation of layer properties as well as of point stability. Schweizer et al. (2008b) concluded that a wide range of variability exist, but weak layers are often spatially continuous and show less variation than slab layers (e.g. Kronholm and Schweizer (2003); Birkeland et al. (2004b)). Furthermore, they pointed out, that the scale of variation is a key factor for assessing the propensity of fracture propagation. Fracture character, rutschblock release type and shear quality are more continuous than scores of stability tests and are therefore less subjected to spatial variations. Numerical models suggest that spatial variation hinder fracture propagation (e.g. Fyffe and Zaiser (2004);Kronholm and Birkeland (2005)). The sampling design affects the estimated correlation length (Kronholm and Birkeland, 2007). This fact and the different applied

methods made comparison of the different studies questionable and partly explain the contradictionary results of spatial variability studies.

Recent studies not included in Schweizer et al. (2008b) are compiled in Table 1.1. Floyer (2008) performed transects of penetrometer measurements using the SABRE probe (Mackenzie and Payten, 2002) across different terrain features such as wind affected slopes or across the unreleased snow cover next to an avalanche. Simenhois and Birkeland (2009) and Hendrikx et al. (2009) both studied spatial variations using the Extended column test (ECT) (Simenhois and Birkeland, 2006). Simenhois and Birkeland (2009) found no or very little variation in their test results. On the other hand, the ECT results by Hendrikx et al. (2009) showed large variations. Lutz (2009) analyzed the temporal evolution of spatial variability of weak layer properties for one slope with a nested sampling design. He found that spatial variability increased over time and spatial variability decreased after large loading events.

These findings from the latest studies on spatial variability of layer properties and point stability essentially coincide with the conclusions made by Schweizer et al. (2008b).

1.4 Summary and aims

To summarize, spatial variability exists and various degrees of spatial variability at different scales were observed. Weak layers were found to be continuous showing less variation than slab layers. Spatial variability affects the avalanche formation process. Spatial variability of weak layer and slab layer properties affect fracture initiation as well as fracture propagation. Critical weak layer properties are required over distances smaller than 10 m to reach the critical length. In fact, correlation length of layer properties < 10 m were observed at the slope scale.

Throughout all studies some trends seemed to emerge supporting the theory of how spatial variability affects snow slope stability. Observation showed that a slope can be triggered by a second person skiing after and beside the first person. This observation might be related to spatial variability of layer properties, since the fracture initiation and propagation propensity might differ at the slope scale due to the spatial variability of weak and slab layer properties. Therefore, and the above described example supports this, one can hypothesize that spatial variability is particular relevant if variation occurs between stable and unstable conditions and the unstable regions are large enough to favor fracture initiation as well as propagation. This limits the relevance of spatial variability for avalanche forecasting to time periods between storm events.

A slope which is not triggered during investigation can only be rated as stable in terms of an avalanche release. That means, slope instability can not be readily measured and a slope stability classification remains elusive.

Table 1.1: Recent spatial variability studies not included in Schweizer et al. (2008b) with property under study and major results.

Study	Property	Results
Floyer (2008)	Penetration resistance (SABRE probe)	- Different terrain features have been analyzed; a wind affected slope, a rain gully, a boulder field, elevation and aspect changes and the unreleased snow adjacent to an avalanche - Transect length and spacing differ depending on terrain feature; length 1.3 - 2000 m; spacing 5 cm - 400 m - Penetration resistance layer thickness and depth were found to vary considerably over surveyed features. - Features particular associated with high spatial variability were wind ridges, aspect changes, elevation changes, snow surrounding boulders and runnels caused by rain events.
Simenhois and Birkeland (2009)	Point stability (ECT)	- ECT stability tests have been performed on two slopes - The results were spatial uniform while within one grid all test propagate and the other shows a clustering of propagation and non propagation.
Hendrikx et al. (2009)	Point stability (ECT)	- Two slopes, a windy and a sheltered one, were investigated - Considerable variation in propagation potential was observed - Resistance of propagation and clustering increased over time
Lutz (2009)	Strength, point stability, penetration resistance (SMP)	- Temporal evolution of weak layer properties for one slope. - Spatial variability of measured parameter increased over time. - Spatial variability of parameter decreased after large loading events.

The aim of this study is to quantify spatial variations of snow cover properties at the slope scale and asses the relevance of the variations for slope stability to support the above described hypothesize. This aim should be achieved by 1) identifying snow cover parameter associated with snow cover instability 2) identifying their spatial structure and 3) relating this spatial structure to slope instability.

Methods

This chapter summarizes and discusses the manual observations, introduces the SnowMicroPen and finally describes the statistical methods used to analyze the data. The data were collected during three winters between 2006 - 2009 in the region of Davos, Switzerland. Sampling methods as well as the sampling design are also presented in this chapter.

2.1 Sampling design

In this section some parameters relevant for sampling designs are defined. Furthermore, some general questions regarding sampling strategy are addressed. Finally, the sampling design used in this study is introduced and the accuracy of detecting the range of the variable under investigation is estimated.

Blöschl (1999) suggested a framework for studies where scale issues are of particular importance. For this framework he introduced three scales the process scale, the measurement scale and the model scale. The aim of a spatial variability study is to measure and quantify the process scale. The measurement scale is described by the scale triplet (spacing, extent and support) and the scale triplet is defined as:

Spacing - The spacing is defined as the distance between measurement locations. Two main sampling strategies exist, regular sampling and random sampling. With regular sampling the spacing is constant. The spacing with random sampling varies.

Extent - The extent of a sampling design is defined as the maximum possible distance between measurement locations. To study avalanche release the extent should not be smaller then about 10 m, since this is the expected upper length scale required for fracture propagation leading to avalanche release (Schweizer, 1999).

Support - The support of the sampling design is defined as the area needed to perform

the measurement at each measurement location. For example the compression test has a support of 900 cm^2, the rutschblock of 3 m^2 and the SnowMicroPen (SMP) a support of 19.6 mm^2.

2.1.1 Comments on sampling design

The sampling design is of particular importance for a reliable interpretation of spatial structures (see definition below). As mentioned above the extent should not be smaller then 10 m, a reasonable upper limit seems to be about 20 m, because surveys on larger, steeper slopes are often too dangerous in terms of avalanche release. Sampling designs with a smaller extent allow one to perform more than one survey on the same slope, since the amount of available slopes within an experimental site is limited. In addition, this procedure enables one to capture the temporal evolution of spatial variability on potential avalanche slopes. Kronholm and Birkeland (2007) analyzed different sampling designs (regular and random) and assessed whether these sampling designs were able to detect a pre-defined structure. They concluded that the sampling design should contain some randomness if the correlation length is unknown. However, in practice, randomly distributed measurement points are difficult to locate on grids where the extent is small (< 20 m), i.e. locating points, for example, by GPS requires differential GPS.

A large amount of sampling locations improves the reliability of the geostatistical analysis. Different authors suggest to use more then hundred points to ensure a reliable statistical analysis (e.g. Webster and Oliver (2007)). However, performing many measurements is often not practical since it is time consuming and snow conditions might change during the day.

Skøin and Blöschl (2006) analyzed the bias on the correlation length estimate if extent, spacing and support change. They found that the estimated correlation length is biased depending on the choice of these parameters. Furthermore they pointed out, that the sampling design should be adapted to the expected correlation length. As a rule of thumb, Skøin and Blöschl (2006) suggested for an optimized sampling design an extent larger and a spacing smaller than the expected correlation length.

For snow the correlation length is unknown. Also, the number of processes acting on the snow cover, e.g. wind or radiation, and the typical length scale of these processes are not sufficiently known. Many processes such as wind cause variations at different scales. As this study focus on avalanche formation, particularly on the effect of spatial variability on avalanche formation, an assumption on the length scale can be made that might be most relevant. This scale is related to the avalanche release process which can be described in terms of fracture mechanics. In order for an initial failure to propagate so that eventually the slab becomes detached, the failure has to reach a critical size. Independent estimates suggest that the critical size is < 10 m but larger than the slab thickness (Schweizer et al., 2003). Therefore the sampling design should be such that a

correlation length of a few meters can be determined - at least approximately.

2.1.2 Partly randomized sampling design

The sampling design used in this study was developed for a grid of 18 m x 18 m (Figure 2.1). This area was divided into nine sub-grids of 6 m x 6 m. Each sub-grid contained five SMP measurements in a L-shaped design as suggested by Cline et al. (2001). The distance between each SMP measurement within a sub-grid differed (0.25 m, 0.5 m, 1 m).
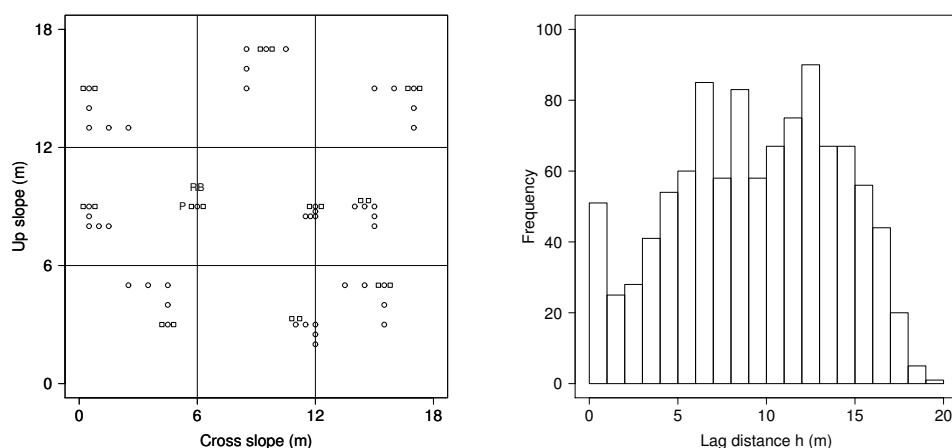
Figure 2.1: Left: Sampling design of the present study. Dots indicate locations of SMP measurements, squares location of compression tests adjacent to the SMP measurement. The position of the manual profile is indicated by P, where two additional compression tests and a SMP measurement were performed. RB locates the position of the rutschblock test. The SMP measurements are 0.25 m, 0.5 m and 1 m apart. Right: Frequency distribution of lag distance h for the sampling design shown on the left.

The point pairs within each lag distance class are well distributed (Figure 2.1). For lag distances $h = 4$ - 17 m the number of point pairs is > 30. Journel and Huijbregts (1978) suggested a minimum of 30 - 50 point pairs within each lag distance. The mean spacing of the sampling design is 9 m and the extent is about 20 m. According to Skøin and Blöschl (2006) the spacing for a regular grid with a fixed spacing should be smaller than the expected correlation length. The sampling design is partly randomized and has therefore no fixed spacing. The mean spacing is on the order of the maximum expected correlation length and might therefore be somewhat too large. However, the random

sampling design also includes distances smaller then the expected correlation length, which allows one to cover the small-scale variability.

2.1.3 Testing design accuracy

Geostatistical analysis is influenced by the sampling design (Skøin and Blöschl, 2006). To assess the applicability of the sampling design introduced above for our specific purpose (presence or absence of a range of a few meters), Gaussian random fields with defined initial covariance parameters ($\sigma = 1 \pm 0.2$; $\tau = 0$; $R = 2$ m, 5 m and 8 m $\pm$ 0.2 m, 100 simulations per range) were generated using the grf-function implemented in the RandomFields-package (Schlather, 2001) for R (R Development Core Team, 2009). The fields were generated on a rectangular grid with a regular spacing of 0.25 m (5328 points). Each point of the sampling location was assigned to the corresponding value of the generated field and a sample variogram was calculated. A spherical model λ was fitted to each sample variogram and the parameter range R, sill σ and the nugget τ were determined ($\lambda = R, \sigma, \tau$). A method suggested by Cressie (1993) was used to estimate the best fitting variogram. This method used the weighted least-squares approach given by the function J:

$$J(\lambda) = \sum_{i=1}^{K} N(h(i)) \left\{ \frac{\gamma(h(i)) - \overline{\gamma}(h(i)); \lambda}{\overline{\gamma}(h(i)); \lambda} \right\}^2 \tag{2.1}$$

where $N(h(i))$ is the number of point pairs separated by the lag distance $h(i)$ ($i = 1, , K$), and γ is the experimental variogram and $\overline{\gamma}$ the theoretical variogram. The function J gives more weight to smaller lags and to lags with more point pairs $N(h(i))$. The initial covariance parameters of the theoretical variogram were the same as those used to generate the random fields.

Figure 2.2 shows the variation of simulated ranges for the three generated ranges of 2 m, 5 m and 8 m sampled with the sampling design used in this study. The median, mean and the standard errors of the simulated ranges are given in Table 2.1. The differences between the mean simulated range and the generated range varied from 1.4 m to 2.4 m, while the deviation from the median of the simulated ranges was always smaller than 1 m. The largest standard error ($\pm$ 0.7 m) was observed for the generated 2 m range, the smallest standard error ($\pm$ 0.3 m) for the 5 m range. The sampling design should be such that a correlation length of a few meters can be determined - at least approximately. A robust estimate is not possible with this sampling design, but it can be used to clarify if a correlation length of a few meters exists or not.
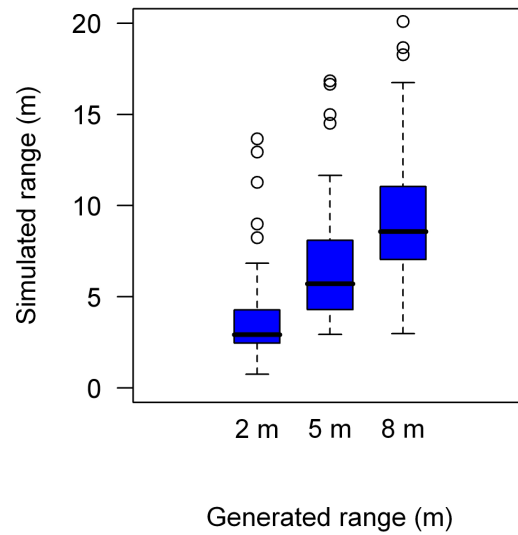
Figure 2.2: Distribution of simulated ranges for the three generated ranges of 2 m, 5 m and 8 m. Boxes span the interquartile range. Open circles indicate outliers.

Table 2.1: Summary statistics for the sampling design testing. Given are the generated range, the median of the simulated range, the mean of the simulated range as well as the standard error of the mean (SE).

Generated Range m	Median m	Mean m	SE m
2	2.9	4.4	0.7
5	5.7	6.4	0.3
8	8.5	9.8	0.5

2.2 Manual observations

2.2.1 Snow profile

Within a grid a manual snow profile was recorded by an experienced observer. Usually prior to recording the stratigraphy, a resistance profile was taken using the rammsonde (Bader et al., 1939). Grain type and size as well as the hardness of the layers were recorded according to Fierz et al. (2009). A density and a temperature profile completed the manual profile. After profiling, the stability at the profile location was tested using a rutschblock test as well as two compression tests. These manual observations provided help to identify the weak layer within the SMP signal and to assign the results from spatially distributed compression tests to a specific layer.

The manual snow profiles were classified into five stability classes (1: very poor, 2: poor, 3: fair, 4: good, 5: very good) according to Schweizer and Wiesinger (2001). This classification is based on the rutschblock score, the resistance profile and on weak layer characteristics.

2.2.2 Stability test

Stability tests are used to identify weak layers and to assess the probability of slab avalanche release. Various stability tests have been developed during the last decades. The two most commonly used stability tests are the compression test (CT) and the rutschblock test (RB) which are used by avalanche professionals as well as by backcountry skiers. Isolated columns are loaded and fractures in weak layers are observed. Based on the loading step the point stability, i.e. the local release potential, can be estimated.

The rutschblock test

The rutschblock test described by Föhn (1987) has a size of 3 m^2 (2 m x 1.5 m). After isolating the block from the snow cover, the block is loaded by a skier in six steps until a fracture occurs (Table 2.2). The loading steps ranges from, (1) fracture occurs during isolating the block to (6) jumping onto the upper third of the block. After a fracture occurred the loading step (1 to 6) is recorded as well as the release type. No release corresponds to a rutschblock score 7. The release type, i.e. how much of the block slides away, can be either whole block (wb), below skies (bs) or an edge (e). The fracture type can either be clean, rough or irregular. Low scores and a whole block release can be related to high triggering potential. On the other hand, high scores, as well as a release below skies or of only an edge of the block, indicate low triggering potential.

The rutschblock serves as a reference to define the most prominent weak layer. The

weak layer identified with the rutschblock test was defined as the primary weak layer of the grid.

Table 2.2: Rutschblock scores 1 to 7 and the corresponding loading steps.

RB score	Loading step
1	A release while cutting.
2	A release while stepping onto the upper third of the rutschblock.
3	A release during one of three pushes from the knees.
4	A release after the first jump from above the block.
5	A release after the second or third jump from above the block.
6	A release after jump from above without skis
7	No release

The compression test

The compression test (Jamieson, 1999) (CT) has a much smaller support than the rutschblock test (900 cm^2). A column of 30 cm x 30 cm is isolated from the snow cover with a saw. Then, a shovel is placed on the top of the column to ensure uniform load distribution. The column is loaded while tapping on the shovel blade, moving the hand 10 times from the wrist, 10 times from the elbow, and finally 10 times from the shoulder. When a weak layer fractures the number of taps corresponds to the compression test score. In addition, the fracture type according to van Herwijnen and Jamieson (2007a) is recorded. van Herwijnen and Jamieson (2007a) introduced five fracture types: sudden planar (SP), sudden collapse (SC), resistant planar (RP), progressive collapse (PC) and break (B) (see Table 2.3 for further explanation).

Low compression test scores and sudden fractures are related to poor stability (van Herwijnen and Jamieson, 2007a). That means fracture initiation and fracture propagation are possible. However, the small support of the compression test does not allow to quantify the propagation propensity at the slope scale.

The fracture initiation and propagation propensity at the slope scale are difficult to estimate and cannot directly be determined. Currently, no test method exists to estimate both processes at the slope scale, without disturbing or triggering the slope, i.e. bombing or ski-cutting. However, Gauthier and Jamieson (2006) developed the propagation saw test (PST). This test enables one to estimate the local propagation propensity of a weak

Table 2.3: Classification of compression test fracture type according to van Herwijnen and Jamieson (2007a).

Fracture type	Code	Fracture characteristics
Progressive Compression	PC	Fracture usually crosses column with one loading step, followed by gradual compression of the layer with subsequent loading steps.
Resistant Planar	RP	Planar or mostly planar fracture that requires more than one loading step to cross column and/or block does not slide easily on weak layer.
Sudden Planar	SP	Planar fracture suddenly crosses column with one loading step and the block slides easily on weak layer.
Sudden Collapse	SC	Fracture suddenly crosses column with loading step and causes noticeable slope normal displacement.
Non-planar Break	B	Irregular fracture surface.
No Fracture	NF	No fracture occurs

layer. A beam of typically 1 m length and 30 cm width is isolated. Afterwards, a failure is artificially initiated while cutting the weak layer with a saw, until the fracture propagates. With this test the propagation propensity can be estimated, since the fracture propagates through the entire weak layer or might arrest. However, the fracture propagation propensity at the slope scale remains unknown, since the PST test is only 1 m long. To estimate the fracture propagation propensity at the slope scale a PST test covering the whole slope would be required. Obviously, this procedure is too time consuming since it requires intensive digging, i.e. fracture propagation propensity needs to be extrapolated.

The compression test score and fracture type (van Herwijnen and Jamieson, 2007a) were combined to provide the point stability classification used for further analysis. In the following point stability classes are indicated by lower case letters and slope stability (see below) by upper case letters. This study uses three stability classes $poor$, $fair$ and $good$.

The two sudden fractures (SP and SC), were grouped as well as the non-sudden fractures (RP,PC,B). If no fracture (NF) occurred, i.e. the weak layer identified with the rutschblock did not fracture during a compression test, the corresponding compression test fracture type was assigned to the group of non-sudden fractures.

Table 2.4 shows how compression test score and fracture character are combined for point stability classification. A compression test score $\leq$ 13 observed with a sudden fracture

Table 2.4: Point stability classification

Point stability	CT score	Fracture type		CT score	Fracture type
poor	≤ 13	SP, SC			
fair	< 20	RP,PC,B	or	≥ 13	SP, SC
good	≥ 20	RP,PC,B			

was rated as *poor* point stability. Scores < 20 with a non-sudden fracture character were rated as *fair* point stability, as well as scores ≥ 13 and sudden fracture character. If the compression test score was ≥ 20 and had a non-sudden fracture the point stability was rated as *good*.

2.2.3 Slope stability classification

The slope stability can not readily be measured or determined, but several stability tests allow one to estimate slope stability. Compression tests were performed spatially distributed as shown in Figure 2.6 and classified into point stability classes of *poor*, *fair* and *good*. This point stability classification considered compression test score and fracture character, which are related to fracture initiation and fracture propagation, respectively.

It is assumed that homogeneous and continuous weak layers and stiff slabs favor fracture propagation. Sudden fractures in stability tests are related to larger propagation propensity (Gauthier, 2007). Low compression test scores indicate high failure initiation probability. All this information is included in the point stability classification. That means, the spatial distribution of point stability, derived from the compression tests, can be considered to estimate slope stability.

The compression test results were classified into point stability classes *poor*, *fair* or *good* as described above. Slopes where all compression test scores were classified as of either *poor*, *fair* or *good* point stability were classified as slopes with $POOR$, $FAIR$ or $GOOD$ slope stability, respectively. As described above, the critical length is assumed to be < 10 m. Slopes where the point stability, derived from the compression test, was either *poor*, *fair* or *good* over distances > 10 m, i.e. the critical length is definitely covered, were classified as $POOR$, $FAIR$ or $GOOD$ depending on which point stability class was observed. Slopes that showed consistent or varying point stability classes over distances < 10 m were classified as slopes of $GOOD$ stability.

2.3 Meteorological observations

Seven automatic weather stations (AWS) are located within the experimental site where measurements were performed during the winters 2006 to 2009 (Figure 2.3). These seven stations include three so-called meteorological stations and four so-called wind stations. A meteorological station measures air temperature (ventilated) and humidity, short-wave and long-wave radiation (incoming as well as outgoing), surface temperature, snow height and additional wind speed and direction. The data are available as 10 minute averages. A wind station measures speed and direction and in addition with a separate anemometer the speed of the three wind components u,v,w. Each wind stations measures also the snow height.
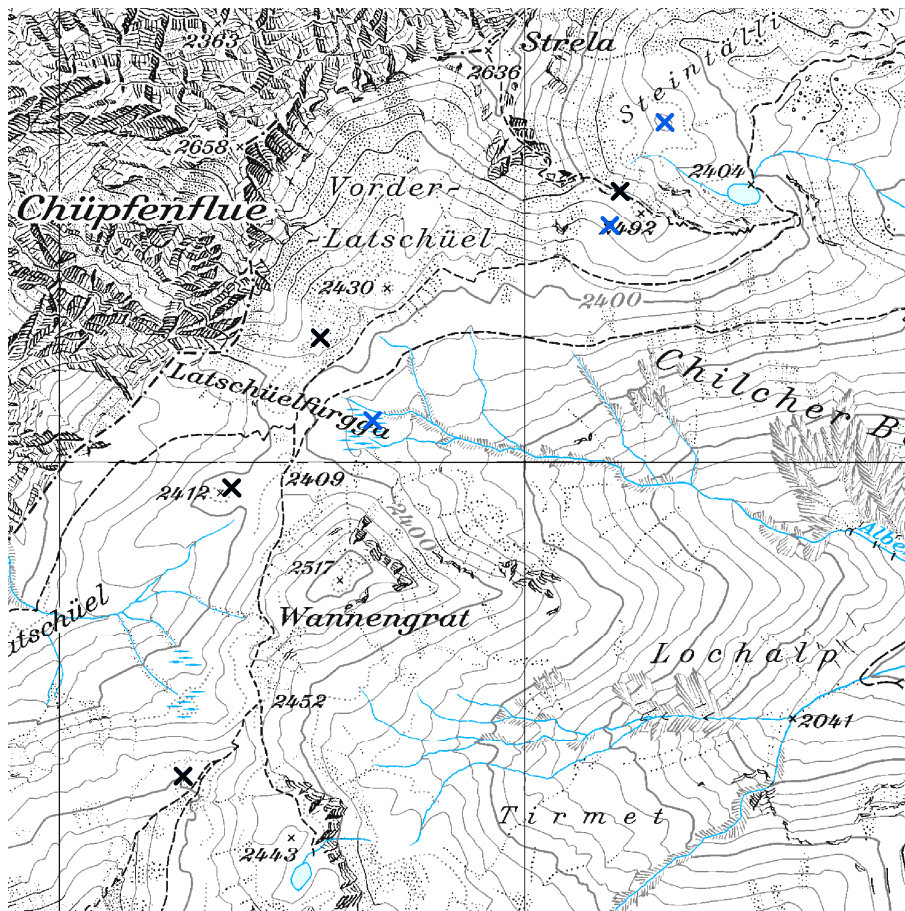
Figure 2.3: Location of the seven automatic weather stations (AWS). Meteorological stations (blue crosses) as well as wind stations (black crosses).

2.4 SnowMicroPen (SMP)

The SnowMicroPen (SMP) developed by Schneebeli and Johnson (1998) has become a valuable tool to derive snow mechanical properties. The following section describes the technical components of the SMP and the signal analysis. Finally, general limitations and error sources are described.

2.4.1 Design

The SMP (Figure 2.4) consists of a rod which is driven into the snow cover by a motor unit with a constant speed of 20 mm s^{-1} (Schneebeli and Johnson, 1998). The movable cone shaped tip (Figure 2.5) with a diameter of 5 mm and an included angle of 60° transfers changes in penetration resistance to a piezo-electric force sensor. The force sensor measures penetration resistance (range 0-42 N) every 4 μm, which corresponds to a data sampling rate of 5 kHz. As most of the penetration resistance is due to the contact of the upper part of the cone (not the tip) with the ice matrix, it is assumed that the layer resolution of the SMP corresponds to the height of a truncated cone with a lateral area that is two thirds of the lateral surface area of the whole cone, that is 1.8 mm.

Figure 2.4: SnowMicroPen during sampling. See text for detailed explanation.
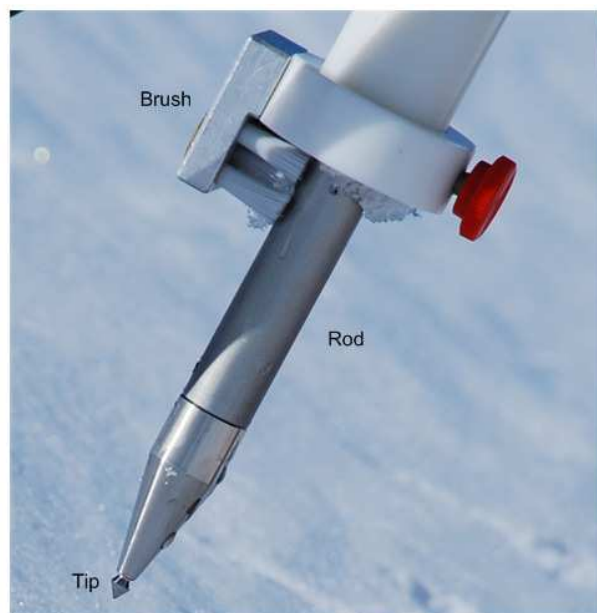
Figure 2.5: Tip of the SnowMicroPen. Cone shaped tip on top of the rod. The force sensor is located inside the silver colored part of the rod. The brush should prevent that too much frozen snow at the rod is transported into the motor unit.

2.4.2 Micro-structural model

Snow consists of sintered ice particles and the strength of snow increases during the sintering process due to bond growth (Kaempfer and Schneebeli, 2007). The porosity of snow layers that are part of a dry-snow slab avalanches exceeds 70%. This high porosity allows the SMP to measure the deformation and failure of micro-structural elements that can be used for a quantitative analysis of the SMP penetration profile.

To derive structural information, failures of individual micro-structural elements need to be identified in the SMP signal. The SMP measures a force distance profile. The resistance measurement in low density snow (50 - 300 kgm^{-3}) is caused by the rupture and deflection of the micro-structural elements, i.e. the rupture of bonds (Johnson and Schneebeli, 1999). In high density snow (above 300 kgm^{-3}), additionally, the friction between the ice and the sensor tip needs to be taken into account. A schematic SMP signal for two different snow types is shown in Figure 2.6. A micro-structural element will rupture within a typical length of dimension L_n, and will induce a peak force in the SMP signal F_{max} (Figure 2.6). The element length L_n is defined through the number of peaks (elements) within a volume zA:

$$L_n = \left(\frac{zA}{n_{peaks}} \right)^{\frac{1}{3}} \tag{2.2}$$

with z the depth interval in mm, n_{peaks} the number of peaks within the distance z and A the lateral surface area of the sensor tip (≈ 39 mm^2). The rupture force f_r is defined as the difference between the peak force F_{max} and the corresponding minimum F_{min}. The micro-structural strength can be derived from the rupture force f_r and the element length L_n and is defined as:

$$S = \frac{f_r}{L_n^2} \qquad (2.3)$$
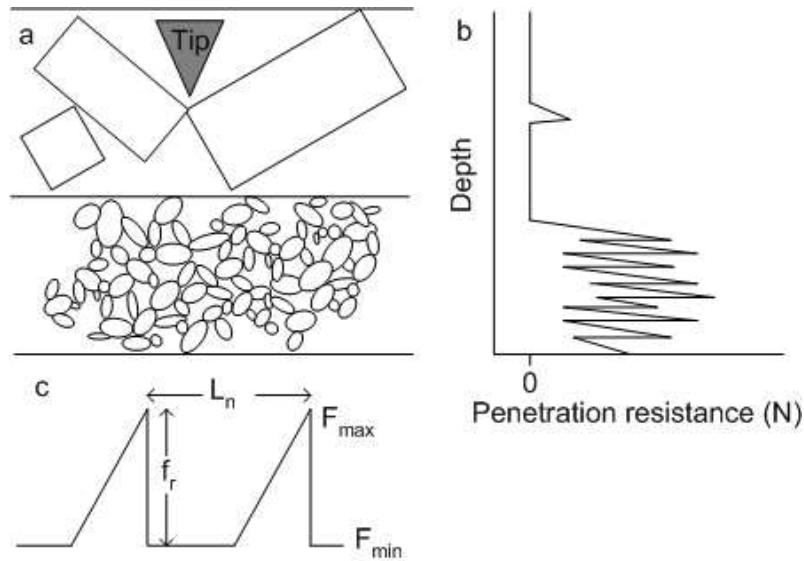
Figure 2.6: (a) Schematic of poorly bonded (top) and well-bonded (bottom) snow layers and (b) the corresponding schematic SMP signals. (c) The definition of the microstructural parameters, rupture force f_r, element length L_n and peak force F_{max} and the corresponding minimum F_{min}. The number of peaks n_{peaks} corresponds to the number of ruptures per unit length.

2.4.3 Limitations and error sources

Common practice while analyzing SMP profiles in order to derive weak layer properties is a visual inspection of the signal. Changes in penetration resistance are attributed to layer boundaries. A change of the signal variance is also an indicator of changing snow types (Schneebeli et al., 1999). In combination with the manual profile and a stability test, experienced users can identify weak layers manually in SMP profiles. However, this procedure is subjective and even two experienced users might identify different layers or boundaries. The boundaries of a snow layer in the SMP profile are not discrete as

suggested in manually observed profiles, but a transition zone between two layers exists, that is the hardness changes gradually between two layers of different hardness. The transition zone is partly an artifact of the measuring device since the measuring cone shaped tip has a finite length (4.33 mm). Transition zones between layers with large differences in penetration resistance are on the order of the layer resolution, but can be larger within softer snow, which makes the definition of layer boundaries more difficult. These transition zones have to be taken into account when analyzing the force-distance signal.

Measurement errors can occur due to, variable penetration speed and mechanical as well as electronical problems. To ensure a constant penetration speed the operator should hold the motor casing steady to prevent the device from lifting because of the reaction force of the SMP against the snow. Mechanical problems might occur if the sensor is frozen. An O-ring seal should impede that snow reaches the sensor. However, this O-ring seal is not water proof and after a few dozen measurements water may reach the sensor and might freeze up. Warming up and cooling down of the device also produces moisture next to the sensor. SMP signals affected by a frozen sensor can easily be identified and should be excluded. The sensor is often subject to large temperature changes during the measurement. These temperature changes affect the casing surrounding the piezo-electric sensor, which results in a deformation of the piezo-crystal which may cause signal drift. To minimize these effects the SMP should be cooled down before each measurement.

2.5 Statistical methods

2.5.1 Geostatistics

During the last years geostatistical analysis has been applied to snow studies, e.g. Kronholm (2004). One aim of a geostatistical analysis is to identify the correlation length of observed properties. Typically the variable of interest Z at sampling locations $x = (X, Y)$ is divided into a trend $T(x)$ and a residual part $R(x)$ (Cressie, 1993):

$$Z(x) = T(x) + R(x) \tag{2.4}$$

It is assumed that $R(x)$ is stationary with constant mean and variance over the entire area under study. Both the trend $T(x)$ (see next section) and the residual part $R(x)$ need to be quantified to describe the spatial structure of the variable under study. Figure 2.7 shows the orientation of the coordinates X (cross-slope) and Y (up-slope).
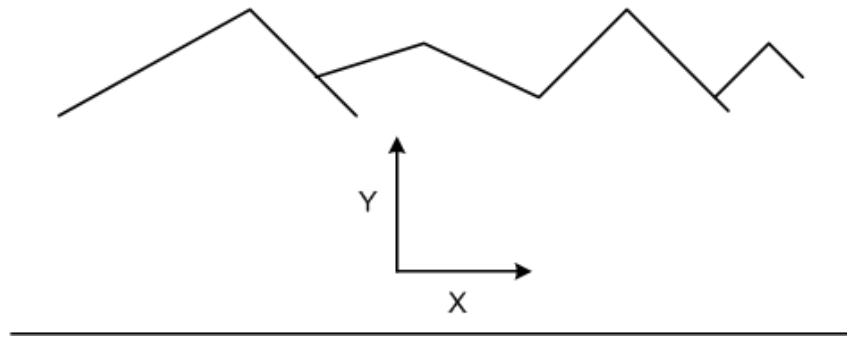
Figure 2.7: Orientation of coordinates X (cross-slope) and Y (up-slope).

Trend removal

Often spatial trends of a property exist spanning the entire area of investigation. These trends need to be removed before calculating the variogram. Trends introduce a non-stationarity of the property under investigation. Trends of snow properties can often be directly explained by meteorological conditions such as wind. For example, the variation of snow depth at the slope scale may be explained by snow drift.

Trends have been quantified in this study by applying a first order polynominal to the data such that:

$$T(x) = a + bX + cY \qquad (2.5)$$

with the coefficients a,b and c. The sampling locations are described by X, Y, where X is positive in the orographic left direction (cross-slope) and Y is positive up-slope. The usage of a linear trend does not imply that the trend was linear. However, a linear trend allows one to directly interpret slope scale trends. That means, a positive correlation of the variable of interest in X direction corresponds to an increase of this variable cross the slope (compare Figure 2.7).

Variogram

The semi-variogram (Webster and Oliver, 2007) is used to describe spatial properties of the residual part $R(x)$. It is assumed that $R(x)$ is stationary over the entire area of interest. That means, the mean and variance are constant over the area and the spatial dependence of the data Z is only a result of the distance between sampling locations and not of their absolute position. These assumptions are typically ensured after trend removal (Webster and Oliver, 2007).

The semi-variogram $\gamma(h)$ calculates the half mean squared differences between sampling locations separated by distance h. In the following the semi-variogram is referred to as

simply the variogram to avoid excessive jargon. Usually point pairs with similar distances are grouped into classes of lag distances to increase the number of point pairs per class. This grouping increases the robustness of the statistical analysis. For each lag distance h the experimental variogram (open circles, Figure 2.8) can be calculated following Cressie and Hawkins (1980).

$$\gamma(h) = \frac{\left[\frac{1}{N(h)} \sum_{i=1}^{N(h)} |Z(x_i + h) - Z(x_i)|^{\frac{1}{2}}\right]^4}{(0.914 + \frac{0.988}{N(h)})} \qquad (2.6)$$

with Z the variable of interest at sampling location $x_i = (X_i, Y_i)$ and $N(h)$ the number of point pairs separated by the lag distance h. The variogram is a measure of variation. The variance increases with lag distance h as the measurements become more dissimilar.
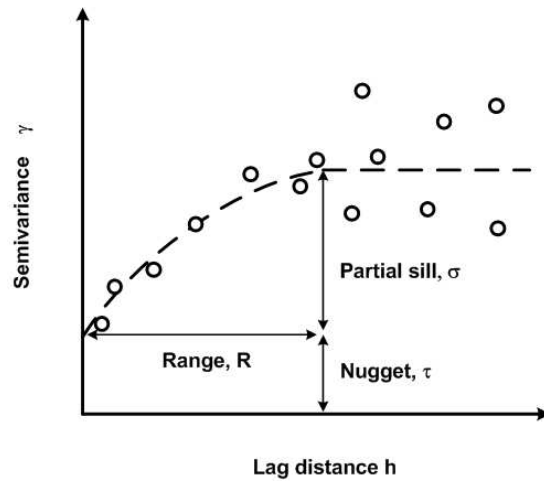
Figure 2.8: Schematic of a variogram. Experimental variogram (open circles) as well as the theoretical variogram (dashed line) are shown with the descriptive parameter partial sill σ , nugget τ, and range R.

To each experimental variogram $\gamma(h)$ a theoretical variogram $\overline{\gamma}(h)$ (dashed line in Figure 2.8) can be fitted. A spherical variogram was fitted to each experimental variogram as previously done for snow properties by Kronholm (2004). The spherical model is defined such that:

$$\overline{\gamma}(h) = \begin{cases} 0 & h = 0, \\ \tau + \sigma \left[\frac{3h}{2R} - \frac{1}{2}(\frac{h}{R})^3\right] & 0 < h \leq R \\ \tau + \sigma & h > R \end{cases} \qquad (2.7)$$

and fitted using weighted least square method.

Variogram interpretation

Figure 2.8 shows a schematic variogram with the descriptive covariance parameters, partial sill σ, nugget τ and range R. The sill (partial sill + nugget) is reached when the theoretical variogram reaches a plateau. The distance where the sill is reached corresponds to the range R. Values separated by distances smaller than the range R are similar (correlated), beyond the range values are dissimilar (uncorrelated). The nugget variance τ is caused by measurement errors and variations smaller than the minimum spacing.

Theoretical variograms should only be interpreted to half the extent (Cressie, 1993), since the range estimate becomes unreliable. However, this rule of thumb is subjective and depends on the sampling design as well as on the amount of available point pairs within each lag (Journel and Huijbregts, 1978). Journel and Huijbregts (1978) suggested 30 - 50 point pairs within each lag for a variogram estimation. The sampling design used in this study fulfilled this requirement for almost all lag distances (compare Figure 2.1). For this study all lag distances were considered for the variogram estimation, but the theoretical variogram was only interpreted to about half the extent.

Three typical variograms are shown in Figure 2.9. The pure-nugget variogram (Fig. 2.9a) indicates no spatial dependence of the variable under study, after trend removal, over the entire area of interest ($\sigma = 0$). A pure nugget variogram indicates, that a possible variation is only caused by a slope scale trend or variations have scales larger than the study area.

A unbounded variogram, i.e. the variance γ increase linearly with increasing lag distance is shown in Figure 2.9c. The unbounded variogram indicates a non-stationary process of the residuals of the variable under study. This implies that the applied trend should be of a higher order, i.e. it is not linear. For completeness a variogram where a range R can be identified is shown in Figure 2.9b.
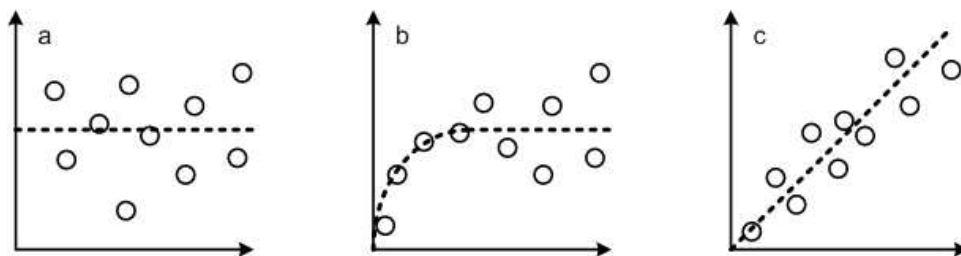
Figure 2.9: Three typical variograms. a) pure-nugget b) the theoretical variogram, in this case a spherical, reaches a sill and c) an unbounded variogram.

If a range R or correlation length can be determined by the variogram, a spatial structure

spanning the scale of the range R exists. Values are spatially variable if large variations of this value occur over small distances. The value is less spatially variable if small variations are observed over large distances. The extent at which the variable of interest is investigated is of particular importance. A correlation length of 10 m at slope scale might indicate low spatial variability, but might indicate high spatial variability at for example the basin scale.

2.5.2 Moran's I

In addition to the geostatistical analysis, the spatial structure was estimated with the Moran's I coefficient, a measure of spatial autocorrelation (Moran, 1948) that has been recently applied in a snow study by Hendrikx et al. (2009). The coefficient ranges from -1 (dispersion) to +1 (clustered). A value of zero indicates a random pattern (Figure 2.10). The null hypothesis chosen was "no spatial autocorrelation exists". For this study, we choose a level of significance $p < 0.05$ to reject the null hypothesis. The Moran's I statistics was calculated with the Moran.I - function implemented in the ape-package (Paradis et al., 2004) for R (R Development Core Team, 2009) and is defined as:

$$I = \frac{N}{\sum_i \sum_j w_{ij}} \frac{\sum_i \sum_j w_{ij}(Z_i - \overline{Z})(Z_j - \overline{Z})}{\sum_i (Z_i - \overline{Z})^2} \qquad (2.8)$$

where N is the number of sampling locations indexed by i and j, $\overline{Z}$ is the mean of the variable under study and w_{ij} is a matrix of spatial weights. This study uses an inverse distance matrix which gives more weight to smaller distances. Note that the Moran's I coefficient describes the spatial structure of the variable of interest including a possible slope scale trend, i.e. the data were not de-trended.
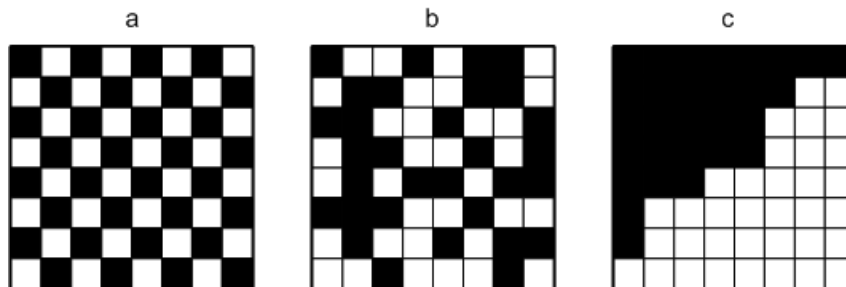
Figure 2.10: Schematic of three theoretical patterns. Representing a) a dispersed pattern (Moran's I $\Rightarrow$ -1) b) a random pattern (Moran's I = 0) and c) a clustered pattern (Moran's I $\Rightarrow$ +1).

2.5.3 Non-spatial statistics

Non-spatial statistics, i.e. the measurement location was not considered for statistical analysis, have been used in this study to describe the data. All parameters analyzed in this study were tested for normal distribution. They passed the Kolmogorov Smirnov test ($p < 0.05$) (Spiegel and Stephens, 1999), but were often slightly skewed. Therefore, the median, the semi-interquartile range (SIQR) as well as the quartile coefficient of variation (QCV) were used to describe the observed data.

The semi-interquartile range (SIQR) was used to describe the absolute dispersion of the observed data. The SIQR (Spiegel and Stephens, 1999) is defined as:

$$SIQR = \frac{Q3 - Q1}{2} \qquad (2.9)$$

with Q1 the 1st (25% of the data) and Q3 (75% of the data) the 3rd quartile.

The quartile coefficient of variation (QCV) as a relative measure of dispersion is defined as:

$$QCV = \frac{Q3 - Q1}{Q3 + Q1} \qquad (2.10)$$

For comparison with other studies the quartile coefficient of variation (QCV) can be related to the coefficient of variation (CV) such that:

$$CV = \frac{3}{2} QCV \qquad (2.11)$$

Tree statistics and performance measures

Univariate tree statistics (Breiman et al., 1998) were used to derive threshold values for stability classification (see chapter 4.1), i.e. distinguish between the stability classes of $poor$ and $fair - to - good$. Bellaire et al. (2009) used this stability classes for the stability classification of SMP profiles. For these classification profiles with a rutschblock score ≤ 3 were assigned to the group of $poor$, profiles with a rutschblock score > 3 as $fair - to - good$ point stability. To estimate the performance of these different cross-correlated prediction models contingency tables as schematically shown in Table 2.5 were generated (Wilks, 1995). Various performance measures can be derived from these contingency tables (Doswell et al., 1990).

Table 2.5: Schematic of a contingency table.

		Observation	
		poor	**fair-to-good**
Model	**poor**	a	b
	fair-to-good	c	d

This study focused on 3 measures. The hit rate (HR)

$$HR = \frac{a+d}{a+b+c+d} \tag{2.12}$$

is a measure of the overall accuracy. The poorest hit rate is zero if $a = d = 0$, whereas the best possible hit rate is 1 ($b = c = 0$). The second parameter is the probability of detection (POD) defined as:

$$POD = \frac{a}{a+c} \tag{2.13}$$

A POD of 1 indicates a perfect prediction of *poor* stability. Finally the probability of non-events (PON) is 1 if all observations classified as $fair-to-good$ are modeled correctly.

$$PON = \frac{d}{b+d} \tag{2.14}$$

Data

This chapter introduces the data sets used for this study. A summary of all 23 grids measured during the winters of 2006-2009 is given as well as information about the performed measurements within each grid including compression tests and SMP measurements. In addition, the dataset used by Bellaire et al. (2009), which was supplemented with additional SMP signals for this study, is presented.

3.1 Grids

During three winters between 2006 and 2009 twenty three grids were carried out on different slopes above timberline (at about 2400 m a.s.l.) in the region of Davos, Switzerland (Figure 3.1,Table 3.1). The slopes had four different aspects (N, NE, S, SW) and the slope angle varied between 18° and 35°. Five grids were discarded since the majority of the SMP measurements were erroneous. One grid, performed on a strongly wind affected slope was also discarded, because the weak layer could not be identified in most of the SMP signals. Therefore, only 17 out of 23 grids were analyzed in this study.

In nine out of the remaining 17 grids the weak layer consisted mainly of persistent grain types (Jamieson and Johnston, 1998) and in three cases at least the secondary grain type was persistent (Table 3.1). The remaining five weak layers or interfaces were either mixtures of decomposed fragmented precipitation particles and small rounded grains (3) or hardness changes across a layer interface between layers of small rounded grains (2).

The selection of a grid location was strongly depending on the avalanche danger as well as on weather conditions during the field day. A slope was selected by the most experienced member of the field crew. No specific slopes or aspects were preferred for sampling. The slopes had a rather uniform snow depth distribution and were undisturbed. The meteorological conditions were recorded by the automatic weather stations. To relate

observed snow cover conditions to meteorological parameters, generally slopes close to weather stations were sampled. During the winter of 2007-2008 fortnightly measurements have been performed on a south-west facing slope (blue open circles, zoom Figure 3.1) to follow stability over time.
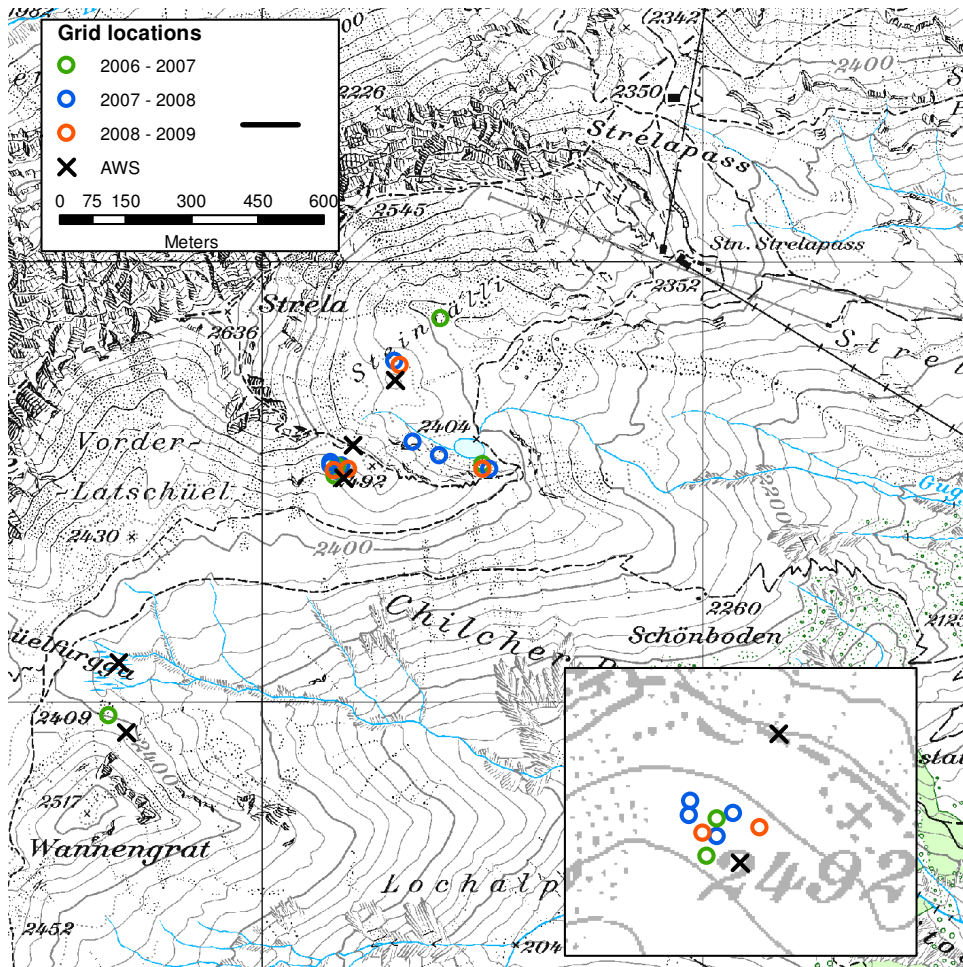
Figure 3.1: Map of the experimental site. The locations of the automatic weather station (X) are shown as well as the grid locations for the three winters between 2006 and 2009 (colored open circles). The small map represents a zoom of the south-west facing slope where many of the grids have been performed.

3.2 Stability tests

Each grid contained a manual snow profile supplemented with a rutschblock test. Seventeen rutschblock tests were analyzed. The layer identified by the rutschblock was defined as the weak layer. Rutschblock scores and the release types are shown in Table

Table 3.1: Summary information for the 23 carried out grids. Beside date and location, aspect slope angle and weak layer primary grain type(WL) are given as well as the profile type (PT) according to Schweizer and Wiesinger (2001) the rutschblock score (RB) and release types (RT). Additional given are the mean compression test score (CT), the absence or presence (x) of signs of instability, notes and finally if the grid was used (x).

No.	ID	Date	Coordinates		Asp.	Angle °	WL	PT	RB	RT	CT	Signs	Notes	Used
			X	Y										
1	1-0607	25.01.2007	779164	186514	SW	19	RG	3	4	wb, c	RR		Rammrutsch	x
2	2-0607	02.02.2007	779404	186872	NE	20	RG	5	7	-	17.5			x
3	3-0607	16.02.2007	779500	186540	N	30	FC	3	5	wb, c	13			x
4	4-0607	06.03.2007	779296	186774	N	18	DH	4	6	bs, c	15	x	frozen sensor	
5	5-0607	08.03.2007	779170	186535	SW	23	DF	3	5	E, c	12			x
6	6-0607	15.03.2007	778650	185970	N	33	DH	2	3	wb, r	12	x		x
7	1-0708	10.01.2008	779170	186525	SW	22	FC	2	2	wb, c	10.5	x		x
8	2-0708	17.01.2008	779515	186529	N	32	RG	3	5	wb, c	11.5			x
9	3-0708	23.01.2008	779179	186538	SW	22	DH	1	2	wb, c	11	x		x
10	4-0708	31.01.2008	779300	186775	N	20	FCmx	3	4	wb, c	14.5			x
11	5-0708	07.02.2008	779154	186537	SW	22	DH	3	4	wb, r	12.5	x		x
12	6-0708	15.02.2008	779401	186560	N	32	FC	4	6	E, c	22.5			x
13	7-0708	19.02.2008	779155	186545	S	23	FCmx	3	3	bs, r	14			x
14	8-0708	06.03.3008	779171	186571	S	18	DH	4	6	E, r	16.5	x	frozen sensor	
15	9-0708	18.03.2008	779341	186591	NE	34	RG	4	4	bs, s	19	x		x
16	1-0809	09.01.2009	779155	186532	SW	23	FC	4	6	bs, c			frozen sensor	
17	2-0809	14.01.2009	779312	186765	N	20	RG	4	5	E, s	13.5			x
18	3-0809	29.01.2009	779164	186546	SW	20	DH	3	3	bs, r	12	x	frozen sensor	
19	4-0809	30.01.2009	779499	186530	N	30	RG	3	4	bs, c	11			x
20	5-0809	05.02.2009	779275	186781	N	20	SH	3	5	wb, c	19		frozen sensor	
21	6-0809	19.02.2009	779162	186527	S	20	DH	4	5	bs, c	13	x		x
22	7-0809	26.02.2009	779194	186530	SW	21	FCmx	4	6	wb, r	18			x
23	8-0809	17.03.2009	778635	185959	N	35	DH	3	4	bs, r	18		no continuous weak layer	

3.1. Rutschblock scores ranged from 2 to 7 (no release). Most release types were whole block releases (10 out of 17). Four rutschblocks released below skis and in three grids only an edge released.

Compression tests were also carried out in all grids. Each grid contained 10 pairs of compression tests. In total 340 compression tests were analyzed. The median compression test scores ranged from 10.5 to 22.5. Only compression test scores for the weak layer identified by the rutschblock test were taken into account for this study. The minimum score of two side by side compression tests was used. The median difference between two adjacent compression tests was 1 score (3rd quartile: 3 scores). In most cases, the RB failure layer also failed in both of the two adjacent compression tests. In 19 out of 170 compression test pairs, only one compression test of the pair failed on the weak layer identified by the rutschblock test. In 12 out of 170 compression test pairs the weak layer identified with the rutschblock could not be fractured with the compression test.

3.3 SMP measurements

3.3.1 Grids

To quantify snow cover properties SMP profiles were measured at 46 locations over the entire grid. In total 1058 SMP signals were recorded. From these 1058 profiles 295 profiles had to be discarded due to erroneous signals (Table 3.1). All SMP signals were visually inspected. So far no method exist to identify erroneous signals automatically. Pielmeier and Marshall (2009) used a four level quality check (C1-C4) to rate signal quality (Table 3.2).

Before the sensor tip touches the snow surface, the tip travels through the air while measuring. The signal measured in air should only be affected by vibrations from the motor and can be used as a baseline signal (micro-variance) to identify erroneous signals. A typical air signal oscillates around zero with a maximum amplitude of $\pm$ 0.02 N depending on the specific SMP. If the sensor is frozen this amplitude is much smaller. Within the snow cover, an erroneous signal due to a frozen tip can be identified by a nearly linear increase in penetration resistance.

All analyzed SMP signals belong to the group C1, i.e. no trends and off-set visible. The remaining 763 profiles were analyzed as described in the Methods section. IDL procedures (IDL version 6.4) were used for signal processing. These procedures were based on the micro-structural model introduced by Johnson and Schneebeli (1999) and on the stability formulation introduced by Bellaire et al. (2009).

Table 3.2: Four level SMP signal quality check suggested by Pielmeier and Marshall (2009).

Quality	Type of SMP signal error
C1	None
C2	Trend or offset in absolute SMP force
C3	Dampened or disturbed SMP force micro-variance
C4	Both C2 and C3

3.3.2 Stability algorithm

To verify the SMP stability algorithm introduced by Bellaire et al. (2009) a dataset consisting of 71 SMP profiles from the eastern Swiss Alps was used. These profiles were measured close ($<$ 0.5 m) to a manual snow profile completed with a stability test. Stability tests used were the rutschblock test (in 59 cases) and the compression test (in 12 cases). This data set is similar to the data set used by Bellaire et al. (2009), but was supplemented with additional SMP measurements. The old data set was verified using the four level quality check (C1-C4) introduced by Pielmeier and Marshall (2009). Following this procedure erroneous signals (about 10%) had to be discarded from the original data set.

Compression test scores were converted into comparable rutschblock scores according to Schweizer and Jamieson (2003). The rutschblock scores covered the entire range (1 to 7) with a median score of 4.

In 41% of the 71 observed profiles the primary grain type in the failure layer was faceted crystals. In another 22 profiles, the failure layer primarily consisted of either depth hoar (16%), rounded facets (13%) or buried surface hoar (1%). In the remaining failure layers (29%) melt forms, graupel and mixtures of rounded grains and decomposed and fragmented precipitation particles were observed. The failure depth ranged from 5 cm to 62 cm, with a median value of 30 cm.

For the stability classification of the SMP stability index proposed by Bellaire et al. (2009) the profiles (N = 71) were grouped into two stability classes based on the rutschblock score. Scores $\leq$ 3 indicated rather $poor$ (N = 28), scores $\geq$ 4 $fair-to-good$ stability (N = 43).

Results

This chapter summarizes the results of this study. First, a re-analysis of the SMP stability algorithm introduced by Bellaire et al. (2009) is presented. Second, the results of a spatial and non-spatial analysis of the data are shown. Finally, the observations are related to snow slope stability.

4.1 SMP Stability algorithm

4.1.1 Introduction

Collecting stability information, i.e. performing stability tests like the compression test or the rutschblock test, is time consuming. Measuring the snow stratigraphy over one meter with the SMP takes about two minutes. In contrast, a manual snow profile supplemented with stability tests lasts about one hour. A SMP signal based stability information would therefore increase the amount of available stability information and would reduce the uncertainty of estimating slope stability with a single stability tests. That means, additional objective stability information would be available.

The following re-analysis which is used for further analysis in this study is based on the proposed algorithm by Bellaire et al. (2009), but uses an extended dataset (see section 3.3.2). The re-analysis of the algorithm includes, beside the analysis made by Bellaire et al. (2009), a more detailed analysis of micro-structural parameters, which may be used to assess slope stability.

The algorithm estimates stability by a stepwise sequential analysis of micro-structural parameters - see method section for details - derived from the SMP signal. First, the four weakest transitions between layers are identified. Second, for each of the four weakest transitions the corresponding weak layer boundaries are defined. Third, by taking into

account the layer structure, the layer that will most likely fail is selected from the four potential weak layers. Finally, based on an analysis of weak layer and slab properties SMP signals are classified into two stability classes of $poor$ and $fair-to-good$.

4.1.2 Model development

This section provides the theoretical background of the algorithm. The stability algorithm is based on four assumptions (Bellaire et al., 2009) which are mainly based on the micro-structural parameters as introduced above.

a) The microstructural element length L_n is larger for poorly bonded snow than it is for well-bonded snow (Johnson and Schneebeli, 1999). As a consequence the number of ruptures n_{peaks} per unit length is much smaller for poorly bonded snow than for well-bonded snow.

b) A weak layer can often be described as a region of poorly bonded grains, i.e. fewer bonds per unit volume. The rupture force f_r in a layer of poorly bonded grains is lower than the ruptures force in a layer of well-bonded grains (Johnson and Schneebeli, 1999).

c) Large discontinuities in structure (hardness and grain size) between layers indicate weak areas or interfaces (Schweizer and Jamieson, 2003).

d) Weak layers buried deep within the snow cover are less prone to skier triggering, because the additional skier-induced stress strongly decreases with increasing depth (Föhn, 1987).

Weak layer detection

Following assumptions (a) and (b) a parameter relating to the structure of layers named Ψ is defined:

$$\Psi = \frac{\bar{f}_r n_{peaks}}{A} \tag{4.1}$$

where $\overline{f_r}$ (N) is the rupture force averaged over 1 mm of the SMP signal, n_{peaks} the number of peaks within 1 mm and A is the lateral surface area of the sensor tip (39 mm^2). The parameter Ψ is smaller for poorly bonded than for well-bonded grain types (see assumptions (a) and (b)).
Following assumption (c), that is large discontinuities in properties between layers indicate a weakness, the gradient of Ψ (1 mm) is calculated over the entire signal. The gradient of Ψ, which can be interpreted as a layer boundary property, is only relevant for instability when the peak force F_{max} is also small and indicates low strength. Therefore,

the gradient of Ψ is scaled by the ratio of the peak force F_{max} to the lateral surface area A of the sensor tip:

$$B = \frac{A \; grad\Psi}{F_{max}} \qquad (4.2)$$

As the peak force F_{max} is typically smaller for poorly bonded layers than for well-bonded layers, sections of the SMP signal with $F_{max} > 0.5 \; N$ are not considered for further analysis. This value of 0.5 N is used a pre-filter, since weak layers have to be weak, and was derived empirically.

In early winter thick depth hoar layers may form at the base of the snowpack. These layers may persist for the whole winter, but can usually not be skier triggered when they are buried deeper than about 1 m. However, in the SMP signal they are often identified as a weak transition, because Ψ is much smaller for larger grains than for smaller grains. To avoid this, the parameter B was additionally weighted by a depth dependent factor w, which was derived from the frequency distribution of slab thickness. This factor corresponds to the Weibull density distribution:

$$w(z) = f(z, \alpha, \beta) = \frac{\alpha}{\beta} \; z^{\alpha-1} \; e^{-(\frac{z}{\beta})^\alpha} \qquad (4.3)$$

where z is the slab thickness and α and β are the coefficients of the Weibull distribution. These latter coefficients were obtained from the frequency distribution of thicknesses of snow slabs above the failure surface from 512 stability tests done in Switzerland and Canada (updated from Schweizer and Jamieson (2003) (Figure 4.1)) where z is the slab thickness, and α and β are the coefficients of the Weibull density distribution: $\alpha = 2.5$, $\beta = 500$. Without this weighting factor w the snow surface is in most cases identified as the weakest transition (air/snow).

Combining Equations (4.2) and (4.3) yields to the final parameter Δ to seek potential weaknesses in a SMP profile:

$$\Delta = \frac{A \; grad\Psi}{F_{max}} \; w(z) \qquad (4.4)$$

The parameter Δ can be negative for transitions between poorly-bonded layers and well-bonded layers, and positive for bonded/poorly-bonded transitions, i.e. a potential weak transition (WT) is located where Δ either reaches a maximum or a minimum value. For further analysis, the two primary (min and max) and the two secondary extreme values that were closer to the surface than the primary ones, were used. Furthermore, a transition once identified by either a minimum or a maximum can not be selected again. That means four independent weak layers are identified by the algorithm.
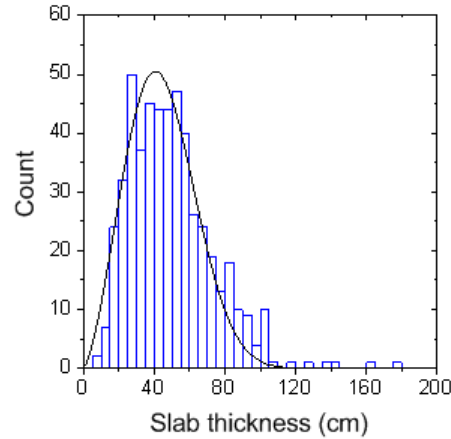
Figure 4.1: Histogram of slab thickness from 512 stability tests performed in the Swiss Alps and the Columbia Mountains of western Canada, and the fitted Weibull distribution (solid line).

Figures 4.2 a to f summarize the above described procedure for identifying the critical weak layer in SMP signals. First, the SMP signal is averaged over 250 measurements, i.e. over 1 mm (Fig. 4.2a). Four extreme values of the parameter Δ are identified (Fig. 4.2b). Transition number two (Fig. 4.2b) was the observed weak layer in the rutschblock test (depth z_{WL} = 465 mm). The Figures 4.2c to 4.2f show the region of the weak layer for the penetration resistance F, the parameter Ψ, the rupture force f_r and the number of ruptures n_{peaks}. The parameter Ψ is shown in Figure 4.2d. Ψ is equally small for persistent as for non-persistent layers, what indicates similar bonded layers. The weak layer (transition number two) in this example is a layer of rounded facets (FCmx) below a layer of small rounded grains (RG) that is harder than the weak layer. Figure 4.2e shows the rupture force. The rupture forces below and above the hard layer are quite similar. In fact, similar grain sizes (i.e. similar bond sizes) were observed, supporting assumption (b). As a result in this case, following Equation (4.1), Ψ can only be smaller if the number of ruptures is smaller, which is often the case for layers of poorly bonded grains (Fig. 4.2f). In the example shown, the layer of rounded facets has slightly fewer bonds than the layers above the harder layer. This figure also shows the difficulty of detecting weak layers that have structural parameters that are similar to those of layers that are not weak layers.
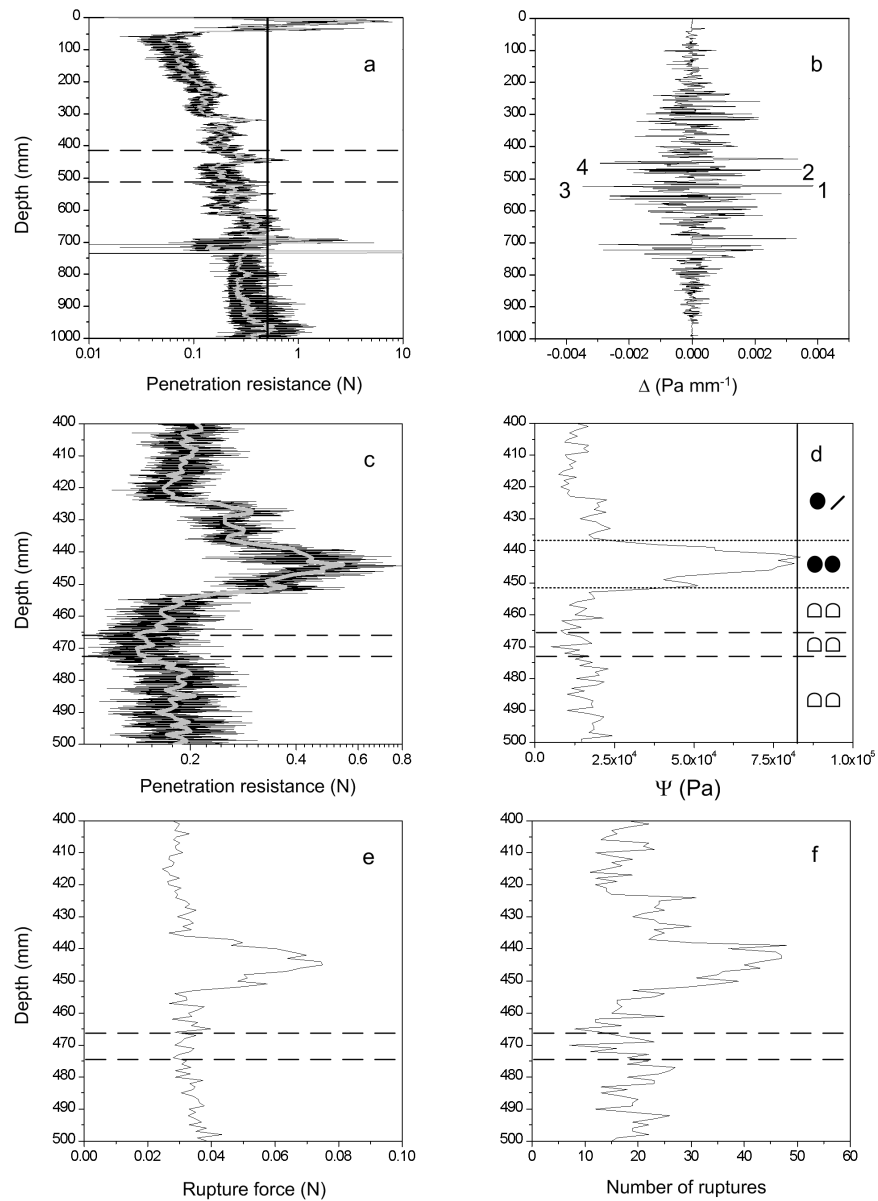
Figure 4.2: (a) Original (black solid) and averaged SMP signal (gray solid line, 1 mm average). (b) Parameter Δ to find potential weak transitions. The locations are indicated by the numbers 1 to 4. (c) Zoom to the region of weak layer (dashed lines in a) with original (solid black line) and averaged (solid gray line) SMP signal. Dashed lines show upper and lower boundaries indicated by the algorithm. (d) Parameter Ψ at the depth of the weak layer with grain types for both the observed weak layer and adjacent layer. (e) Averaged rupture force for the depth of the weak layer. Dashed lines show layer boundaries of the weak layer. (f) Number of ruptures for the region of the weak layer. Dashed lines show upper and lower boundaries of the weak layer defined by the algorithm.

Defining weak layer boundaries

The parameter Δ identifies four potential weak transitions, i.e. poorly bonded regions in the resistance-depth profile. Colbeck et al. (1990) defined a layer as a stratum which is different in at least one respect (hardness, grain size, shape) from the stratum above and below. To define the upper and lower boundaries of the potential weak layer, the minimum force F_{min} within 1 cm either above and below the weak transition (WT) was identified. If the minimum force F_{min} (averaged over 1 mm) was found above the weak transition, WT was defined as the lower layer boundary, otherwise as the upper layer boundary. To define the other layer boundary the coefficient of variation was calculated. The local coefficient of variation (CV) is defined as the standard deviation divided by the mean over 1 mm of penetration force signal. It is assumed that a layer boundary is located where the gradient of the CV is larger than 0.1. The value of 0.1 was derived empirically by comparing the gradient of the CV to the observed manual profiles and their layering. The locations where the threshold of 0.1 is exceeded correspond to the upper and lower boundary, respectively. However, the upper and lower boundaries often fall within the transition zone, as hardness changes gradually between two layers of different hardness. Therefore the final upper and lower boundaries are assumed to be located in the middle between the boundaries and the position of the minimum force F_{min}. The above described procedure is illustrated in Figure 4.3.
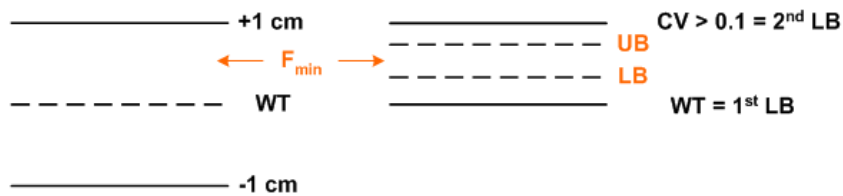
Figure 4.3: Schematic of layer boundary detection. Left: Picking of weak transition (WT) by Δ and searching for the minimum penetration resistance F_{min} within ± 1 cm. Right: Defining the weak transition as first temporary layer boundary and searching for the first position where the coefficient of variation is > 0.1 (second temporary boundary layer). The middle between these two positions and the minimum penetration resistance is defined as upper (UB) and lower (LB) boundary, respectively.

Critical weak layer detection

In order to test the algorithm, the failure depth of the automatically picked critical weak layers was compared to the depth of the failure layer that was identified manually in the SMP profile with the help of the manual snow profile and the stability test. When applying the algorithm, i.e. seeking the four potential weak layers in the profiles, in 90% of cases (64 out of 71) one of the four potentially weak layers derived from the SMP signal coincided with the observed weak layer (Fig. 4.4a).

As described above four potential weak layers are identified by the algorithm. To decide which of the four potential weaknesses is most prone to be skier triggered, two potential critical layers were selected from the four identified layers by choosing the two layers with the lowest penetration resistance. Then, the layer (one of these two) that showed the maximum difference in penetration resistance between the slab and the weak layer is defined as the layer which is most prone to be skier triggered. Different combinations of various micro-structural parameters and their differences between slab and weak layer were tested. However, the above described procedure performed best and in 58% of the 64 SMP signals the weak layer identified by the algorithm corresponded to the observed weak layer (Figure 4.4b), random picking yields to 25%. This accuracy is comparable to the performance of stability field tests such as the Compression Test or the Extented Column Test (Winkler and Schweizer, 2009). These stability tests performed adjacent to each other identified the same weak layer only in about 60% of the cases.

For comparison, Figure 4.4c shows that the depth of the minimum penetration resistance was poorly related to the observed failure depth. The agreement was only 11%. This implies that micro-structural properties and micro-mechanical strength derived from the SMP signal are essential for weak layer detection.

4.1.3 Stability formulation

Various weak and slab layer properties were contrasted for the stability classes of *poor* and $fair-to-good$ (Fig. 4.5). These properties included the penetration resistance (F), the number of peaks (n_{peaks}), the element length (L), the rupture force (f_r), the micro-structural strength (S) and the parameter Ψ. For the comparison only those 64 profiles were considered where one of the potential weaknesses was the observed weak layer.

The profiles rated as *poor* had lower median values for all variables, except the element length L, than the profiles rated as $fair-to-good$ (Figure 4.5). For all variables, except the weak layer penetration resistance ($p_{wl} = 0.286$, $p_{slab} = 0.293$), the observed differences were judged to be statistically significant (p < 0.05) based on a nonparametric Mann-Whitney U-Test (Spiegel and Stephens, 1999).

For the significant variables a threshold value was determined using univariate 10-fold cross-validated tree statistics (Breiman et al., 1998) to classify the profiles into the two stability classes. The performance of the different classifiers is indicated by the hit rate (HR), the probability of non-events (PON) and the probability of detection (POD), as shown in Table 4.1. The best hit rate (75%) were observed for the micro-structural strength and for the parameter Ψ of the slab layers. Furthermore, both parameter showed the same threshhold value (15 kPa). This can partly be explained by the fact that the micro-strength and the parameter Ψ are comparable (compare equation (2.3 and 4.1). However, the parameter Ψ was a slightly better predictor of weak layer instability since
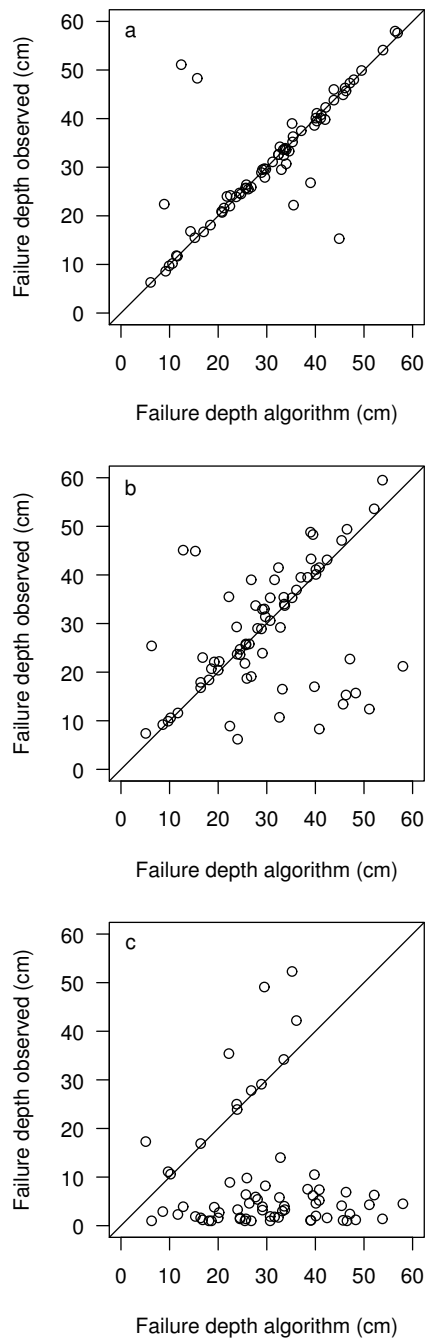
Figure 4.4: (a) Failure depth derived from rutschblock test and compression tests vs. failure depth as selected manually from the four suggested weak layers (accuracy: 90%). (b) Comparison of the observed failure depth to the failure depth of the weak layer derived automatically by the algorithm (accuracy: 58%). (c) Comparison of the position of the lowest measured penetration resistance to the observed failure depth (accuracy: 11%). The solid line in each graph shows the "one-to-one" relationship.

the POD was larger for Ψ than for S.

As described in the method section a reliable detection of *poor* stability is preferred. The best performance was for the weak layer Ψ with a POD of 88% and a threshold value of 15 kPa. This value is three times larger than the value found by Bellaire et al. (2009). Bellaire et al. (2009) used a different dataset (not cross-validated) which could explain this difference. More data are required for a robust estimation of threshold values. The parameter Ψ for the slab layers showed a lower POD (57%), however the probability of detecting non-events (PON) was 87% with also a treshhold value of 15 kPa.

Using these threshold values to select the most critical weak layer (one out of four) instead of the above described procedure did not perform better, revealing the complexity of an automatic detection of weak layers. In addition, a multivariate classification, i.e. all parameter of weak and slab layers were used for the classification, results in a classification only based on the parameter Ψ.

Table 4.1: Threshold values, hit rate (HR), standard deviation of (HR), probability of non-detection (PON) as well as probability of detection (POD) for various weak and slab layer properties: Penetration force (F), the number of peaks (n_{peaks}), the element length (L), the rupture force (f_r), the micro-strength (S) and the parameter Ψ.

Weak layer								
Parameter	Unit	Threshold	HR %	STD %	PON %	STD %	POD %	STD %
F	N	< 0.115	50	0.04	48	0.06	54	0.09
n_{peaks}	-	< 10.5	67	0.02	62	0.04	75	0.03
L	mm	> 1.5	61	0.02	62	0.03	59	0.05
f_r	N	< 0.035	72	0.004	63	< 0.001	85	0.01
S	kPa	< 15	71	0.03	62	0.04	85	< 0.001
Ψ	kPa	< 15	66	0.03	50	0.02	88	0.07
Slab layers								
F	N	< 0.065	56	0.05	70	0.07	36	0.07
n_{peaks}	-	< 5.8	68	0.03	74	0.05	59	0.04
L	mm	> 1.9	67	0.03	74	0.05	57	0.04
f_r	N	< 0.025	71	0.02	79	0.03	58	0.02
S	kPa	< 15	75	0.03	74	0.02	77	0.07
Ψ	kPa	< 15	75	0.01	87	0.01	57	0.03
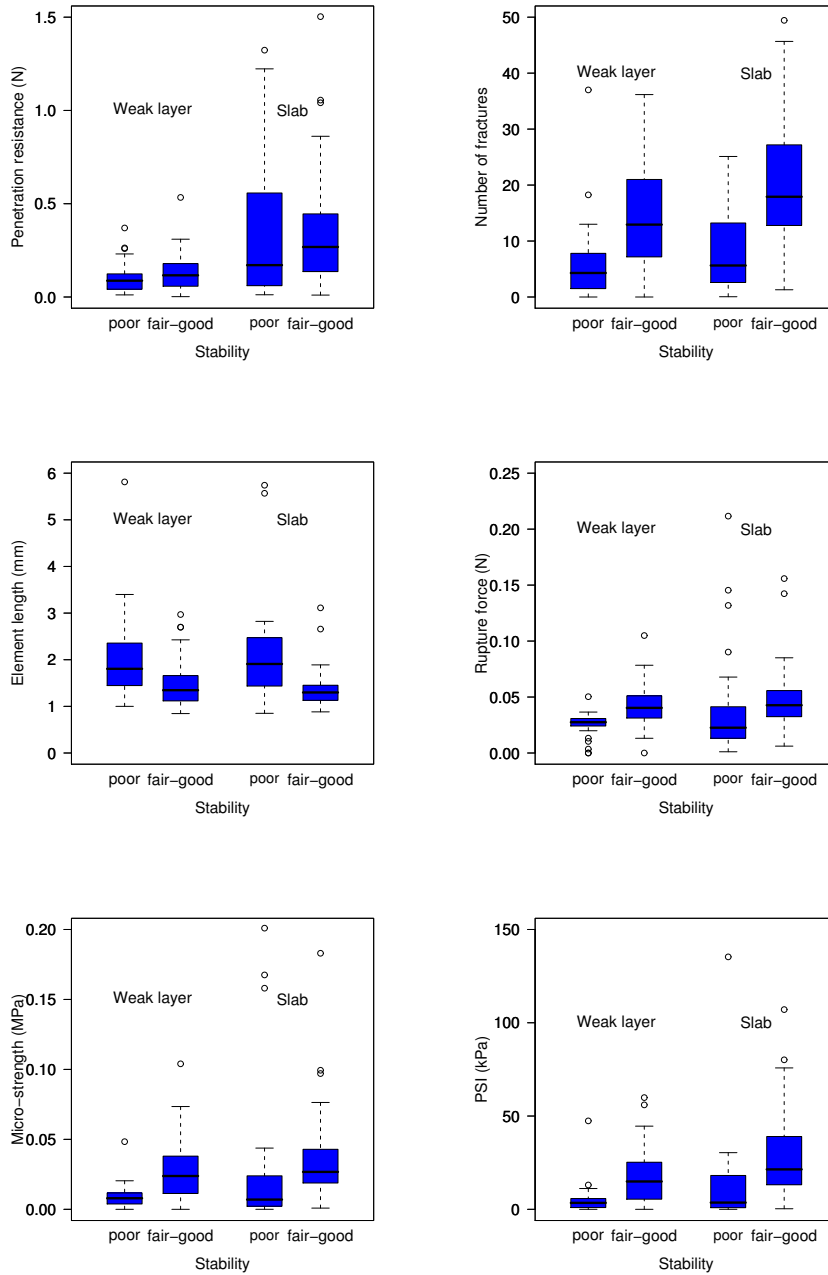
Figure 4.5: Comparison of various properties for weak layer and slab layers. Shown are the the penetration force (F), the number of peaks (n_{peaks}), the element length (L), the rupture force (f_r), the micro-strength (S) and the parameter Ψ.

4.2 Non-spatial analysis of grid data

4.2.1 Introduction

The following section presents a non-spatial analysis of four layer properties. These four parameters are, the mean penetration resistance F, the maximum penetration resistance F_{max}, the parameter Ψ as introduced in section 4.1 and finally the layer thickness D. Each parameter was calculated for the weak layer as well as for the slab layers.

These four layer properties were chosen because:

1. Penetration resistance F: Small penetration resistance indicates low strength. Weak layers are typically layers of low strength. A slab consisting of new snow, has a small penetration resistance and failure initiation is likely, but fracture propagation is unlikely. On the other hand, slab layers of well consolidated snow (e.g. small rounded grains) show typically high penetration resistance which favors fracture propagation (van Herwijnen and Jamieson, 2005).

2. Maximum penetration resistance F_{max}: Crusts have a much higher penetration resistance and might hinder fracture initiation if they are part of the slab layers (van Herwijnen and Jamieson, 2005; Habermann et al., 2008).

3. The parameter Ψ: The parameter Ψ relates to the structure of layers. Ψ is smaller for poorly bonded snow (fracture propagation is likely) and larger for well bonded snow (fracture propagation is unlikely)(Bellaire et al., 2009).

4. Depth D: Weak layers located near the surface ($<$ 15 cm) and deeper than 1 m are rarely ski triggered (Föhn, 1987; Schweizer and Jamieson, 2003).

The degree of variation of these parameters and of point stability were determined as well as possible slope scale trends. The aim of this analysis was to relate the variation and absolute values to slope stability.

Various degrees of variation were observed for the snow cover properties and point stability. However, the interpretation of these results especially with regard to avalanche formation remains challenging. In the following a possible interpretation of point stability (compression test) patterns with regard to failure initiation and fracture propagation is introduced.

4.2.2 Layer properties

Variation of layer properties

Statistics for all parameters and each grid are shown in Tables A.1 - A.4 (Appendix A). The median values of the penetration resistance and the parameter Ψ were typically higher for the slab layers than for the weak layer (14 out of 17). Obviously, the median thickness D and the maximum penetration resistance F_{max} were always larger for the slab than for the weak layer (17 out of 17). The semi-interquartile range (SIQR) of the penetration resistance was smaller for the weak layer in 12 out of 17 cases. For the parameter Ψ the SIQR was smaller for the weak layer in 13 out of 17 cases. Similar to the median values, the SIQR of the layer thickness D and maximum penetration resistance F_{max} was always smaller for the weak layer than for the slab layers.

Table 4.2 summarizes values of the median as well as of the the semi-interquartile range (SIQR) for the 17 grids. In addition, the minimum and maximum values of the quartile coefficient of variation (QCV) is shown. The semi-interquartile range (SIQR) can be interpreted as a measure of variation since it is a measure of the absolute spread of the data. The quartile coefficient of variation (QCV) describes the relative variation.

The median values of all parameters were higher for the slab layers than for the weak layer. The semi-interquartile range (SIQR) was smaller for the weak layer than for the slab. That means, the observed weak layer properties showed smaller absolute variations than the same properties within the slab. The quartile coefficient of variation (QCV) showed a large range for all parameters. The coefficient was typically smaller for the slab layers than for the weak layers. The largest range was observed for the weak layer Ψ and the smallest for the weak layer maximum penetration resistance F_{max}.

Table 4.2: Summary statistics of the four parameters, Ψ, F_{max}, F, and D. Given are median values for the weak layer and the slab layer properties of all 17 grids. Shown are the median, the semi-interquartile range (SIQR) and the minimum and maximum of the quartile coefficient of variation (QCV).

		Weak layer			Slab layer		
		Median	SIQR	QCV Min - Max	Median	SIQR	QCV Min - Max
Ψ	kPa	8.86	3.52	0.08 - 0.81	30.29	6.29	0.04 - 0.48
F_{max}	N	0.22	0.05	0.12 - 0.31	2.75	0.38	0.11 - 0.38
F	N	0.10	0.02	0.14 - 0.62	0.20	0.05	0.10 - 0.46
D	cm	1.79	0.34	0.07 - 0.61	30.23	2.48	0.04 - 0.38

Relation between properties

To estimate the relation between weak and slab layer properties in the seventeen grids Pearson correlation coefficients were calculated. All parameter passed the Kolomogorov-Smirnov test (p < 0.05) to ensure normality. Calculation was done for the median and the semi-interquartile range of all four parameters, Ψ, F_{max}, F and D. The median was taken instead of the mean because the data were slightly skewed.

No correlation was observed between the weak and slab layer thickness. The correlation coefficients are displayed in Table 4.3. Strong positive correlation was observed for the three other parameters. The parameter Ψ showed the strongest correlation between weak layer and slab layers for the semi-interquartile range (SIQR) and the median, 0.9 and 0.7, respectively. That means, large variations or median values of the slab layers were related to large variations or median values of the weak layer and vice versa.

Table 4.3: Pearson correlation coefficients between weak and slab layer properties calculated for the parameter Ψ, the penetration resistance F, the maximum penetration resistance F_{max} and the thickness D. Correlation coefficients are given for the median and the semi-interquartile range.

	Median	SIQR
Ψ	0.7	0.9
F	0.6	0.6
F_{max}	0.4	0.5
D	< 0.1	< 0.1

Point stability variation

Summary statistics for the compression test scores and fracture character of the each weak layer are given in Table 4.4. The weak layer was identified by the rutschblock test and assigned to the compression tests.

For eight grids the median compression test score was ≤ 13, two grids showed median scores ≥ 20 and for the remaining seven grids the median compression test score was between 14 and 19. The semi-interquartile range (SIQR) for seven out of the eight grids with compression test score ≤ 13 was below 1. That means, the variation was less than 2 scores for 50% of the data. The SIQR of the grids with intermediate and high compression test scores was larger than 1. Except for grid 5 and 7 from winter 2007-2008, these grids show an SIQR below or equal to 1, respectively. However, the variation occure across classes of intermediate and high compression test scores.

Fracture characters were grouped into either sudden fractures (0) or non-sudden fractures

(1). Ten compression tests were chosen as described in section 2.5.1. The proportion (Ratio in Table 4.4) of sudden to non-sudden fractures was calculated. Seven grids showed sudden fractures over the entire grid (Ratio = 0/10). For two grids only one pair of compression tests showed a non-sudden fracture (Ratio = 1/10). The weak layer of grid 2-0809 was associated with non-sudden fractures (Ratio = 10/10). The compression test fracture character of the remaining seven grids showed non-sudden fractures as well as sudden fractures. Ratios varied from 3/10 to 7/10.

To obtain a relation between point stability variation and snow cover properties the median and semi-interquartile range of the four parameter (F, F_{max}, Ψ, D) were correlated with the point stability variation (SIQR) as shown in Table 4.4. Table 4.5 shows the correlation coefficients for the weak layer and slab layers. The strongest correlation was observed for the parameter Ψ. The semi-interquartile range as well as the median of the parameter Ψ were positively correlated with point stability variation. That means, the point stability variations were related to variation of the structural parameter Ψ. The other parameters showed no or weak correlation with point stability and its variation.

4.3 Spatial analysis of grid data

4.3.1 Introduction

It is assumed that the spatial structure of snow cover properties affects snow slope stability. To determine the correlation length in the measurements a geostatistical analysis was performed. In addition, the Moran's I coefficient, a measure of spatial autocorrelation was calculated. These two statistical methods were applied to the four weak and slab layer properties assumed to be relevant for the avalanche formation process. Prior to the geostatistical analysis the data need to be de-trended to ensure stationarity. The trend analysis is also shown in this section.

4.3.2 Slope scale trends

Slope scale trends were described by fitting a linear model (Eq. 2.5) to the data. All regression coefficients are displayed in Tables A.5 to A.8 in Appendix A for the four parameters under study.

Table 4.6 summarizes the number of observed trends in either X, Y or both directions of the four parameters for the 17 grids. Depending on the parameter, trends were present in up to 12 grids out of 17 for the weak layer (Ψ). The correlation coefficient R^2 varied between < 0.01, i.e less than 1% of the variation can be explained by slope scale trends, and 0.44 depending on the parameter.

Table 4.4: Basic statistics of the compression test scores and type (N = 10) for all seventeen grids. Shown are the minimum and maximum compression test score as well as the median, mean, 1st (Q1) and 3rd (Q3) quartile and the resulting semi-interquartile range and quartile coefficient of variation. Ratio gives the number of non-sudden fractures out of 10 compression tests.

				Compression Test					
			Score						Fracture type
Grid ID	Min	Max	Median	Mean	Q1	Q3	SIQR	QCV	Ratio
1-0607	11	35	27.5	26.6	20	35	7.5	0.27	7/10
2-0607	13	21	17.5	17.3	16	19	1.5	0.09	0/10
3-0607	11	35	13.5	19.8	13	30.5	8.75	0.40	4/10
5-0607	11	35	12	14.2	11.25	12	0.375	0.03	3/10
6-0607	5	13	12	11.5	11.25	13	0.875	0.07	0/10
1-0708	3	11	10.5	9.1	7.75	11	1.625	0.17	0/10
2-0708	11	12	11.5	11.5	11	12	0.5	0.04	4/10
3-0708	3	14	11	10.6	11	11.75	0.375	0.03	0/10
4-0708	11	22	14.5	15.9	13	19.5	3.25	0.20	3/10
5-0708	10	14	12.5	12.3	12	13	0.5	0.04	0/10
6-0708	18	35	24	27.3	22.25	35	6.375	0.22	4/10
7-0708	9	16	14	13.8	13	15	1	0.07	0/10
9-0708	18	35	19.5	21.3	19	21.5	1.25	0.06	4/10
2-0809	12	35	14	18.2	13	17.5	2.25	0.15	10/10
4-0809	11	15	11	12	11	12.75	0.875	0.07	1/10
6-0809	11	15	13	13.2	13	14	0.5	0.04	1/10
7-0809	15	21	18	18	16.25	19.75	1.75	0.10	0/10

Table 4.5: Results of the correlation between the variation of point stability (SIQR Table 4.4) with the semi-interquartile range and the median of the four parameters under study. Given are the correlation coefficients for the weak layer and the slab layers.

	Weak layer		Slab layers	
	Median	SIQR	Median	SIQR
Ψ	0.44	0.56	0.46	0.44
F_{max}	0.25	0.02	-0.03	0.15
F	0.07	< 0.01	0.23	0.13
D	-0.01	0.12	0.07	-0.11

In contrast, the trends observed for the slab layers (up to 10 grids out of 17) explain up to 95% of the slope scale variation (Table 4.7). These 95% were observed for the slab layer thickness of grid 6 of winter 2006 - 2007. That means, only 5% of the variation was related to variation of the residuals. In fact, this grid was observed at a wind affected slope where slab thickness decreased from the lower right to the upper left corner (looking uphill).

The weak layer thickness is the only parameter which showed only uni-directional trends, i.e. significant coefficients in only one direction. The layer thickness increased either in up-slope or in orographic left direction. The weak layer maximum penetration resistance as well as the parameter Ψ tended to decrease in up-slope direction as well as in orographic left direction. The penetration resistance of the weak layer decreased in up-slope direction.

Slab layer thickness decreased in up-slope direction as well as the maximum penetration resistance and the parameter Ψ. The mean penetration resistance of the slab layers increased in up-slope direction.

Contour plots of grid properties

For visualization contour plots, i.e a linear interpolation between measurements point (not de-trended), of the parameter Ψ, thickness D, maximum penetration resistance F_{max} and penetration resistance F for weak layer and slab layer of all seventeen grids are shown in Appendix B - E.

The contour plots of the measured weak layer and slab layer properties under study suggest that in most of the cases no clear spatial pattern exists. However, the slab layers properties showed more often spatial patterns than the weak layers, suggesting that weak layers are more uniform.

Table 4.6: Slope scale trends observed for the four parameters, F, Ψ, F_{max} and D for the weak layer. See Tables A.5 to A.8 in Appendix A for details. Given are the number of grids (out of 17) having significant trends in either X or Y direction and the number of grids showing a trend in both directions. Total indicates the total number of grids with trends. Also given is the median and the minimum and maximum of the correlation coefficient R^2.

	Spatial trends				Variation explained	
	X	Y	Both	Total	Median R^2	Min - Max R^2
F	4	2	3	9	0.12	< 0.01 - 0.41
Ψ	6	4	2	12	0.18	0.02 - 0.35
F_{max}	5	3	2	10	0.12	0.01 - 0.44
D	3	5	0	8	0.11	0.01 - 0.42

Table 4.7: Slope scale trends observed for the four parameters, F, Ψ, F_{max} and D for the slab layer. See Tables A.5 to A.8 in Appendix A for details. Given are the number of grids (out of 17) having significant trends in either X or Y direction and the number of grids showing a trend in both directions. Total indicates the total number of grids with trends. Also given is the median and the minimum and maximum of the correlation coefficient R^2.

	Spatial trends				Variation explained	
	X	Y	Both	Total	Median R^2	Min - Max R^2
F	2	3	5	10	0.16	< 0.01 - 0.75
Ψ	2	4	4	10	0.20	0.01 - 0.67
F_{max}	1	5	2	8	0.10	0.01 - 0.57
D	2	2	5	9	0.21	< 0.01 - 0.95

The slab layer thickness D (Appendix E) showed patterns for almost all grids. This can partly be explained by slope scale trends, since the slab layers are affected by wind, e.g. snow drift. In fact, the modeled trends showed the largest correlation coefficients (R^2, Table 4.7). In contrast, the weak layer thickness seems to be more uniform with small variations.

4.3.3 Geostatistical analysis

Variogram analysis

The modeled correlation length, i.e. the range, of each grid for the weak layer and slab layers of the four parameters (Ψ, F_{max}, Ψ, D) are compiled in Table 4.8. The variogram plots are shown in Appendices B to E.

A summary of Table 4.8 is displayed in Table 4.9. Correlation length can only be reliably be determined up to about half of the extent (Journel and Huijbregts, 1978). Therefore, variograms with correlation length ≥ 8 m were classified as unbounded. These variograms reach their sill, i.e. a plateau, close to half the extent and were therefore questionable.

More unbounded and pure-nugget variograms (see Figure 2.3) were modeled for the weak layer than for the slab layers (Table 4.9). This means that a correlation length smaller than half the extent was more often observed for the slab layers than for the weak layers, indicating that slab properties were more often spatially correlated than weak layer properties.

The median correlation length R was larger for the slab layer properties than for the weak layer properties (Table 4.9). However, the minimum and maximum correlation spanned almost all possible correlation length for all observed properties. The fact, that a correlation length was observed more often for the slab layer properties than for the weak layer properties suggest that different processes affect weak and slab layers. This is also supported by the fact that the median correlation length was larger for the slab than for the weak layer properties.

4.3.4 Moran's I

The Moran's I coefficient is an index of spatial autocorrelation and was calculated for the four parameters ,Ψ, F, F_{max} and D, within each grid. Median values for the weak layer and the slab layers are displayed in Table 4.10 (coefficients for each grid and parameter, see Appendix A ,Tables A.9-12).

Comparing the median Moran's I coefficients of the four parameters for the weak layer and slab layers showed that the medians were larger for the slab layers except for the maximum penetration resistance. For the parameter Ψ the Moran's I was larger for the

Table 4.8: Correlation length R for the parameter Ψ, the penetration resistance F, the maximum penetration resistance F_{max} and the weak and slab layer thickness (D) given for each grid. "-" indicates a pure nugget variogram (no range), "≥ 8" indicates an unbounded variogram.

	Weak layer				Slab layers			
ID	Ψ	F	F_{max}	D	Ψ	F	F_{max}	D
	m	m	m	m	m	m	m	m
1-0607	2	2	3	≥ 8	4	6	4	3
2-0607	≥ 8	≥ 8	≥ 8	7	≥ 8	7	4	4
3-0607	≥ 8	≥ 8	≥ 8	3	4	6	3	≥ 8
5-0607	≥ 8	3	3	-	6	4	6	3
6-0607	-	-	-	-	≥ 8	6	-	7
1-0708	≥ 8	6	3	2	2	3	6	4
2-0708	≥ 8	≥ 8	-	3	≥ 8	≥ 8	5	4
3-0708	-	4	-	≥ 8	3	3	≥ 8	5
4-0708	≥ 8	≥ 8	≥ 8	5	7	6	4	≥ 8
5-0708	≥ 8	≥ 8	-	4	2	≥ 8	≥ 8	5
6-0708	6	3	3	5	7	7	3	6
7-0708	7	3	5	-	≥ 8	6	-	≥ 8
9-0708	3	3	3	≥ 8	≥ 8	≥ 8	≥ 8	3
2-0809	≥ 8	≥ 8	≥ 8	≥ 8	≥ 8	≥ 8	3	≥ 8
4-0809	3	3	3	-	4	3	3	3
6-0809	3	3	3	2	5	6	3	6
7-0809	≥ 8	≥ 8	-	1	≥ 8	3	≥ 8	≥ 8

Table 4.9: Summary of Table 4.8. Given are the number of unbounded variograms, pure-nugget variograms and variograms with a sill for the weak layer and slab layers parameters (Ψ, F, F_{max}, D). In addition, the median correlation length and the range of correlation length is given.

	Weak layer				Slab layers			
	Ψ	F	F_{max}	D	Ψ	F	F_{max}	D
Unbounded	9	7	3	4	7	4	4	5
Pure nugget	2	1	5	4	0	0	2	0
Sill (Range)	6	9	9	9	10	13	11	12
Median (m)	3	3	3	3	5	6	4	5
Min - Max (m)	2-7	2-6	3-5	1-7	2-7	3-7	3-6	3-7

Table 4.10: Median values of the Moran's's I coefficients of weak layer and slab layer properties Ψ, F, F_{max} and D for all 17 grids. In addition, the number of grids out of 17 for which the weak layer Moran's I was smaller than the slab layer Moran's I (Ratio) are given.

	Weak layer	Slab	Ratio
Ψ	0.14	0.26	11/17
F	0.12	0.26	14/17
F_{max}	0.10	0.10	7/17
D	0.08	0.26	14/17

slab layers in about 65%, for F and D in about 82% and for F_{max} in about 41% of the 17 cases.

The Moran's I statistics suggests that the parameters of the slab layers were more clustered than those of the weak layer. This observation is consistent with the results of the geostatistical analysis where larger correlation length were observed for the slab layer properties, except for the parameter F_{max} which showed similar correlation length for the slab and weak layers.

Point stability patterns

The point stability, derived from compression tests, was classified into stability classes of $poor$, $fair$ and $good$ as described in the Methods section (Table 2.4). Figures 4.6 to 4.8 show point stability for each grid grouped by the winter when the grid was performed.

Three different regimes were observed. First, uniform conditions within one stability class over the entire grid, e.g. grid 5 of winter 2006-2007 or grid 4 of winter 2008-2009. Second, variations across two stability classes, e.g. grid 2 of winter 2007-2008 and third all classes were present over the entire grid (e.g. grid 3, winter 2006-2007).

4.4 Relating observations to slope stability

4.4.1 Introduction

Slope stability was estimated using the point stability observations as outlined in section 2.2.3. In the following, correlation length R and Moran's I are compared to slope stability.

4.4.2 Classification

Compression test scores were classified into point stability classes of $poor$, $fair$ and $good$ (section 2.2.2). Based on point stability and the spatial distribution of point stability (Figure 4.6 - 4.8) slopes were classified into three stability classes $POOR$, $FAIR$ and $GOOD$ (section 2.5.2). In the following, this slope stability estimate will be referred to as "Slope Stability I". Using this classification, eight slopes were classified as $POOR$, five slopes as $FAIR$ and the remaining four slopes as $GOOD$.

Bellaire and Schweizer (2010) suggested a different slope stability classification, referred to as "Slope Stability II". It is based on the profile classification into five stability classes according to Schweizer and Wiesinger (2001) (section 2.2.1), the mean point stability of the grid (using the compression tests) and the presence or absence of signs of instability
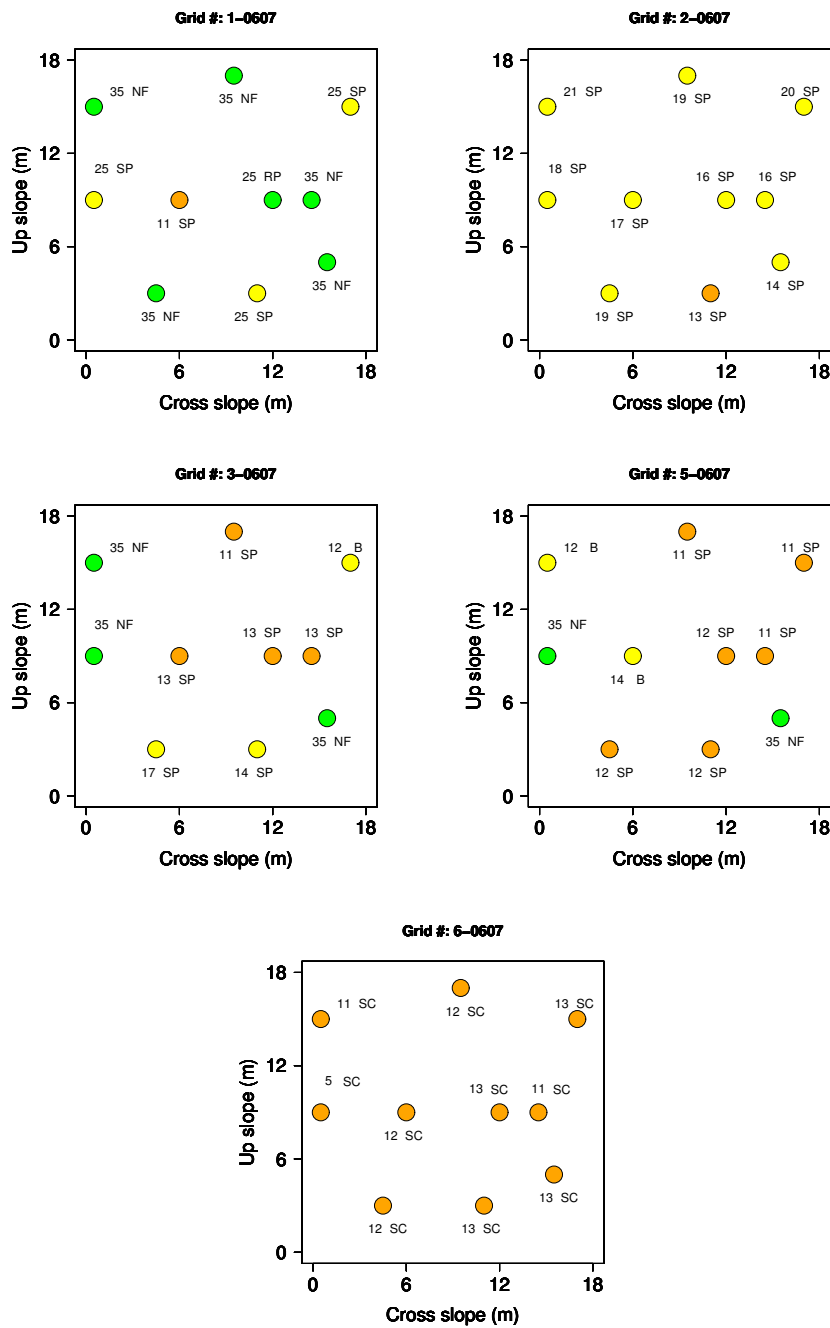
Figure 4.6: Point stability for the grids observed during the winter of 2006 - 2007. The color of the circles indicates either *poor* (orange), *fair* (yellow) or *good* (green) point stability.

Figure 4.7: Point stability for the grids observed during the winter of 2007 - 2008. The color of the circles indicates either *poor* (orange), *fair* (yellow) or *good* (green) point stability.
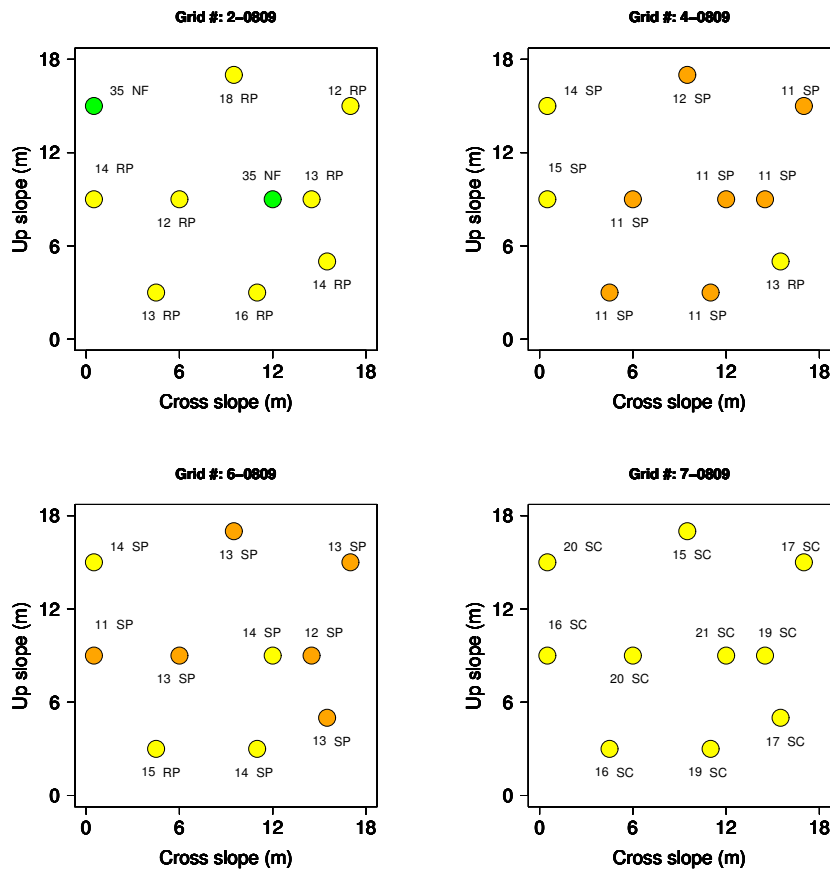
Figure 4.8: Point stability for the grids observed during the winter of 2008 - 2009. The color of the circles indicates either *poor* (orange), *fair* (yellow) or *good* (green) point stability.

(section 2.2.3). Using this classification, only three grids were classified as $POOR$, five as $FAIR$ and the remaining nine as $GOOD$.

A comparison of both slope stability classifications is given in Table 4.11. Comparing Slope Stability I and II shows that a) all slopes classified with Slope Stability II as $FAIR$ were shifted into the group of $POOR$ with Slope Stability I and b) five grids classified as $GOOD$ with II moved to the group of $FAIR$ with Stability I. This shift towards unstable conditions using Stability I can be explained by the high sensitivity of the compression test results, i.e. compression tests tend to underestimate stability. Hence, "Slope Stability I" is a more conservative estimate of slope stability than "Slope Stability II" which takes observed signs of instability into account.

The classification used by Bellaire and Schweizer (2010) seems to provide a more realistic view of slope stability in accordance to the observations of the field crews. However, the spatial distributed compressions tests, i.e. fracture character and score, allows one a

Table 4.11: Slope stability classification. Shown are the grid ID, the rutschblock score (RB) where a bold score indicates a whole block release, the profile classification (PC) into five stability classes (1: very poor, 2: poor, 3: fair, 4: good, 5: very good) according to Schweizer and Wiesinger (2001) as well as the median point stability, i.e. the median of all compression test scores. A "x" in the column "Signs" marks the grids where signs of instabilities were observed. Slope Stability I corresponds to the slope stability classification as introduced in section 2.5.4. Slope stability II corresponds to the stability classification used by Bellaire and Schweizer (2010).

ID	RB	PC	MPS	Signs	Slope Stability I	Slope Stability II
1-0607	**4**	3	RR		GOOD	GOOD
2-0607	7	5	17.5		FAIR	GOOD
3-0607	**5**	3	13		POOR	FAIR
5-0607	5	3	12		POOR	FAIR
6-0607	**3**	2	12	x	POOR	POOR
1-0708	**2**	2	10.5	x	POOR	POOR
2-0708	**5**	3	11.5		POOR	FAIR
3-0708	**2**	1	11	x	POOR	POOR
4-0708	**4**	3	14.5		GOOD	GOOD
5-0708	**4**	3	12.5	x	POOR	FAIR
6-0708	6	4	22.5		GOOD	GOOD
7-0708	3	3	14		FAIR	GOOD
9-0708	4	4	19	x	FAIR	GOOD
2-0809	5	4	13.5		GOOD	GOOD
4-0809	4	3	11		POOR	FAIR
6-0809	5	4	13	x	FAIR	GOOD
7-0809	**6**	4	18		FAIR	GOOD

more detailed insight into the spatial distribution of compression test results and how it affects slope stability. For this reason the following analysis is based only on the slope classification I.

Layer properties

Descriptive statistics of the parameter Ψ, the maximum penetration resistance F_{max}, the mean penetration resistance F and the thickness D for the weak layer and slab layers for all seventeen grids are compiled in Table A.1 - A.4 in Appendix A. The seventeen grids are grouped into either $POOR$, $FAIR$ or $GOOD$ slope stability (I) as described above. Median values of the semi-interquartile range (SIQR), the quartile coefficient of

variation (QCV) and the median were calculated and are shown in Table 4.12.

The median as well as the SIQR of the parameter Ψ for the weak layer increased with increasing stability. The quartile coefficient of variation, on the other hand, decreased with increasing stability from 43% to 28%. The semi-interquartile range was about four times larger for the slopes classified as $GOOD$ than for the slopes classified as $POOR$. Ψ was larger for the slab than for the weak layer. Furthermore, lower values of the QCV were observed for the slab than for the weak layer. This shows that the relative variations in Ψ were smaller for the slab than for the weak layer.

For the maximum penetration resistance F_{max} of the weak layer the median slightly increased with increasing stability. No trend was observed for the semi-interquartile range while the coefficient of variation decreased with increasing stability. The median QCV ranged from 15% to 23%. The maximum penetration resistance was larger for the slab layers than it was for the weak layer. Similar to the weak layer the maximum penetration resistance increased with increasing slope stability. For the slab, the semi-interquartile range and the QCV increased with increasing stability.

The median penetration resistance F of the weak layer showed no clear trend for the median and the semi-interquartile range or the QCV with increasing stability. For the slab layers only the median penetration resistance slightly increased with increasing stability.

The median thickness D of the weak layer decreased with increasing stability, as did the semi-interquartile range and the quartile coefficient of variation. The slab thickness increased with increasing stability. However, no trend was observed for the semi-interquartile range, and the quartile coefficient of variation decreased. In addition the smallest relative variations were observed for the slab layer thickness (10% to 8%).

Point stability

The results of the compression test scores for each grid (Table 4.4) were sorted by increasing slope stability and are compiled in Table 4.13. The mean and median compression test scores increased with increasing stability. The median semi-interquartile range (SIQR) of the compression test scores per slope stability class increased with increasing stability ($POOR = 0.7$, $FAIR = 1.3$, $GOOD = 4.8$). Slopes classified as $POOR$ or $FAIR$ showed more often sudden fractures of the weak layer compared to slopes classified as $GOOD$.

Geostatistics

The median correlation length for each stability class of the four parameters are given in Table 4.14. No significant relation between the estimated correlation length and slope stability was observed. The used sampling design allows one to detect correlation length

Table 4.12: Descriptive statistics for all four parameters grouped according to slope stability class. For each stability class the median, the semi-interquartile range (SIQR) and of the quartile coefficient of variation (QCV) are given for weak layer and slab layers separately.

	Weak layer			Slab layer		
	Median kPa	SIQR kPa	QCV	Median kPa	SIQR kPa	QCV
			Ψ			
	Median kPa	SIQR kPa	QCV	Median kPa	SIQR kPa	QCV
POOR	4.1	2.3	0.4	26.0	5.9	0.30
FAIR	8.9	4.5	0.3	38.3	1.6	0.15
GOOD	30.5	8.1	0.3	61.3	13.5	0.22
			F_{max}			
	Median N	SIQR N	QCV	Median N	SIQR N	QCV
POOR	0.2	0.04	0.23	1.9	0.3	0.22
FAIR	0.2	0.06	0.20	2.8	0.3	0.14
GOOD	0.3	0.05	0.15	3.4	1.1	0.37
			F			
	Median N	SIQR N	QCV	Median N	SIQR N	QCV
POOR	0.08	0.02	0.29	0.19	0.04	0.22
FAIR	0.12	0.02	0.16	0.20	0.02	0.16
GOOD	0.09	0.02	0.27	0.29	0.08	0.26
			D			
	Median cm	SIQR cm	QCV	Median cm	SIQR cm	QCV
POOR	2.7	0.7	0.33	25.4	2.3	0.10
FAIR	1.8	0.3	0.16	31.2	3.6	0.05
GOOD	1.1	0.4	0.20	36.6	2.6	0.08

Table 4.13: Compression test results (compare Table 4.4) of the seventeen grids sorted by increasing slope stability. Shown are the minimum and maximum compression test score as well as the median, mean, 1st (Q1) and 3rd (Q3) quartile and the resulting semi-interquartile range and quartile coefficient of variation. Ratio gives the number of non-sudden fractures out of 10 compression tests. In addition, all median are shown (bold) below each stability class.

		Compression test								
		Score								Fracture type
Grid ID	Slope stability	Min	Max	Median	Mean	Q1	Q3	SIQR	QCV	Ratio
3-0607	$POOR$	11	35	13.5	19.8	13	30.5	8.75	0.40	4/10
5-0607	$POOR$	11	35	12	14.2	11.25	12	0.375	0.03	3/10
6-0607	$POOR$	5	13	12	11.5	11.25	13	0.875	0.07	0/10
1-0708	$POOR$	3	11	10.5	9.1	7.75	11	1.625	0.17	0/10
2-0708	$POOR$	11	12	11.5	11.5	11	12	0.5	0.04	4/10
3-0708	$POOR$	3	14	11	10.6	11	11.75	0.375	0.03	0/10
5-0708	$POOR$	10	14	12.5	12.3	12	13	0.5	0.04	0/10
4-0809	$POOR$	11	15	11	12	11	12.75	0.875	0.07	1/10
Median		**11**	**14**	**12**	**12**	**11**	**12**	**0.7**	**0**	**1/10**
2-0607	$FAIR$	13	21	17.5	17.3	16	19	1.5	0.09	0/10
7-0708	$FAIR$	9	16	14	13.8	13	15	1	0.07	0/10
9-0708	$FAIR$	18	35	19.5	21.3	19	21.5	1.25	0.06	4/10
6-0809	$FAIR$	11	15	13	13.2	13	14	0.5	0.04	1/10
7-0809	$FAIR$	15	21	18	18	16.25	19.75	1.75	0.10	0/10
Median		**13**	**21**	**18**	**17**	**16**	**19**	**1.3**	**0**	**0/10**
1-0607	$GOOD$	11	35	27.5	26.6	20	35	7.5	0.27	7/10
4-0708	$GOOD$	11	22	14.5	15.9	13	19.5	3.25	0.20	3/10
6-0708	$GOOD$	18	35	24	27.3	22.25	35	6.375	0.22	4/10
2-0809	$GOOD$	12	35	14	18.2	13	17.5	2.25	0.15	1/10
Median		**12**	**35**	**19**	**22**	**17**	**27**	**4.8**	**0**	**6/10**

with an accuracy of about 2 m. Observed trends (Table 4.14) fall within the range of this accuracy.

Most of the modeled pure-nugget and unbounded variograms fall into the class of $POOR$ slope stability. This may be interpreted as rather uniform layer conditions since lower variations of layer properties were also assigned to the slope stability class of $POOR$.

Table 4.14: Median correlation length of the parameter Ψ, the penetration resistance F, the maximum penetration resistance F_{max} and the thickness D of weak layer and slab layers per slope stability class.

	Correlation length					
	Weak layer			Slab layers		
	$POOR$	$FAIR$	$GOOD$	$POOR$	$FAIR$	$GOOD$
	m	m	m	m	m	m
Ψ	3	3	4	3	5	7
F	4	3	2	3	6	6
F_{max}	3	3	3	5	3	4
D	3	2	5	4	4	5

Moran's I

Clear trends of the Moran's I coefficient were observed for only the mean penetration resistance F of the slab and for the weak layer thickness D (Table 4.15). However, all parameters showed a positive Moran's I index, i.e the properties showed clustered patterns. The clustering for the other parameters of weak and slab layer tended to increase with increasing stability.

Table 4.15: Median Moran's I coefficient per slope stability class for the parameter Ψ, the penetration resistance F, the maximum penetration resistance F_{max} and the thickness D of weak layer and slab layers.

	Weak layer			Slab layers		
	POOR	FAIR	GOOD	POOR	FAIR	GOOD
Ψ	0.14	0.19	0.19	0.26	0.08	0.31
F	0.09	0.17	0.12	0.17	0.28	0.29
F_{max}	0.10	0.17	0.11	0.09	0.03	0.20
D	0.07	0.08	0.12	0.22	0.35	0.23

Discussion

5.1 Introduction

How does spatial variability of snow cover properties affect snow slope stability? To answer this question typical avalanche slopes were investigated. These investigations were performed utilizing the SnowMicroPen and manual snow cover observations. The first section (5.2) of this chapter contains some general comments on the dataset. The SnowMicroPen signal was analyzed to derive snow cover stability estimates using an algorithm introduced by Bellaire et al. (2009). A re-analysis of this algorithm is discussed in section 5.3. Data collected on 17 slopes were analyzed using non-spatial as well as spatial statistical methods. These results are discussed in sections 5.4 and 5.5. Some possible error sources of the applied methods are discussed at the end of each section. Finally, a hypothetical concept on how spatial variability may influence snow slope stability is presented (section 5.6).

5.2 Data

During three winters between 2006 and 2009 twenty three grids were recorded. Six grids had to be discarded due to technical problems with the SMP. Field observations are always challenging especially those performed during winter time. Equipment as well as people are exposed to extreme conditions. Often no observations could be performed at all due to severe weather conditions and for safety reasons. Research tools like the SMP were developed to stand these extreme conditions, but are still prone to errors. Currently, no other method exists which quantifies the stratigraphy of mountain snow covers with high resolution within a reasonable time and is directly related to the mechanical properties. However, the time needed to investigate a slope such as done in this study was

between three and four hours with three experienced persons, i.e only one grid could be performed per day. These problems and the occasional lack of suitable weak layers reduced the number of grids available for analysis. Despite the limited data set some trends seem to emerge.

5.3 Stability algorithm

The developed algorithm (section 4.1) was used to detect structural weaknesses in SMP signals. The re-analysis with a slightly larger dataset showed no major differences compared to the findings presented by Bellaire et al. (2009). In the majority of the cases (90%) one of the four potential weaknesses derived from the SMP signal coincided with the observed weak layer (Figure 4.4). A different procedure than suggested by Bellaire et al. (2009) was used to automatically detect weak layers. This new procedure takes the slab layer properties above each weak layer into account. The accuracy of both procedures (60% and 58%) are similar to the performance of stability field tests such as the compression test or extended column test (Winkler and Schweizer, 2009). These stability tests performed adjacent to each other identified the same weak layer only in about 60% of the cases.

Weak layer as well as slab properties were considered to classify measured SMP profiles into stability classes of $poor$ and $fair - to - good$ (Table 4.1). All variables provided plausible results. $Poor$ stability is expected with a low number of ruptures, low rupture force and a low value of Ψ in the weak layer, and with rather soft slab layers. The latter finding agrees with results of van Herwijnen and Jamieson (2007b) and Habermann et al. (2008) who found that hard layers within the slab impede failure initiation. A larger dataset would certainly improve the stability estimation and might also allow a multivariate approach. Furthermore, the low probability of detection (POD, Table 4.1) of the slab layer parameters is likely related to the fact that soft slab layers have a rather low Ψ, but avalanche release is rather unlikely (van Herwijnen and Jamieson, 2007a). A larger dataset would allow one to derive an upper and lower threshold for the slab layer Ψ where skier triggering or avalanche release is most probable.

Weak layer detection and stability estimation is based on a single SMP measurement which is compared to a manual profile and a stability test that cannot be done at the exact same location. Some spatial variations in layer properties between the location of the SMP measurement and the location of the rutschblock may occur. The uncertainty in the stability test result ($\pm$ 1 score) may further affect the results of the stability classification since only two stability classes were used. Pielmeier and Marshall (2009) showed that a set of SMP measurements, covering the area of the rutschblock, improved the accuracy of the stability estimate. The automatic weak layer detection could also be improved using a multiple signal approach. Multiple signals, measured for instance around the rutschblock like done by Pielmeier and Marshall (2009), could be combined

to identify the most critical weak layer. Furthermore, multiple measurements would allow one to determine spatially related layer properties that favor fracture propagation, and to take those into account for the automatic weak layer detection and stability estimation.

Some of the lack of accuracy might be due to technical problems of the SMP device - although the signal quality was checked. The sensitivity of the SMP sensor to temperature changes might have caused erroneous signals that affected the layer boundary definition. This signal drift, i.e. positive or negative offset, can often not be recognized by a visual inspection and might affect the derivation of the structural properties. The signals were analyzed by two experienced persons, however some uncertainty remains.

The dataset used for this analysis contained 71 SMP signals. Most of the weak layers consisted of persistent grain types such as faceted crystals or depth hoar. A larger dataset with various types of weak layers might improve the weak layer detection and stability estimation. More SMP signals would allow one to create test and training datasets, which would substantially improve the reliability and accuracy of the algorithm.

Still, the SMP, in combination with the algorithm and standard field observations (rutschblock test plus manual profile), can be used to quantify and analyze spatial variability patterns faster than with standard observation methods. However, more validation of the SMP signals is required before the SMP can become a valuable tool for avalanche warning services.

5.4 Non-spatial analysis

The non-spatial analysis suggests that the median values of the weak layer properties are lower and show less variation than the corresponding slab layer properties (Tables A.1-A.4, Appendix A). This supports the findings first made by Kronholm (2004) and summarized by Schweizer et al. (2008b).

Slope scale trends were observed for most of the weak and slab layer properties (Tables A.5-A.8, Appendix A). Trends were responsible for a large part of the variation of the slab layer properties (e.g. 95%, grid 6 winter 2006/2007). In contrast, slope scale trends within the weak layer explained less of the variation (Table 4.6). Therefore, it is likely that different processes affect slab and weak layer properties and cause spatial variability. Several metorological parameters are acting together to form a mountain snow cover above tree line. Slab layers are likely affected by wind and topography at the slope scale. Weak layers often form at the snow surface, e.g. surface hoar or surface faceting. The formation of a weak layer within the snow cover, i.e. not at the snow surface, is rare and the energy balance at the snow surface is similar at the slope scale causing few variations. However, the analysis of such a complex system requires the coupling of snow cover and topographical models with high-resolution meteorological models including small scale windfield modeling.

It remains unknown what processes caused spatial variations of the weak layer residuals. Trends might be explained by meteorological parameters such as wind if weak layers are formed at the snow surface. Complex metamorphic processes might contribute to the variation of the weak layer properties. However, these metamorphic processes are strongly influenced by the entire snow cover structure and the ground. The correlation between weak layer and slab layer variations showed that in case of a variable weak layer, the slab layers were often variable too (Table 4.3). This might be a hint that metamorphic processes, forced by different temperature gradients, are important for weak layer variation.

Grids with low median compression test scores showed less variation than grids with intermediate or high compression test scores (Table 4.4). The large number of grids with low median compression test scores can be explained by the large sensitivity of the compression test, typically resulting in an underestimation of point stability (Winkler and Schweizer, 2009). The fact that the variation of scores increased with increasing score suggests that the weak layer, on a slope with low median compression test score, was spatially continuous and rather uniform. The fracture type was often less variable than the compression test score as suggested by van Herwijnen et al. (2009). Some grids showed even no variation of fracture type. In case the fracture type was observed to be sudden, one can assume that fracture propagation is more likely (van Herwijnen and Jamieson, 2007a).

The finding that the variation of compression test scores increased with increasing stability supports the hypothetical concept that spatial variability is only important with intermediate scores. Simply stated, if a single stability test performed on a slope indicates the stability to be poor, stability can be assumed as poor everywhere or at least over areas large enough to favor self-propagating fractures. That means, frailure initiation as well as propagation are possible and an avalanche may release. On the other hand, if tests indicate good stability, larger variations at the slope scale can be expected suggesting that fracture initiation and fracture propagation are less likely. The distribution, i.e. the length scale, of poor stability test results on slopes with intermediate test results becomes crucial in regard to avalanche release.

The variation of spatially distributed compression test scores was related to the variation of the snow cover properties derived from the SMP measurements (Ψ, F, F_{max}, D). In particular, the variation of the parameter Ψ correlated ($R^2 \approx 0.5$) with the point stability variation, expressed as the semi-interquartile range of all compression tests (Table 4.5). The structural parameter Ψ introduced by Bellaire et al. (2009) and the micro-strength S are comparable. Both were related to point stability (Bellaire et al., 2009; Pielmeier and Marshall, 2009). This supports the choice of Ψ (or S) for signal analysis and slope stability estimation.

5.5 Spatial analysis

5.5.1 Geostatistics

The geostatistical analysis showed no significant trends, i.e. the estimated correlation length was not related to slope stability, and is in that respect inconclusive. This might be due to the fact that a) the sampling design was not adequate to measure the variability b) the slope stability classification was not adequate and slope stability cannot readily be measured c) the observations were not performed at the right place and time or d) there is no relation.

With the sampling design used in this study (section 2.2) ranges up to 10 m can be detected with an accuracy of about 2 m. Hence, the sampling design should be sufficiently reliable to capture spatial structures smaller than the maximum length scale ($\approx$ 10 m) assumed to be crucial for the avalanche formation process.

Each stability classification is subjective. Currently, no method exists which estimates stability without slope investigation. The SMP stability algorithm was a first attempt for an objective stability classification, but also requires slope access. Really unstable conditions can only be found when an avalanche is triggered on the study slope. Simply spoken, the stability of a slope which was not released during investigation has to considered as at least marginally stable. Or in other words, really poor slope stability can hardly be measured. This might partly explain why so far no spatial variability study exists which linked snow cover variability to slope stability. However, the presence of weak layers and signs of instability and the knowledge about the avalanche formation process allows one to classify slopes as rather poor. A slope can be estimated as of rather poor stability if either:

1. A weak layer is present over the entire slope and the slab layers are stiff enough to favor fracture propagation without hindering fracture initiation.

2. Spatially distributed point stability observations show consistent results related to instability, e.g. compression test score $\leq$ 13 and sudden fractures.

3. Signs of instability such as "whumpfs" or cracking are observed on the investigated slope or on slopes of similar aspects.

Clearly, rather poor slopes often fulfill all three requirements.

The often investigated south-west facing slope (Figure 3.1) often showed critical weak layers with low rutschblock scores (e.g. 1-0708, 2-0707; Table 3.1). This slope has a slope angle of about 20° and is therefore not steep enough for avalanche release, but one could imagine that the same conditions on a steeper slope would result in avalanche release. Only one slope (grid 6, winter 2006/2007) was whumpfed and cracks occurred during investigation, and can therefore be classified as unstable. However, it is questionable

if measurements performed on a slope that was whumpfed are still representative for unstable slopes. In that specific case the measurements can be assumed as representative since the weak layer was a thick layer of depth hoar. The differences in stability of the slopes not whumpfed might be too small for reliable discrimination. In other words, except for one slope (grid 6, winter 2006/2007) all other slopes were stable or at most marginally stable. This might explain the lack of patterns of spatial variations with regard to slope stability in the data analyzed.

A trend removal, also done in this study, is required before a geostatistical analysis is performed to distinguish between variations introduced by slope scale trends and variations caused by the residuals. The separation of the trend and the residuals allows one to relate variations at different scales. However, the trend removal might only be relevant for the weak layer properties since the trend explained a small part of the observed variations (Table 4.6). The slab layers often showed strong slope scale trends (Table 4.7). This variation might be at least as important for the avalanche formation process as the variation of the residuals. This result might also explain the inconclusive geostatistical analysis and questions the applicability of the geostatistical analysis.

5.5.2 Moran's I

The Moran's I coefficients were positive and larger for the slab layers than for the weak layer. This observation can partly be explained by the presence of slope scale trends, since these trends were not removed. Slope scale trends are often a result of wind effects, for example the slab layer penetration resistance is influenced by wind. Wind influence on the snow cover results in patterns which are clustered, as indicated by positive Moran's I coefficients. That means further, the slab layers showed more often spatial structure. This may be interpreted as contradicting the findings first made by Kronholm et al. (2004) and summarized by Schweizer et al. (2008b) who concluded that slabs may be more variable than weak layers.

However, the result that slab layers were more clustered than weak layers does not necessarily mean that they were spatially less variable. Slab layers tend to have a larger absolute spread than weak layers (Table 4.2). Furthermore, Kronholm et al. (2004) argued that slab layers showed more complex structures than the weak layer, without any further explanation. Their estimated correlation length for the slab layers varied from about 4 m to correlation length larger than half the extent which implies, at least for some slab layers, a spatial structure. Their investigated weak layers showed no correlation length and small variations indicating uniform conditions, i.e. they were still spatially variable but with small variations.

5.6 Hypothesis

Hypothesis: Variations and their length scales are only relevant when the variations are around the threshold between rather unstable and rather stable conditions.

The results presented showed that weak layers were less clustered than slab layers and show less variation, i.e. weak layers were more uniform than slab layers. This suggests in case a weak layer is present and shows weak structure, that the variability of the slab layers might control the avalanche formation process.

Numerical modeling of spatial variations, e.g. Fyffe and Zaiser (2004), Kronholm and Birkeland (2005) suggests that an increase in strength of weak layer, hinders fracture propagation. This means that avalanche release becomes less likely. Therefore, the correlation length of layer properties favoring fracture propagation, becomes particularly important.

Figure 5.1 shows a schematic of a hypothetical concept of how spatial stability variations might be considered for slope stability estimation. Variations and length scales are less relevant if they occur within the stable or unstable range (a and c). Spatial variability, especially the correlation length R, becomes crucial if variations occur across stability classes (b). The wave length of b) does not necessarily have to be greater than the wave length of a) or c) - at least not over the entire slope. However, unstable areas have to be large enough (critical length) to favor self-propagating fractures. Stability could be derived from any source, e.g. point stability observations like the compression or rutschblock test or from layer properties derived from the SMP. A suitable threshold needs to be defined to distinguish between the stable and the unstable range.

Grid 6-0607 was whumpfed during investigation in the upper left corner. This is certainly one of the most affect (obviously variable, by naked eye) in the area (compare Schweizer et al. (2008a)). Figure 5.2a shows the contour plots of the parameter Ψ for the weak layer and the slab layers. This slope was strongly wind affected from the right. The parameter Ψ shows a spatial pattern, i.e. a gradual decrease in Ψ from the lower right to the upper left, especially for the slab layers. The variation of the parameter Ψ for the weak and slab layer is shown in Figure 5.2b. All SMP measurements are shown starting with the one at the lower right corner and ending at the upper left corner in the grid. The measurement locations within the dashed vertical lines correspond to the area were the grid was whumpfed while approaching the slope. The solid line in Figure 5.2.b at 15 kPa corresponds to the threshold value estimated for the parameter Ψ (section 4.3). The variation of the parameter Ψ for the slab layers appeared above the threshold i.e. within the stable range. The weak layer on the other hand, showed variation around the threshold (across stability classes), and the unstable areas coincide with the areas where the slope was triggered.

Following the hypothetical concept introduced in Figure 5.1, showed that the variations
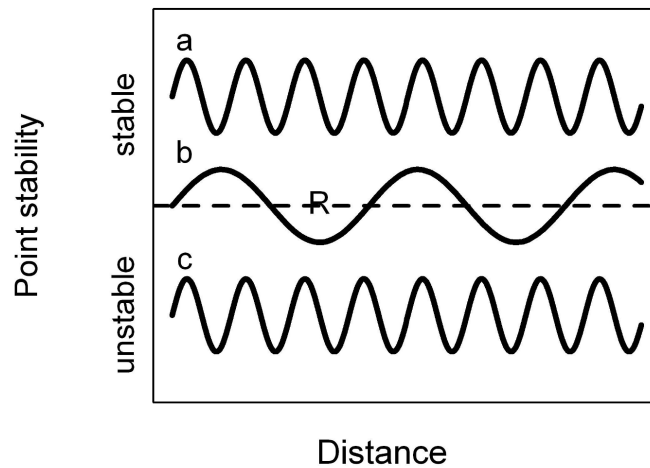
Figure 5.1: Relevance of stability variation for slope stability estimation. Dashed line indicates a stability threshold value. a) Stability variations within the stable range resulting in stable slope stability. b) variations across the stable and unstable range. The correlation length R controls the slope stability and c) variation within the unstable range result in unstable conditions.

of the parameter Ψ occurred above the threshold. However, the values within the area where the slope was triggered were lower than the values in the areas where the slope could not be triggered. Therefore, a new threshold value for the slab layer is suggested by grouping the values of the slab layer Ψ at these sampling locations and assigning them to the class of $POOR$ stability. The remaining points were assigned to the class of $GOOD$ stability.

These two classes were compared and a threshold value of 43 kPa was determined to distinguish between $POOR$ (smaller than threshold) and $GOOD$ (larger than threshold) slope stability. As described above soft slab layers (low Ψ values) hinder fracture initiation. Therefore, a threshold of 15 kPa seems to be a reasonable lower threshold for the slab layer, since the slab layers should not show smaller Ψ values than the weak layer. For the weak layer a threshold of < 15 kPa was chosen to distinguish between the two stability classes. These threshold values are indicated by solid horizontal lines (Figure 5.2b). Figure 5.2c shows a contour plot of stability estimates based on the above described thresholds, whereas the red areas indicate $POOR$ stability and the yellow areas $GOOD$ stability.

Figure 5.2c and especially Figure 5.2b support the concept described above that spatial variability is only relevant if variations occur between the stable and unstable range and

the correlation length of the unstable region is large enough to favor fracture propagation. Clearly, one observation is not sufficient for verification of this concept. More investigations on slopes with "unstable" areas are required. In addition, numerical simulations such as done by Kronholm and Birkeland (2005) (cellular automata) can be used to verify this concept.
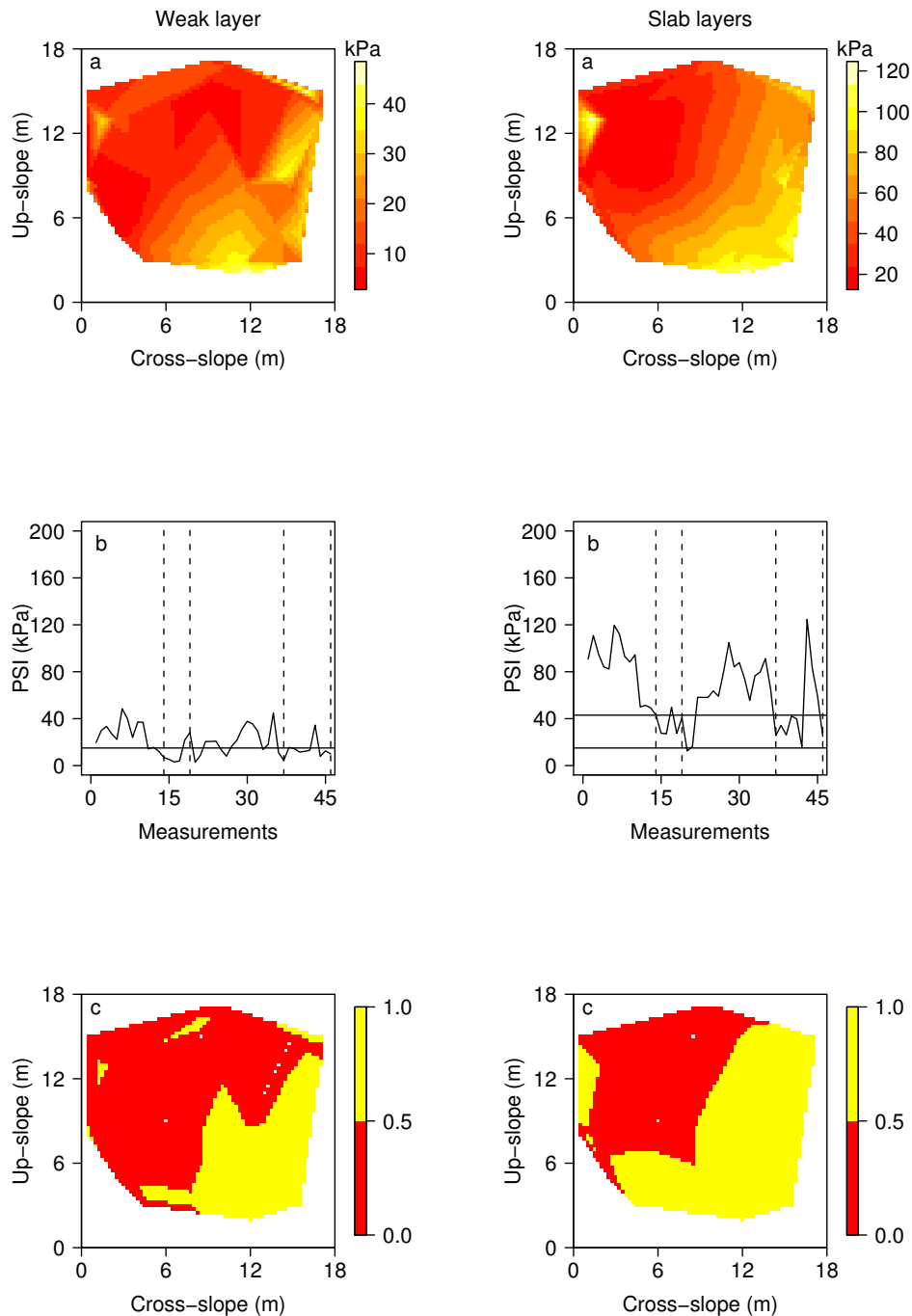
Figure 5.2: Summary plot of grid 6 winter 2006-2007 for the weak (left) and slab layers (right). a) Contour plots of the parameter Ψ. b) Variation of the parameter Ψ. The vertical dashed lines indicate the areas of the grid where the slope was triggered. Horizontal solid lines corresponds to the derived threshold values for the slab and weak layer. c) Contour plots of the suggested slope stability classification (red = poor; yellow = good) based on parameter Ψ (see text for explanation).

Chapter 6

Conclusions

Spatial variations of weak layer and slab layer properties at the slope scale were measured above timberline near Davos, Switzerland. Aim of these investigations was to identify snow cover parameter associated with snow cover instability and identify their spatial structure with the goal to relate this spatial structure to slope instability.

A novel partly randomized sampling design for efficient field observations, of snow cover properties and point stability, was developed and tested. The SnowMicroPen (SMP) was used to derive the snow cover properties. The sampling design consisted of 46 SMP measurement locations. The relative small number of sampling locations enables the field crew to sample slopes in a reasonable time. The sampling design further includes, a full snow profile and 20 compression tests. The sampling design was adapted for geostatistical analysis. The correlation length of investigated properties can be estimated with an accuracy of about $\pm$ 2 m. This is not sufficient if the exact estimate of the correlation length is required. However, determining whether a correlation length of a few meters is present or not is possible.

Twenty three slopes were sampled near Davos, Switzerland. The data from seventeen slopes were analyzed. The SMP is a valuable tool for snow cover investigations. However, SMP signals still need to be analyzed with care to ensure high data quality. For the present study about 25% of the data had to be discarded due to poor signal quality.

Unstable snow cover conditions were rare during the three winters between 2006 and 2009, making the interpretation of the data in terms of slope stability challenging. Furthermore, sampling during periods of high avalanche hazard is not possible due to safety concerns. In addition, the definition of slope stability in the course of field studies seems problematic. Nevertheless, some important conclusions can be made even from this limited dataset.

Earlier studies, e.g. Kronholm and Schweizer (2003) or Kronholm (2004), were unable to relate spatial SMP measurements to the manual stability observations partly due to (a)

the sampling design that did not allow a spatial analysis for the manual stability observations and (b) the lack of an SMP derived stability parameter. Therefore, an algorithm for the analysis of SMP profiles that detects a potential weakness and provides a stability estimate was developed and compared to 71 manually observed profiles (Appendix F). The stability algorithm identified weak layers with an accuracy of 90%. An automatic detection of the most critical weak layer was however not satisfactory. The accuracy of detecting the most critical weak layer was 58%, comparable to traditional methods of stability estimation. Various weak layer and slab layer properties were tested to classify SMP signals into stable or unstable. One of the best classifiers was the parameter Ψ which is a measure of the snow layer structure. The stability algorithm combines microstructural properties of snow with expert rules. Therefore, the algorithm in combination with the SMP shows promising potential for providing high resolution, objective stability estimates as input data for avalanche forecasting.

The non-spatial analysis showed that the investigated weak layers were spatially continuous, i.e. were identified in almost all SMP signals, and the properties showed less variations (absolute value) than the slab layer properties. The slab layers showed more variation than weak layers suggesting that the spatial variability of the slab layers may even be more relevant for avalanche formation than the weak layer variability.

Slope scale trends were calculated for the weak and slab layer properties. Most of the variation of the slab layers were explained by slope scale trends. This suggests the importance of meteorological conditions, during and after deposition, as driving agents for spatial variability of the slab layers at the slope scale. Varying weak layer properties were found to be positively correlated with varying slab layer properties suggesting that either the variation of slab layer properties influence the variation of weak layer properties, or that the same processes affected both weak and slab layer properties.

Grids with low median compression test scores showed less variation than grids with intermediate or high compression test scores. That means, stability increases with increasing variation. The fact that the variation of compression test scores increased with increasing score suggests that for low scores the spatially continuous weak layers were relatively uniform. This suggests that if compression tests (at least two about 10 m apart) are performed on an avalanche slope and both indicate consistent low results, spatial variability can be assumed to be small indicating rather unfavorable conditions. This finding suggests an efficient sampling strategy for avalanche forecasters for slope stability assessment. In addition, the fracture type showed less variation than the compression test score (Schweizer and Bellaire, 2010) suggesting again uniformity of weak layers.

The geostatistical analysis showed a variety of correlation lengths, but a certain correlation length could not be related to slope stability. Therefore, the effect of length scale on slope stability remains unknown. However, slab layers more often showed a correlation length than the corresponding weak layers. This was also supported by the Moran's I index, which was positive and larger, i.e. more clustered structure, than the weak layers

Moran's I. This was also consistent with the observation that trends account for more of the slab layer variation.

A hypothetical concept was proposed how spatial variability influences the avalanche formation process. This concept suggests that spatial variations are only relevant if they occur between stable and unstable conditions and the unstable areas are large enough to favor self-propagating fractures. Variations within stable or unstable conditions become irrelevant. This concept should be interpreted as preliminary since only one grid, but the only proven unstable one, supports the hypothesis. More data are required to validate this concept. However, slope instability cannot readily be measured and a verification might only be possible by modeling the effect of spatial variability on fracture initiation and propagation propensity.

This study provides new insight into the nature of spatial variations at the slope scale and points out the difficulties that need to be tackled in order to clarify the effect of spatial variations on avalanche release. In particular, the definition of slope stability in the course of field studies seems questionable. The effect of meteorological conditions on the snow cover, especially on weak layer and slab layer formation, remains unknown for the time being. The SMP, still supplemented with some manual observation shows promising potential for snow cover surveys not only at the slope scale.

Suggestions for further research

The sampling design is of particular importance for a reliable estimation of the correlation length. Different sampling designs were used during snow cover investigations through out the years. Still, sampling designs have to be adapted to the specific research questions. Therefore, more analysis of sampling designs is required to identify the optimal sampling design. It might even be possible that different sampling designs are required for snow cover investigations at different scales. This means, a snow survey at the slope scale might require a sampling design with a regular spacing, but for a survey at the basin or mountain range scale a L-shaped design such as used in this study might be more practical since less sampling locations are required. In addition, sampling designs should contain some randomness if the correlation length is unknown, but robust estimates of the correlation length are only possible with a large number of sampling locations.

The SMP shows promising potential for snow cover observations. The new micro-structural model Marshall and Johnson (2009) was not used for this study. Pielmeier and Marshall (2009) showed an improvement in stability estimation with the new model compared to the old model introduced by Johnson and Schneebeli (1999). This suggests also an improvement of the performance of the stability algorithm, especially for the automatic weak layer picking, introduced by Bellaire et al. (2009) and re-analyzed in this study. Furthermore, an automatic layer identification and quality check would allow the usage of the SMP as an operational tool for avalanche forecasting services. This would substantially increase the number of available snow cover observations and might therefore improve the reliability of avalanche forecasts.

The propagation propensity at the slope scale can only be measured if a propagation test covering the entire slope or grid is performed. However, performing a test of this extent is not practical. The propagation saw test (PST) (Gauthier and Jamieson, 2006) in conjunction with SMP measurements allows one to link propagation and non-propagation events to snow cover properties and extrapolation of propagation propensity might become possible. This would substantially improve the understanding of the complex interaction of

weak and slab layer properties with propagation potential.

The meteorological conditions within the entire experimental site have been measured by seven automatic weather stations (AWS). Combining these meteorological observations, especially wind and radiation, with the snow cover observations might give insight into how these conditions affect spatial variability at the slope scale. This would allow one to identify the causes of spatial variability and would substantially improve the avalanche forecasting even for single slopes.

Since slope instability cannot readily be measured, modeling of different spatial variability patterns at the slope scale would allow one to estimate the effect of these variations on snow slope stability. This modeling can also be used to verify the proposed concept of how spatial variability might affect snow slope stability. The data collected in this study can serve as input data for three dimensional snow cover modeling.

Different processes cause spatial variability at different scales. Therefore, spatial variability has to be interpretated separately for each scale, i.e. the slope scale, the regional scale and the mountain range scale. Spatial variability exists, but might only be relevant if occurring between the stable and unstable range as proposed in this study. These situations might be the only relevant situations when spatial variability has to be considered for slope stability estimation. To verify this hypothesis numerical modeling is required since this situations might be difficult to measure. The data collected during this study can be used as input data for numerical modeling with cellular automata models such as used by Kronholm and Birkeland (2005).

Future studies on spatial variability should utilize the SMP to measure snow cover properties at the slope scale nearby automatic weather stations, to identify the causes of spatial variability. The measured snow cover properties should be used as input data for cellular automata models to estimate the slope stability in order to identify the state of the snow cover most critical for slope instability. This is probably possible with the data collected during this study and would form the base for an avalanche forecasting model.

Bibliography

Akitaya, E. (1974). Studies on depth hoar. *Contrib. Inst. Low Temp. Sci.*, 26(A):1–67.

Bader, H., Haefeli, R., Bucher, E., Neher, J., Eckel, O., and Thams, C. (1939). *Der Schnee und seine Metamorphose*. Beiträge zur Geologie der Schweiz - Geotechnische Serie - Hydrologie, Lieferung 3. Kümmerly and Frey, Berne, Switzerland: 1-61.

Bellaire, S., Pielmeier, C., Schneebeli, M., and Schweizer, J. (2009). Stability algorithm for snow micro-penetrometer measurements. *J. Glaciol.*, 55(193):805–813.

Bellaire, S. and Schweizer, J. (2010). Measuring spatial variations of weak layer and slab properties with regard to snow slope stability. *Cold Reg. Sci. Technol. (2010), doi:10.1016/j.colregions.2010.08.013*.

Birkeland, K., Kronholm, K., Schneebeli, M., and Pielmeier, C. (2004a). Changes in shear strength and micropenetration hardness of a buried surface-hoar layer. *Ann. Glaciol.*, 38:223–228.

Birkeland, K., Logan, S., and Kronholm, K. (2004b). A comparison of the spatial structure of the penetration resistance of snow layers in two different snow climates. In *Proceedings ISSMA-2004, International Symposium on Snow Monitoring and Avalanches*, pages 3–11. Snow and Avalanche Study Establishment, India, Manali, India, 12-16 April 2004.

Birkeland, K. W. and Chabot, D. (2006). Minimizing "false stable" stability test results: Why digging more snowpits is a good idea. In Gleason, J. A., editor, *Proceedings ISSW 2006. International Snow Science Workshop*, pages 498–504. Telluride CO, U.S.A., 1-6 October 2006.

Blöschl, G. (1999). Scaling issues in snow hydrology. *Hydrol. Process.*, 13:2149–2175.

Breiman, L., Friedman, J. H., Olshen, R. A., and Stone, C. J. (1998). *Classification and regression trees*. CRC Press, Boca Raton, U.S.A., 386 pp.

Cline, D., Armstrong, R., Davis R., Elder K., and Liston G. (2001). Nasa cold land processes field experiment plan. http://www.nohrsc.nws.gov/cline/clpx.html.

Colbeck, S. C., Akitaya, E., Armstrong, R., Gubler, H., Lafeuille, J., Lied, K., McClung, D., and Morris, E. (1990). *The international classification for seasonal snow on ground*. International comission on Snow and Ice (ICSI). International Association of Scientific Hydrology, Wallingford,Oxon, U.K., 23 pp.

Cressie, N. A. C. (1993). *Statistics for spatial data*. Wiley series in probability and mathematical statistics. John Wiley & Sons, Inc., New York, revised edition, 900 pp. edition.

Cressie, N. A. C. and Hawkins, D. M. (1980). Robust estimation of the variogram: I. *Math. Geol.*, 12(2):115–125.

Doswell, C. A., Davie-Jones, R., and Keller, D. L. (1990). On summary measures of skill in rare event forecasting based on contingency-tables. *Weather and Forecasting*, 5(4):576–585.

Föhn, P. M. B. (1987). The stability index and various triggering mechanisms. In Salm, B. and Gubler, H., editors, *Symposium at Davos 1986 - Avalanche Formation, Movement and Effects, IAHS Publ., 162*, pages 195–214. International Association of Hydrological Sciences, Wallingford, Oxfordshire, U.K.

Fierz, C., Armstrong, R. L., Durand, Y., Etchevers, P., Greene, E., McClung, D. M., Nishimura, K., Satyawali, P. K., and Sokratov, S. A. (2009). *The International Classification for Seasonal Snow on the Ground*. The International Association of Cryospheric Sciences IACS.

Floyer, J. A. (2008). *Layer detection and snowpack stratigraphy characterisation from digital penetrometer signals*. PhD thesis, University of Calgary, 270 pp.

Floyer, J. A. and Jamieson, J. B. (2008). Avalanche weak layer tracing and detection in snow penetrometer profiles. In Locat, J., Perret, D., Turmel, D., Demers, D., and Leroueil, S., editors, *Proceedings of the 4th Canadian Conference on Geohazards: From Causes to Management, Québec, Canada, 20-24 May 2008*, pages 161–168. Presse de l'Université Laval, Québec, Canada.

Föhn, P. M. B. (1987). The rutschblock as a practical tool for slope stability evaluation. In Salm, B. and Gubler, H., editors, *Symposium at Davos 1986 - Avalanche Formation, Movement and Effects, IAHS Publ., 162*, pages 223–228. International Association of Hydrological Sciences, Wallingford, Oxfordshire, U.K.

Fyffe, B. and Zaiser, M. (2004). The effects of snow variability on slab avalanche release. *Cold Reg. Sci. Technol.*, 40(3):229–242.

Gauthier, D. and Jamieson, J. B. (2006). Evaluating a prototype field test for weak layer fracture and failure propagation. In Gleason, J. A., editor, *Proceedings ISSW 2006. International Snow Science Workshop*, pages 107–116. Telluride CO, U.S.A., 1-6 October 2006.

Gauthier, D. M. (2007). *A practical field test for fracture propagation and arrest in weak snowpack layers in relation to slab avalanche release*. PhD thesis, University of Calgary, 302 pp.

Habermann, M., Schweizer, J., and Jamieson, J. B. (2008). Influence of snowpack layering on human-triggered snow slab avalanche release. *Cold Reg. Sci. Technol.*, 54(3):176–182.

Hendrikx, J., Birkeland, K., and Clark, M. (2009). Assessing changes in the spatial variability of the snowpack fracture propagation propensity over time. *Cold Reg. Sci. Technol.*, 56(2-3):152–160.

Jamieson, J. B. (1999). The compression test - after 25 years. *The Avalanche Review*, 18(1):10–12.

Jamieson, J. B. and Johnston, C. D. (1993). Rutschblock precision, technique variations and limitations. *J. Glaciol.*, 39(133):666–674.

Jamieson, J. B. and Johnston, C. D. (1998). Refinements to the stability index for skier-triggered dry slab avalanches. *Ann. Glaciol.*, 26:296–302.

Jamieson, J. B. and Johnston, C. D. (2001). Evaluation of the shear frame test for weak snowpack layers. *Ann. Glaciol.*, 32:59–68.

Johnson, J. B. and Schneebeli, M. (1999). Characterizing the microstructural and micromechanical properties of snow. *Cold Reg. Sci. Technol.*, 30(1-3):91–100.

Journel, A. G. and Huijbregts, G. J. (1978). *Mining Geostatistics*. Academic Press, New York, 600 pp.

Kaempfer, T. U. and Schneebeli, M. (2007). Observation of isothermal metamorphism of new snow and interpretation as a sintering process. *J. Geophys. Res.*, 112, D24101, doi:10.1029/2007JD009047.

Kronholm, K. (2004). *Spatial variability of snow mechanical properties with regard to avalanche formation*. PhD thesis, University of Zurich, 192 pp.

Kronholm, K. and Birkeland, K. W. (2005). Integrating spatial patterns into a snow avalanche cellular automata model. *Geophys. Res. Lett.*, 32, L19504, doi:10.1029/2005GL024373.

Kronholm, K. and Birkeland, K. W. (2007). Reliability of sampling designs for spatial snow surveys. *Comput. Geosci.*, 33(9):1097–1100.

Kronholm, K., Schneebeli, M., and Schweizer, J. (2004). Spatial variability of micropenetration resistance in snow layers on a small slope. *Ann. Glaciol.*, 38:202–208.

Kronholm, K. and Schweizer, J. (2003). Snow stability variation on small slopes. *Cold Reg. Sci. Technol.*, 37(3):453–465.

Lutz, E. R. (2009). *Spatial and temporal analysis of snowpack strength and stability and environmental determinants on an inclined, forest opening.* PhD thesis, Montana State University.

Lutz, E. R., Birkeland, K. W., Kronholm, K., Hansen, K. J., and Aspinall, R. (2007). Surface hoar characteristics derived from a snow micropenetrometer using moving window statistical operations. *Cold Reg. Sci. Technol.*, 47(1-2):118–133.

Mackenzie, R. and Payten, W. (2002). A portable, variable-speed, penetrometer for snow pit evaluation. In Stevens, J. R., editor, *Proceedings ISSW 2002. International Snow Science Workshop*, pages 294–300. Penticton BC, Canada, 29 September-4 October 2002.

Marshall, H. P. and Johnson, J. (2009). Accurate inversion of high-resolution snow penetrometer signals for microstructural and micromechanical properties. *J. Geophys. Res.*, 114:F04016,doi:10.1029/2009JF001269.

McClung, D. M. and Schaerer, P. (2006). *The Avalanche Handbook.* The Mountaineers, Seattle, Washington, U.S.A.

Moran, P. (1948). The intepretation of statistical maps. *Journal of Royal Statistical Society*, B(10):243–251.

Paradis, E., Claude, J., and Strimmer, K. (2004). Ape: Analyses of phylogenetics and evolution in r language. *Bioinformatics*, 20:289–290.

Pielmeier, C. and Marshall, H. P. (2009). Rutschblock-scale snowpack stability derived from multiple quality-controlled snowmicropen measurements. *Cold Reg. Sci. Technol.*, 59(2-3):178–184.

Pielmeier, C. and Schweizer, J. (2007). Snowpack stability information derived from the snowmicropen. *Cold Reg. Sci. Technol.*, 47(1-2):102–107.

R Development Core Team (2009). *R: A Language and Environment for Statistical Computing.* R Foundation for Statistical Computing, Vienna, Austria. ISBN 3-900051-07-0.

Satyawali, P. K., Schneebeli, M., Pielmeier, C., Stucki, T., and Singh, A. K. (2009). Preliminary characterization of alpine snow using snowmicropen. *Cold Reg. Sci. Technol.*, 55(3):311–320.

Schlather, M. (2001). *RandomFields: Simulation and Analysis of Random Fields.* R package version 1.3.37.

Schneebeli, M. and Johnson, J. B. (1998). A constant-speed penetrometer for high resolution snow stratigrahy. *Ann. Glaciol.*, 26:107–111.

Schneebeli, M., Pielmeier, C., and Johnson, J. B. (1999). Measuring snow micro structure and hardness using a high resolution penetrometer. *Cold Reg. Sci. Technol.*, 30(1-

3):101–114.

Schweizer, J. (1999). Review of dry snow slab avalanche release. *Cold Reg. Sci. Technol.*, 30(1-3):43–57.

Schweizer, J. (2004). Snow avalanches. *Water Resources Impact*, 6(1):12–18.

Schweizer, J. and Bellaire, S. (2010). On stability sampling strategy at the slope scale. *Cold Reg. Sci. Technol.*, (2010), doi: 10.1016/j.coldregions.2010.02.013.

Schweizer, J., Heilig, A., Bellaire, S., and Fierz, C. (2008a). Variations in snow surface properties at the snowpack depth, the slope and the basin scale. *J. Glaciol.*, 54(188):846–856.

Schweizer, J. and Jamieson, J. B. (2003). Snowpack properties for snow profile analysis. *Cold Reg. Sci. Technol.*, 37(3):233–241.

Schweizer, J. and Jamieson, J. B. (2007). A threshold sum approach to stability evaluation of manual snow profiles. *Cold Reg. Sci. Technol.*, 47(1-2):50–59.

Schweizer, J., Jamieson, J. B., and Schneebeli, M. (2003). Snow avalanche formation. *Rev. Geophys.*, 41(4):1016, doi:10.1029/2002RG000123.

Schweizer, J. and Kronholm, K. (2007). Snow cover spatial variability at multiple scales: Characteristics of a layer of buried surface hoar. *Cold Reg. Sci. Technol.*, 47(3):207–223.

Schweizer, J., Kronholm, K., Jamieson, J. B., and Birkeland, K. W. (2008b). Review of spatial variability of snowpack properties and its importance for avalanche formation. *Cold Reg. Sci. Technol.*, 51(2-3):253–272.

Schweizer, J. and Wiesinger, T. (2001). Snow profile interpretation for stability evaluation. *Cold Reg. Sci. Technol.*, 33(2-3):179–188.

Simenhois, R. and Birkeland, K. W. (2006). The extended column test: a field test for fracture initiation and propagation. In Gleason, J. A., editor, *Proceedings ISSW 2006. International Snow Science Workshop*, pages 79–85. Telluride CO, U.S.A., 1-6 October 2006.

Simenhois, R. and Birkeland, K. W. (2009). The extended column test: Test effectiveness, spatial variability, and comparison with the propagation saw test. *Cold Reg. Sci. Technol.*, 59(2-3):210–216.

Skøin, J. O. and Blöschl, G. (2006). Sampling scale effects in random fields and implications for environmental monitoring. *Environmental Monitoring and Assessment*, 114:521–552.

Spiegel, M. R. and Stephens, L. J. (1999). *Statistics*. McGraw-Hill, New York, 538 pp.

van Herwijnen, A., Bellaire, S., and Schweizer, J. (2009). Comparison of microstruc-

tural snowpack parameters derived from penetration resistance measurements with fracture character observations from compression tests. *Cold Reg. Sci. Technol.*, 59(2-3):193–201.

van Herwijnen, A. and Jamieson, B. (2005). High-speed photography of fractures in weak snowpack layers. *Cold Reg. Sci. Technol.*, 43(1-2):71–82.

van Herwijnen, A. and Jamieson, J. B. (2007a). Fracture character in compression tests. *Cold Reg. Sci. Technol.*, 47(1-2):60–68.

van Herwijnen, A. and Jamieson, J. B. (2007b). Snowpack properties associated with fracture initiation and propagation resulting in skier-triggered dry snow slab avalanches. *Cold Reg. Sci. Technol.*, 50(1-3):13–22.

Webster, R. and Oliver, M. A. (2007). *Geostatistics for environmental scientists*. Statistics in Practice. Wiley, Chichester, West Sussex, U.K., 271 pp.

Wilks, D. S. (1995). *Statistical methods in the atmospheric sciences: an introduction*, volume 59 of *International Geophysics*. Academic Press, San Diego CA, U.S.A, 627 pp.

Winkler, K. and Schweizer, J. (2009). Comparison of snow stability tests: Extended column test, rutschblock test and compression test. *Cold Reg. Sci. Technol.*, 59(2-3):217–226.

List of Figures

List of Tables

Appendix A

Tables of the spatial and non-spatial analysis including results of the variogram analysis, the Moran's I statistics and the basic statistics for all seventeen grids.

Non-Spatial Analysis

Table A.1: Summary statistics of the parameter Ψ for weak layer and slab layers for the 17 grids. Rutschblock score (RB, bold scores indicate a whole block release), PC the profile classification into five stability classes (1: very poor to 5: very good) according to Schweizer and Wiesinger (2001), the mean point stability (MPS) based on CT score, presence (x) or absence of signs of instability, and estimated slope stability are given as well as the number of available SMP measurements for the statistics. Shown are minimum and maximum, the median and the semi-interquartile range (SIQR) as well as the quartile coeffiecient of variation (QCV).

Grid							Weak layer					Slab layers				
ID	RB	PC	MPS	Signs	Slope Stability	N	Min kPa	Max kPa	Median kPa	SIQR kPa	QCV	Min kPa	Max kPa	Median kPa	SIQR kPa	QCV
1-0607	**4**	3	RR		good	46	17.35	138.10	54.98	17.86	0.33	81.65	199.70	134.70	32.05	0.22
2-0607	7	5	17.5		fair	46	15.73	106.00	61.94	5.36	0.08	17.74	45.42	38.25	1.59	0.04
3-0607	**5**	3	13		poor	42	7.94	90.93	20.65	5.09	0.27	11.78	61.20	24.14	4.23	0.17
5-0607	5	3	12		poor	44	0.00	27.78	1.73	1.70	0.81	30.71	89.55	53.28	7.56	0.15
6-0607	**3**	2	12	x	poor	46	2.81	48.46	17.19	8.67	0.42	12.50	124.60	59.21	22.92	0.36
1-0708	**2**	2	10.5	x	poor	46	0.36	15.95	1.58	0.87	0.47	0.97	9.04	3.49	1.42	0.36
2-0708	**5**	3	11.5		poor	46	11.89	162.20	53.00	10.98	0.20	19.80	173.90	67.59	14.70	0.21
3-0708	**2**	1	11	x	poor	44	0.10	19.91	5.09	2.52	0.42	0.52	22.40	7.70	3.66	0.47
4-0708	**4**	3	14.5		good	46	4.66	34.73	12.06	3.52	0.27	19.70	53.11	30.29	6.85	0.21
5-0708	**4**	3	12.5	x	poor	42	0.66	30.08	3.12	2.03	0.50	14.04	64.76	27.97	7.67	0.25
6-0708	6	4	22.5		good	44	16.43	86.80	48.92	12.75	0.25	37.93	178.10	92.38	20.07	0.21
7-0708	3	3	14		fair	41	2.35	32.38	7.94	2.72	0.31	20.44	85.07	42.10	6.29	0.15
9-0708	4	4	19	x	fair	46	0.00	5.45	2.46	0.42	0.16	1.34	29.02	2.14	0.26	0.12
2-0809	5	4	13.5		good	46	1.90	36.52	4.98	1.61	0.29	2.43	34.27	8.05	3.54	0.43
4-0809	4	3	11		poor	46	0.00	1.67	0.57	0.28	0.50	0.08	9.93	2.80	1.20	0.46
6-0809	5	4	13	x	fair	46	0.00	33.04	8.86	4.45	0.48	0.00	2.13	0.51	0.30	0.48
7-0809	**6**	4	18		fair	46	1.57	84.01	22.18	6.82	0.34	20.03	104.30	80.69	12.37	0.16

Table A.2: Summary statistics of the maximum penetration resistance for weak layer and slab layers for the 17 grids. Rutschblock score (RB, bold scores indicate a whole block release), PC the profile classification into five stability classes (1: very poor to 5: very good) according to Schweizer and Wiesinger (2001), the mean point stability (MPS) based on CT score, presence (x) or absence of signs of instability, and estimated slope stability are given as well as the number of available SMP measurements for the statistics. Shown are minimum and maximum, the median and the semi-interquartile range (SIQR) as well as the quartile coeffiecient of variation (QCV).

Grid							Weak layer					Slab layers				
ID	RB	PC	MPS	Signs	Slope Stability	N	Min N	Max N	Median N	SIQR N	QCV	Min N	Max N	Median N	SIQR N	QCV
1-0607	**4**	3	RR		good	46	0.24	0.97	0.44	0.12	0.26	2.42	21.18	8.30	3.52	0.37
2-0607	7	5	17.5		fair	46	0.39	0.96	0.57	0.09	0.15	2.49	6.41	4.26	0.46	0.11
3-0607	**5**	3	13		poor	42	0.18	0.81	0.29	0.03	0.12	0.52	2.74	0.79	0.11	0.14
5-0607	5	3	12		poor	44	0.12	0.51	0.22	0.06	0.25	4.42	19.74	7.52	1.59	0.23
6-0607	**3**	2	12	x	poor	46	0.20	1.06	0.58	0.14	0.24	1.34	21.94	10.39	3.54	0.34
1-0708	**2**	2	10.5	x	poor	46	0.07	0.36	0.14	0.03	0.21	0.32	1.20	0.54	0.12	0.21
2-0708	**5**	3	11.5		poor	46	0.20	1.42	0.58	0.15	0.24	1.52	4.69	3.06	0.38	0.13
3-0708	**2**	1	11	x	poor	44	0.06	0.36	0.15	0.03	0.20	0.19	2.44	0.75	0.17	0.22
4-0708	**4**	3	14.5		good	46	0.09	0.47	0.22	0.03	0.13	1.23	3.61	2.72	0.53	0.19
5-0708	**4**	3	12.5	x	poor	42	0.07	0.45	0.15	0.05	0.31	3.34	39.92	8.02	2.53	0.29
6-0708	6	4	22.5		good	44	0.20	0.82	0.52	0.07	0.14	1.39	13.88	3.99	1.65	0.38
7-0708	3	3	14		fair	41	0.08	0.62	0.24	0.05	0.20	3.54	33.66	10.88	2.67	0.24
9-0708	4	4	19	x	fair	46	0.06	0.31	0.15	0.02	0.12	0.19	1.81	0.28	0.04	0.14
2-0809	5	4	13.5		good	46	0.05	0.26	0.09	0.02	0.17	0.15	1.49	0.58	0.22	0.37
4-0809	4	3	11		poor	46	0.02	0.10	0.06	0.01	0.19	0.08	1.06	0.35	0.08	0.23
6-0809	5	4	13	x	fair	46	0.05	0.56	0.20	0.06	0.30	0.07	0.55	0.24	0.07	0.25
7-0809	**6**	4	18		fair	46	0.24	0.87	0.41	0.09	0.20	1.81	5.46	2.75	0.31	0.11

Table A.3: Summary statistics of the penetration resistance F for weak layer and slab layers for the 17 grids. Rutschblock score (RB, bold scores indicate a whole block release), PC the profile classification into five stability classes (1: very poor to 5: very good) according to Schweizer and Wiesinger (2001), the mean point stability (MPS) based on CT score, presence (x) or absence of signs of instability, and estimated slope stability are given as well as the number of available SMP measurements for the statistics. Shown are minimum and maximum, the median and the semi-interquartile range (SIQR) as well as the quartile coeffiecient of variation (QCV).

Grid							Weak layer					Slab layers				
ID	RB	PC	MPS	Signs	Slope Stability	N	Min N	Max N	Median N	SIQR N	QCV	Min N	Max N	Median N	SIQR N	QCV
1-0607	**4**	3	RR		good	46	0.11	0.49	0.24	0.07	0.29	0.37	1.09	0.70	0.14	0.20
2-0607	7	5	17.5		fair	46	0.18	0.61	0.28	0.05	0.16	0.08	0.38	0.20	0.02	0.11
3-0607	**5**	3	13		poor	42	0.05	0.33	0.10	0.02	0.20	0.11	0.39	0.19	0.02	0.12
5-0607	5	3	12		poor	44	0.08	0.43	0.16	0.05	0.29	0.30	1.17	0.54	0.11	0.20
6-0607	**3**	2	12	x	poor	46	0.00	0.36	0.14	0.04	0.31	0.10	1.12	0.50	0.18	0.36
1-0708	**2**	2	10.5	x	poor	46	0.02	0.21	0.04	0.01	0.26	0.05	0.16	0.08	0.01	0.14
2-0708	**5**	3	11.5		poor	46	0.12	1.13	0.39	0.12	0.29	0.18	1.42	0.51	0.12	0.22
3-0708	**2**	1	11	x	poor	44	0.02	0.18	0.06	0.02	0.30	0.03	0.19	0.08	0.03	0.32
4-0708	**4**	3	14.5		good	46	0.04	0.15	0.07	0.01	0.17	0.16	0.41	0.25	0.05	0.20
5-0708	**4**	3	12.5	x	poor	42	0.00	0.20	0.02	0.02	0.62	0.07	0.61	0.19	0.06	0.30
6-0708	6	4	22.5		good	44	0.02	0.28	0.10	0.03	0.28	0.13	0.73	0.33	0.11	0.32
7-0708	3	3	14		fair	41	0.00	0.20	0.05	0.02	0.40	0.07	0.74	0.26	0.06	0.24
9-0708	4	4	19	x	fair	46	0.02	0.21	0.06	0.01	0.14	0.03	0.23	0.05	0.01	0.16
2-0809	5	4	13.5		good	46	0.00	0.14	0.03	0.01	0.27	0.02	0.15	0.04	0.01	0.34
4-0809	4	3	11		poor	46	0.00	0.06	0.02	0.01	0.28	0.00	0.08	0.04	0.01	0.22
6-0809	5	4	13	x	fair	46	0.03	0.42	0.13	0.04	0.29	0.00	0.11	0.07	0.02	0.46
7-0809	**6**	4	18		fair	46	0.06	0.32	0.12	0.02	0.14	0.41	0.91	0.61	0.06	0.10

Table A.4: Summary statistics of the weak layer and slab layer thickness for the 17 grids. Rutschblock score (RB, bold scores indicate a whole block release), PC the profile classification into five stability classes (1: very poor to 5: very good) according to Schweizer and Wiesinger (2001), the mean point stability (MPS) based on CT score, presence (x) or absence of signs of instability, and estimated slope stability are given as well as the number of available SMP measurements for the statistics. Shown are minimum and maximum, the median and the semi-interquartile range (SIQR) as well as the quartile coeffiecient of variation (QCV).

| Grid | | | | | | | Weak layer | | | | | Slab layers | | | | |
ID	RB	PC	MPS	Signs	Slope Stability	N	Min cm	Max cm	Median cm	SIQR cm	QCV	Min cm	Max cm	Median cm	SIQR cm	QCV
1-0607	**4**	3	RR		good	46	0.1541	3.392	0.8379	0.797	0.61	20.27	32.03	24.61	1.77	0.07
2-0607	7	5	17.5		fair	46	0.707	5.99	2.781	0.1815	0.07	23.09	32.57	26.36	1.41	0.05
3-0607	**5**	3	13		poor	42	0.798	6.706	2.983	1.06	0.32	14.8	50.5	30.23	2.055	0.07
5-0607	5	3	12		poor	44	0.0799	3.152	0.627	0.2408	0.39	10.26	18.44	13.74	1.04	0.07
6-0607	**3**	2	12	x	poor	46	1.277	14.78	7	2.3995	0.34	7.228	80.6	56.71	17.935	0.38
1-0708	**2**	2	10.5	x	poor	46	0.698	4.964	2.426	0.725	0.29	13.17	24.17	18.81	1.995	0.11
2-0708	**5**	3	11.5		poor	46	0.1816	1.785	0.5033	0.2239	0.37	16.24	28.91	22.13	2.475	0.11
3-0708	**2**	1	11	x	poor	44	0.1205	2.386	0.3379	0.1984	0.45	16.46	35.16	28.59	2.67	0.09
4-0708	**4**	3	14.5		good	46	0.2902	6.359	1.129	0.233	0.20	40.82	58.55	48.57	3.51	0.07
5-0708	**4**	3	12.5	x	poor	42	0.8799	4.934	2.926	0.6245	0.21	21.99	85.15	36.31	5.53	0.16
6-0708	6	4	22.5		good	44	0.2992	4.925	2.703	0.476	0.17	39.61	89.02	52.56	7.63	0.14
7-0708	3	3	14		fair	41	0.2234	4.856	1.785	0.732	0.37	12.89	49.45	30.5	1.545	0.05
9-0708	4	4	19	x	fair	46	0.2918	10.87	4.2	0.3215	0.08	21.57	75	31.24	4.62	0.14
2-0809	5	4	13.5		good	46	0.0873	1.687	0.9848	0.1941	0.20	9.559	16.05	11.49	1.025	0.09
4-0809	4	3	11		poor	46	0.5049	8.033	3.502	1.171	0.32	6.132	20.37	16.17	1.155	0.07
6-0809	5	4	13	x	fair	46	0.0766	1.783	0.7475	0.3399	0.47	22.83	58.8	46.59	8.285	0.20
7-0809	**6**	4	18		fair	46	0.4857	2.943	1.623	0.262	0.16	65.63	101.1	82.1	3.635	0.04

Trends

Table A.5: Coefficients of the calculated first order polynominal trend for the mean penetration resistance F. Additional given the correlation coefficient R^2. Bold marked coefficients were significant (p<0.05).

	Weak layer				Slab layers			
ID	a	b	c	R^2	a	b	c	R^2
1-0607	**0.25**	-0.001	0.002	0.01	**0.693**	-0.007	0.008	0.09
2-0607	**0.29**	**-0.006**	**0.009**	0.32	**0.190**	-0.004	**0.008**	0.49
3-0607	**0.16**	-0.003	**-0.003**	0.17	**0.217**	0.001	**-0.004**	0.17
5-0607	**0.20**	-0.002	0.000	0.02	**0.671**	-0.007	-0.003	0.05
6-0607	**0.11**	**0.004**	-0.002	0.12	**0.498**	**0.024**	**-0.021**	0.51
1-0708	**0.07**	0.000	-0.001	0.04	**0.102**	0.000	**-0.002**	0.25
2-0708	**0.40**	-0.009	**0.014**	0.19	**0.649**	**-0.029**	**0.023**	0.61
3-0708	**0.05**	0.001	0.001	0.03	**0.086**	0.001	-0.001	0.07
4-0708	**0.09**	0.000	-0.001	0.06	**0.224**	0.002	0.002	0.03
5-0708	**0.05**	-0.002	0.000	0.09	0.098	0.005	**0.009**	0.16
6-0708	**0.12**	**0.003**	**-0.004**	0.22	**0.164**	**0.021**	0.002	0.44
7-0708	**0.07**	0.001	-0.002	0.08	**0.296**	0.004	-0.006	0.10
9-0708	**0.05**	**0.003**	-0.001	0.37	**0.048**	**0.002**	-0.001	0.14
2-0809	**0.05**	**-0.001**	-0.001	0.14	**0.036**	0.000	0.001	0.04
4-0809	**0.02**	0.000	0.000	0.00	**0.042**	0.000	0.000	0.01
6-0809	**0.22**	**0.003**	**-0.011**	0.41	**0.114**	-0.001	**-0.005**	0.75
7-0809	**0.08**	**0.004**	0.002	0.20	**0.457**	**0.006**	**0.012**	0.35

Table A.6: Coefficients of the calculated first order polynominal trend for the maximum penetration resistance. Additional given the correlation coefficient R^2.Bold marked coefficients were significant (p<0.05).

	Weak layer				Slab layers			
ID	a	b	c	R^2	a	b	c	R^2
1-0607	**0.481**	-0.005	0.005	0.05	**6.713**	**-0.261**	**0.557**	0.40
2-0607	**0.571**	-0.006	**0.009**	0.18	**4.404**	-0.021	0.014	0.04
3-0607	**0.418**	**-0.008**	-0.003	0.14	**1.208**	-0.012	-0.023	0.09
5-0607	**0.266**	-0.003	0.000	0.02	**10.923**	-0.184	-0.084	0.09
6-0607	**0.597**	0.004	-0.005	0.03	**12.191**	0.156	**-0.344**	0.14
1-0708	**0.192**	-0.001	-0.003	0.05	**0.776**	-0.002	**-0.018**	0.19
2-0708	**0.556**	-0.009	**0.018**	0.17	**2.616**	-0.028	**0.079**	0.38
3-0708	**0.154**	0.001	0.001	0.01	**0.999**	-0.011	-0.008	0.03
4-0708	**0.257**	0.000	-0.003	0.04	**2.576**	-0.009	0.018	0.02
5-0708	**0.229**	-0.004	-0.003	0.12	**11.496**	-0.116	-0.052	0.01
6-0708	**0.443**	**0.008**	0.002	0.13	**3.201**	**0.243**	-0.089	0.35
7-0708	**0.363**	-0.002	**-0.010**	0.21	**12.977**	0.091	-0.217	0.04
9-0708	**0.126**	**0.004**	-0.002	0.44	**0.310**	0.009	-0.009	0.09
2-0809	**0.129**	**-0.003**	-0.001	0.19	**0.358**	0.014	0.013	0.10
4-0809	**0.067**	-0.001	0.000	0.03	**0.333**	-0.008	**0.012**	0.18
6-0809	**0.291**	**0.005**	**-0.012**	0.40	**0.382**	0.002	**-0.016**	0.57
7-0809	**0.384**	0.005	0.001	0.05	**1.691**	**0.043**	**0.080**	0.41

Table A.7: Coefficients of the calculated first order polynominal trend for the parameter Ψ. Additional given the correlation coefficient R^2. Bold marked coefficients were significant (p<0.05).

	Weak layer				Slab layers			
ID	a	b	c	R^2	a	b	c	R^2
1-0607	**68.50**	-0.37	-0.85	0.03	**152.90**	-1.52	0.14	0.06
2-0607	**75.57**	**-1.16**	-0.21	0.18	**38.58**	-0.04	-0.10	0.01
3-0607	**37.31**	-0.61	**-0.94**	0.14	**31.45**	0.22	**-0.83**	0.25
5-0607	**6.75**	-0.23	-0.15	0.09	**72.63**	**-0.96**	**-0.98**	0.29
6-0607	**17.64**	**0.99**	**-0.75**	0.33	**57.12**	**2.87**	**-2.20**	0.44
1-0708	**6.12**	-0.14	**-0.24**	0.19	**6.58**	0.05	**-0.34**	0.67
2-0708	**63.11**	**-1.73**	1.32	0.18	**84.48**	**-3.88**	**2.89**	0.63
3-0708	**7.45**	-0.14	0.03	0.04	**8.31**	0.13	-0.12	0.04
4-0708	**16.12**	0.01	-0.23	0.02	**29.02**	0.24	0.14	0.03
5-0708	**10.21**	**-0.43**	-0.15	0.21	**18.47**	**0.72**	0.66	0.20
6-0708	**24.30**	**1.62**	**1.23**	0.35	**37.76**	**4.53**	**2.02**	0.49
7-0708	**16.83**	-0.29	**-0.47**	0.16	**45.70**	0.62	-0.81	0.17
9-0708	**1.92**	**0.10**	-0.03	0.35	3.09	0.09	-0.13	0.04
2-0809	**10.52**	**-0.45**	0.05	0.21	**5.45**	-0.01	**0.43**	0.09
4-0809	**0.54**	-0.01	0.02	0.08	**2.29**	-0.05	0.11	0.11
6-0809	**16.39**	0.21	**-0.89**	0.34	**1.29**	-0.01	**-0.06**	0.44
7-0809	2.55	**1.51**	0.64	0.33	**57.28**	**2.49**	-0.70	0.41

Table A.8: Coefficients of the calculated first order polynominal trend for the weak and slab layer thickness. Additional given the correlation coefficient R^2. Bold marked coefficients were significant (p<0.05).

	Weak layer				Slab layers			
ID	a	b	c	R^2	a	b	c	R^2
1-0607	**1.099**	-0.017	0.033	0.04	**25.259**	0.134	-0.153	0.15
2-0607	**3.349**	0.011	**-0.065**	0.12	**28.835**	**-0.313**	0.070	0.57
3-0607	**1.925**	0.047	**0.099**	0.11	**31.169**	0.051	-0.126	0.02
5-0607	0.317	0.010	0.029	0.07	**12.748**	0.053	0.060	0.06
6-0607	**9.224**	-0.023	**-0.216**	0.10	**29.047**	**3.642**	**-1.687**	0.95
1-0708	**1.785**	-0.020	**0.114**	0.21	**20.459**	**0.176**	**-0.375**	0.58
2-0708	**0.633**	0.017	-0.017	0.12	**29.674**	**-0.417**	**-0.372**	0.76
3-0708	**1.157**	-0.003	**-0.064**	0.32	**23.327**	0.155	**0.392**	0.21
4-0708	**2.209**	-0.035	-0.059	0.11	**48.270**	0.197	-0.010	0.07
5-0708	**3.233**	-0.003	-0.035	0.02	**41.537**	-0.374	-0.076	0.04
6-0708	**2.790**	**-0.059**	0.057	0.21	**35.936**	**1.161**	**0.887**	0.47
7-0708	**2.345**	-0.018	-0.009	0.01	**30.202**	0.013	0.017	0.00
9-0708	**2.142**	**0.117**	0.079	0.18	**30.444**	**0.767**	-0.350	0.30
2-0809	**0.419**	**0.039**	0.017	0.42	**10.820**	0.007	0.065	0.05
4-0809	**4.175**	-0.075	0.032	0.06	**15.095**	-0.074	0.156	0.12
6-0809	**0.638**	0.007	0.011	0.02	**59.686**	-0.020	**-1.876**	0.75
7-0809	**1.676**	-0.029	0.028	0.17	**63.673**	**0.699**	**1.251**	0.63

Moran's I

Table A.9: Results of the Moran's I statistics for the weak and slab layer Ψ. Shown are the grid ID the number of measurement points, the p-value as well as the median.

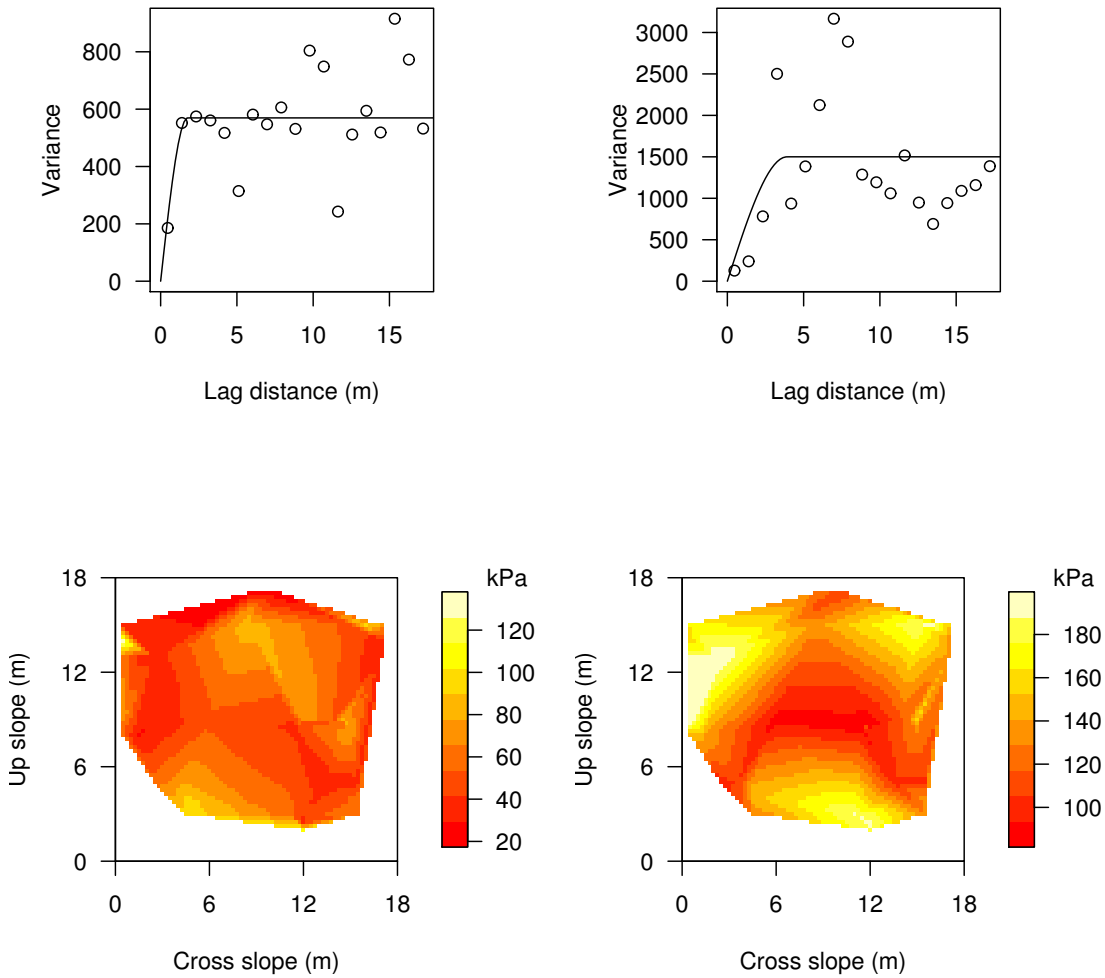|		Weak layer			Slab layer		
ID	N	Moran's I	p	Median KPa	Moran's I	p	Median KPa
1-0607	46	0	0.69	55.0	0.31	0.000	134.7
2-0607	46	0.13	0.00	61.9	-0.04	0.736	38.3
3-0607	42	0.18	0.00	20.6	0.13	0.001	24.1
5-0607	44	0.04	0.11	1.7	0.28	0.000	53.3
6-0607	46	0.21	0.00	17.2	0.30	0.000	59.2
1-0708	46	0.04	0.12	1.6	0.31	0.000	3.5
2-0708	46	0.13	0.00	53.0	0.35	0.000	67.6
3-0708	44	0.07	0.03	5.1	0.24	0.000	7.7
4-0708	46	0.23	0.00	12.1	0.30	0.000	30.3
5-0708	42	0.27	0.00	3.1	0.09	0.019	28.0
6-0708	44	0.37	0.00	48.9	0.56	0.000	92.4
7-0708	41	0.04	0.14	7.9	0.08	0.026	42.1
9-0708	46	0.26	0.00	2.5	-0.02	0.643	2.1
2-0809	46	0.14	0.00	5.0	0.11	0.002	8.1
4-0809	46	0.14	0.00	0.6	0.10	0.003	2.8
6-0809	46	0.25	0.00	8.9	0.26	0.000	0.5
7-0809	46	0.19	0.00	22.2	0.28	0.000	80.7

Table A.10: Results of the Moran's I statistics for the weak and slab layer penetration resistance. Shown are the grid ID the number of measurement points, the p-value as well as the median.

		Weak layer			Slab layer		
ID	N	Moran's I	p	Median N	Moran's I	p	Median N
1-0607	46	0.04	0.162	0.2	0.30	0.000	0.7
2-0607	46	0.21	0.000	0.3	0.28	0.000	0.2
3-0607	42	0.19	0.000	0.1	0.14	0.000	0.2
5-0607	44	0.25	0.000	0.2	0.28	0.000	0.5
6-0607	46	0.06	0.050	0.1	0.26	0.000	0.5
1-0708	46	-0.03	0.874	0.0	0.14	0.000	0.1
2-0708	46	0.10	0.003	0.4	0.35	0.000	0.5
3-0708	44	0.12	0.002	0.1	0.20	0.000	0.1
4-0708	46	0.24	0.000	0.1	0.27	0.000	0.3
5-0708	42	0.08	0.009	0.0	0.12	0.002	0.2
6-0708	44	0.19	0.000	0.1	0.54	0.000	0.3
7-0708	41	0.06	0.081	0.1	0.03	0.220	0.3
9-0708	46	0.17	0.000	0.1	0.05	0.013	0
2-0809	46	0.02	0.263	0.0	0.09	0.006	0
4-0809	46	0.08	0.021	0.0	0.12	0.001	0
6-0809	46	0.30	0.000	0.1	0.37	0.000	0.1
7-0809	46	0.17	0.000	0.1	0.32	0.000	0.6

Table **A.11:** Results of the Moran's I statistics for the weak and slab layer maximum penetration resistance. Shown are the grid ID the number of measurement points, the p-value as well as the median.

		Weak layer			Slab layer		
ID	N	Moran's I	p	Median N	Moran's I	p	Median N
1-0607	46	0.02	0.332	0.4	0.26	0	8.3
2-0607	46	0.17	0	0.6	0.03	0.238	4.3
3-0607	42	0.1	0.003	0.3	-0.07	0.302	0.8
5-0607	44	0.27	0	0.2	0.14	0	7.5
6-0607	46	0.01	0.407	0.6	0.01	0.506	10.4
1-0708	46	-0.03	0.925	0.1	0.11	0.003	0.5
2-0708	46	0.09	0.008	0.6	0.21	0	3.1
3-0708	44	0.04	0.171	0.2	0.01	0.486	0.7
4-0708	46	0.19	0	0.2	0.13	0.001	2.7
5-0708	42	0.12	0.002	0.2	0.08	0.014	8
6-0708	44	0.1	0.007	0.5	0.43	0	4
7-0708	41	0.08	0.022	0.2	0.01	0.5	10.9
9-0708	46	0.23	0	0.1	0.01	0.032	0.3
2-0809	46	0.12	0	0.1	0.1	0.006	0.6
4-0809	46	0.13	0.001	0.1	0.1	0.004	0.4
6-0809	46	0.27	0	0.2	0.27	0	0.2
7-0809	46	0	0.668	0.4	0.24	0	2.7

Table A.12: Results of the Moran's I statistics for the weak and slab layer thickness. Shown are the grid ID the number of measurement points, the p-value as well as the median.

		Weak layer			Slab layer		
ID	N	Moran's I	p	Median cm	Moran's I	p	Median cm
1-0607	46	0.15	0	0.8	0.17	0	24.6
2-0607	46	0.04	0.107	2.8	0.35	0	26.4
3-0607	42	0.07	0.063	3	0.18	0	30.2
5-0607	44	0.01	0.471	0.6	0.12	0.002	13.7
6-0607	46	0.06	0.076	7	0.55	0	56.7
1-0708	46	0.12	0.002	2.4	0.41	0	18.8
2-0708	46	0.07	0.048	0.5	0.43	0	22.1
3-0708	44	0.13	0	0.3	0.26	0	28.6
4-0708	46	0.08	0.008	1.1	0.29	0	48.6
5-0708	42	0.1	0.014	2.9	0.05	0.09	36.3
6-0708	44	0.09	0.012	2.7	0.5	0	52.6
7-0708	41	0.09	0.014	1.8	0.04	0.133	30.5
9-0708	46	0.16	0	4.2	0.19	0	31.2
2-0809	46	0.33	0	1	0.14	0	11.5
4-0809	46	0.07	0.052	3.5	0.13	0	16.2
6-0809	46	0.05	0.109	0.7	0.38	0	46.6
7-0809	46	0.08	0.019	1.6	0.42	0	82.1

Appendix B

Sample (open circles) and theoretical variogram (solid line) of the parameter Ψ for the weak layer and slab layer for the winter between 2006 and 2009. In addition shown are the contour plots of the weak layer and slab layer Ψ. The Ψ values were not detrended.
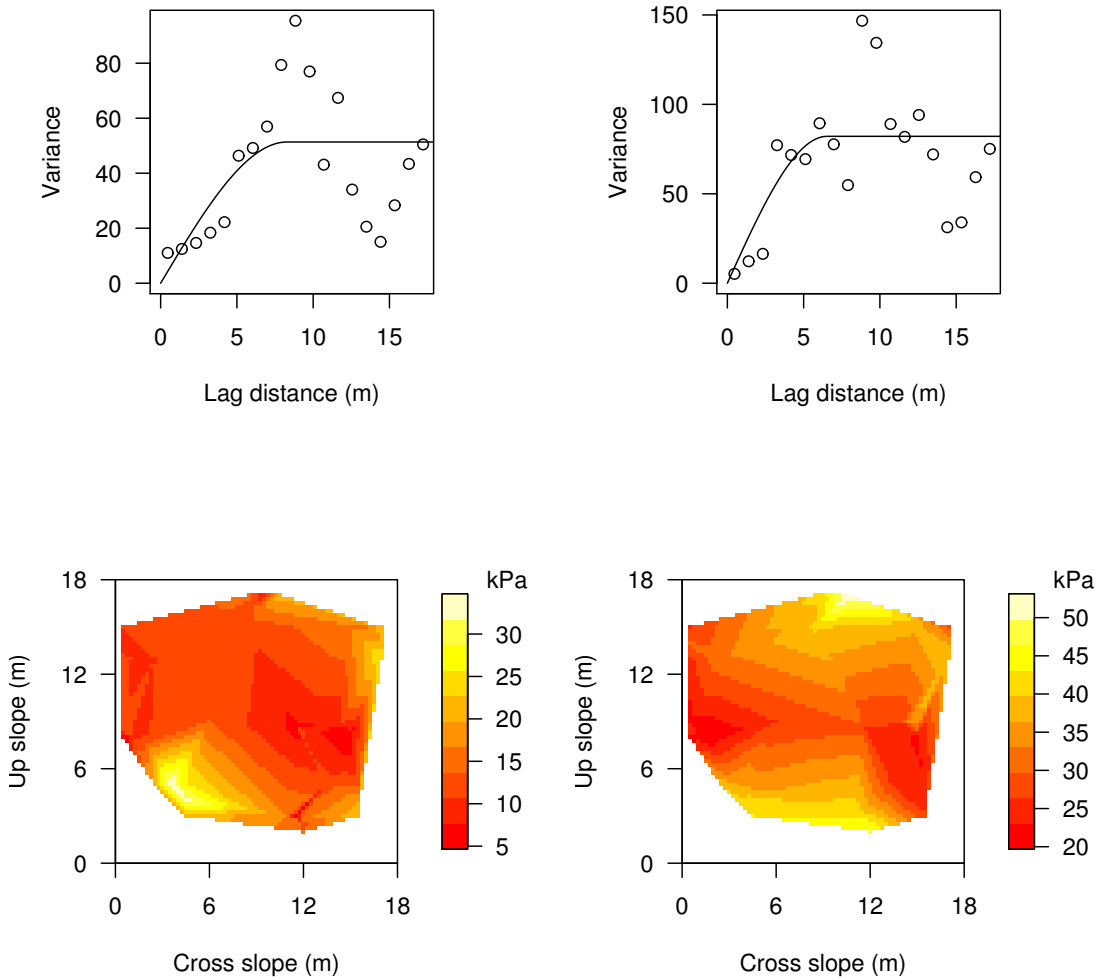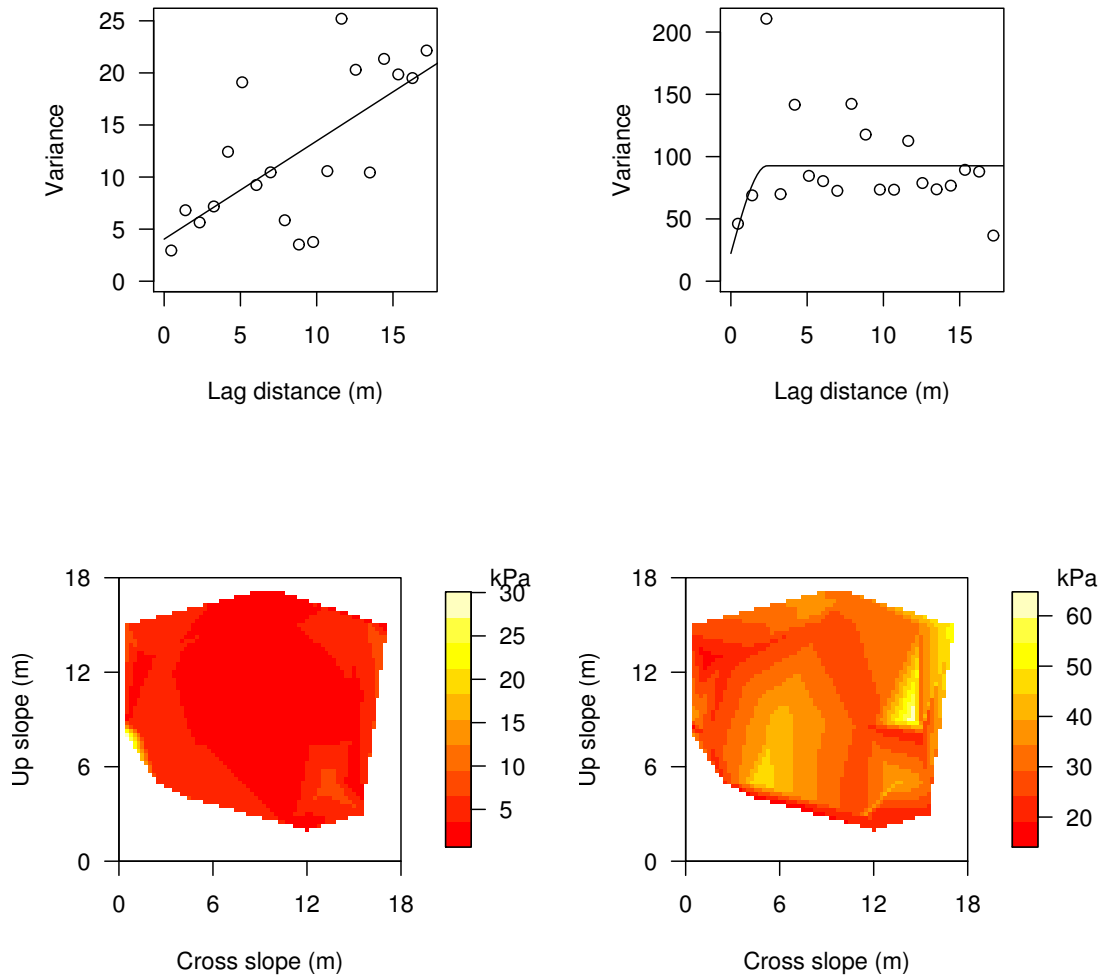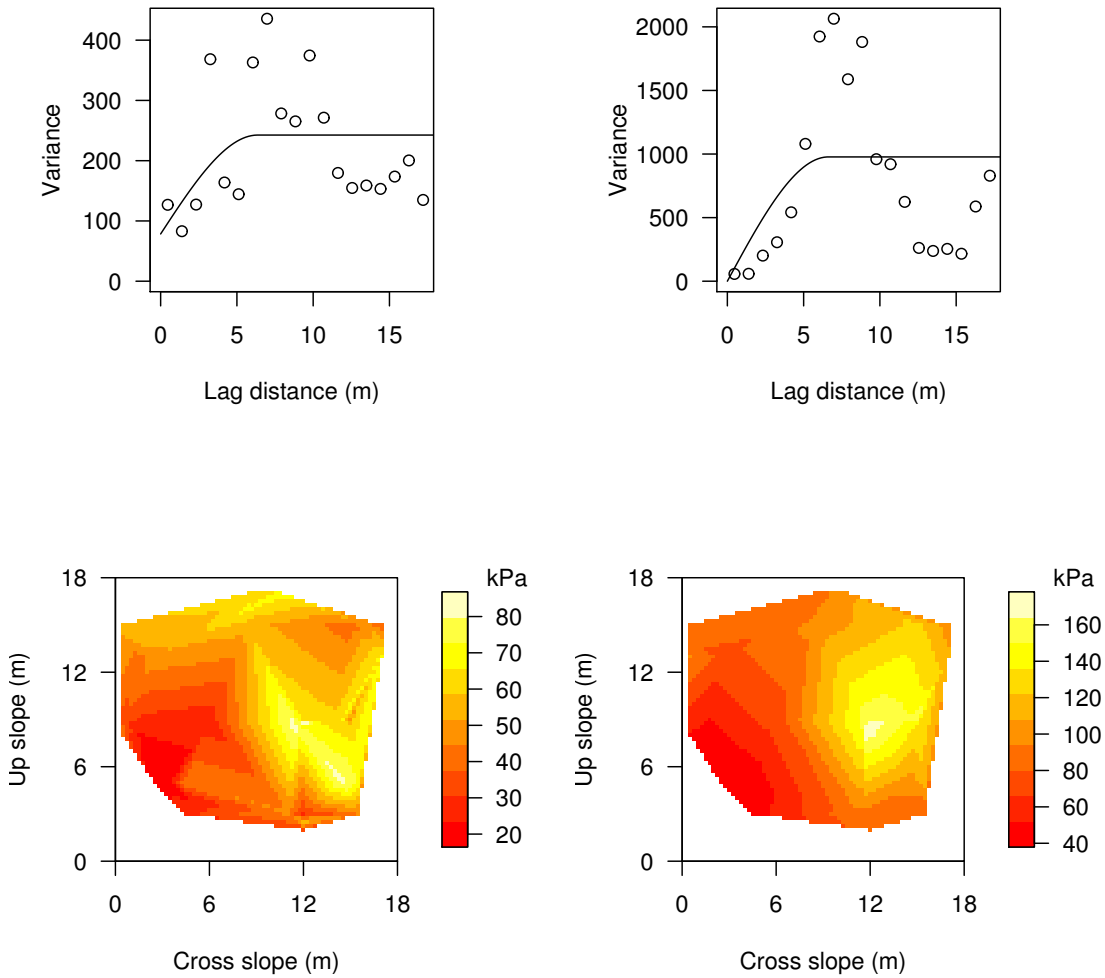
Figure B.1: Grid 1 winter 2006 - 2007. Experimental variogram (open circles) and modeled variogram of the parameter Ψ for the weak layer (top left) and the slab layers (top right). Contour plots of the parameter Ψ for the weak layer (bottom left) and the slab layer (bottom right).
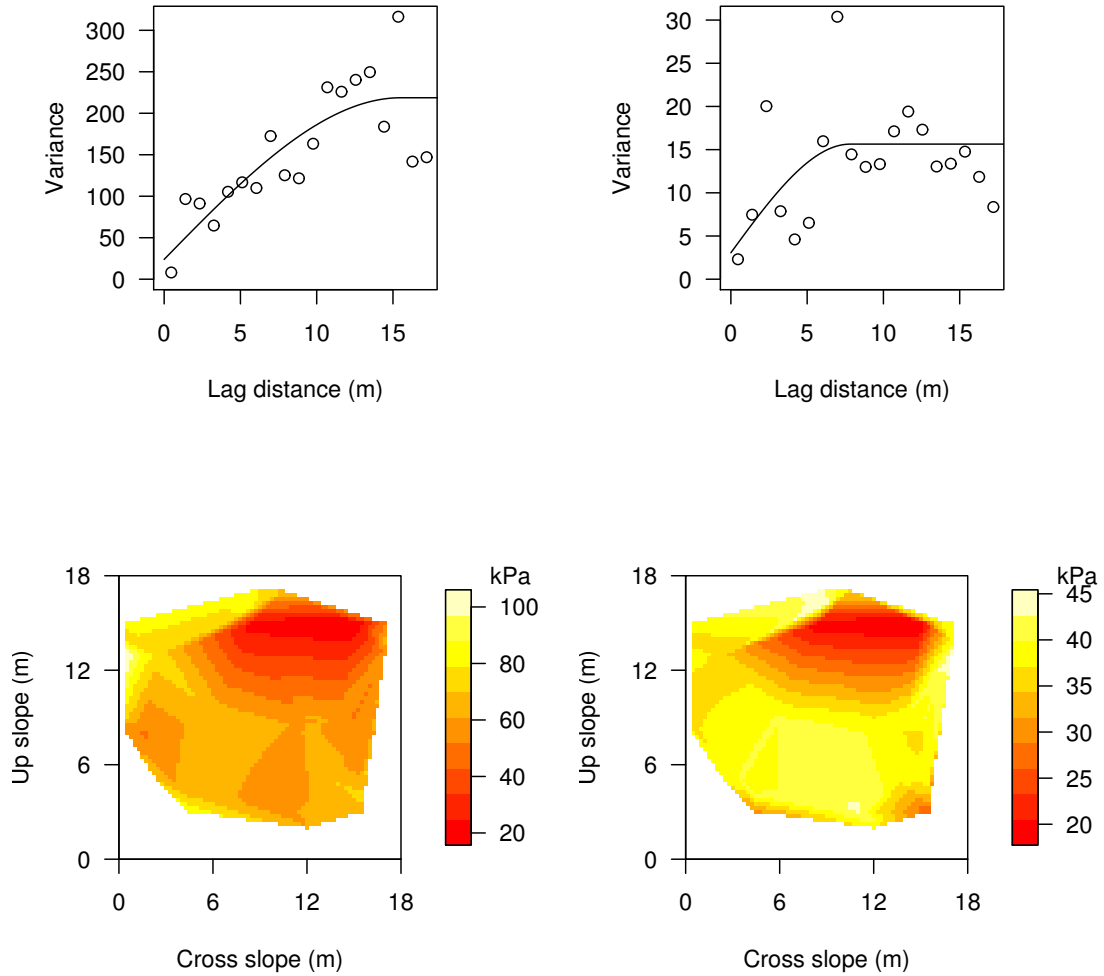
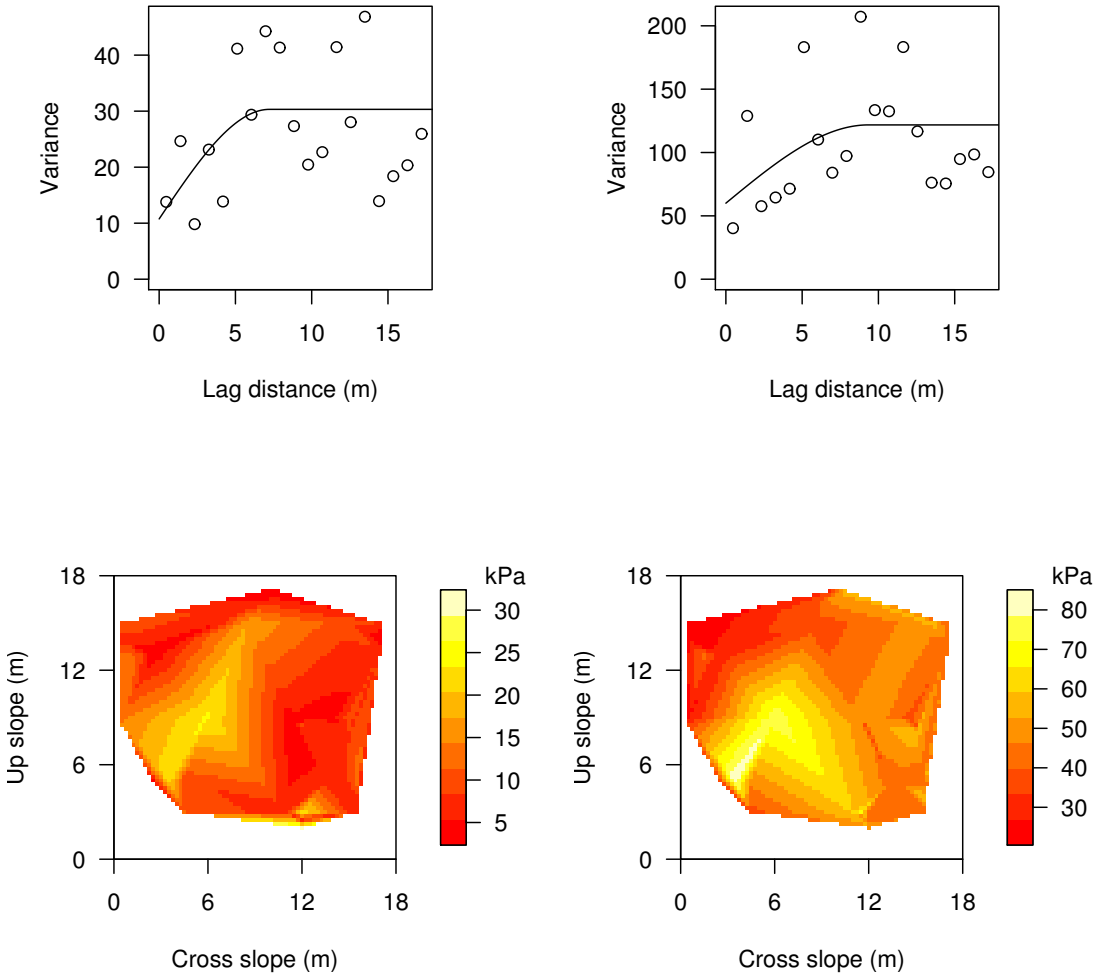**Figure B.2:** Grid 2 winter 2006 - 2007. Experimental variogram (open circles) and modeled variogram of the parameter Ψ for the weak layer (top left) and the slab layers (top right). Contour plots of the parameter Ψ for the weak layer (bottom left) and the slab layer (bottom right).
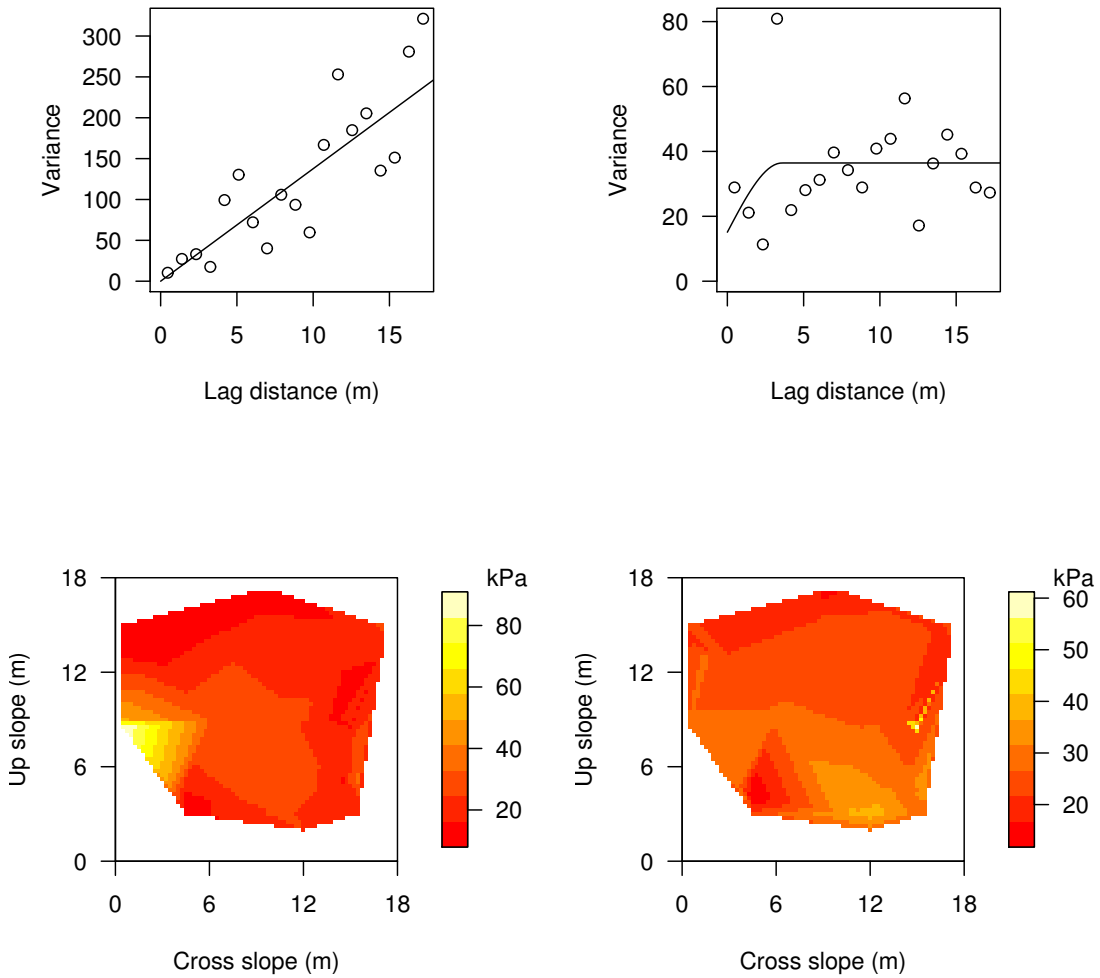
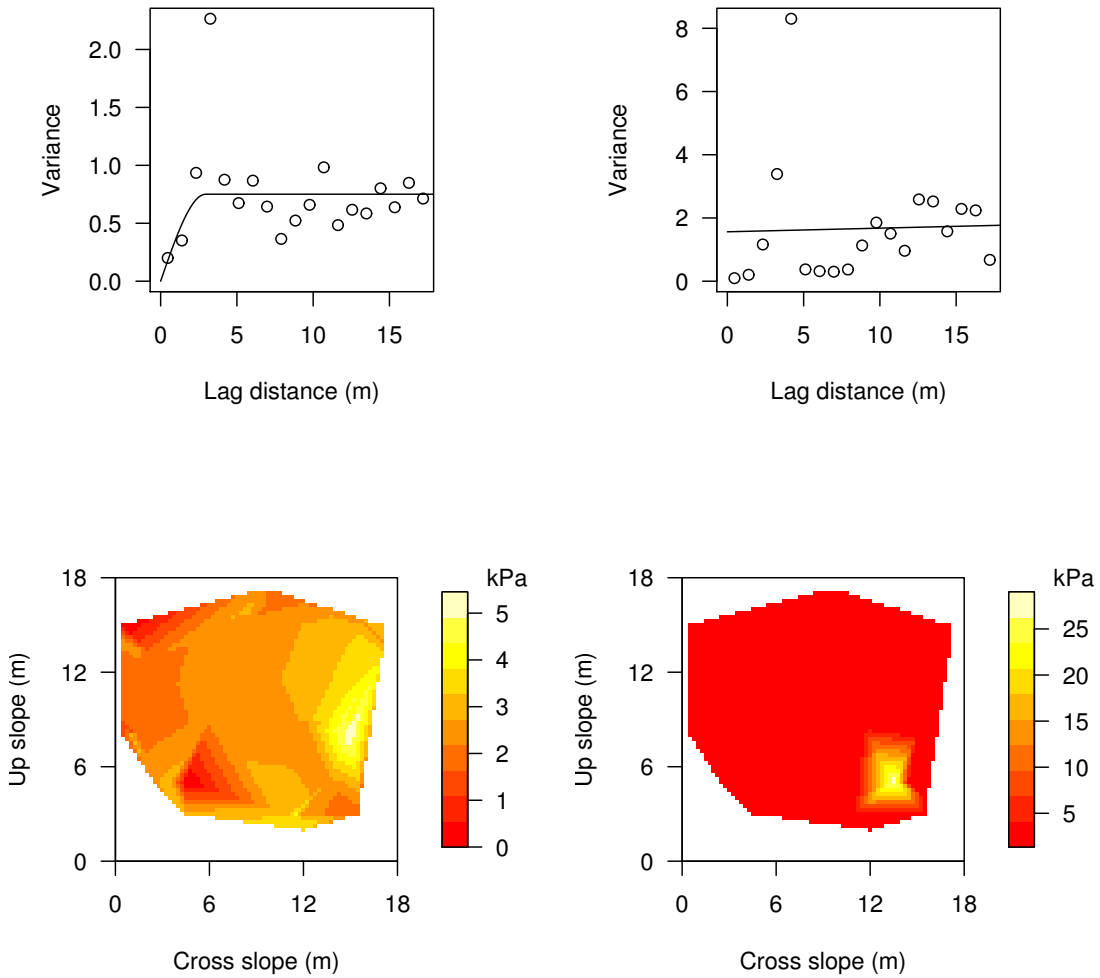**Figure B.3**: Grid 3 winter 2006 - 2007. Experimental variogram (open circles) and modeled variogram of the parameter Ψ for the weak layer (top left) and the slab layers (top right). Contour plots of the parameter Ψ for the weak layer (bottom left) and the slab layer (bottom right).
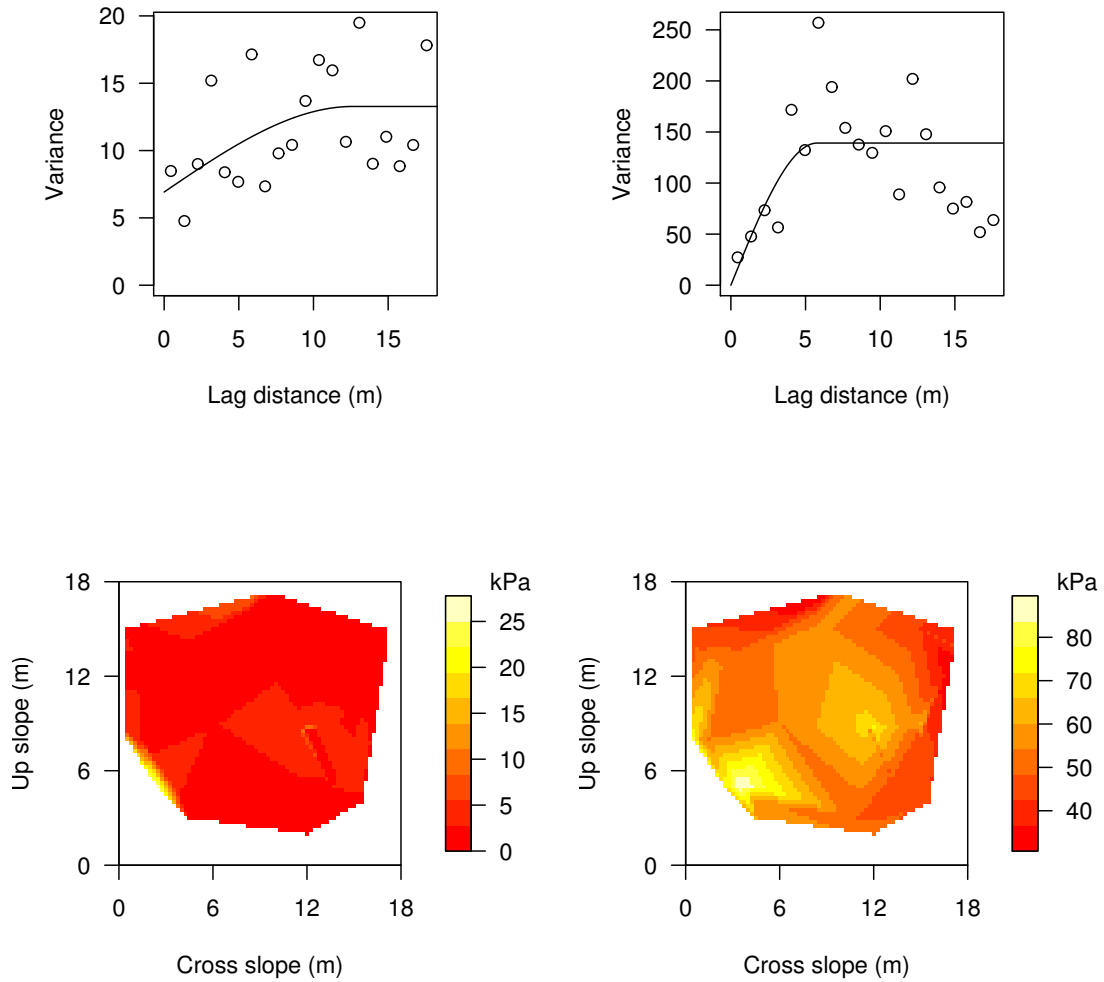
Figure B.4: Grid 5 winter 2006 - 2007. Experimental variogram (open circles) and modeled variogram of the parameter Ψ for the weak layer (top left) and the slab layers (top right). Contour plots of the parameter Ψ for the weak layer (bottom left) and the slab layer (bottom right).
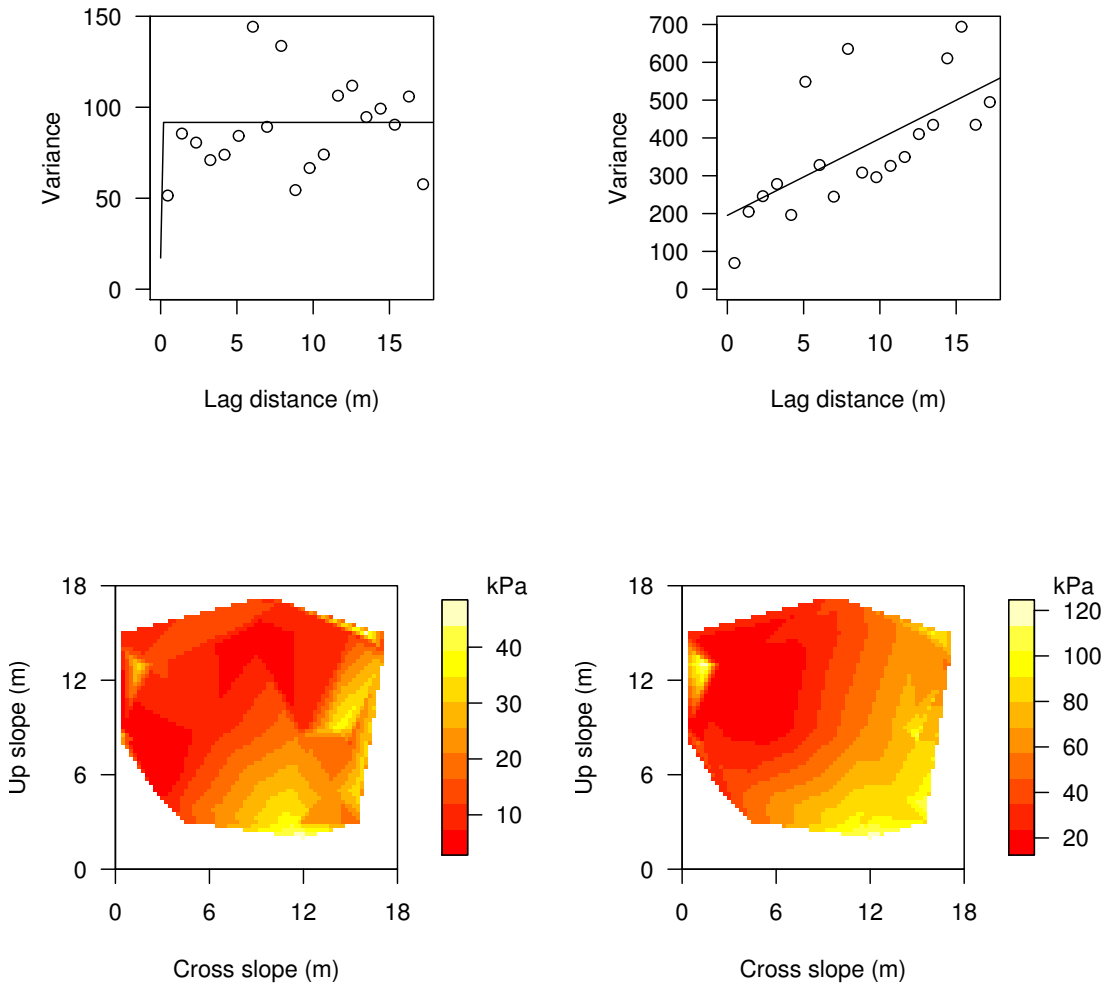
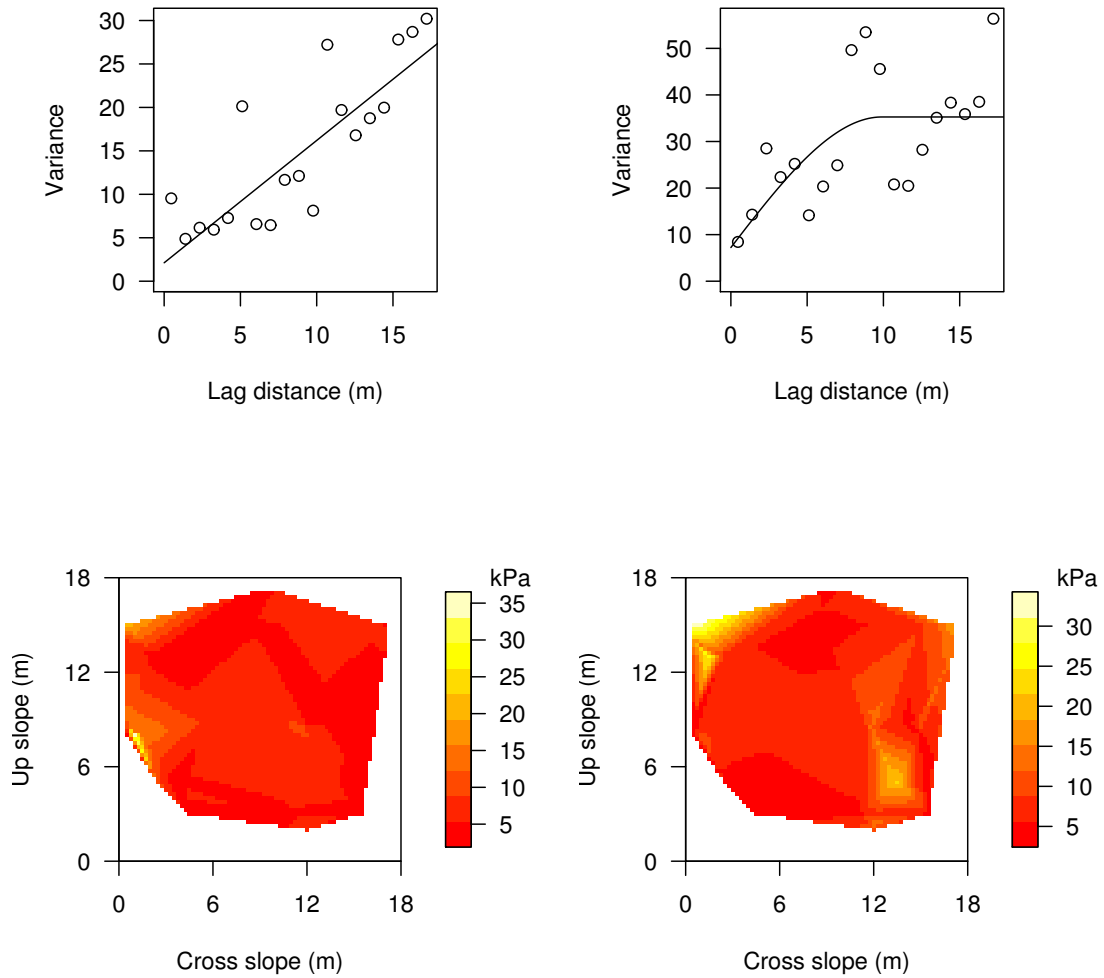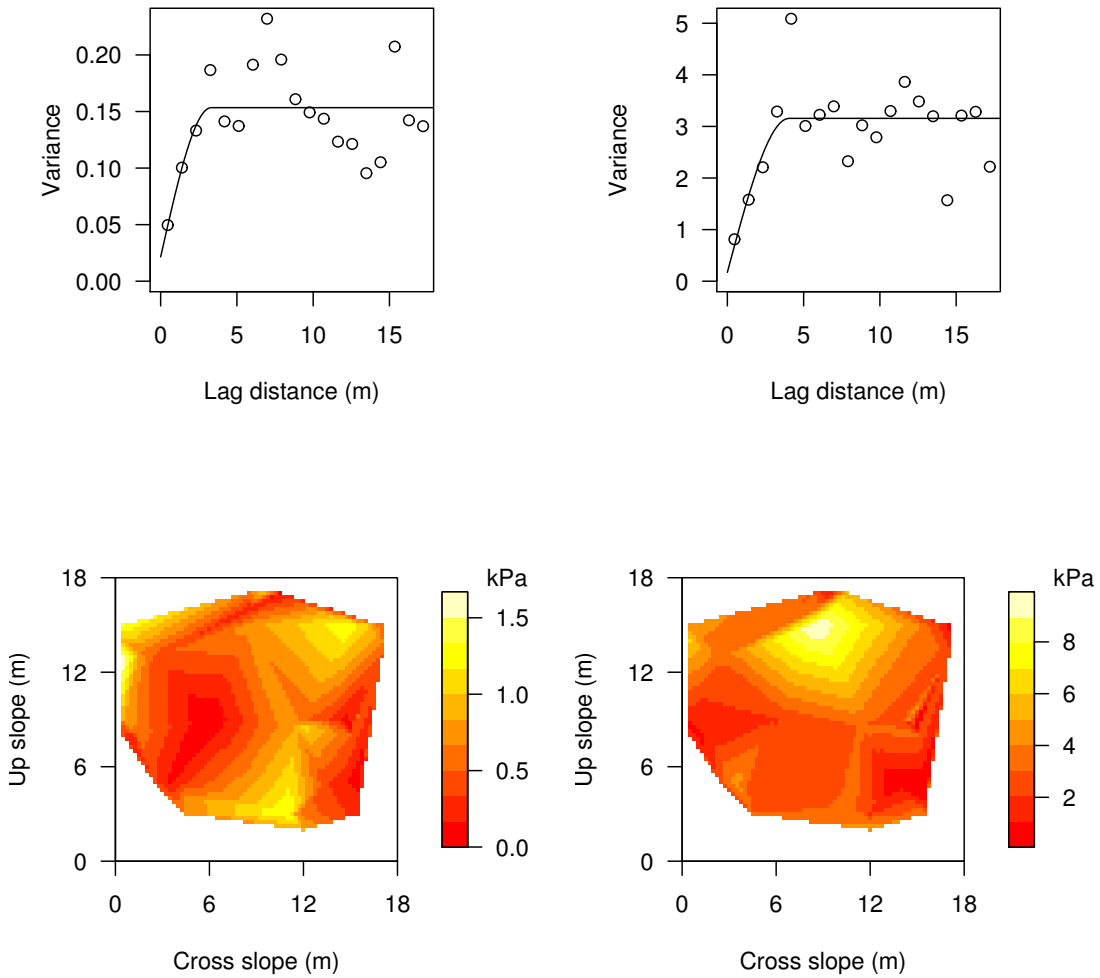**Figure B.5**: Grid 6 winter 2006 - 2007. Experimental variogram (open circles) and modeled variogram of the parameter Ψ for the weak layer (top left) and the slab layers (top right). Contour plots of the parameter Ψ for the weak layer (bottom left) and the slab layer (bottom right).
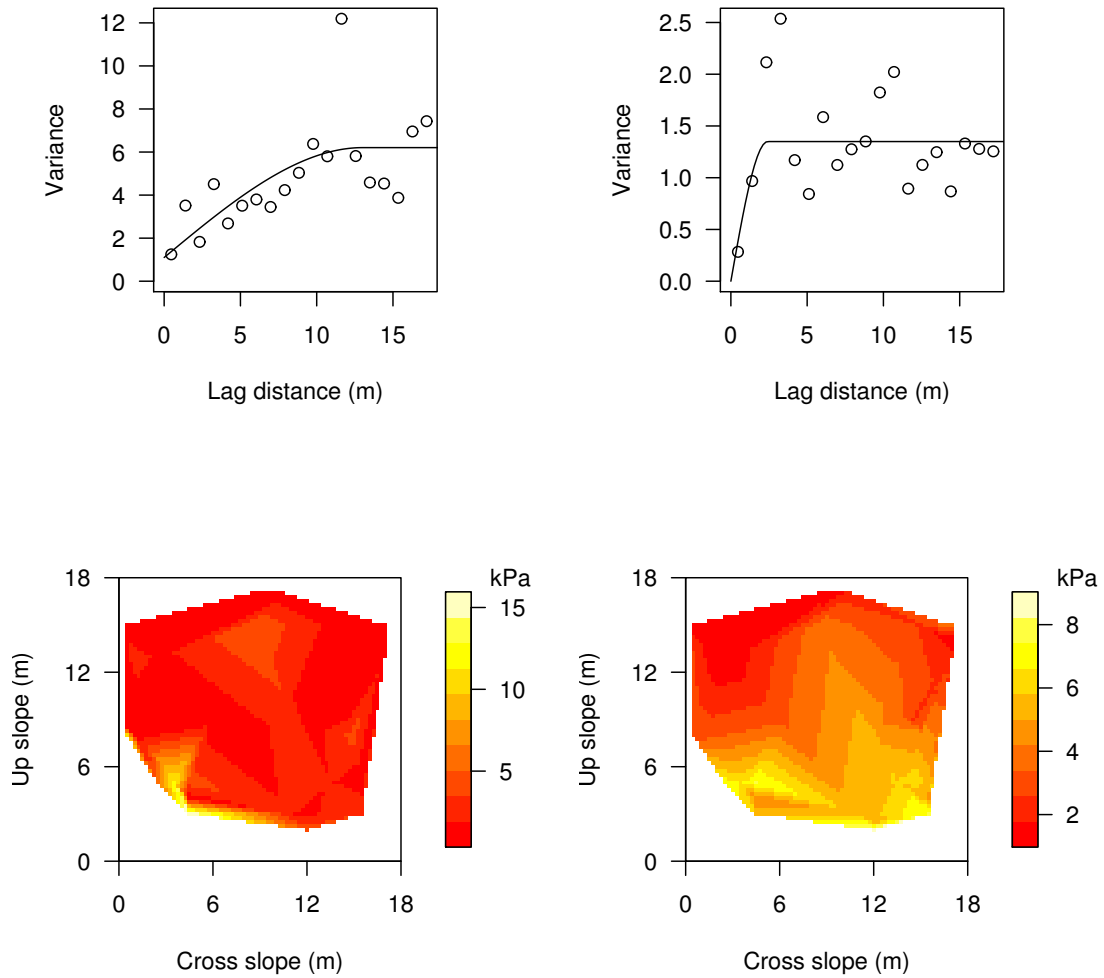
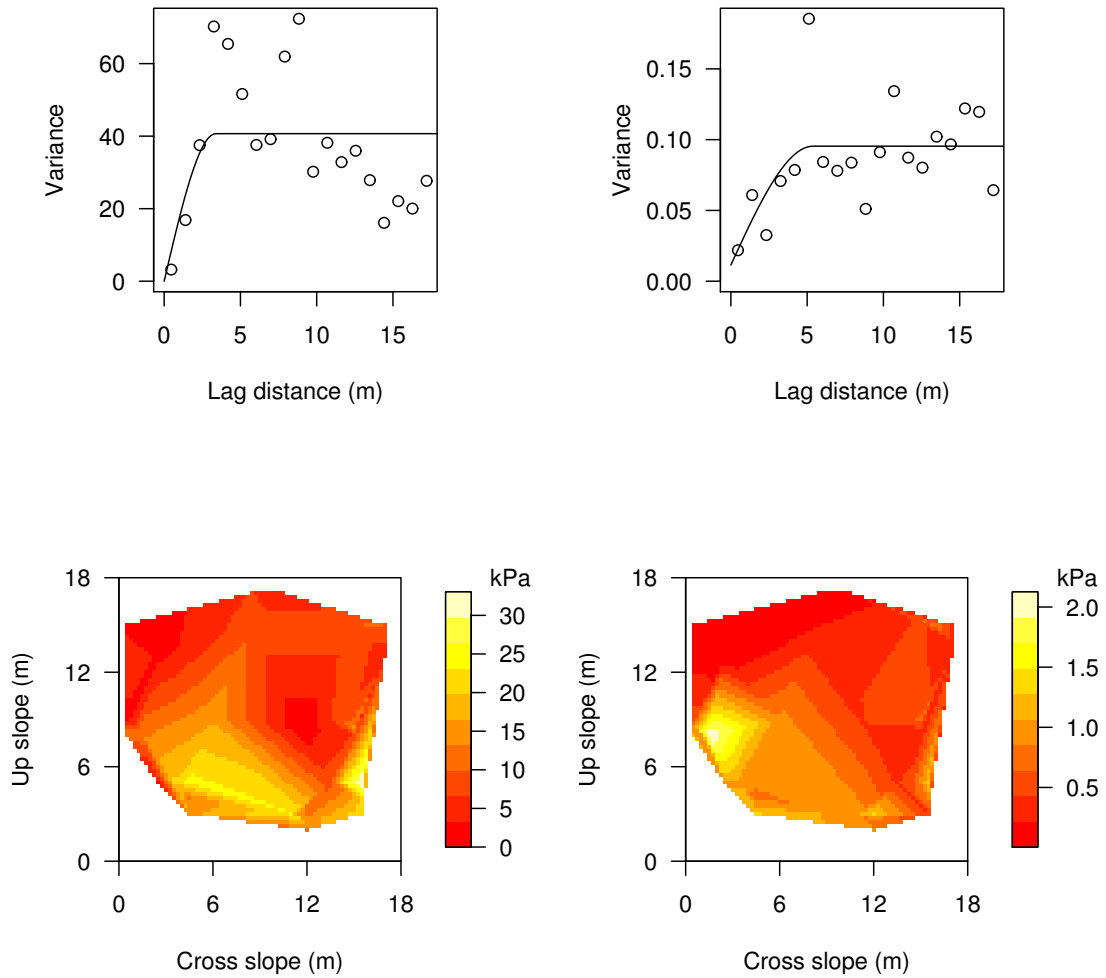**Figure B.6:** Grid 1 winter 2007 - 2008. Experimental variogram (open circles) and modeled variogram of the parameter Ψ for the weak layer (top left) and the slab layers (top right). Contour plots of the parameter Ψ for the weak layer (bottom left) and the slab layer (bottom right).
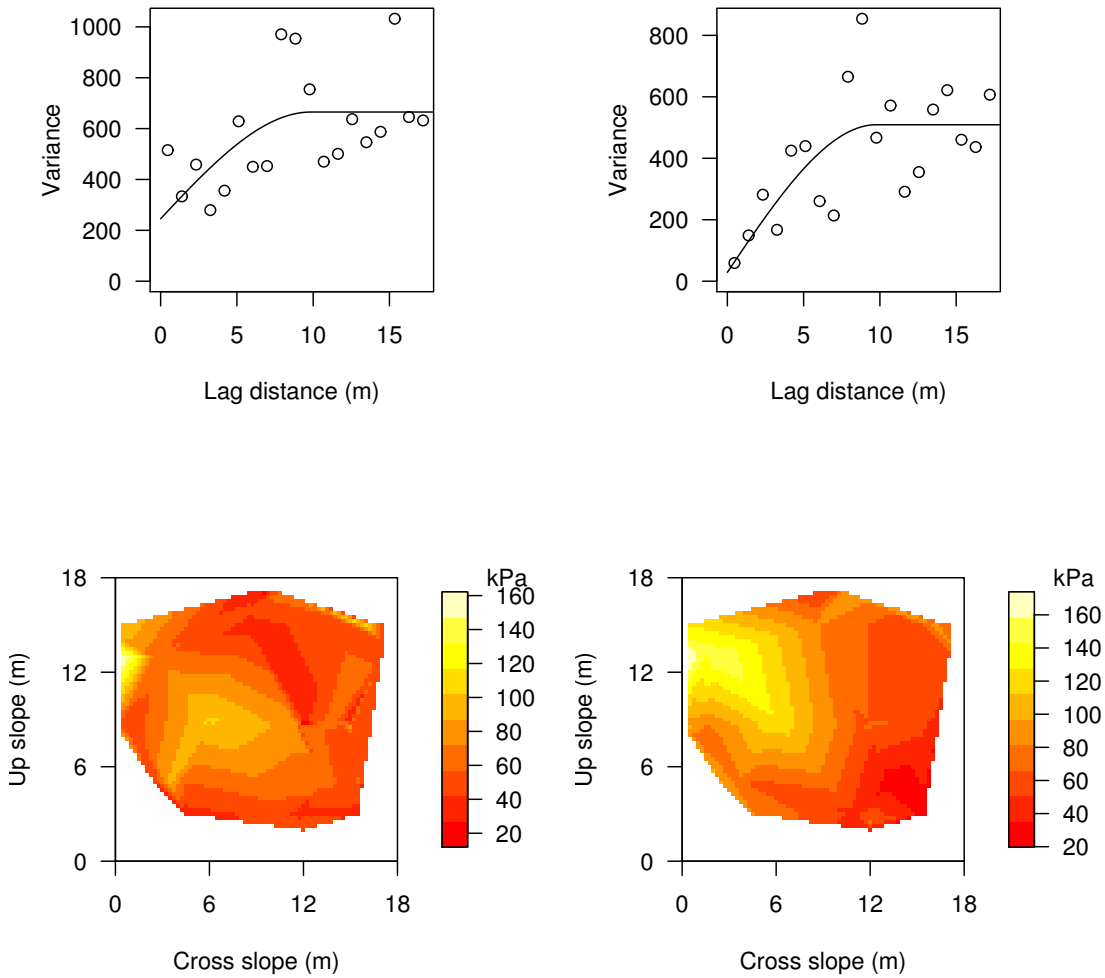
Figure B.7: Grid 2 winter 2007 - 2008. Experimental variogram (open circles) and modeled variogram of the parameter Ψ for the weak layer (top left) and the slab layers (top right). Contour plots of the parameter Ψ for the weak layer (bottom left) and the slab layer (bottom right).
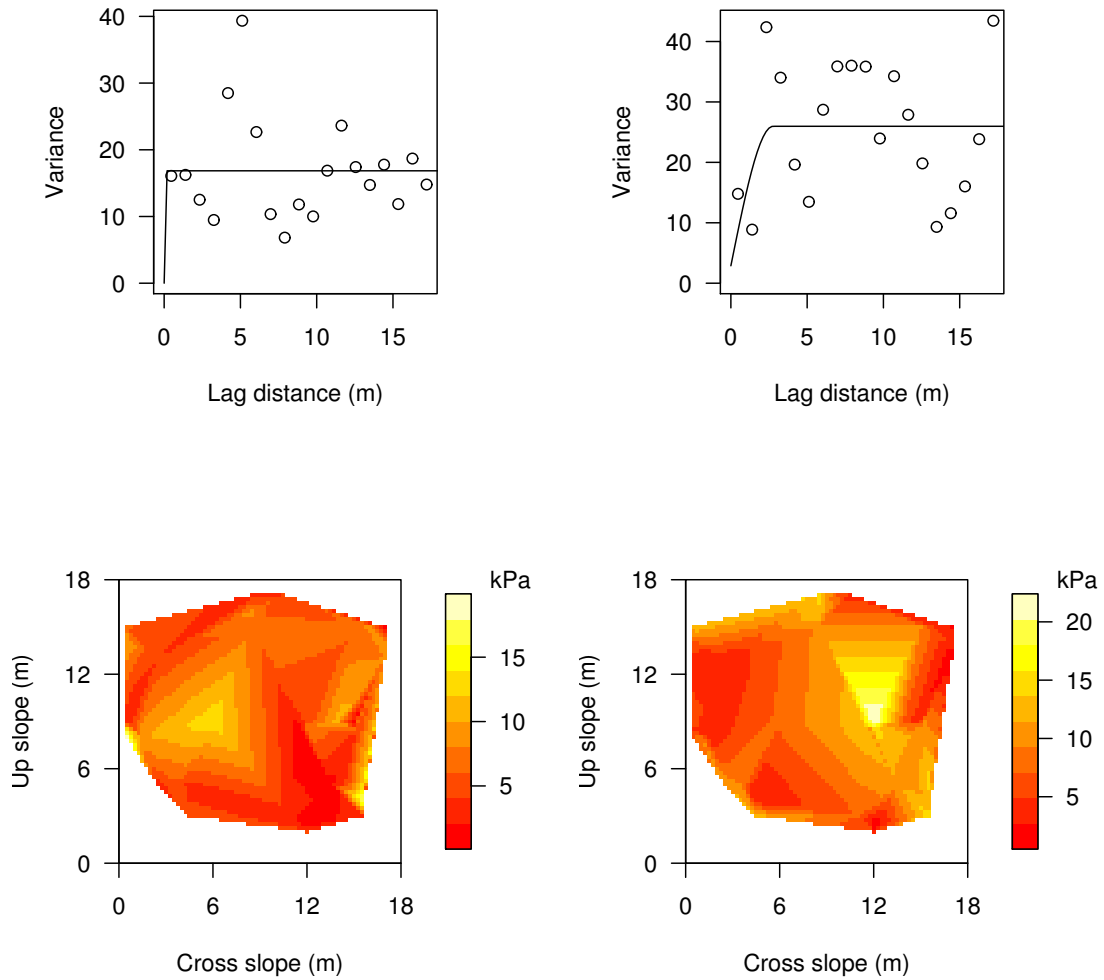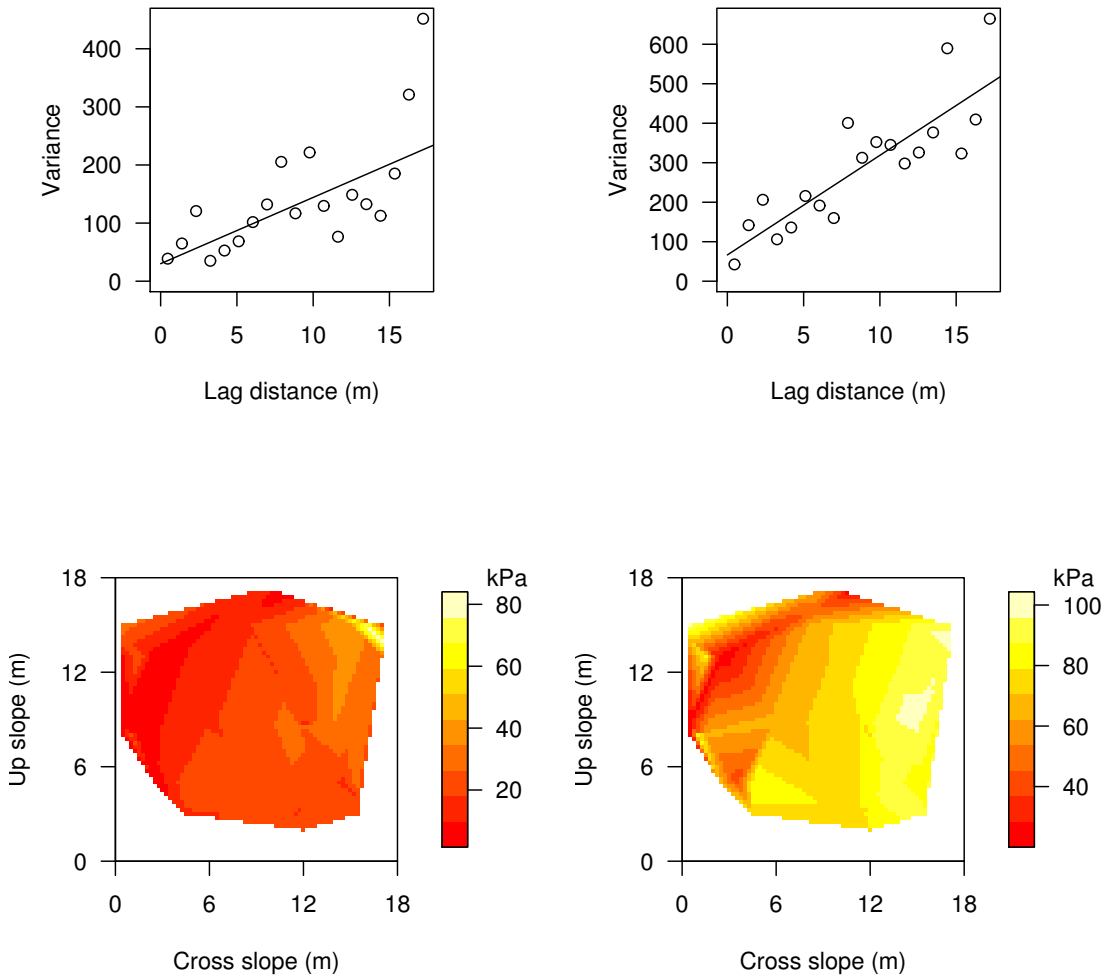
Figure B.8: Grid 3 winter 2007 - 2008. Experimental variogram (open circles) and modeled variogram of the parameter Ψ for the weak layer (top left) and the slab layers (top right). Contour plots of the parameter Ψ for the weak layer (bottom left) and the slab layer (bottom right).

Figure B.9: Grid 4 winter 2007 - 2008. Experimental variogram (open circles) and modeled variogram of the parameter Ψ for the weak layer (top left) and the slab layers (top right). Contour plots of the parameter Ψ for the weak layer (bottom left) and the slab layer (bottom right).
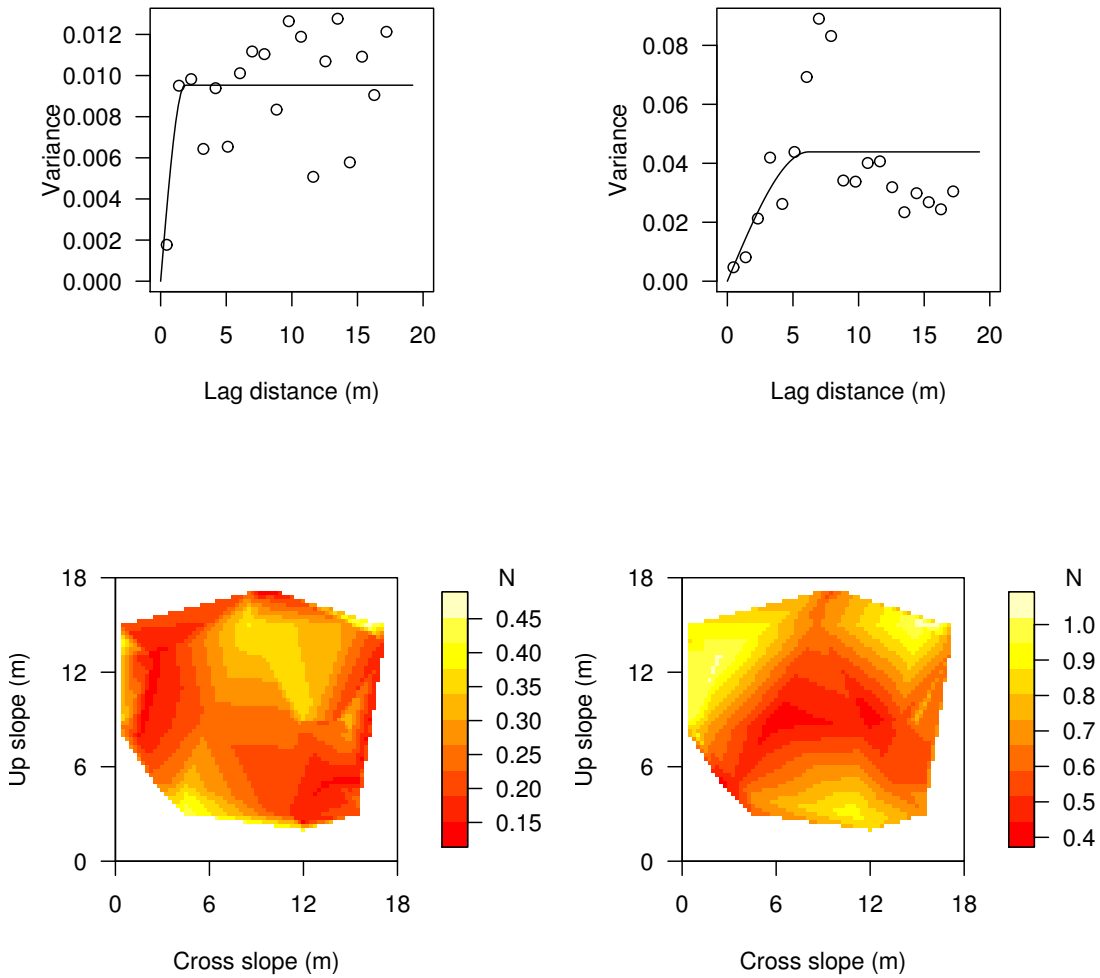
Figure B.10: Grid 5 winter 2007 - 2008. Experimental variogram (open circles) and modeled variogram of the parameter Ψ for the weak layer (top left) and the slab layers (top right). Contour plots of the parameter Ψ for the weak layer (bottom left) and the slab layer (bottom right).

Figure B.11: Grid 6 winter 2007 - 2008. Experimental variogram (open circles) and modeled variogram of the parameter Ψ for the weak layer (top left) and the slab layers (top right). Contour plots of the parameter Ψ for the weak layer (bottom left) and the slab layer (bottom right).

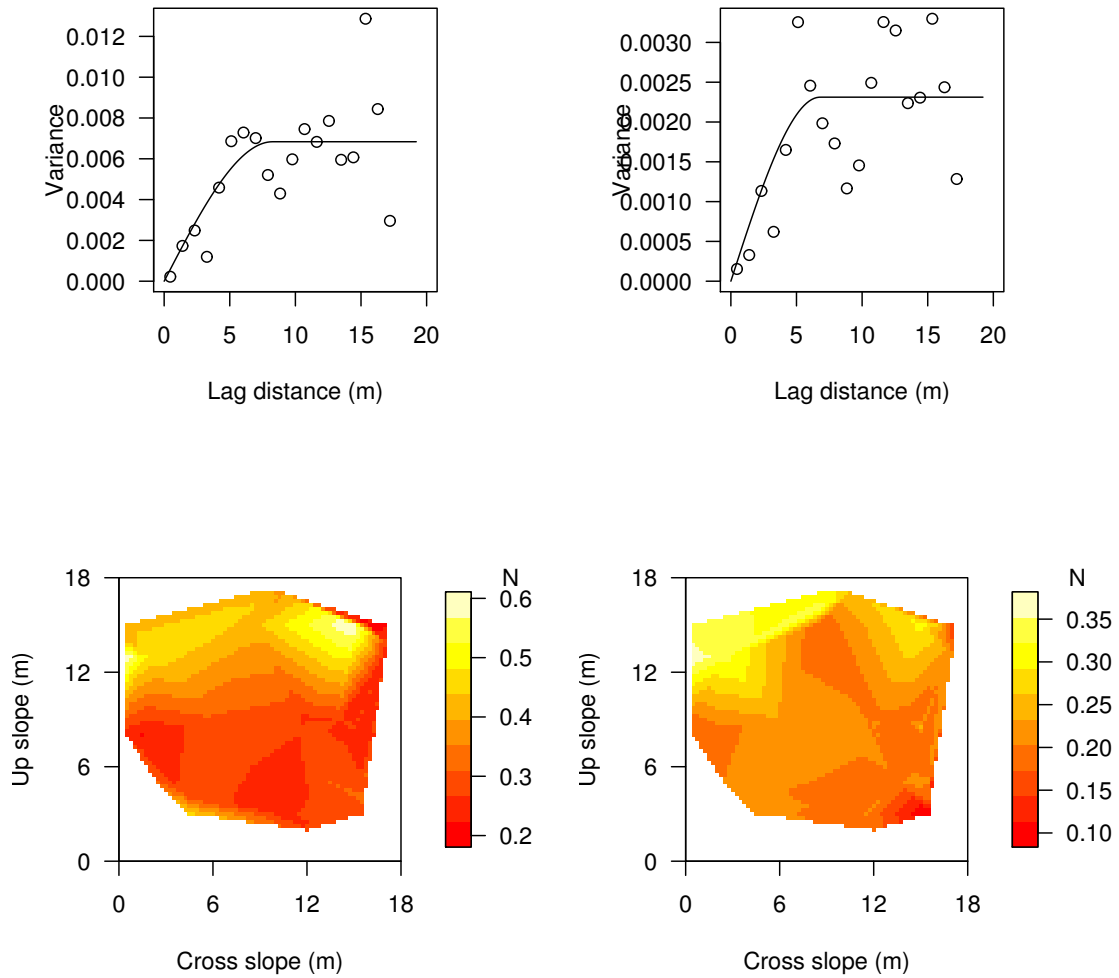**Figure B.12:** Grid 7 winter 2007 - 2008. Experimental variogram (open circles) and modeled variogram of the parameter Ψ for the weak layer (top left) and the slab layers (top right). Contour plots of the parameter Ψ for the weak layer (bottom left) and the slab layer (bottom right).
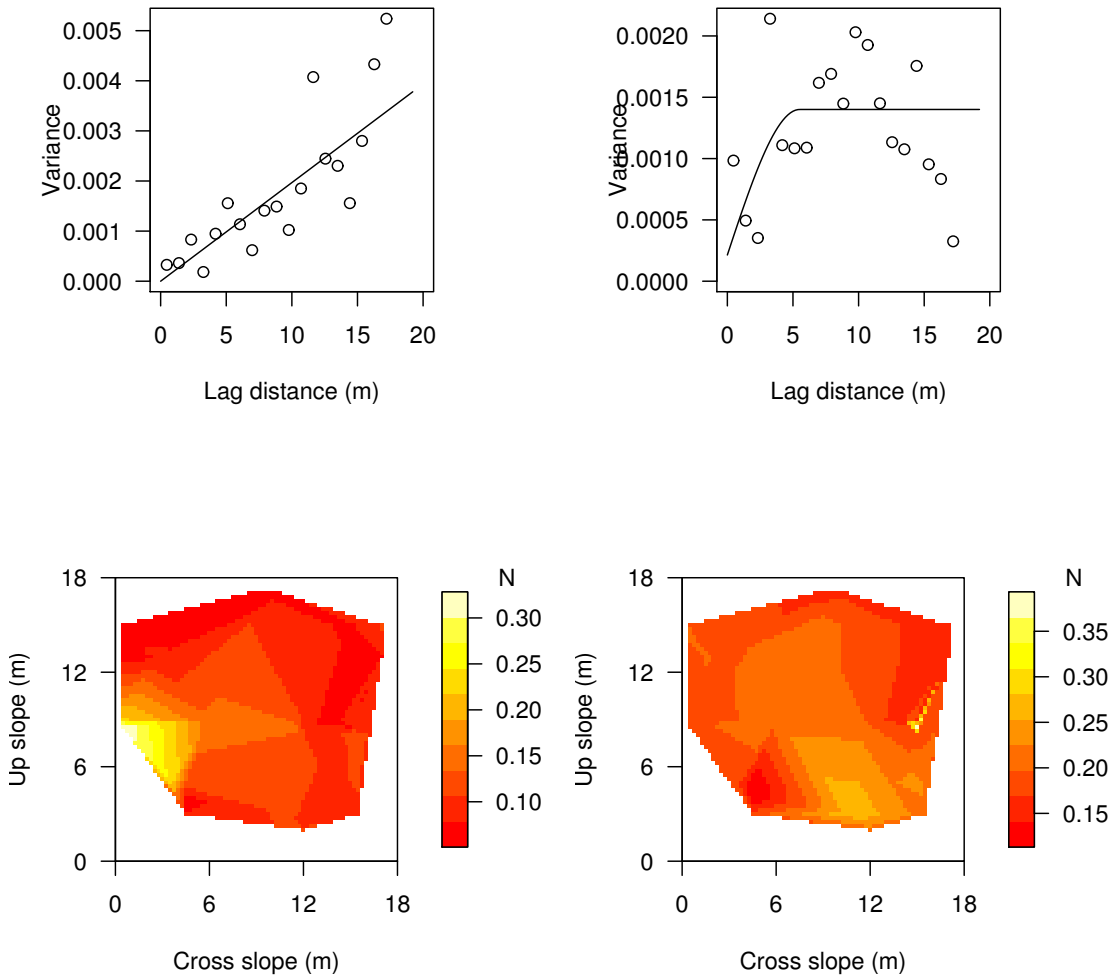
Figure B.13: Grid 9 winter 2007 - 2008. Experimental variogram (open circles) and modeled variogram of the parameter Ψ for the weak layer (top left) and the slab layers (top right). Contour plots of the parameter Ψ for the weak layer (bottom left) and the slab layer (bottom right).

Figure B.14: Grid 2 winter 2008 - 2009. Experimental variogram (open circles) and modeled variogram of the parameter Ψ for the weak layer (top left) and the slab layers (top right). Contour plots of the parameter Ψ for the weak layer (bottom left) and the slab layer (bottom right).
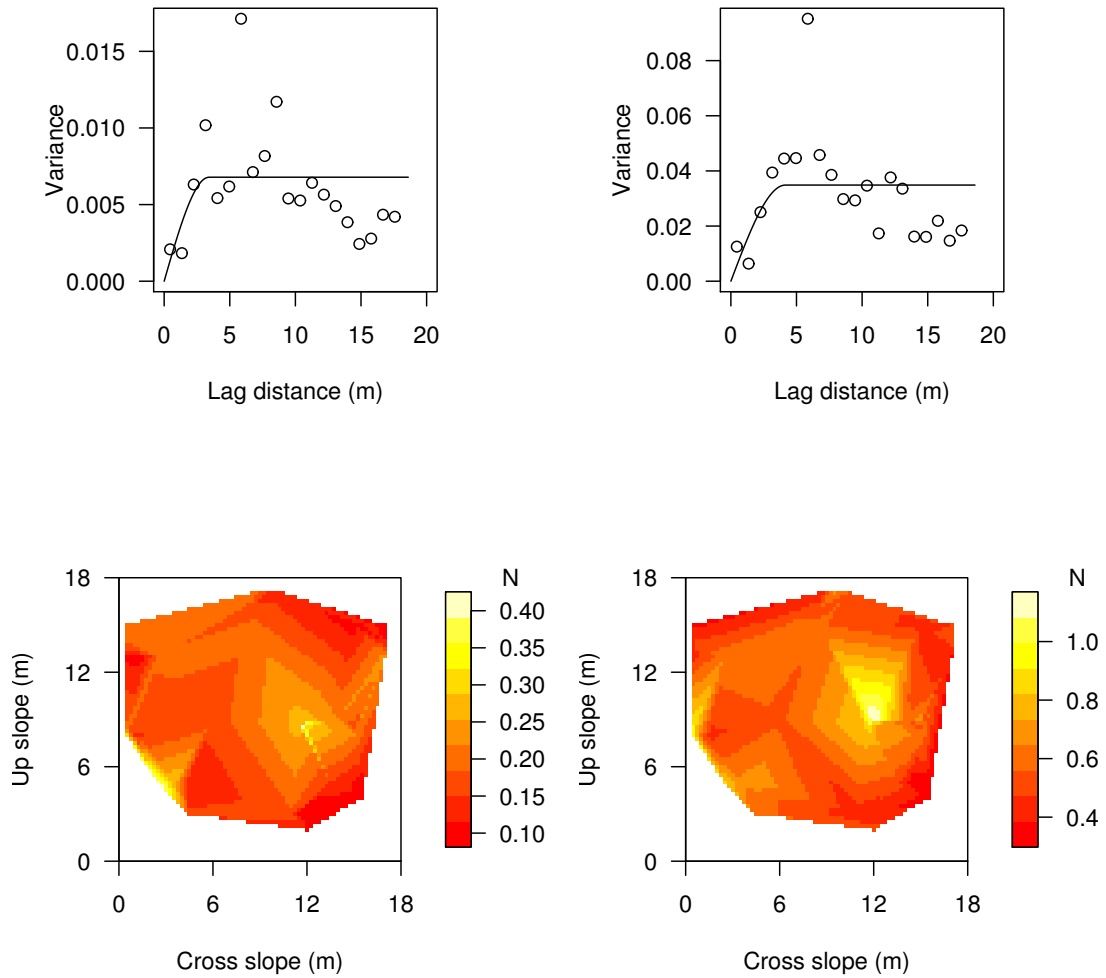
Figure B.15: Grid 4 winter 2008 - 2009. Experimental variogram (open circles) and modeled variogram of the parameter Ψ for the weak layer (top left) and the slab layers (top right). Contour plots of the parameter Ψ for the weak layer (bottom left) and the slab layer (bottom right).
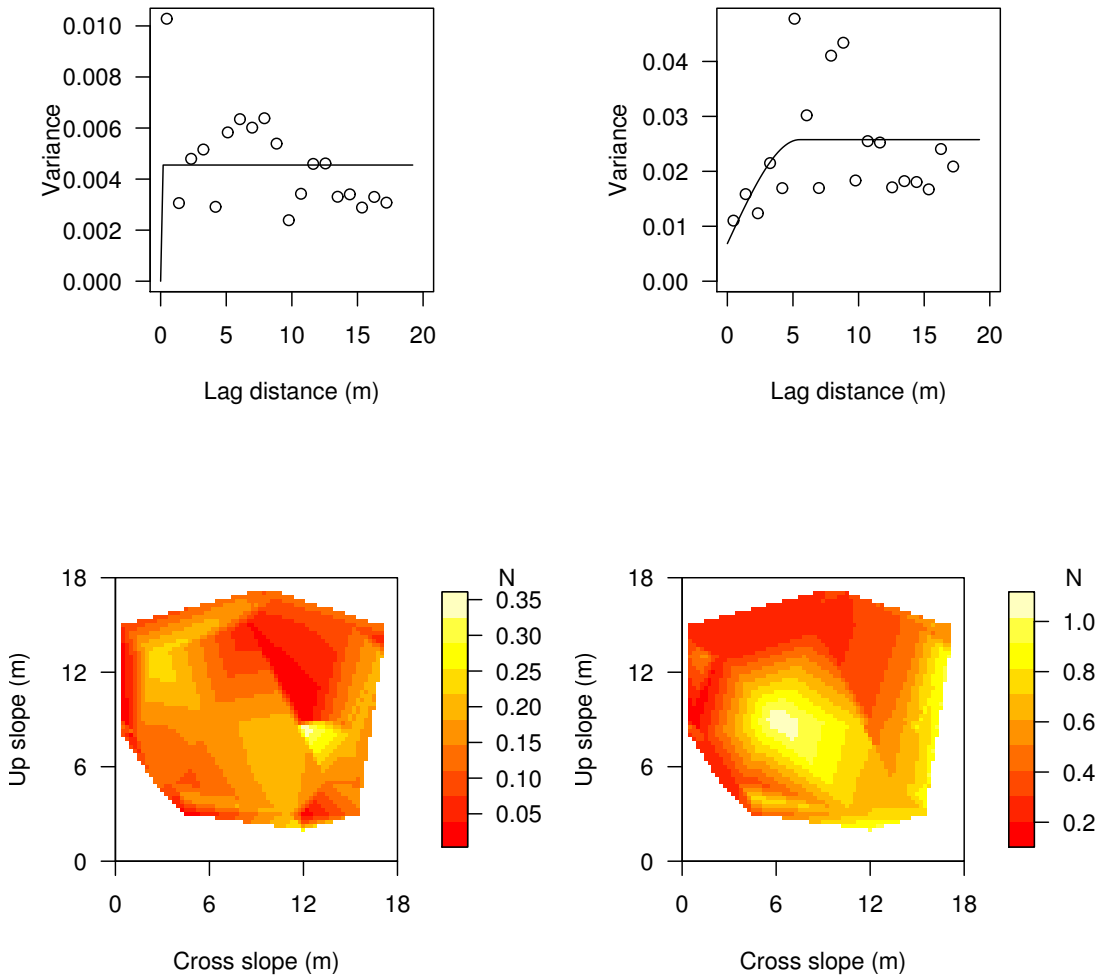
Figure B.16: Grid 6 winter 2008 - 2009. Experimental variogram (open circles) and modeled variogram of the parameter Ψ for the weak layer (top left) and the slab layers (top right). Contour plots of the parameter Ψ for the weak layer (bottom left) and the slab layer (bottom right).
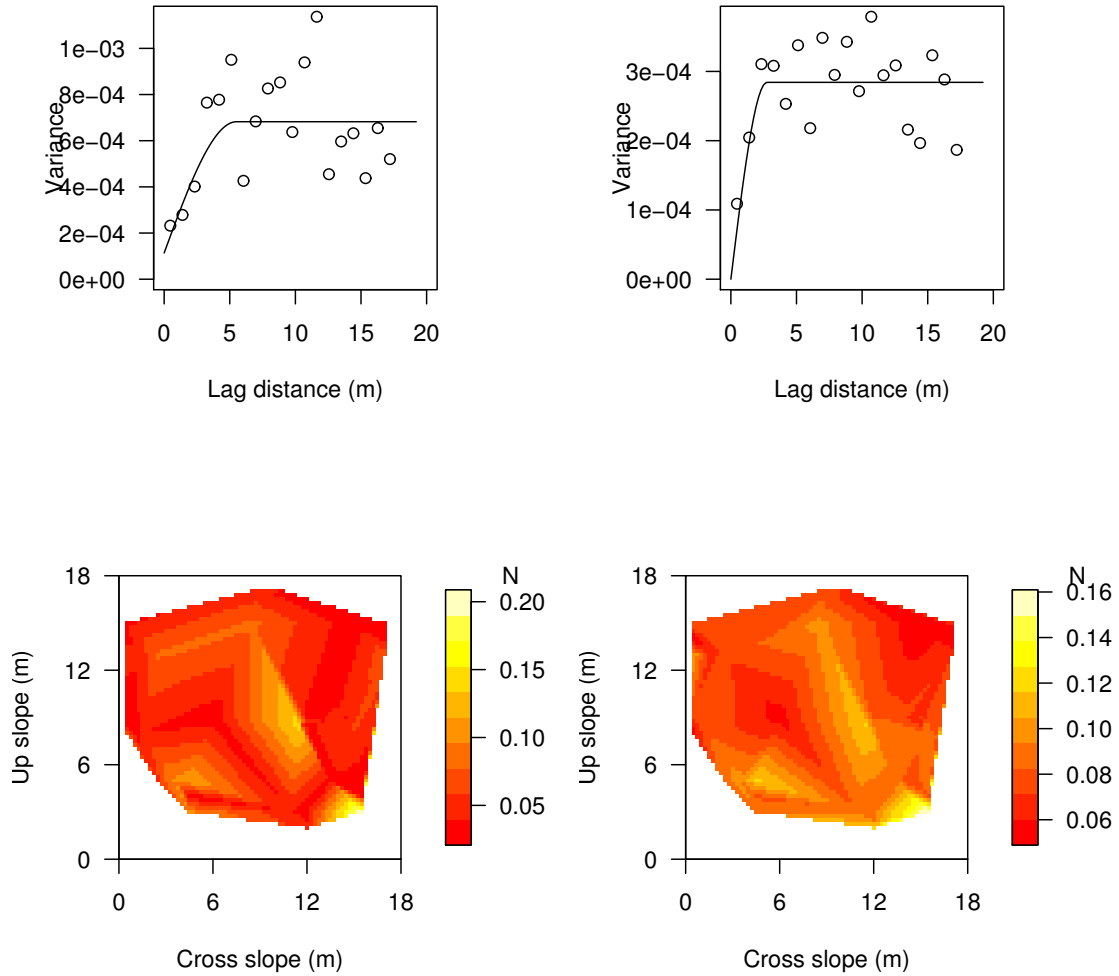
Figure B.17: Grid 7 winter 2008 - 2009. Experimental variogram (open circles) and modeled variogram of the parameter Ψ for the weak layer (top left) and the slab layers (top right). Contour plots of the parameter Ψ for the weak layer (bottom left) and the slab layer (bottom right).

Appendix C

Sample (open circles) and theoretical variogram (solid line) of the weak layer and slab layer mean penetration resistance F for the winter between 2006 and 2009. In addition shown are the contour plots of the weak layer and slab layer mean penetration resistance F. The mean penetration resistance values were not detrended.

Figure C.1: Grid 1 winter 2006 - 2007. Experimental variogram (open circles) and modeled variogram of the mean penetration resistance F for the weak layer (top left) and the slab layers (top right). Contour plots of the mean penetration resistance F for the weak layer (bottom left) and the slab layer (bottom right).
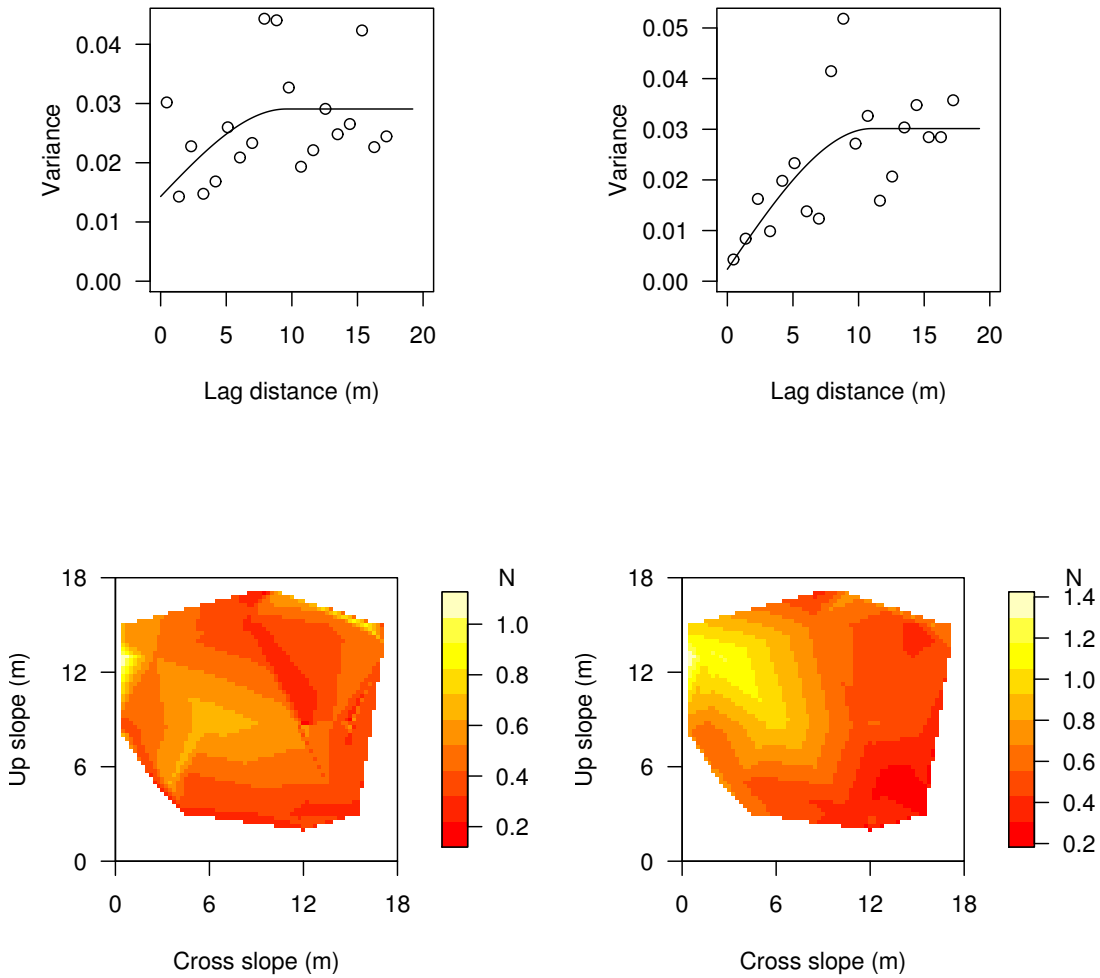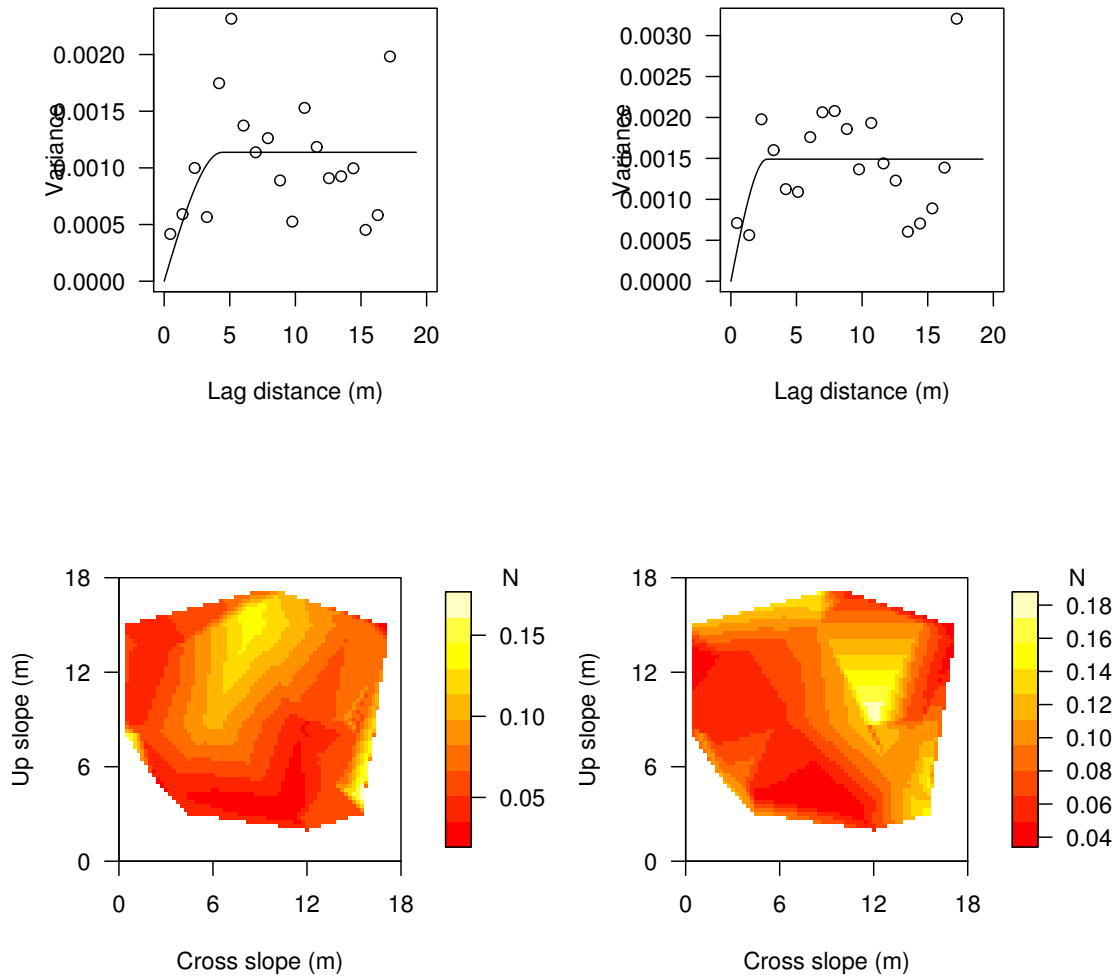
Figure C.2: Grid 2 winter 2006 - 2007. Experimental variogram (open circles) and modeled variogram of the mean penetration resistance F for the weak layer (top left) and the slab layers (top right). Contour plots of the mean penetration resistance F for the weak layer (bottom left) and the slab layer (bottom right).
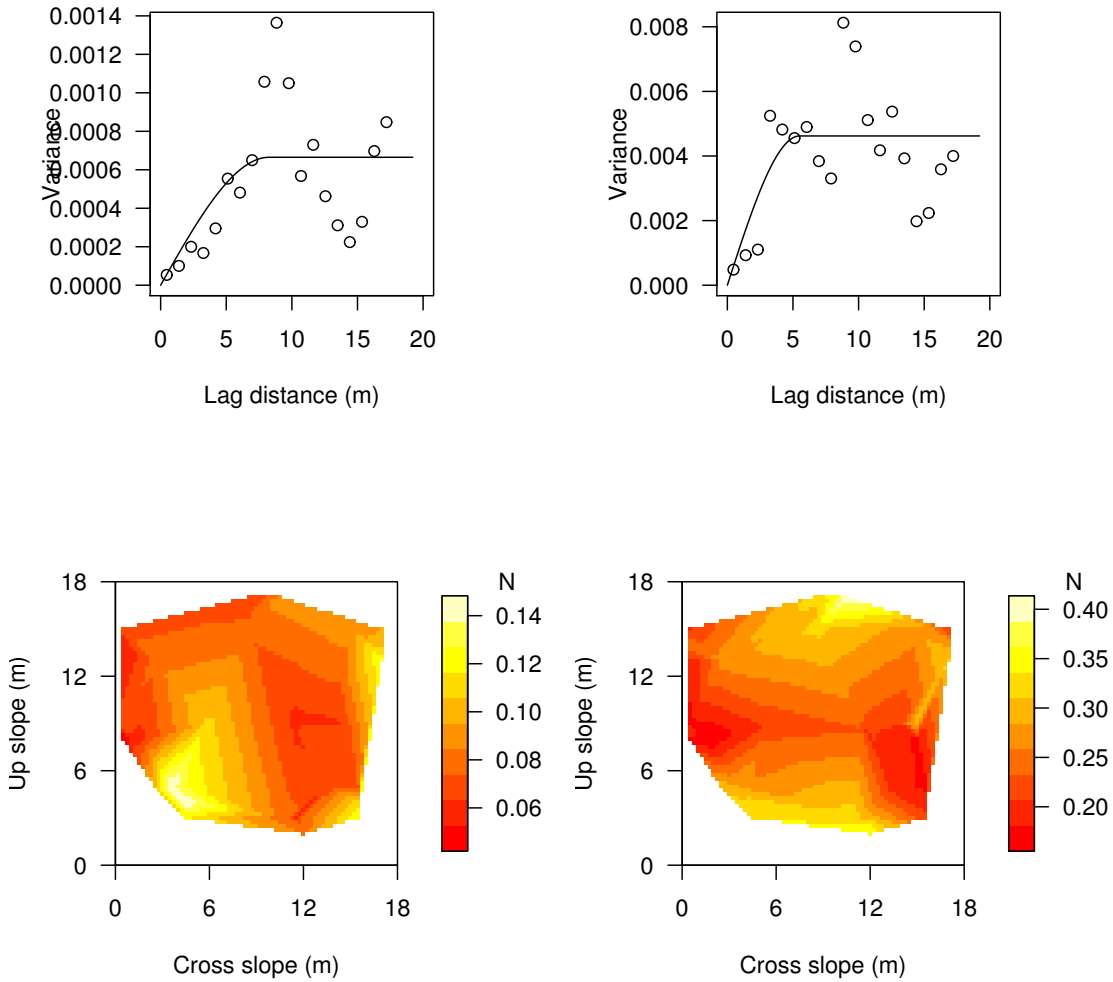
Figure C.3: Grid 3 winter 2006 - 2007. Experimental variogram (open circles) and modeled variogram of the mean penetration resistance F for the weak layer (top left) and the slab layers (top right). Contour plots of the mean penetration resistance F for the weak layer (bottom left) and the slab layer (bottom right).

Figure C.4: Grid 5 winter 2006 - 2007. Experimental variogram (open circles) and modeled variogram of the mean penetration resistance F for the weak layer (top left) and the slab layers (top right). Contour plots of the mean penetration resistance F for the weak layer (bottom left) and the slab layer (bottom right).
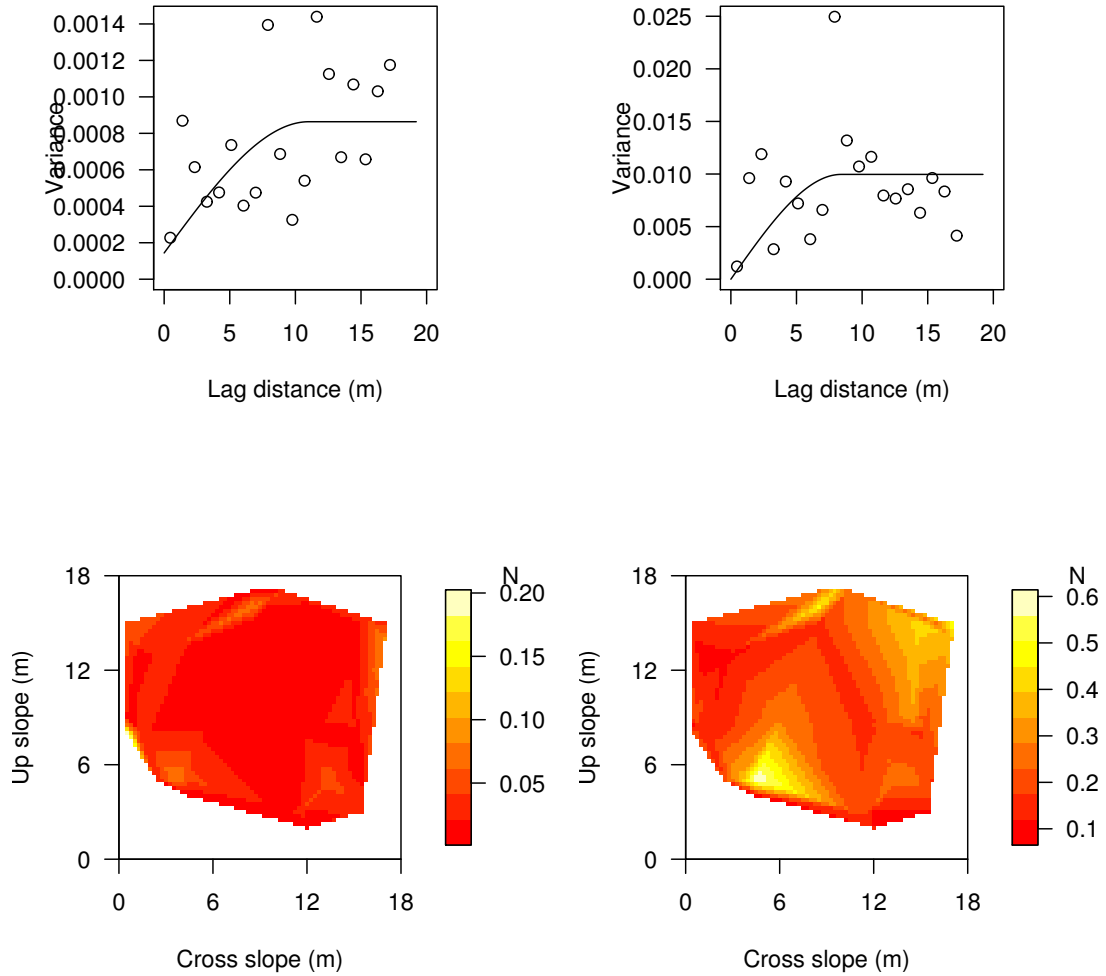
Figure C.5: Grid 6 winter 2006 - 2007. Experimental variogram (open circles) and modeled variogram of the mean penetration resistance F for the weak layer (top left) and the slab layers (top right). Contour plots of the mean penetration resistance F for the weak layer (bottom left) and the slab layer (bottom right).

Figure C.6: Grid 1 winter 2007 - 2008. Experimental variogram (open circles) and modeled variogram of the mean penetration resistance F for the weak layer (top left) and the slab layers (top right). Contour plots of the mean penetration resistance F for the weak layer (bottom left) and the slab layer (bottom right).
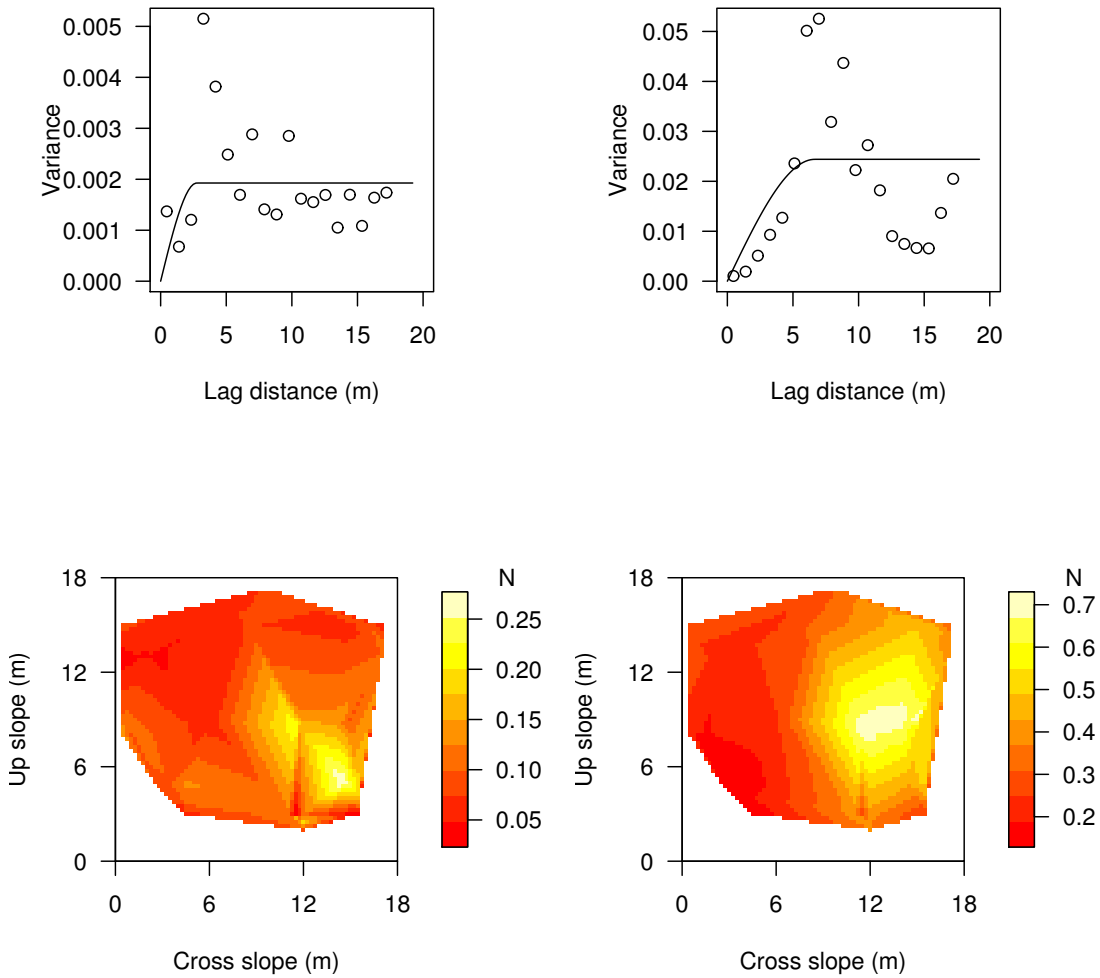
Figure C.7: Grid 2 winter 2007 - 2008. Experimental variogram (open circles) and modeled variogram of the mean penetration resistance F for the weak layer (top left) and the slab layers (top right). Contour plots of the mean penetration resistance F for the weak layer (bottom left) and the slab layer (bottom right).
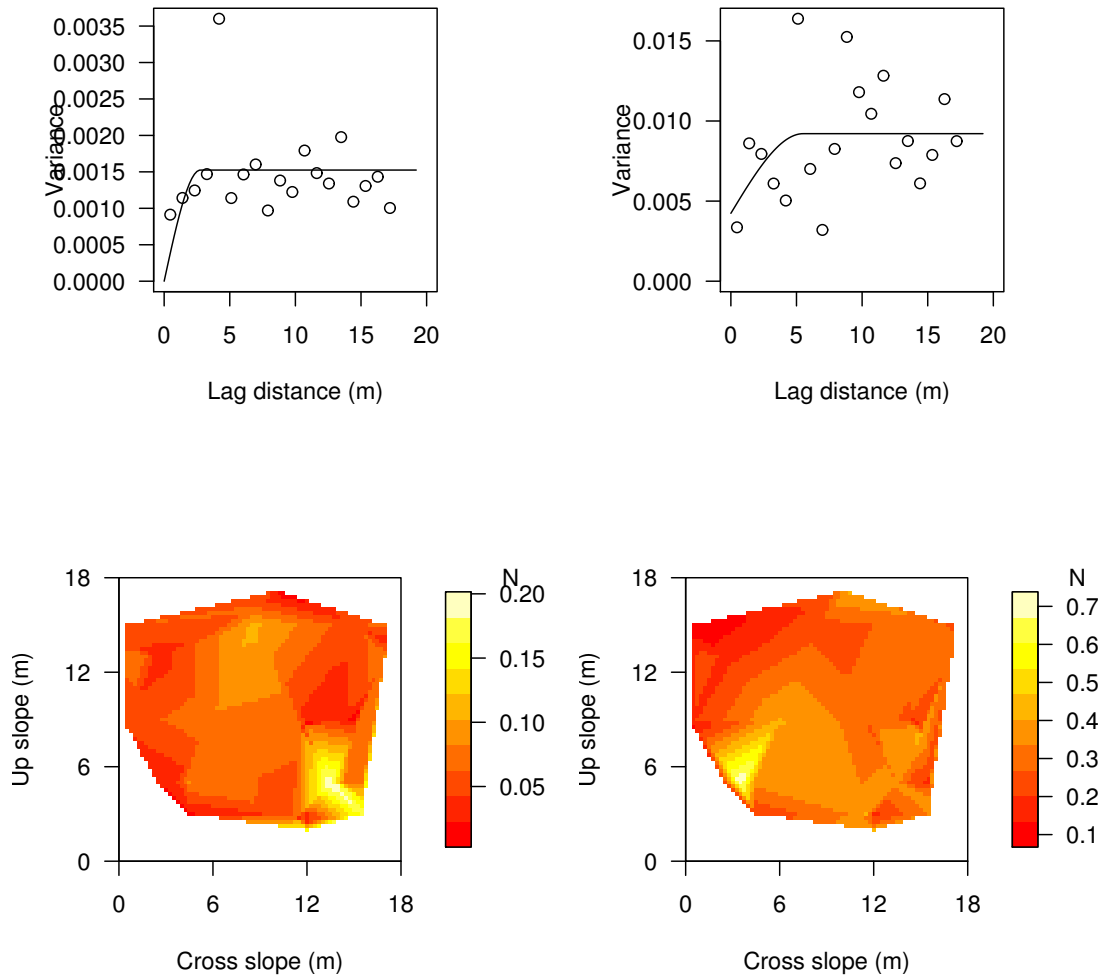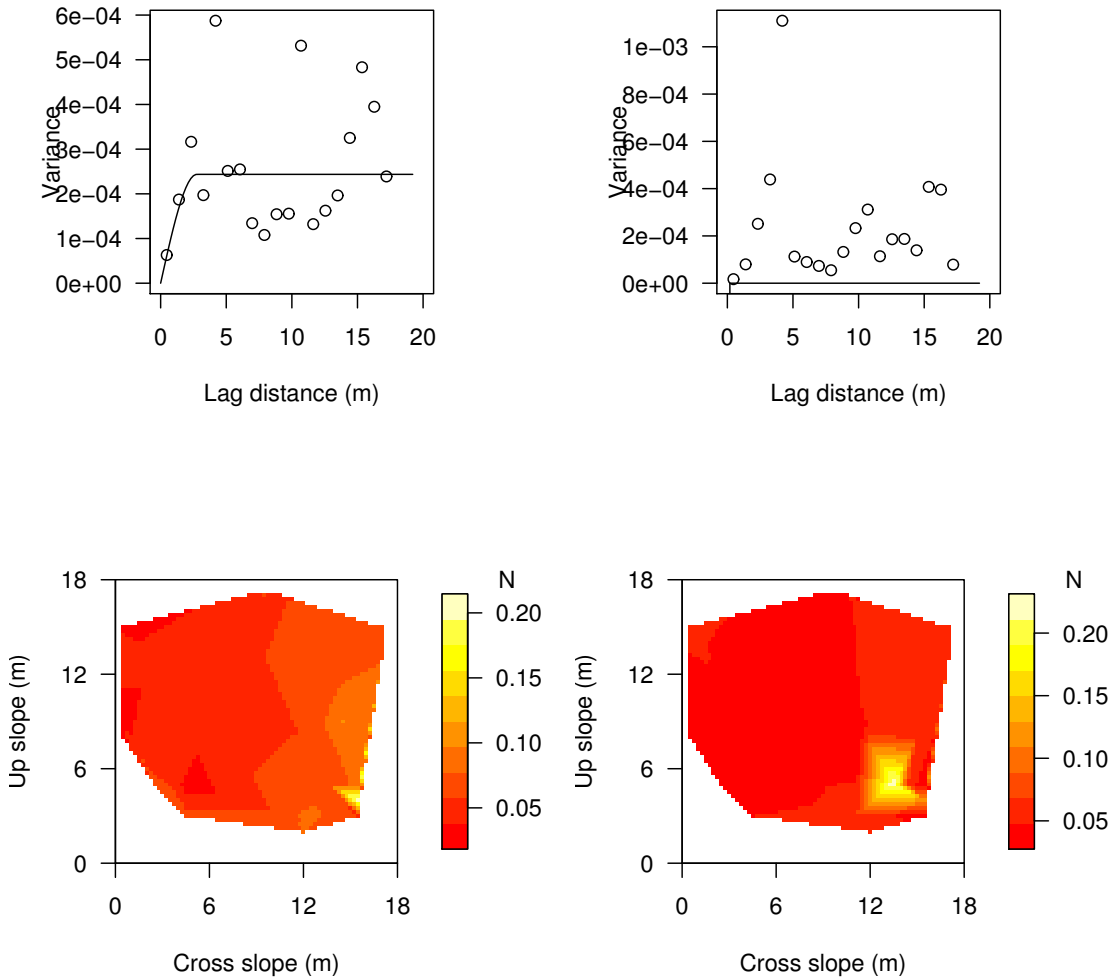
Figure C.8: Grid 3 winter 2007 - 2008. Experimental variogram (open circles) and modeled variogram of the mean penetration resistance F for the weak layer (top left) and the slab layers (top right). Contour plots of the mean penetration resistance F for the weak layer (bottom left) and the slab layer (bottom right).

Figure C.9: Grid 4 winter 2007 - 2008. Experimental variogram (open circles) and modeled variogram of the mean penetration resistance F for the weak layer (top left) and the slab layers (top right). Contour plots of the mean penetration resistance F for the weak layer (bottom left) and the slab layer (bottom right).
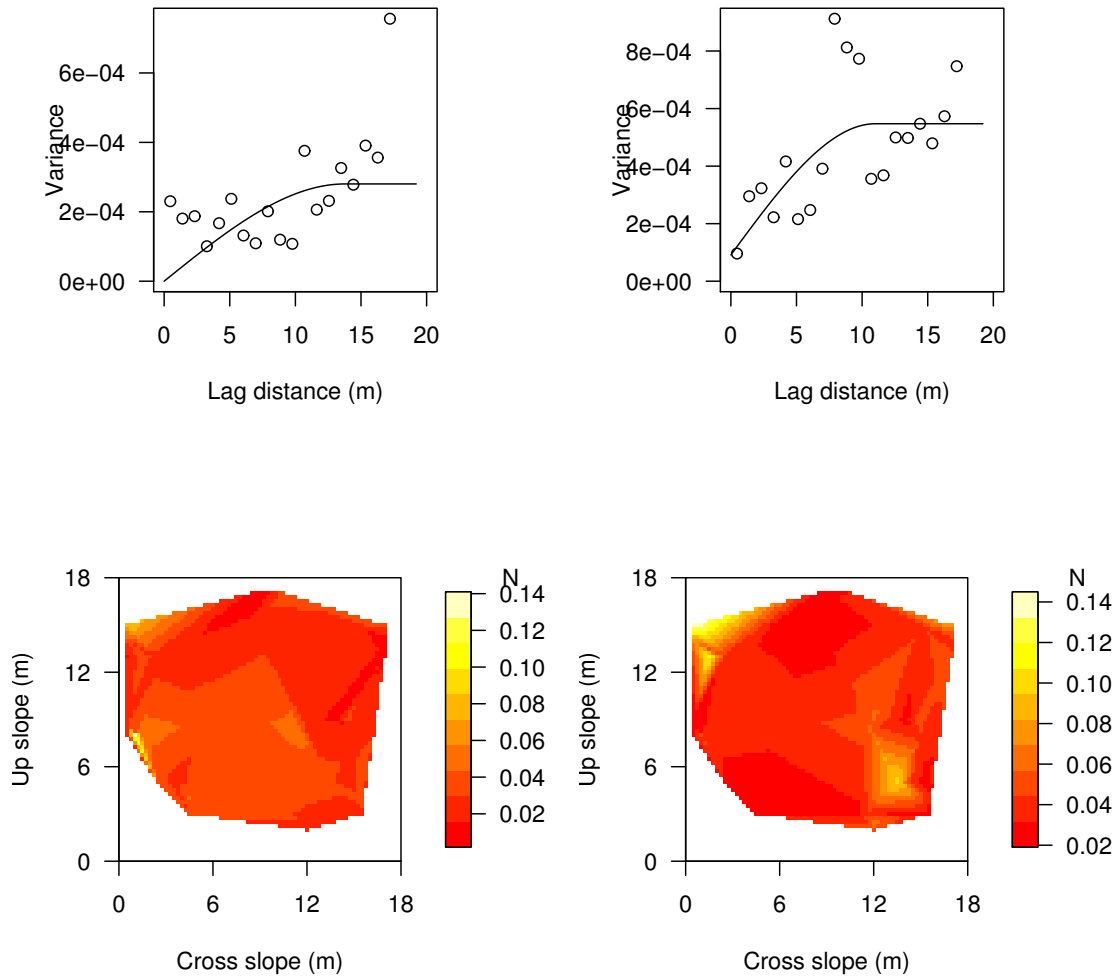
Figure C.10: Grid 5 winter 2007 - 2008. Experimental variogram (open circles) and modeled variogram of the mean penetration resistance F for the weak layer (top left) and the slab layers (top right). Contour plots of the mean penetration resistance F for the weak layer (bottom left) and the slab layer (bottom right).
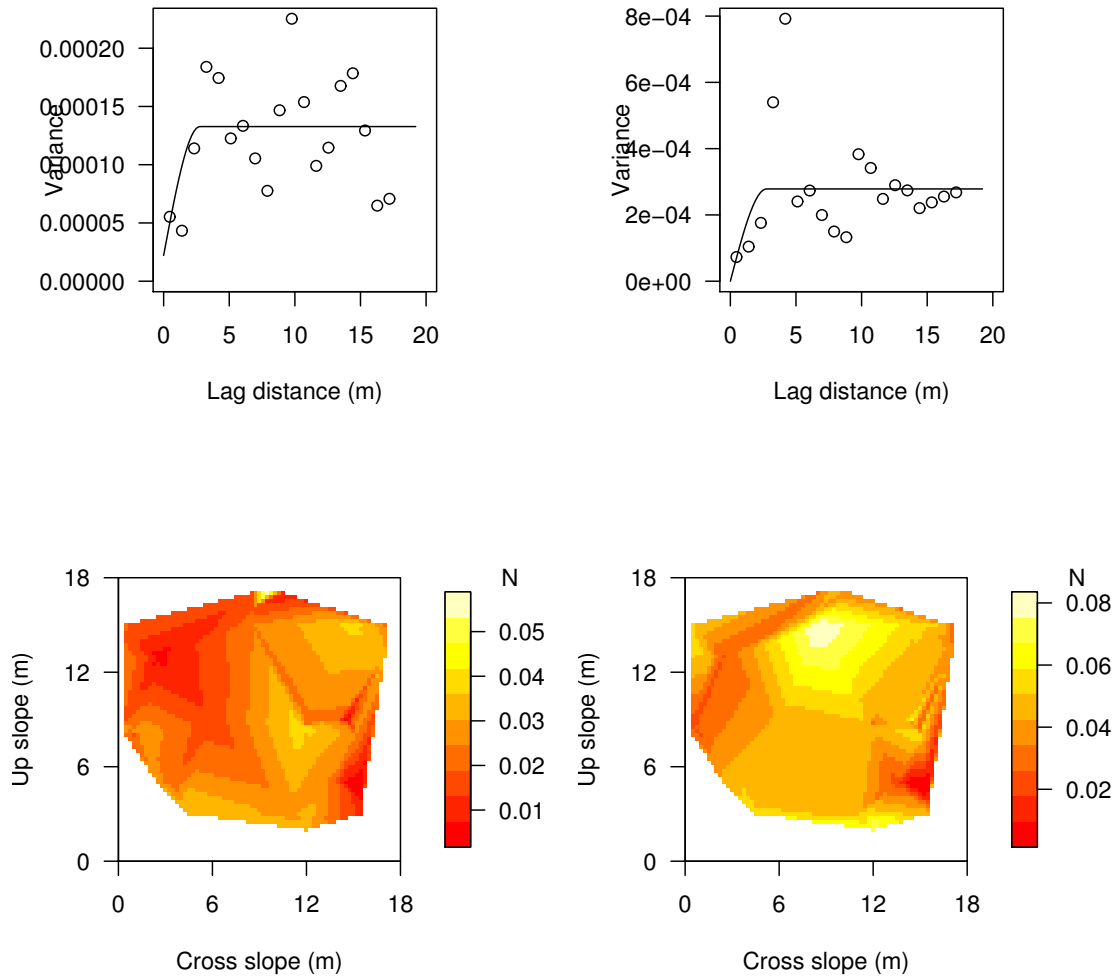
Figure C.11: Grid 6 winter 2007 - 2008. Experimental variogram (open circles) and modeled variogram of the mean penetration resistance F for the weak layer (top left) and the slab layers (top right). Contour plots of the mean penetration resistance F for the weak layer (bottom left) and the slab layer (bottom right).
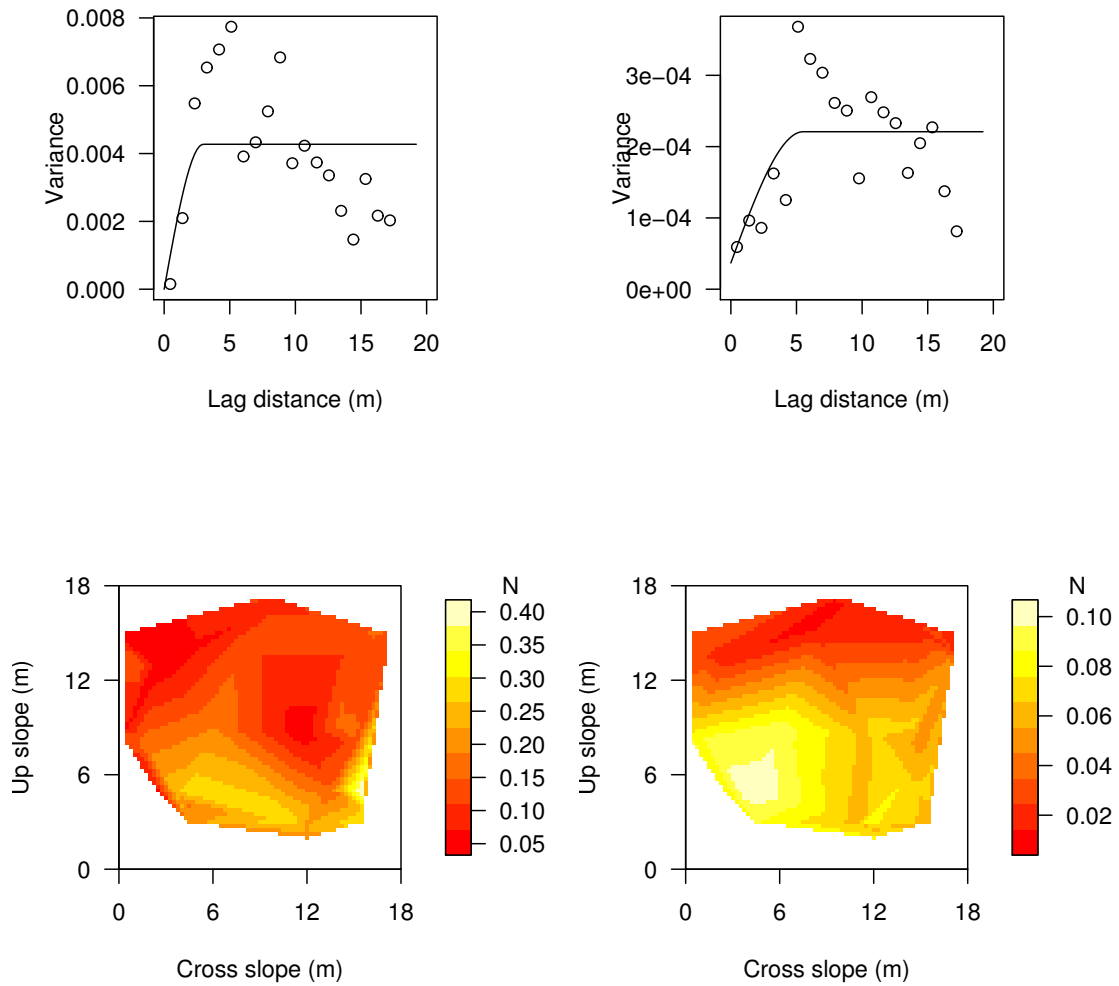
Figure C.12: Grid 7 winter 2007 - 2008. Experimental variogram (open circles) and modeled variogram of the mean penetration resistance F for the weak layer (top left) and the slab layers (top right). Contour plots of the mean penetration resistance F for the weak layer (bottom left) and the slab layer (bottom right).
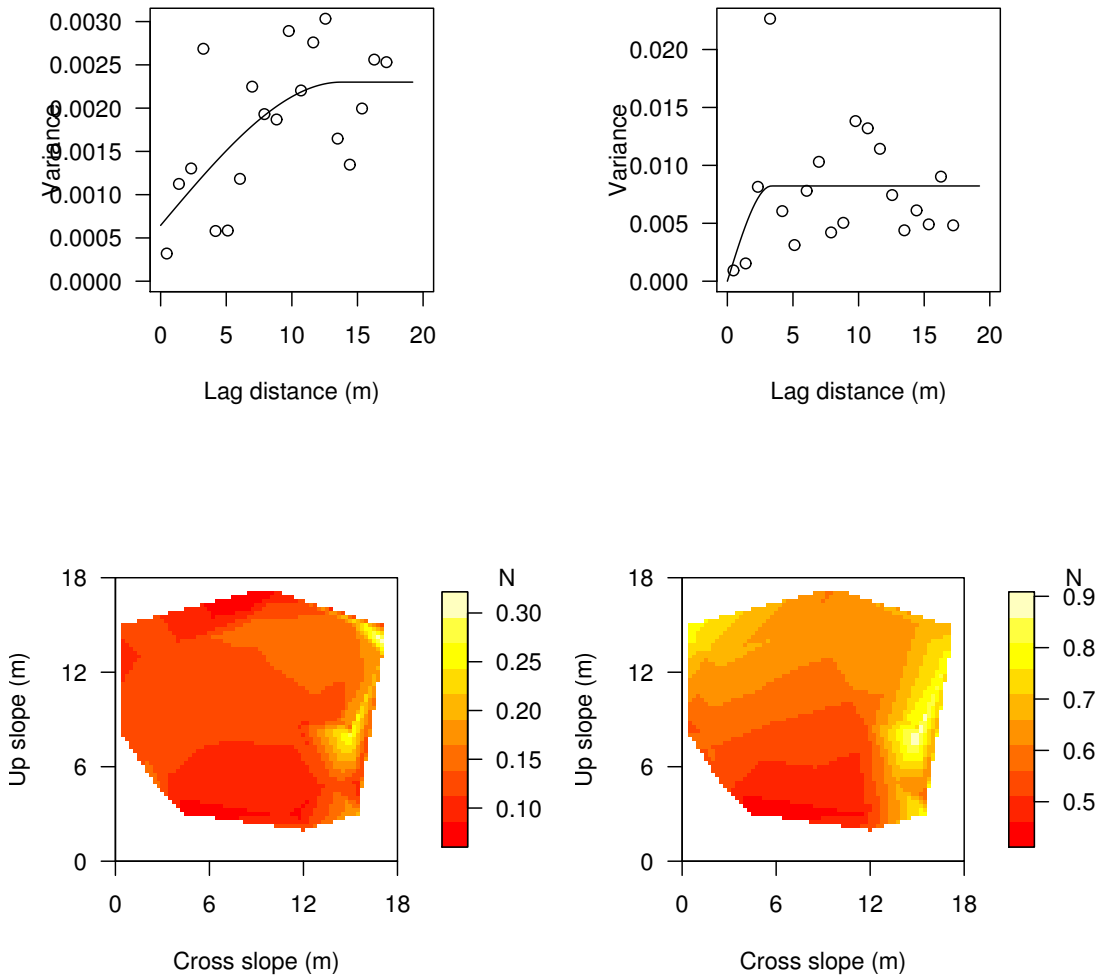
Figure C.13: Grid 9 winter 2007 - 2008. Experimental variogram (open circles) and modeled variogram of the mean penetration resistance F for the weak layer (top left) and the slab layers (top right). Contour plots of the mean penetration resistance F for the weak layer (bottom left) and the slab layer (bottom right).

Figure C.14: Grid 2 winter 2008 - 2009. Experimental variogram (open circles) and modeled variogram of the mean penetration resistance F for the weak layer (top left) and the slab layers (top right). Contour plots of the mean penetration resistance F for the weak layer (bottom left) and the slab layer (bottom right).

Figure C.15: Grid 4 winter 2008 - 2009. Experimental variogram (open circles) and modeled variogram of the mean penetration resistance F for the weak layer (top left) and the slab layers (top right). Contour plots of the mean penetration resistance F for the weak layer (bottom left) and the slab layer (bottom right).
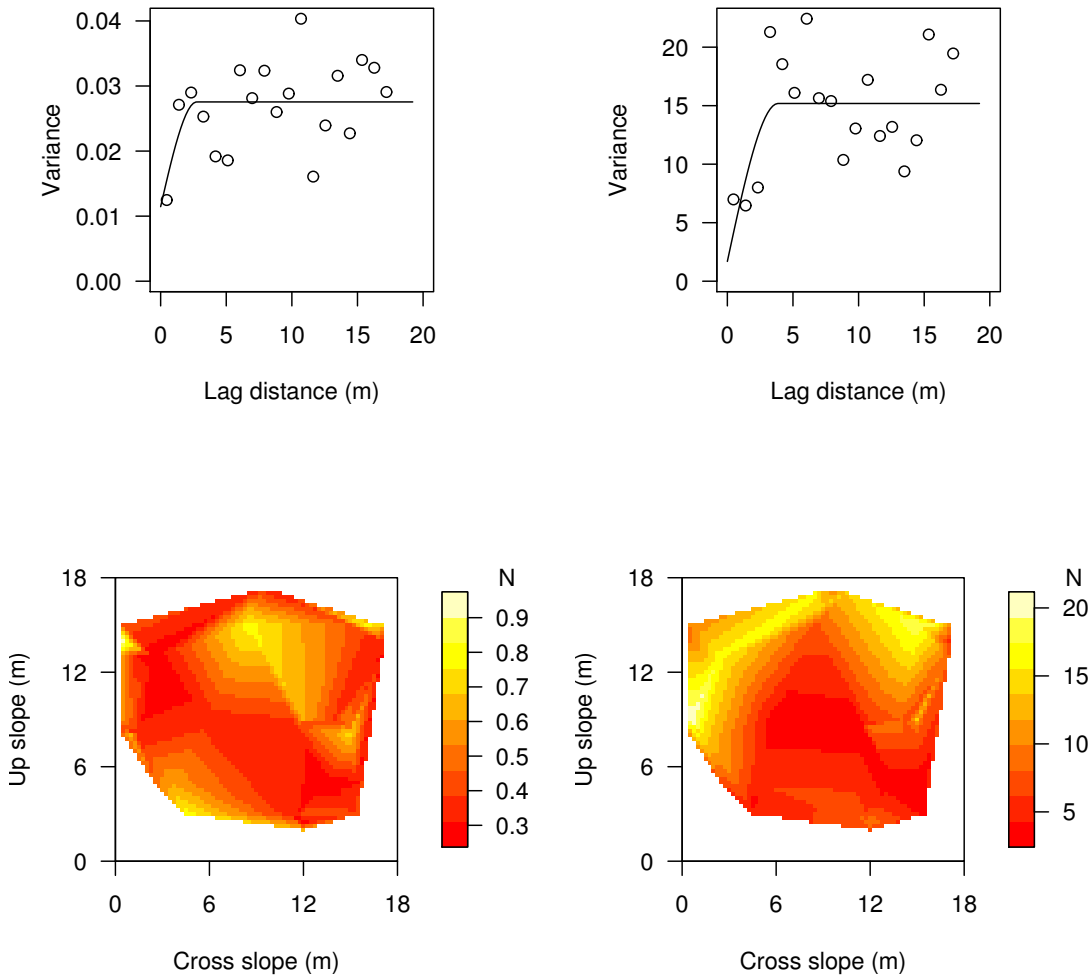
Figure C.16: Grid 6 winter 2008 - 2009. Experimental variogram (open circles) and modeled variogram of the mean penetration resistance F for the weak layer (top left) and the slab layers (top right). Contour plots of the mean penetration resistance F for the weak layer (bottom left) and the slab layer (bottom right).

Figure C.17: Grid 7 winter 2008 - 2009. Experimental variogram (open circles) and modeled variogram of the mean penetration resistance F for the weak layer (top left) and the slab layers (top right). Contour plots of the mean penetration resistance F for the weak layer (bottom left) and the slab layer (bottom right).

Appendix D

Sample (open circles) and theoretical (solid line) variogram of the weak layer and slab layer maximum penetration resistance F_{max} for the winter between 2006 and 2009. In addition shown are the contour plots of the weak layer and slab layer maximum penetration resistance F_{max}. The maximum penetration resistance values were not detrended.
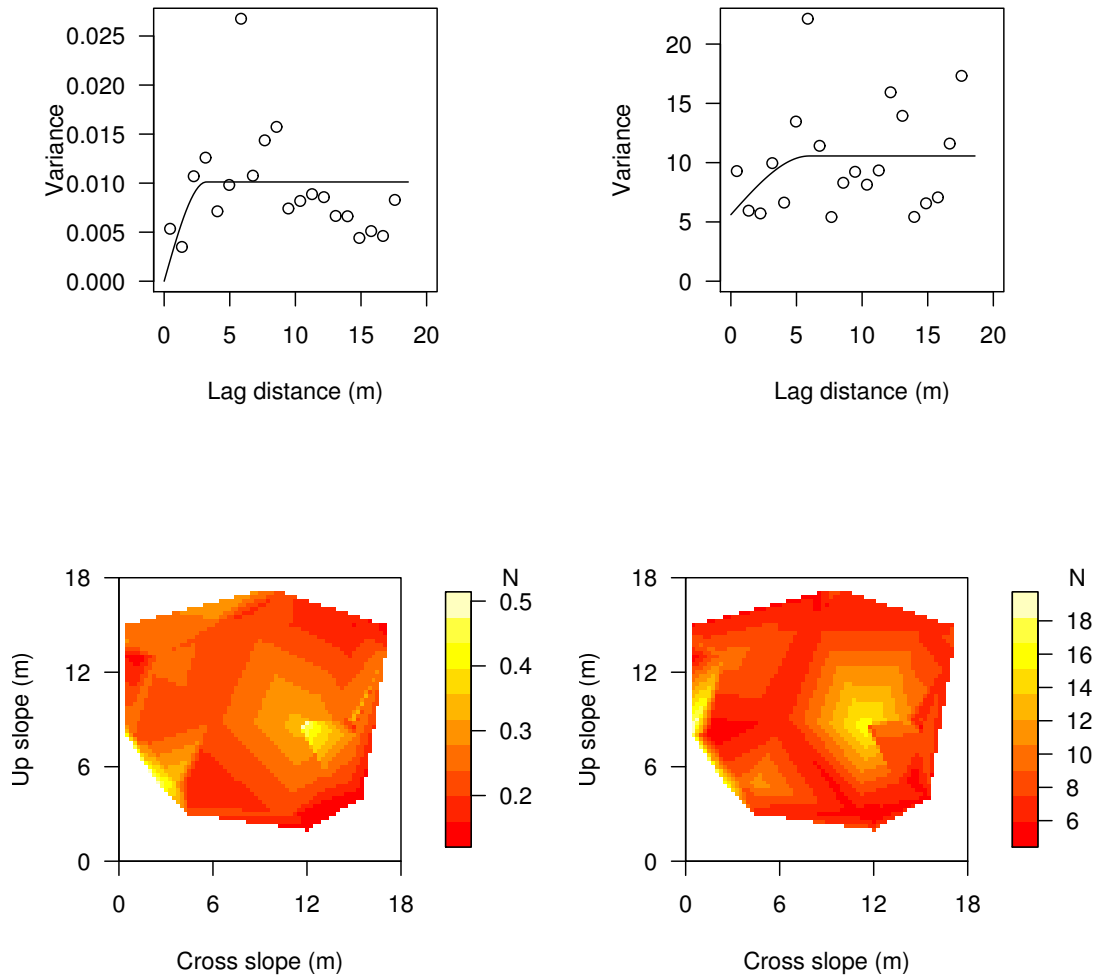
Figure D.1: Grid 1 winter 2006 - 2007. Experimental variogram (open circles) and modeled variogram of the maximum penetration resistance F_{max} for the weak layer (top left) and the slab layers (top right). Contour plots of the maximum penetration resistance F for the weak layer (bottom left) and the slab layer (bottom right).
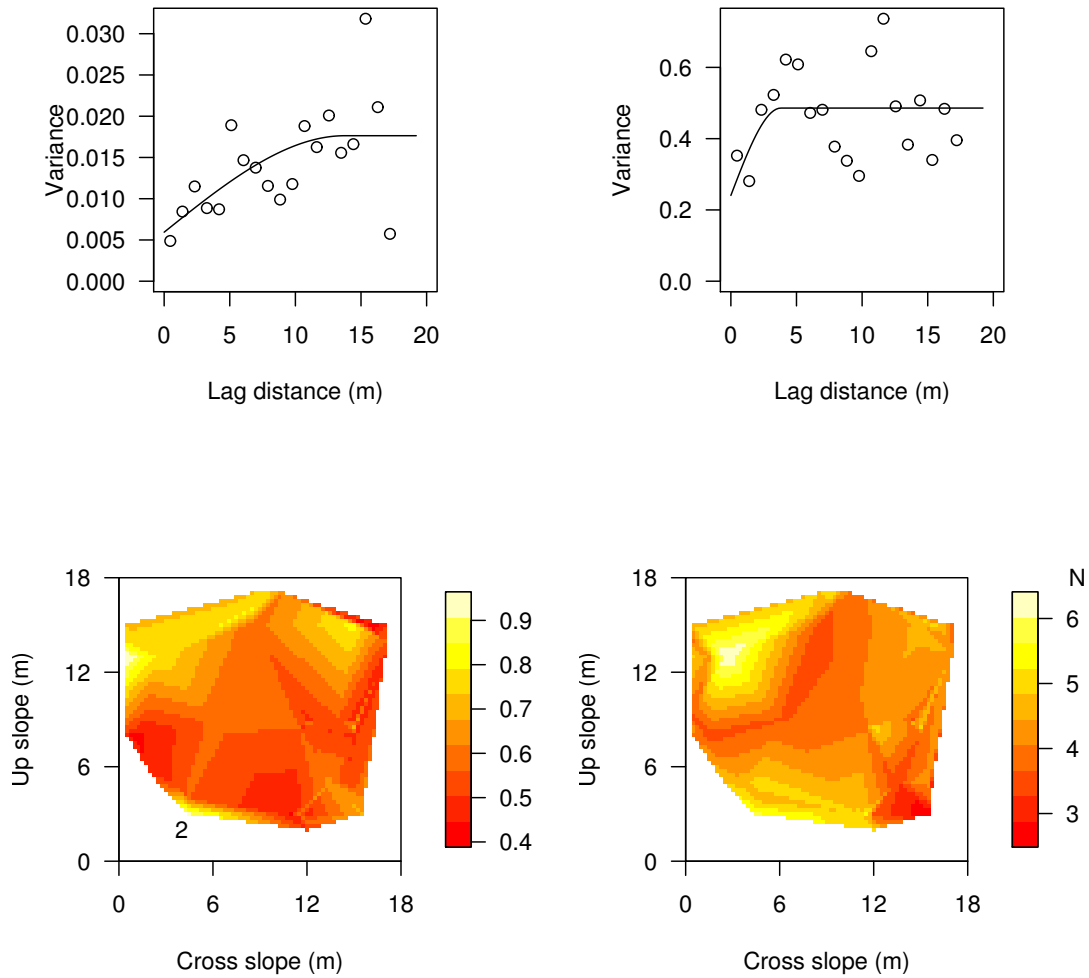
Figure D.2: Grid 2 winter 2006 - 2007. Experimental variogram (open circles) and modeled variogram of the maximum penetration resistance F_{max} for the weak layer (top left) and the slab layers (top right). Contour plots of the maximum penetration resistance F for the weak layer (bottom left) and the slab layer (bottom right).
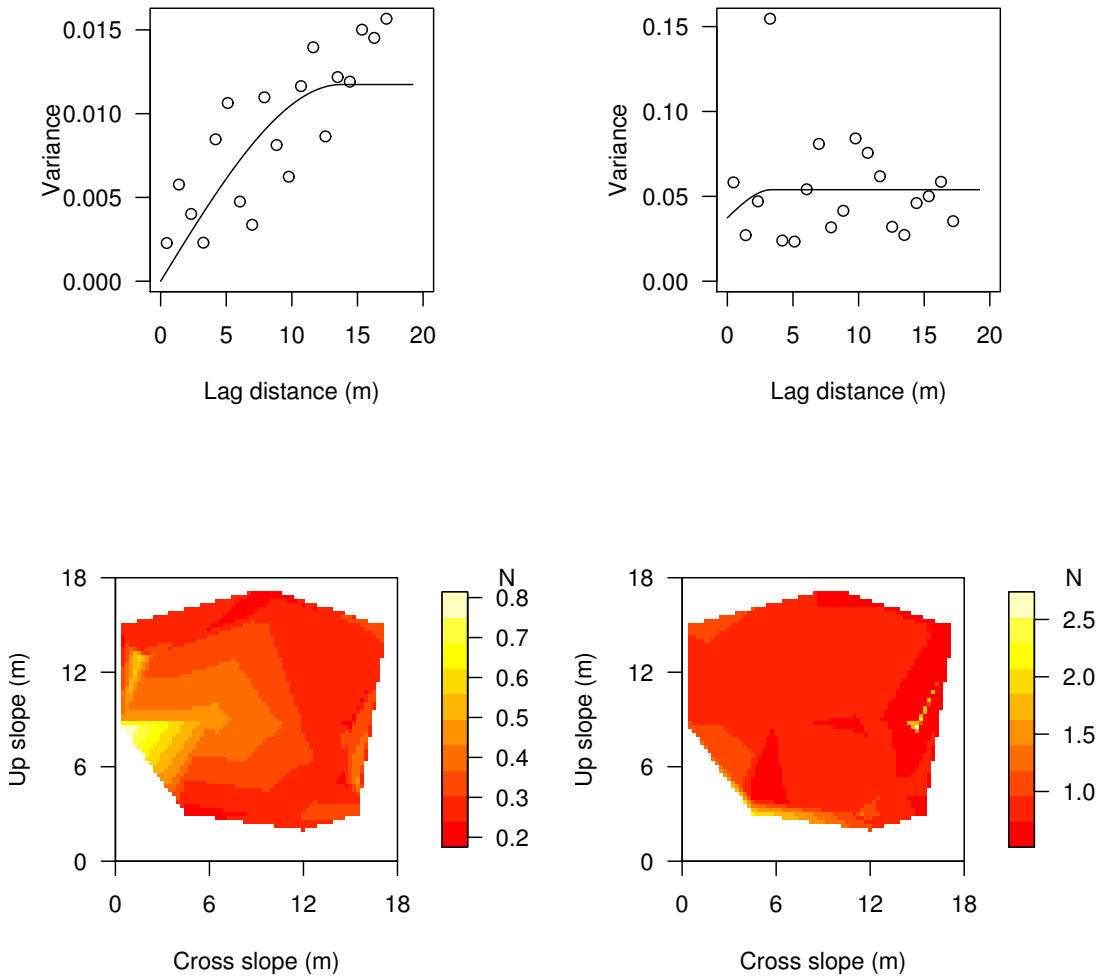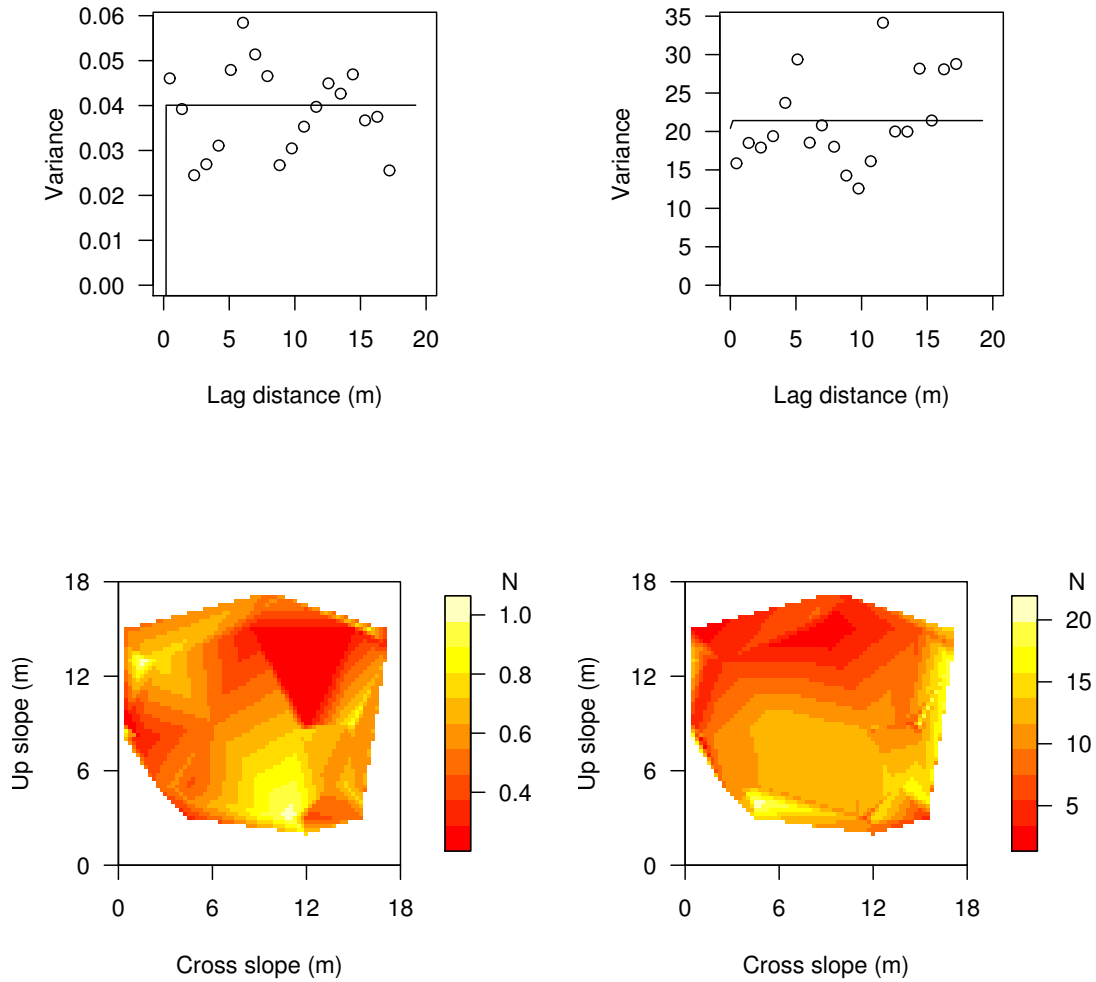
Figure D.3: Grid 3 winter 2006 - 2007. Experimental variogram (open circles) and modeled variogram of the maximum penetration resistance F_{max} for the weak layer (top left) and the slab layers (top right). Contour plots of the maximum penetration resistance F for the weak layer (bottom left) and the slab layer (bottom right).
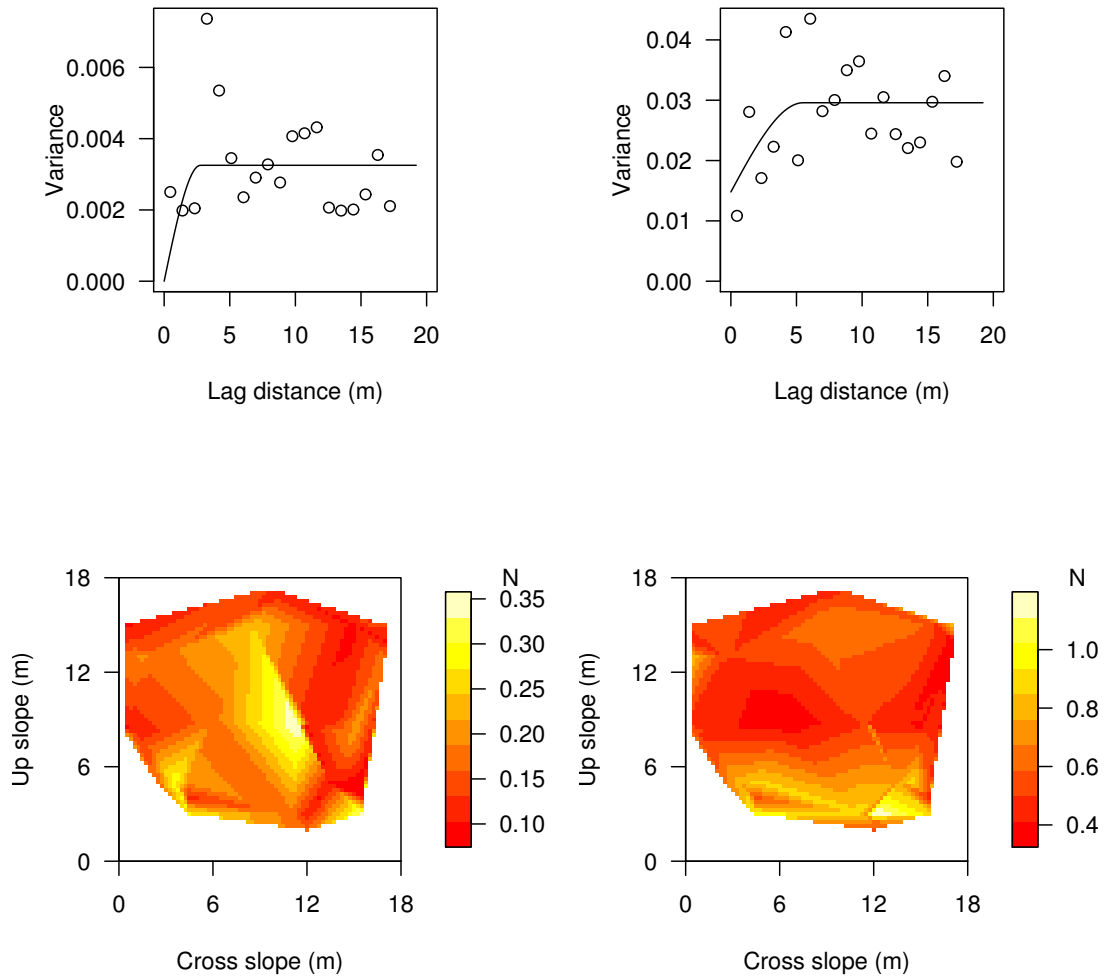
Figure D.4: Grid 5 winter 2006 - 2007. Experimental variogram (open circles) and modeled variogram of the maximum penetration resistance F_{max} for the weak layer (top left) and the slab layers (top right). Contour plots of the maximum penetration resistance F for the weak layer (bottom left) and the slab layer (bottom right).
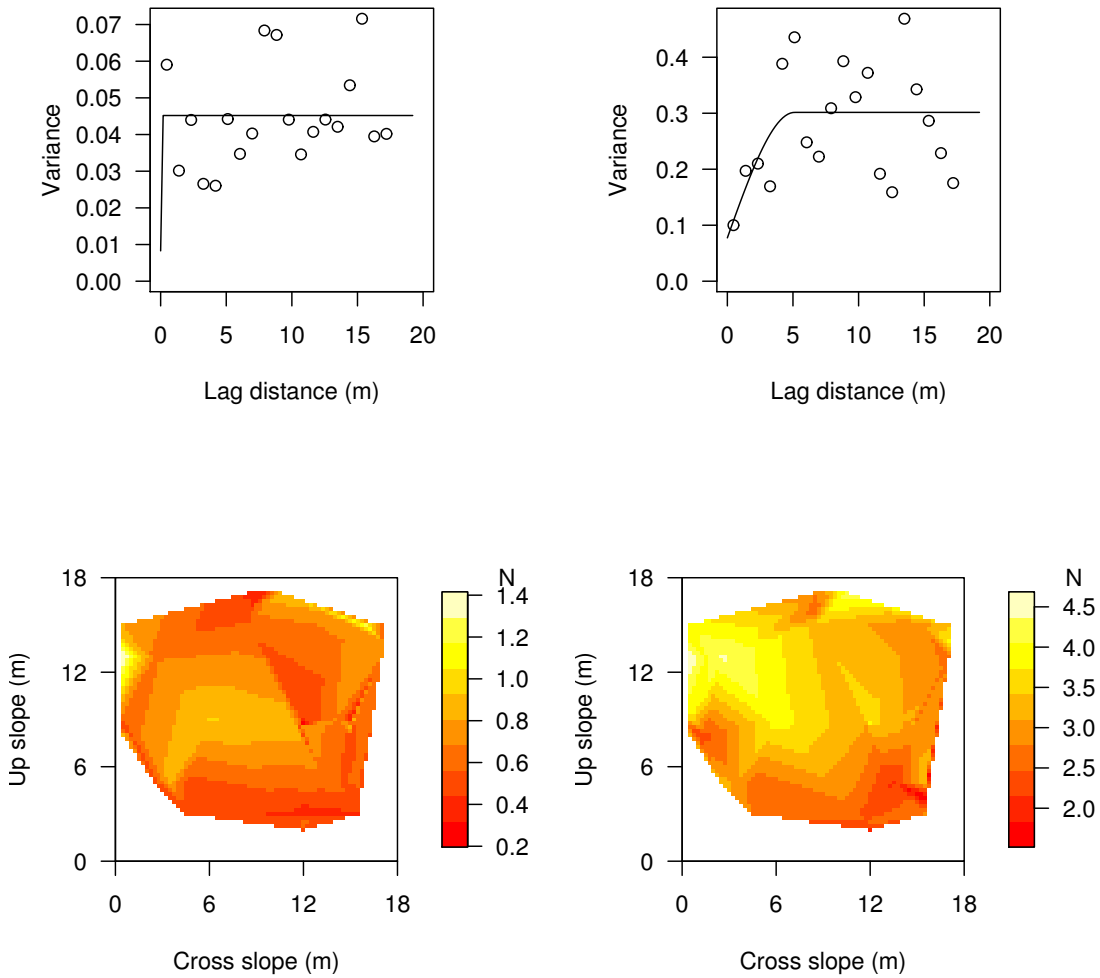
Figure D.5: Grid 6 winter 2006 - 2007. Experimental variogram (open circles) and modeled variogram of the maximum penetration resistance F_{max} for the weak layer (top left) and the slab layers (top right). Contour plots of the maximum penetration resistance F for the weak layer (bottom left) and the slab layer (bottom right).

Figure D.6: Grid 1 winter 2007 - 2008. Experimental variogram (open circles) and modeled variogram of the maximum penetration resistance F_{max} for the weak layer (top left) and the slab layers (top right). Contour plots of the maximum penetration resistance F for the weak layer (bottom left) and the slab layer (bottom right).
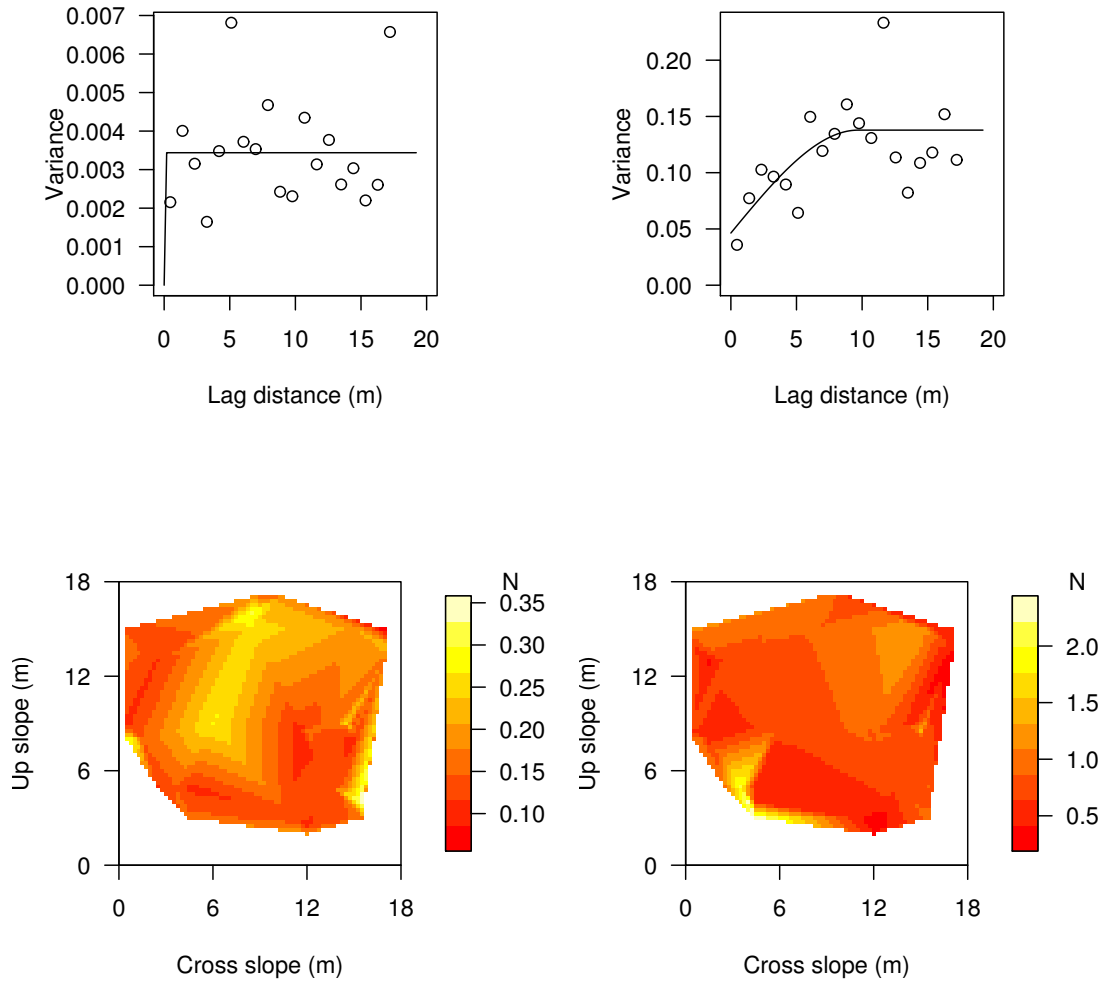
Figure D.7: Grid 2 winter 2007 - 2008. Experimental variogram (open circles) and modeled variogram of the maximum penetration resistance F_{max} for the weak layer (top left) and the slab layers (top right). Contour plots of the maximum penetration resistance F for the weak layer (bottom left) and the slab layer (bottom right).

Figure D.8: Grid 3 winter 2007 - 2008. Experimental variogram (open circles) and modeled variogram of the maximum penetration resistance F_{max} for the weak layer (top left) and the slab layers (top right). Contour plots of the maximum penetration resistance F for the weak layer (bottom left) and the slab layer (bottom right).
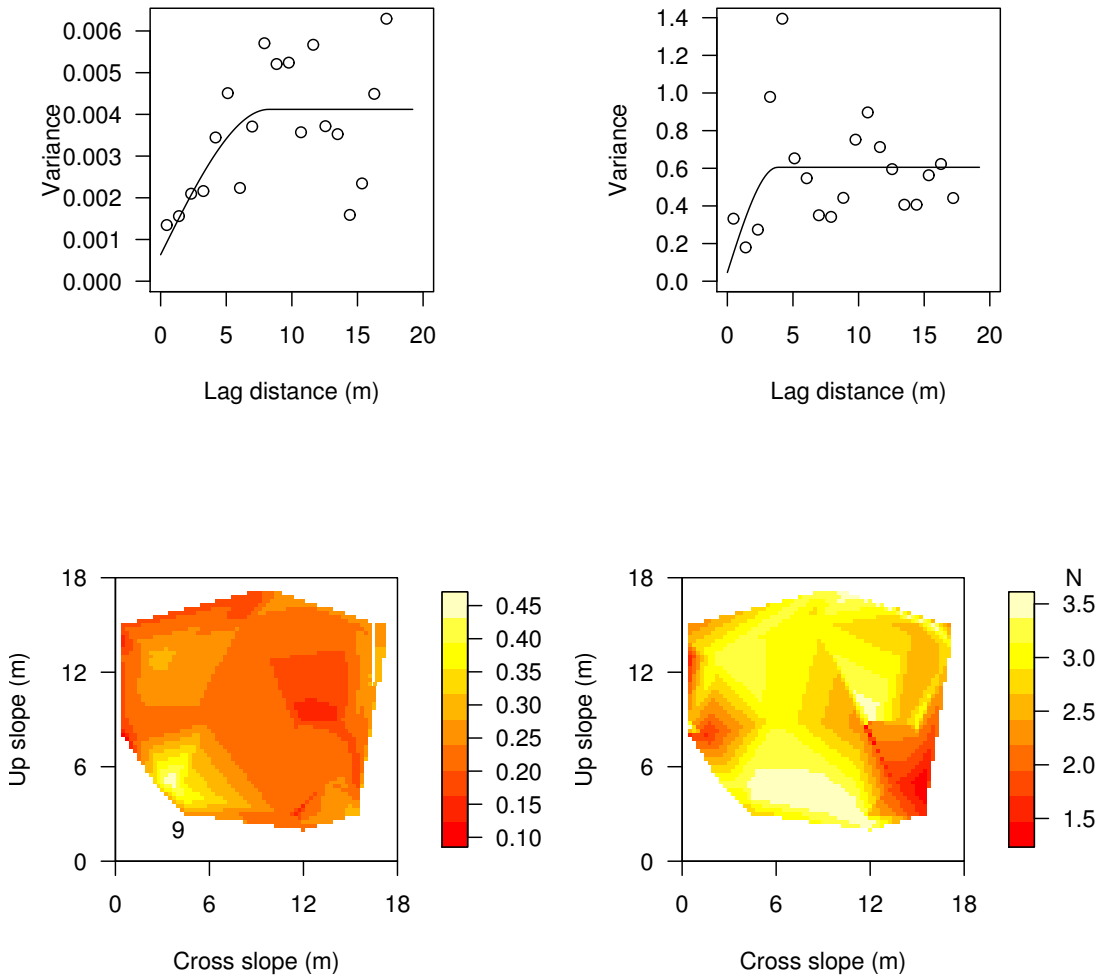
Figure D.9: Grid 4 winter 2007 - 2008. Experimental variogram (open circles) and modeled variogram of the maximum penetration resistance F_{max} for the weak layer (top left) and the slab layers (top right). Contour plots of the maximum penetration resistance F for the weak layer (bottom left) and the slab layer (bottom right).
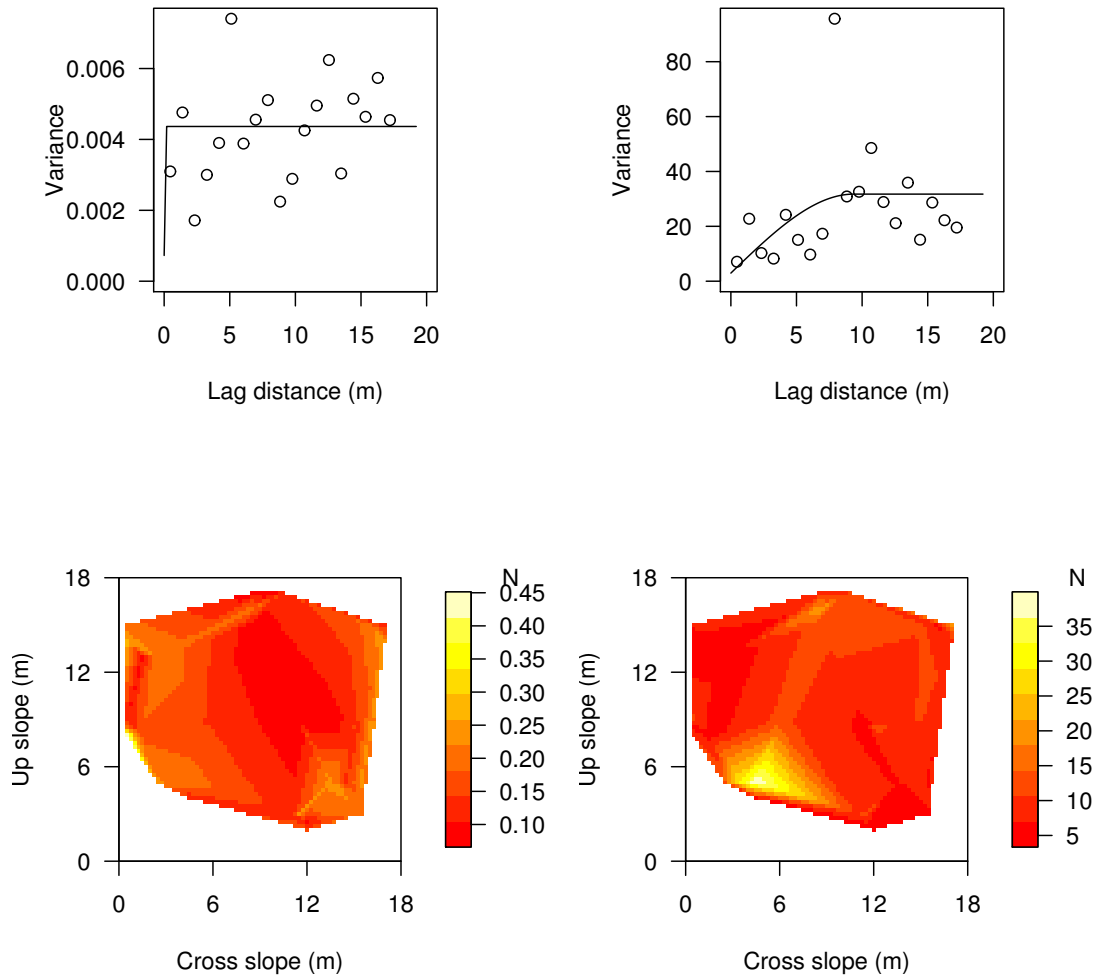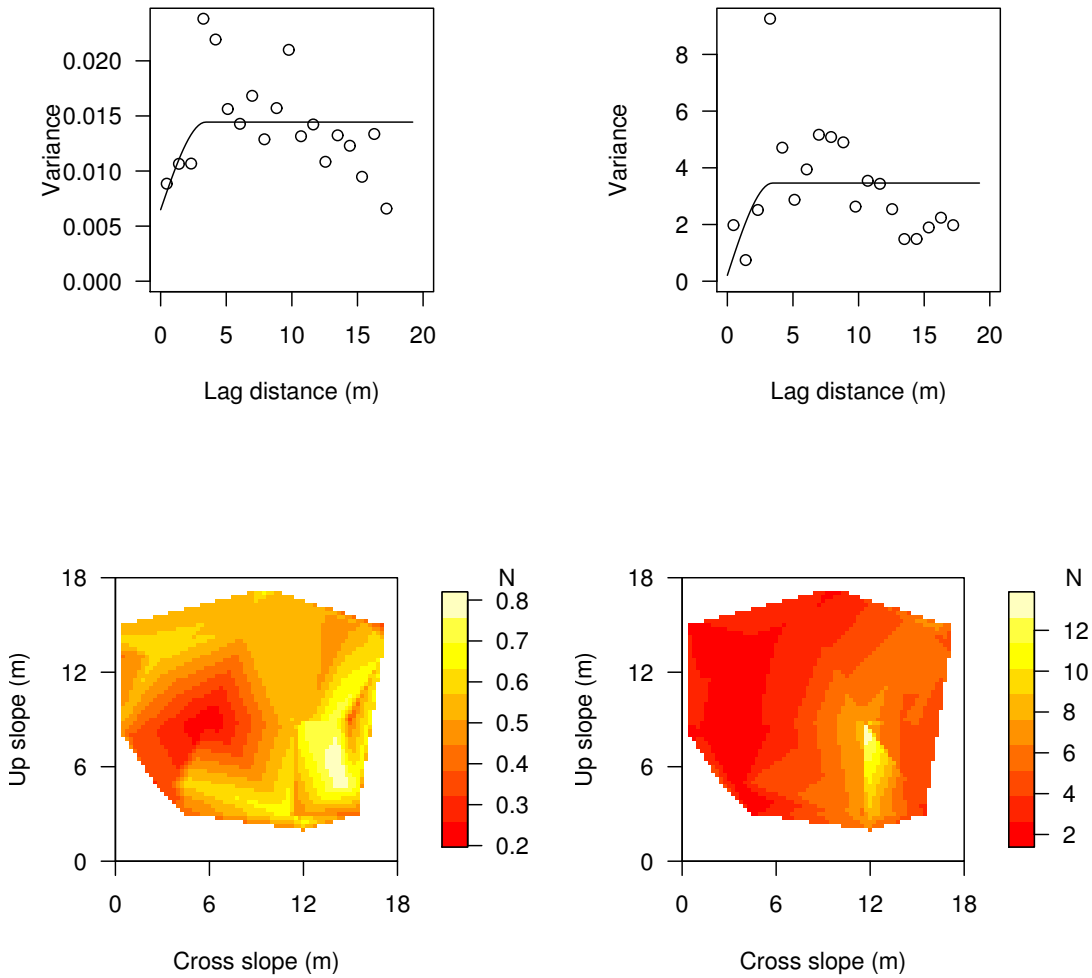
Figure D.10: Grid 5 winter 2007 - 2008. Experimental variogram (open circles) and modeled variogram of the maximum penetration resistance F_{max} for the weak layer (top left) and the slab layers (top right). Contour plots of the maximum penetration resistance F for the weak layer (bottom left) and the slab layer (bottom right).

Figure D.11: Grid 6 winter 2007 - 2008. Experimental variogram (open circles) and modeled variogram of the maximum penetration resistance F_{max} for the weak layer (top left) and the slab layers (top right). Contour plots of the maximum penetration resistance F for the weak layer (bottom left) and the slab layer (bottom right).
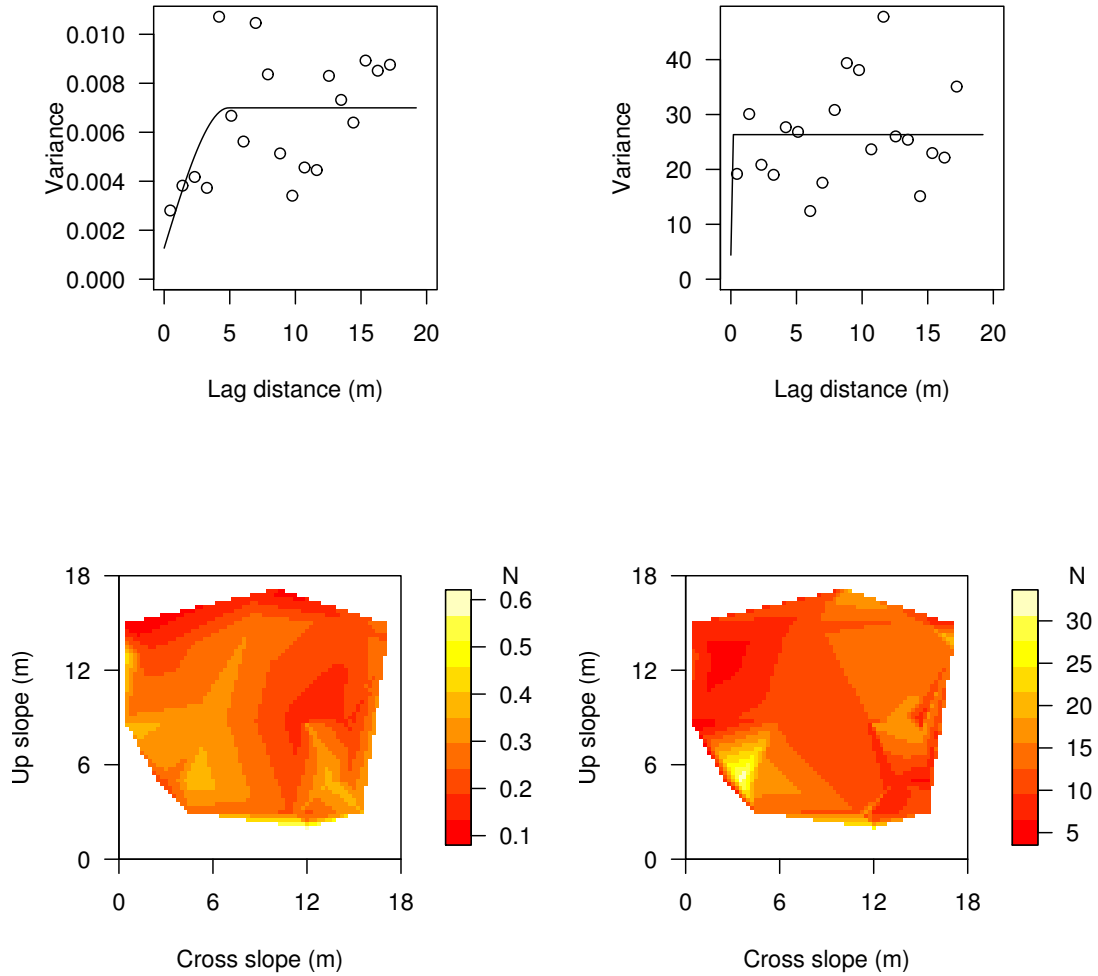
Figure D.12: Grid 7 winter 2007 - 2008. Experimental variogram (open circles) and modeled variogram of the maximum penetration resistance F_{max} for the weak layer (top left) and the slab layers (top right). Contour plots of the maximum penetration resistance F for the weak layer (bottom left) and the slab layer (bottom right).
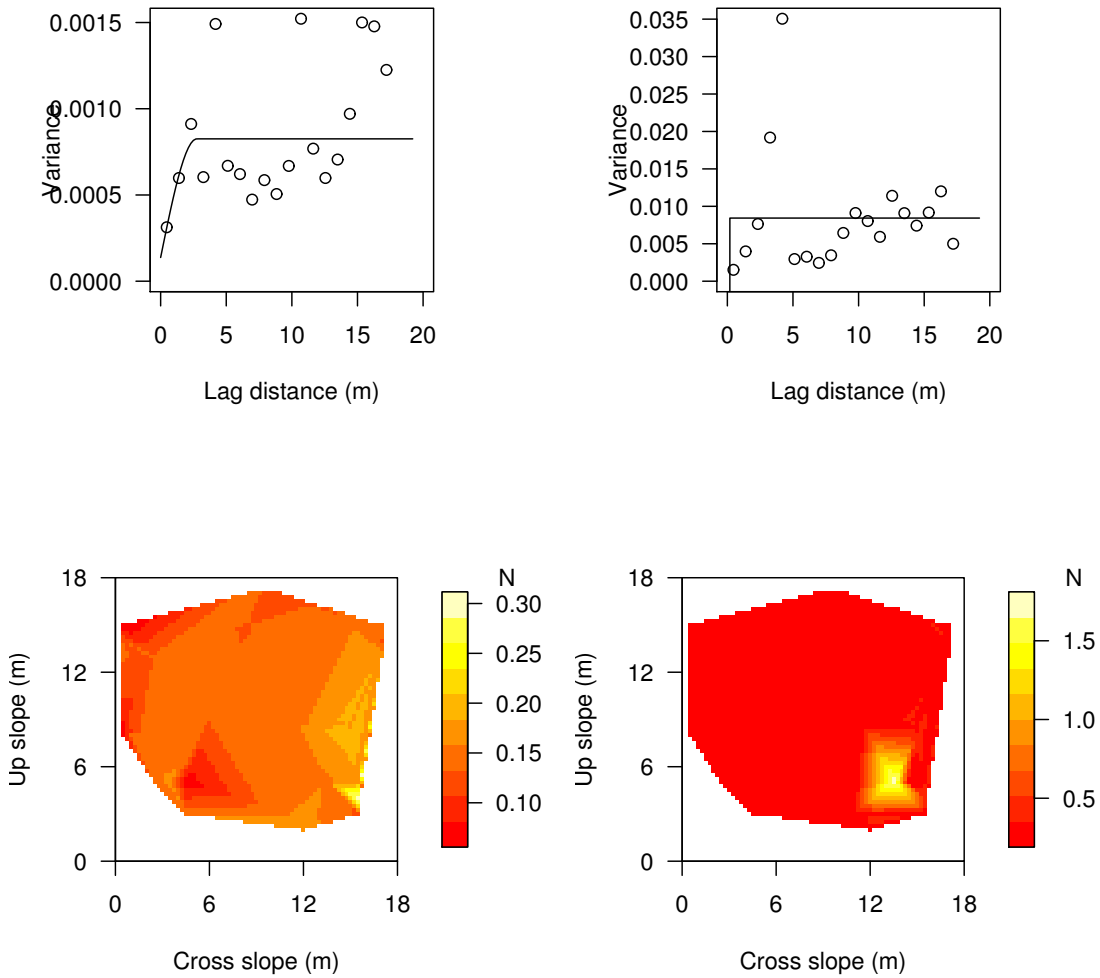
Figure D.13: Grid 9 winter 2007 - 2008. Experimental variogram (open circles) and modeled variogram of the maximum penetration resistance F_{max} for the weak layer (top left) and the slab layers (top right). Contour plots of the maximum penetration resistance F for the weak layer (bottom left) and the slab layer (bottom right).
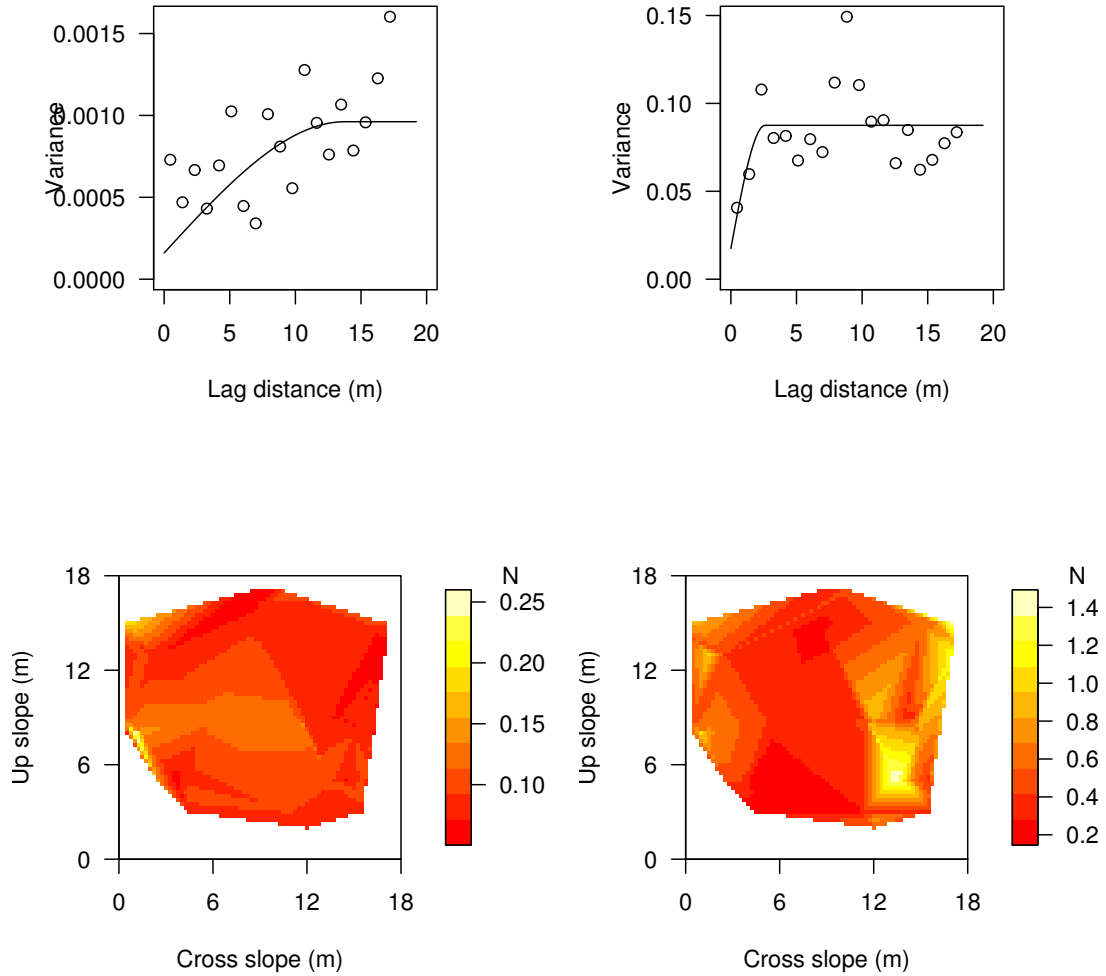
Figure D.14: Grid 2 winter 2008 - 2009. Experimental variogram (open circles) and modeled variogram of the maximum penetration resistance F_{max} for the weak layer (top left) and the slab layers (top right). Contour plots of the maximum penetration resistance F for the weak layer (bottom left) and the slab layer (bottom right).

Figure D.15: Grid 4 winter 2008 - 2009. Experimental variogram (open circles) and modeled variogram of the maximum penetration resistance F_{max} for the weak layer (top left) and the slab layers (top right). Contour plots of the maximum penetration resistance F for the weak layer (bottom left) and the slab layer (bottom right).
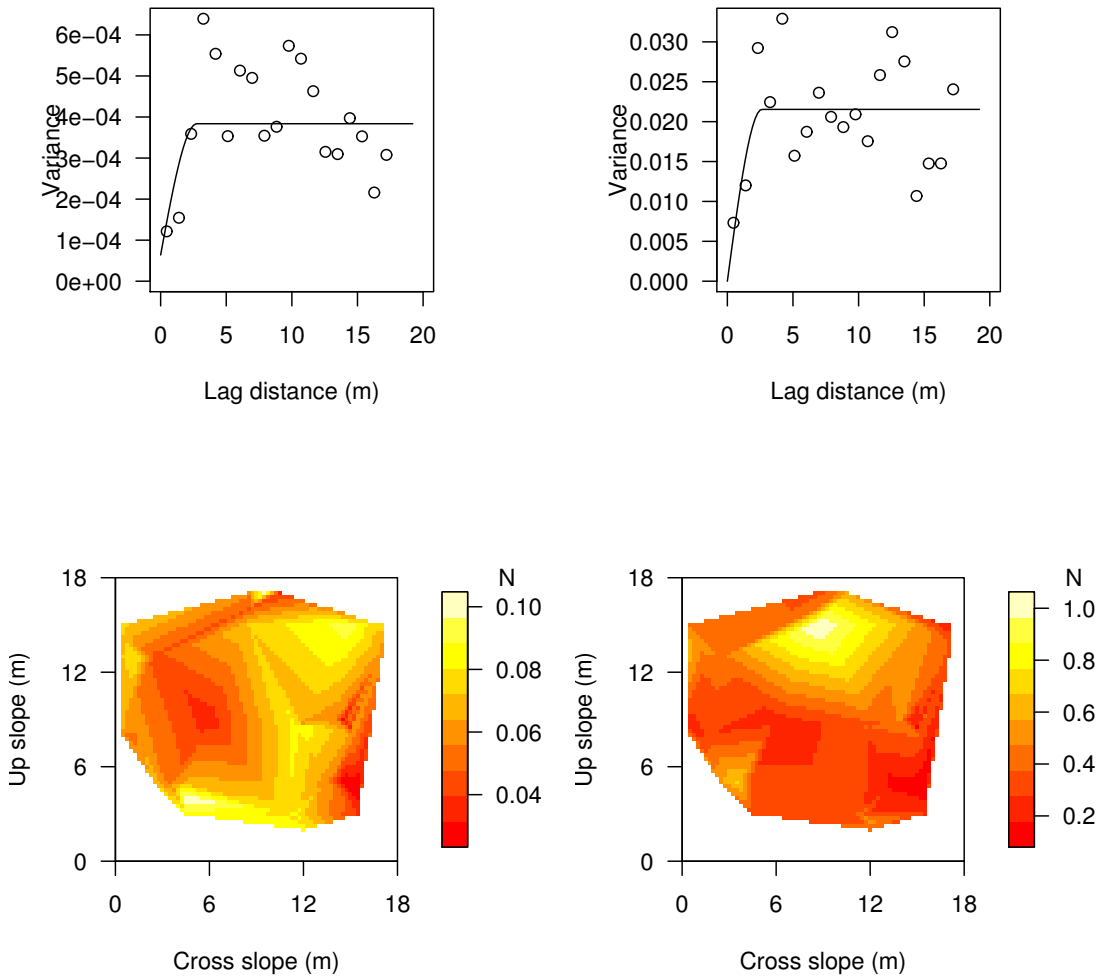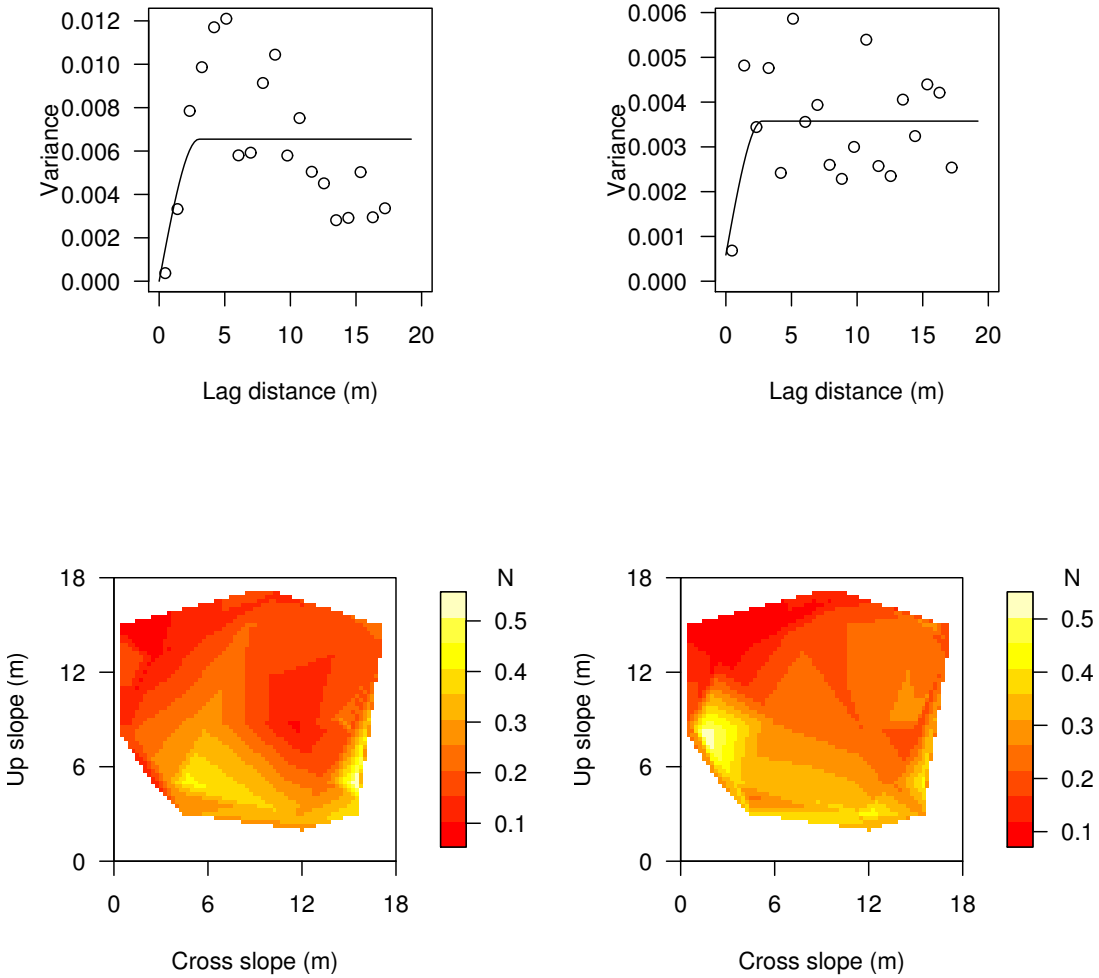
Figure D.16: Grid 6 winter 2008 - 2009. Experimental variogram (open circles) and modeled variogram of the maximum penetration resistance F_{max} for the weak layer (top left) and the slab layers (top right). Contour plots of the maximum penetration resistance F for the weak layer (bottom left) and the slab layer (bottom right).

Figure D.17: Grid 7 winter 2008 - 2009. Experimental variogram (open circles) and modeled variogram of the maximum penetration resistance F_{max} for the weak layer (top left) and the slab layers (top right). Contour plots of the maximum penetration resistance F for the weak layer (bottom left) and the slab layer (bottom right).
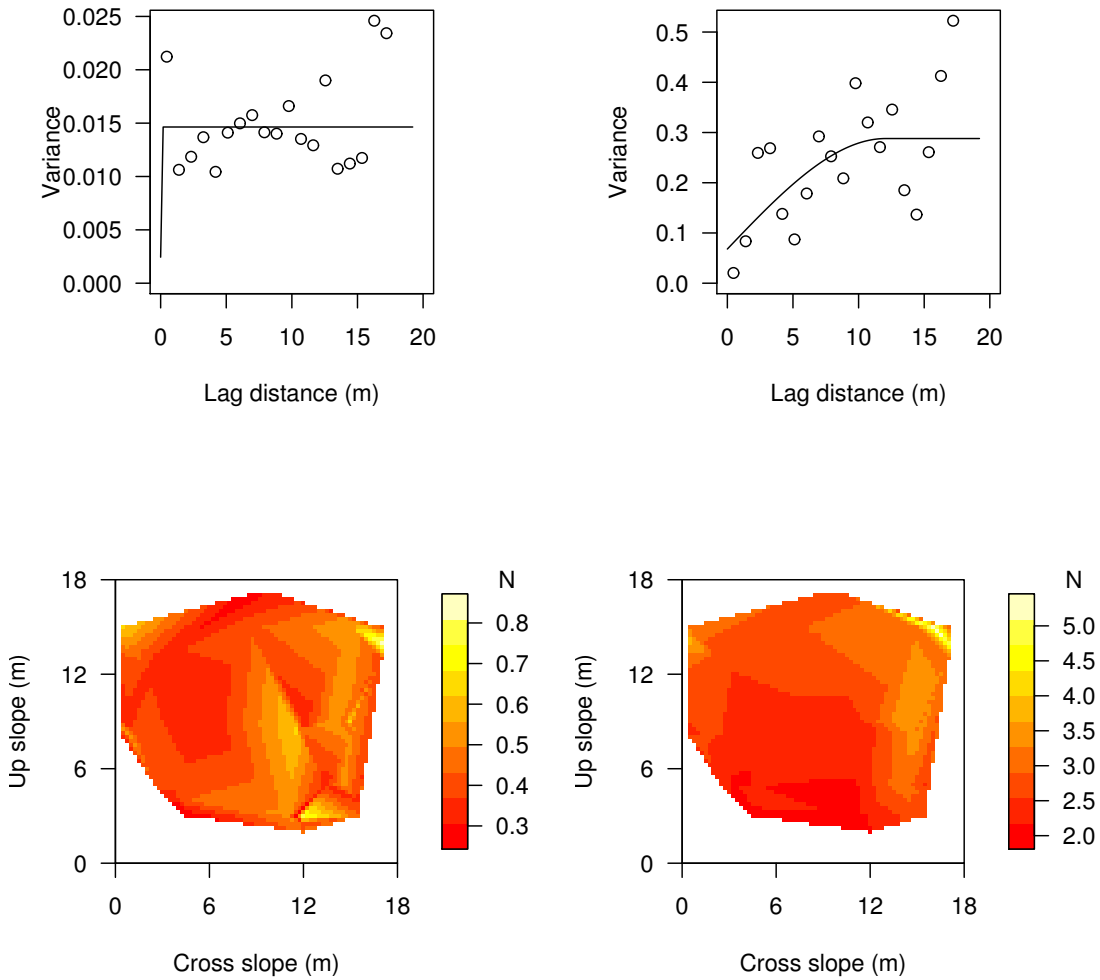
Appendix E

Sample (open circles) and theoretical (solid line) variogram of the weak layer and slab layer thickness D for the winter between 2006 and 2009. In addition shown are the contour plots of the weak layer and slab layer thickness. The thickness D values were not detrended.
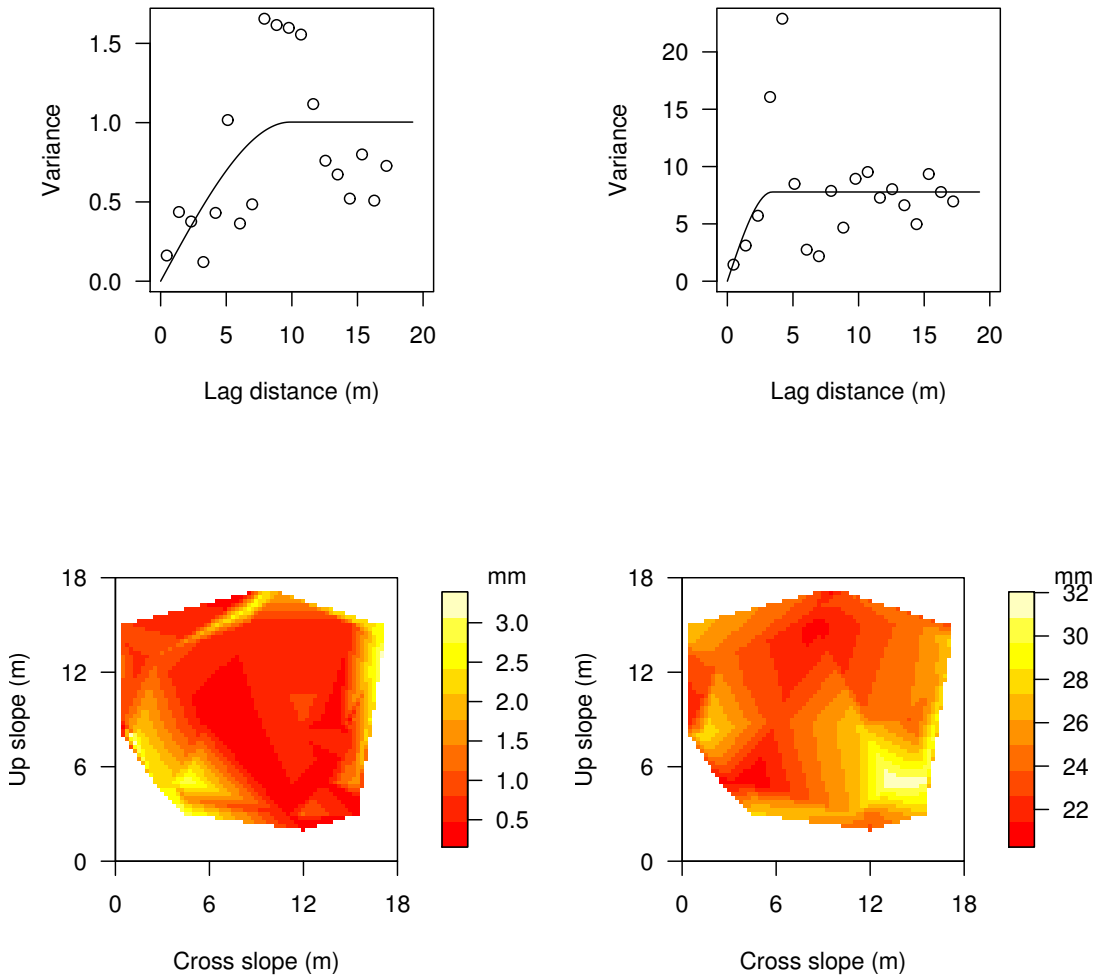
Figure E.1: Grid 1 winter 2006 - 2007. Experimental variogram (open circles) and modeled variogram of the the weak layer (top left) and the slab layers (top right) thickness D. Contour plots of the weak layer (bottom left) and the slab layer (bottom right) thickness D.
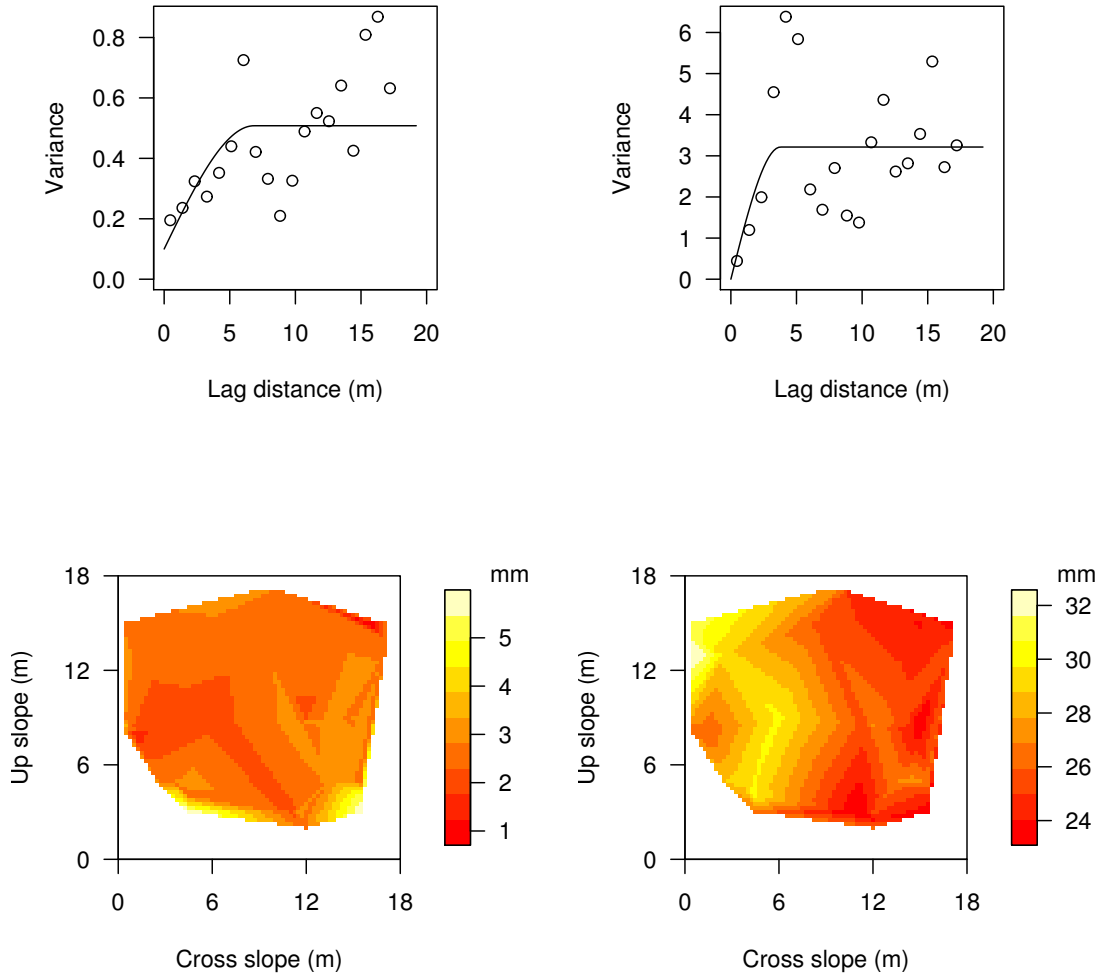
Figure E.2: Grid 2 winter 2006 - 2007. Experimental variogram (open circles) and modeled variogram of the the weak layer (top left) and the slab layers (top right) thickness D. Contour plots of the weak layer (bottom left) and the slab layer (bottom right) thickness D.
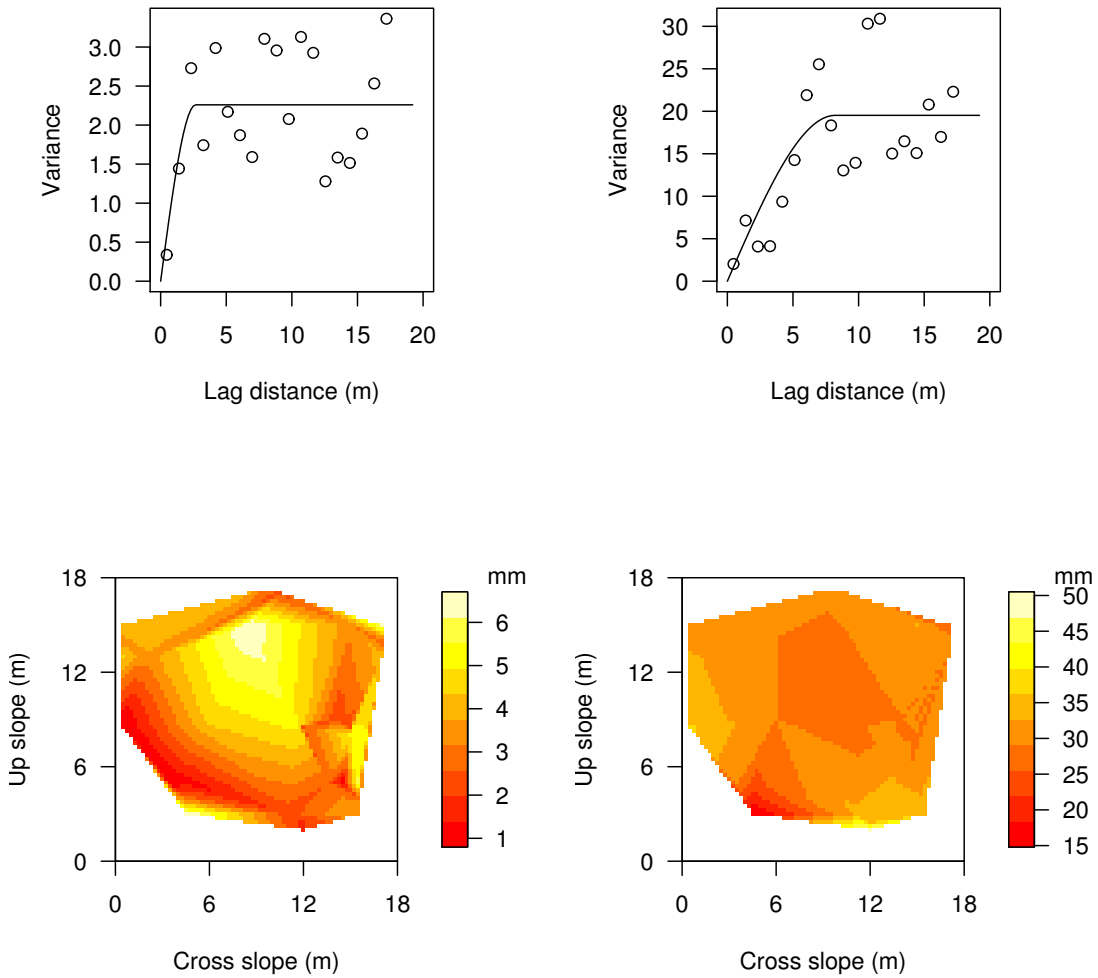
Figure E.3: Grid 3 winter 2006 - 2007. Experimental variogram (open circles) and modeled variogram of the the weak layer (top left) and the slab layers (top right) thickness D. Contour plots of the weak layer (bottom left) and the slab layer (bottom right) thickness D.

Figure E.4: Grid 5 winter 2006 - 2007. Experimental variogram (open circles) and modeled variogram of the the weak layer (top left) and the slab layers (top right) thickness D. Contour plots of the weak layer (bottom left) and the slab layer (bottom right) thickness D.

Figure E.5: Grid 6 winter 2006 - 2007. Experimental variogram (open circles) and modeled variogram of the the weak layer (top left) and the slab layers (top right) thickness D. Contour plots of the weak layer (bottom left) and the slab layer (bottom right) thickness D.

Figure E.6: Grid 1 winter 2007 - 2008. Experimental variogram (open circles) and modeled variogram of the the weak layer (top left) and the slab layers (top right) thickness D. Contour plots of the weak layer (bottom left) and the slab layer (bottom right) thickness D.
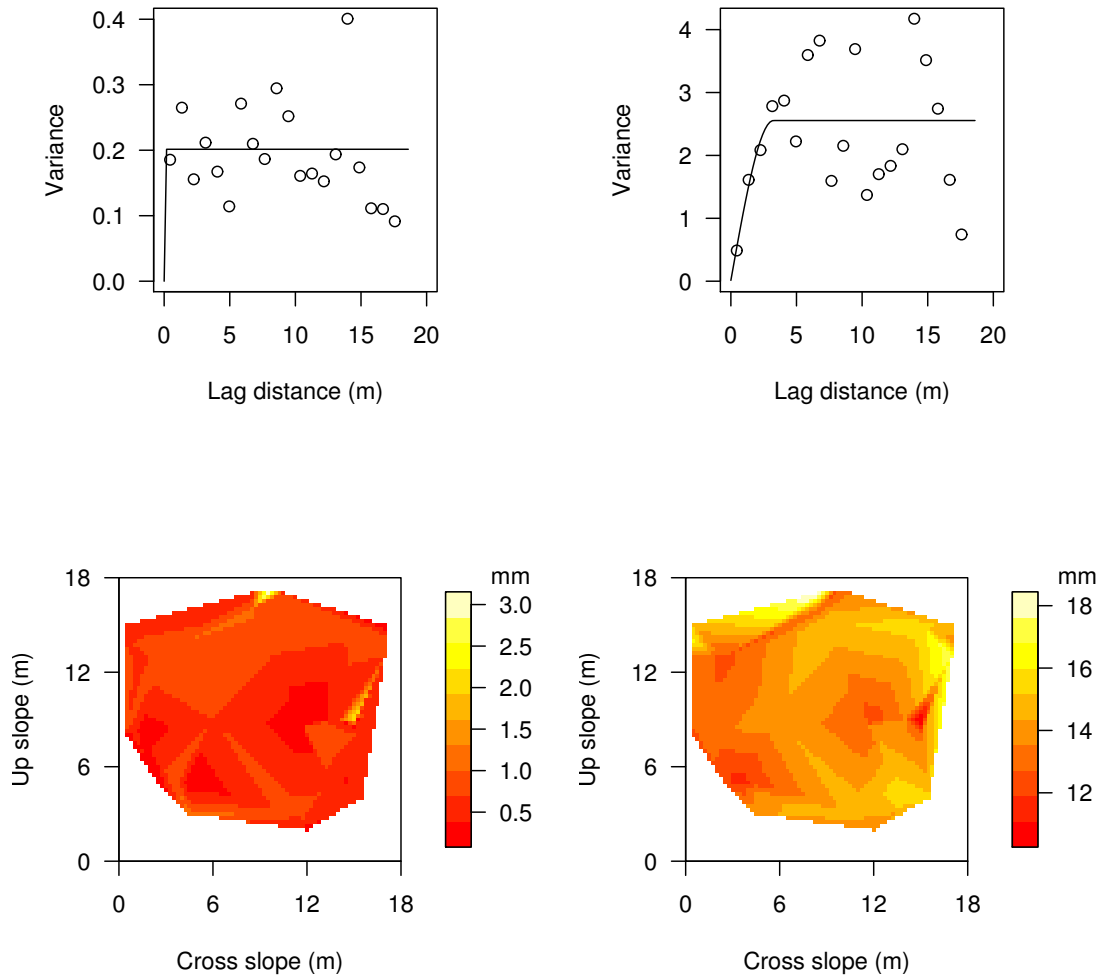
Figure E.7: Grid 2 winter 2007 - 2008. Experimental variogram (open circles) and modeled variogram of the the weak layer (top left) and the slab layers (top right) thickness D. Contour plots of the weak layer (bottom left) and the slab layer (bottom right) thickness D.

Figure E.8: Grid 3 winter 2007 - 2008. Experimental variogram (open circles) and modeled variogram of the the weak layer (top left) and the slab layers (top right) thickness D. Contour plots of the weak layer (bottom left) and the slab layer (bottom right) thickness D.

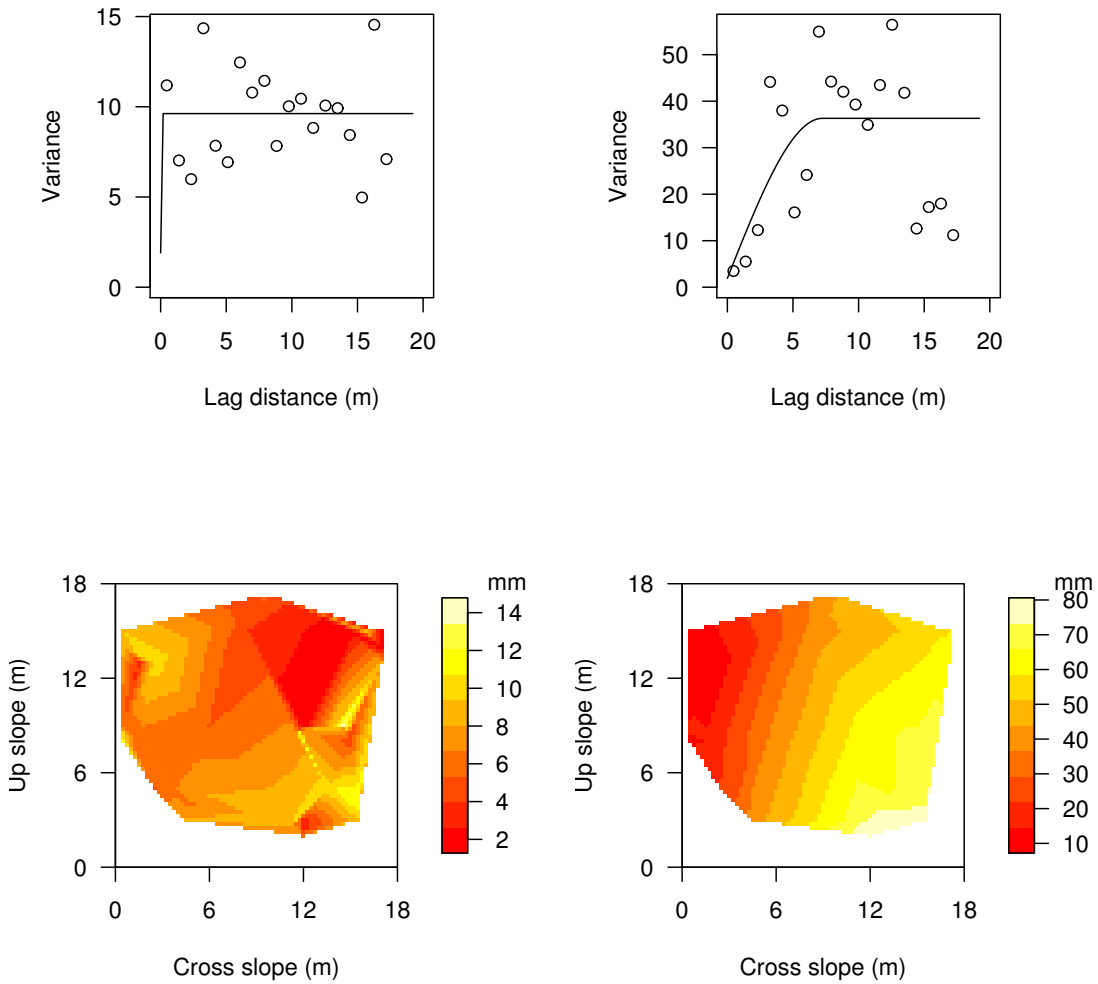**Figure E.9**: Grid 4 winter 2007 - 2008. Experimental variogram (open circles) and modeled variogram of the the weak layer (top left) and the slab layers (top right) thickness D. Contour plots of the weak layer (bottom left) and the slab layer (bottom right) thickness D.

Figure E.10: Grid 5 winter 2007 - 2008. Experimental variogram (open circles) and modeled variogram of the the weak layer (top left) and the slab layers (top right) thickness D. Contour plots of the weak layer (bottom left) and the slab layer (bottom right) thickness D.
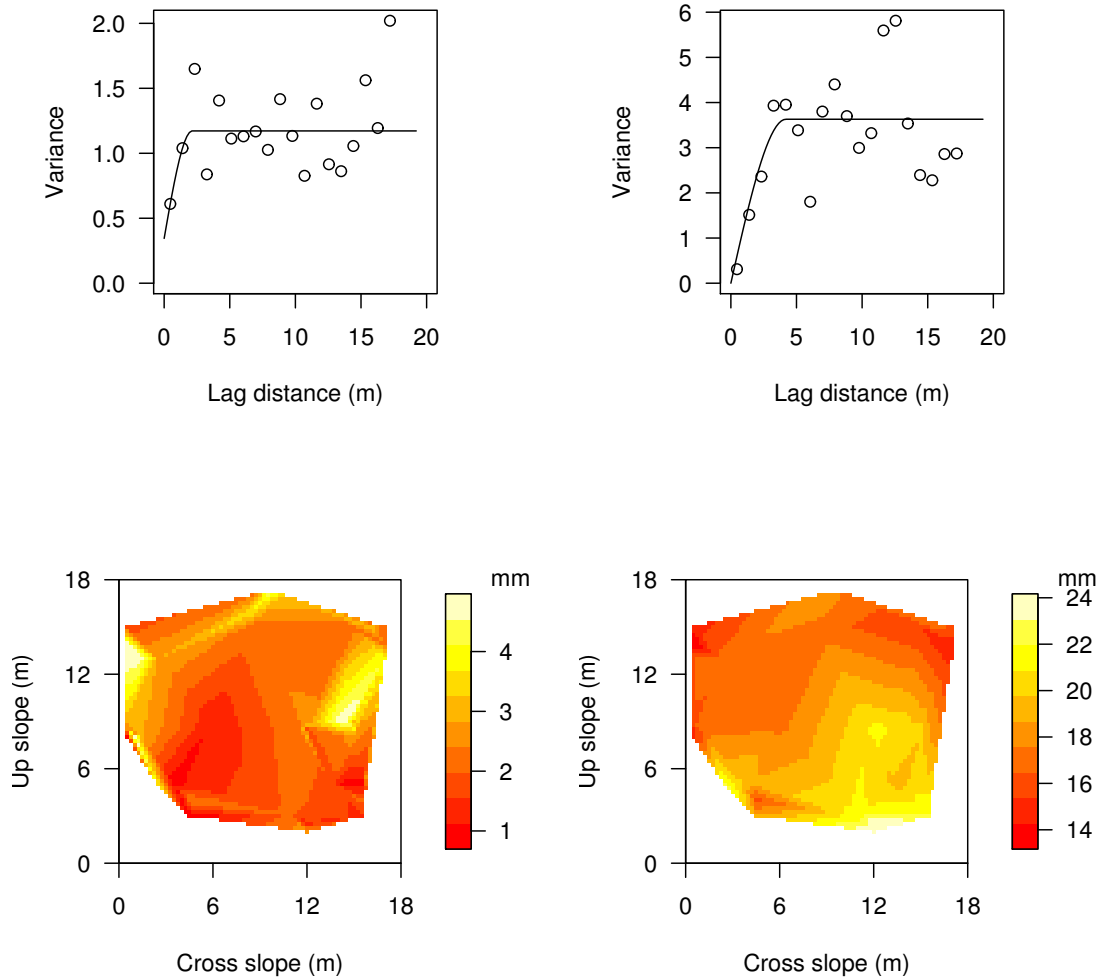
Figure E.11: Grid 6 winter 2007 - 2008. Experimental variogram (open circles) and modeled variogram of the the weak layer (top left) and the slab layers (top right) thickness D. Contour plots of the weak layer (bottom left) and the slab layer (bottom right) thickness D.
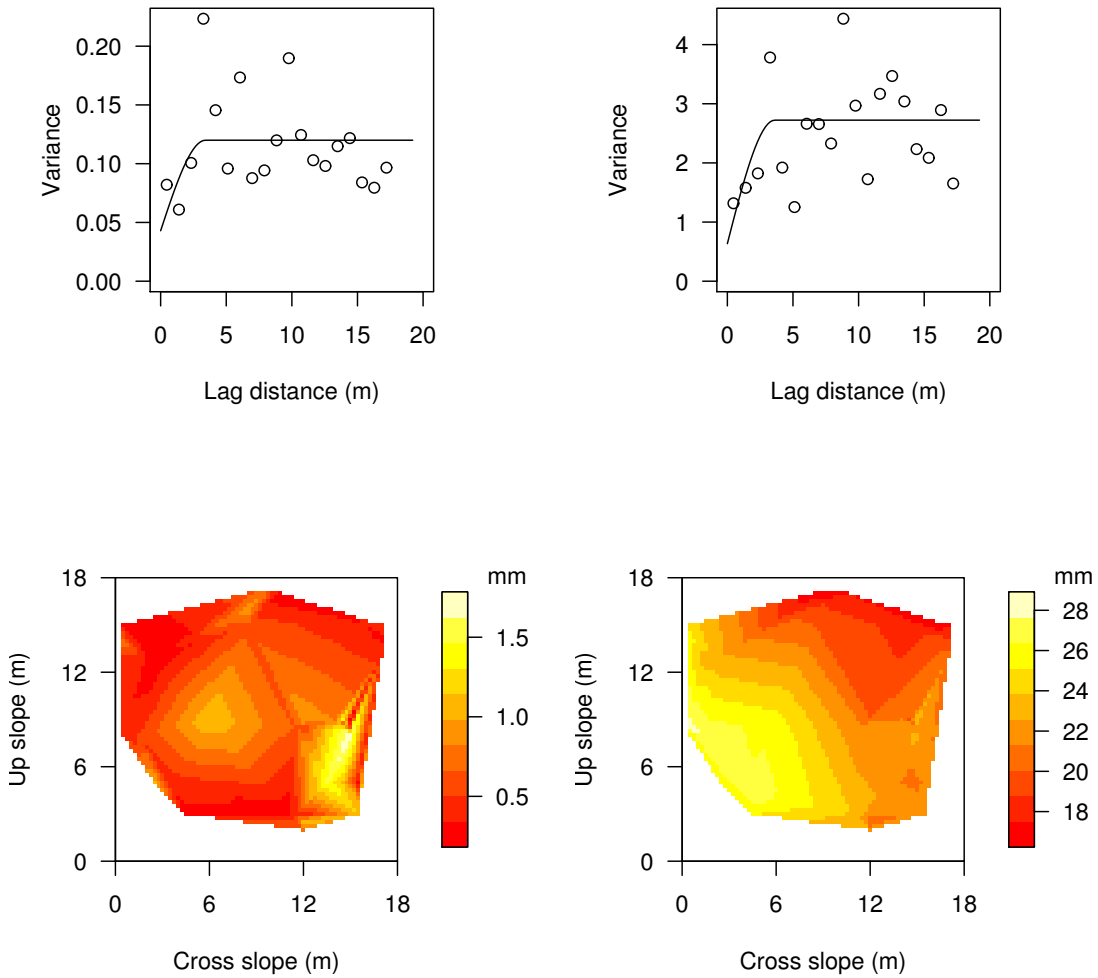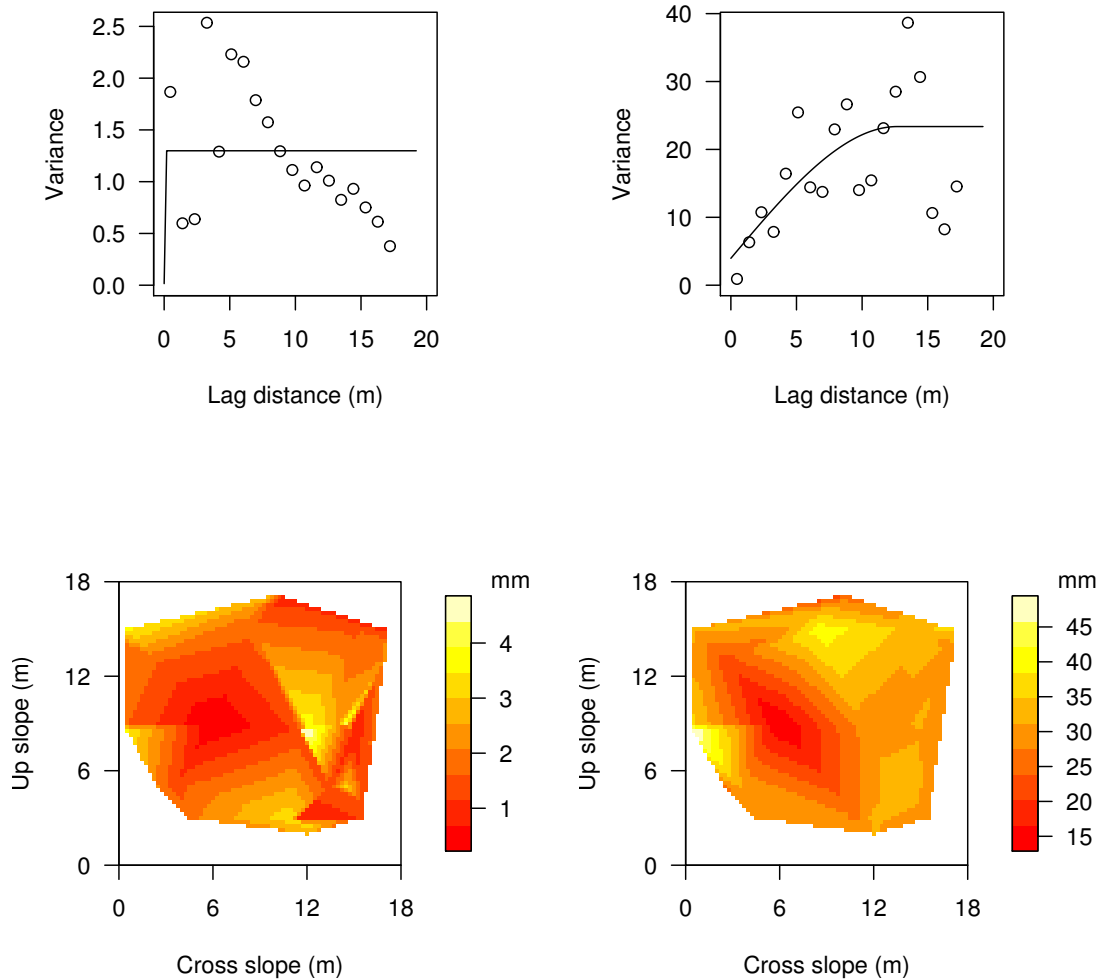
Figure E.12: Grid 7 winter 2007 - 2008. Experimental variogram (open circles) and modeled variogram of the the weak layer (top left) and the slab layers (top right) thickness D. Contour plots of the weak layer (bottom left) and the slab layer (bottom right) thickness D.
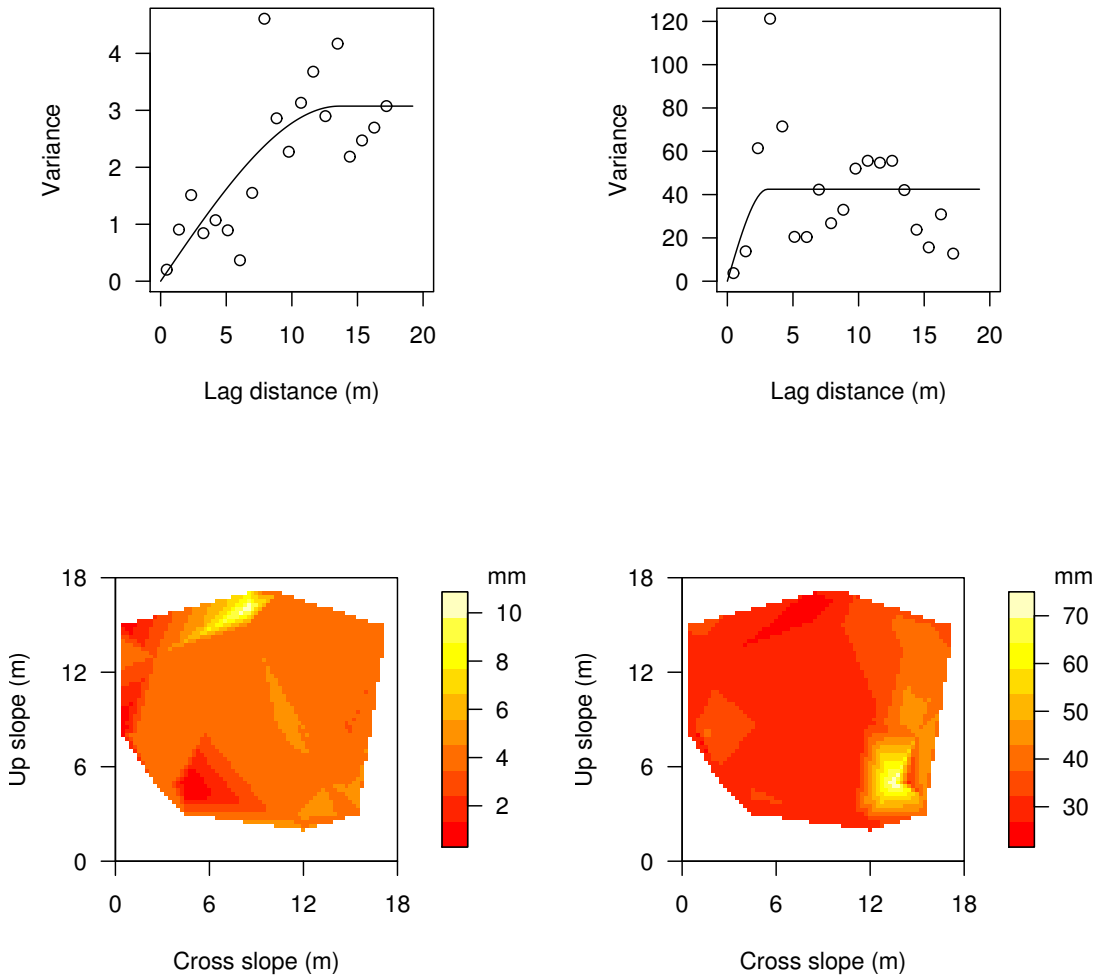
Figure E.13: Grid 9 winter 2007 - 2008. Experimental variogram (open circles) and modeled variogram of the the weak layer (top left) and the slab layers (top right) thickness D. Contour plots of the weak layer (bottom left) and the slab layer (bottom right) thickness D.
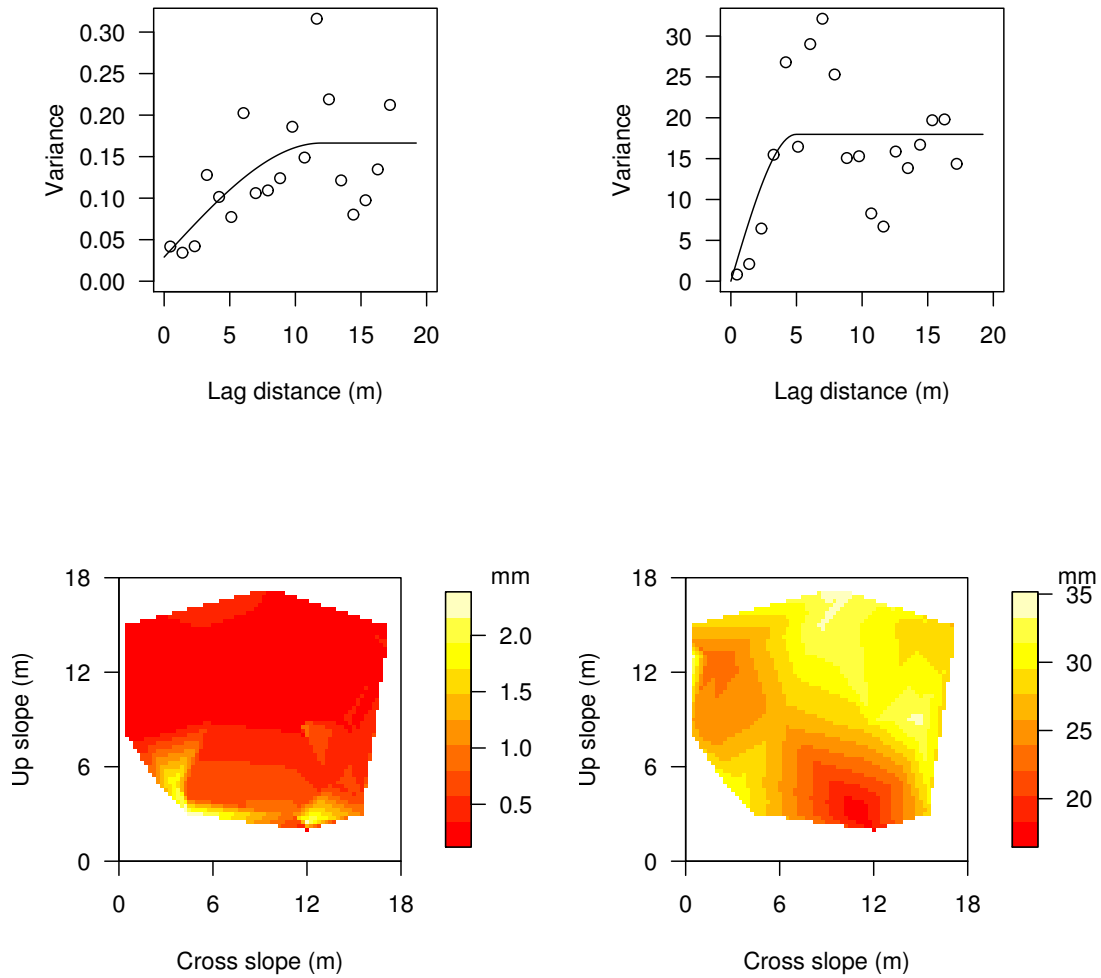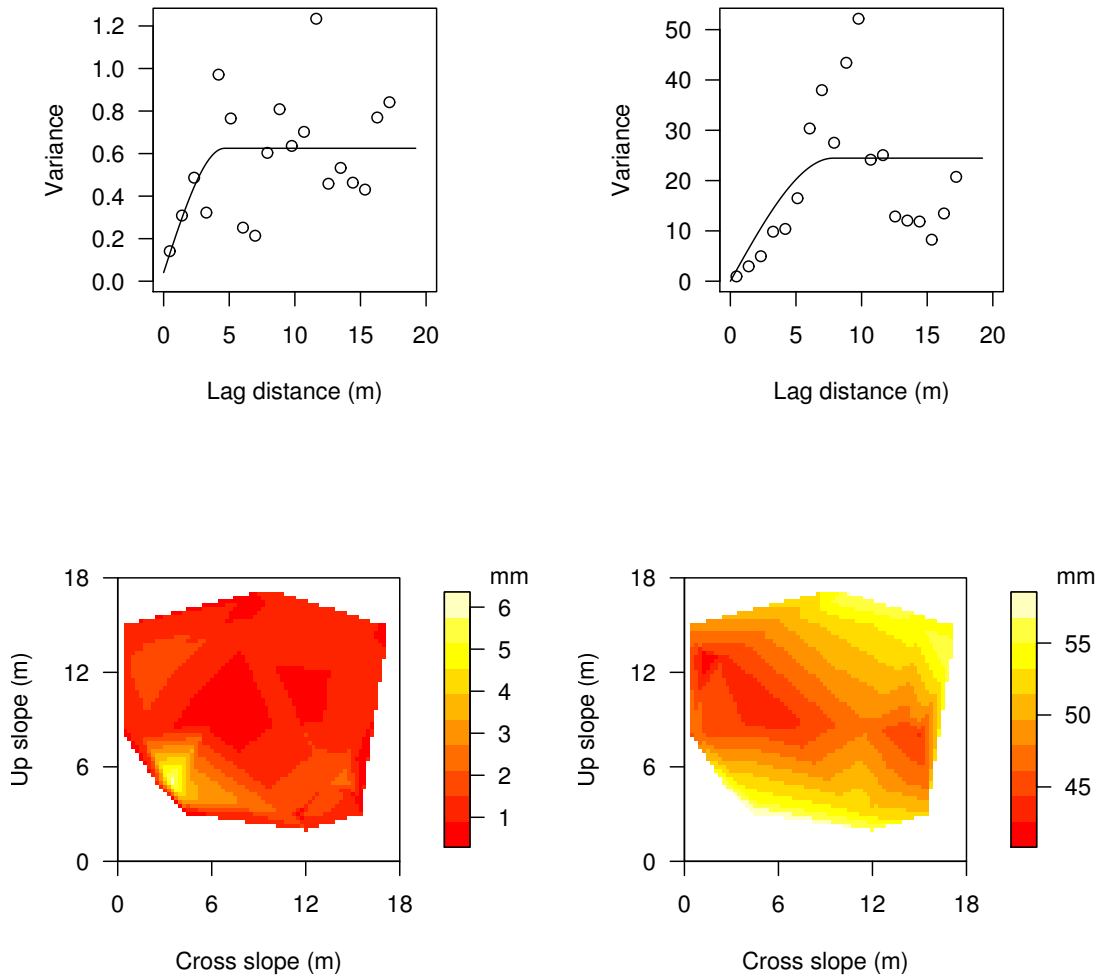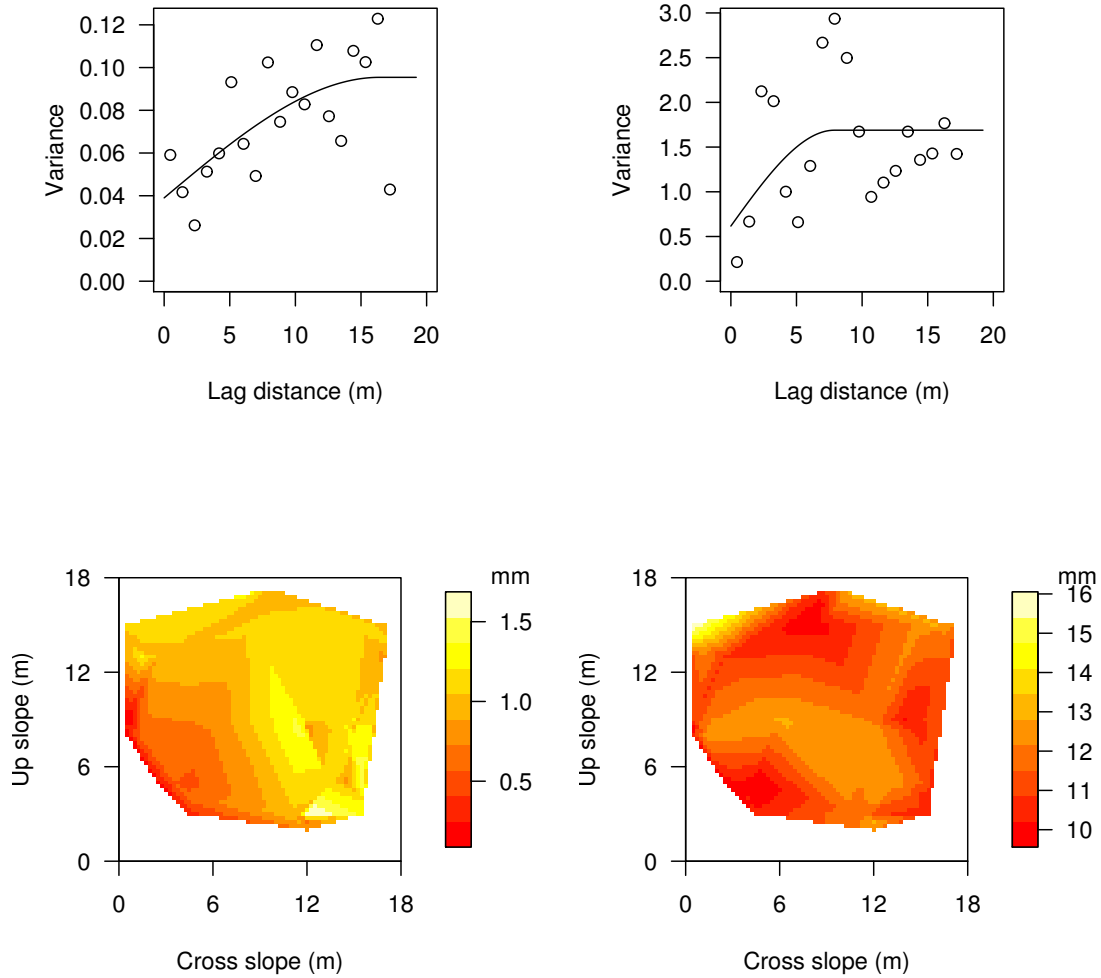
Figure E.14: Grid 2 winter 2008 - 2009. Experimental variogram (open circles) and modeled variogram of the the weak layer (top left) and the slab layers (top right) thickness D. Contour plots of the weak layer (bottom left) and the slab layer (bottom right) thickness D.
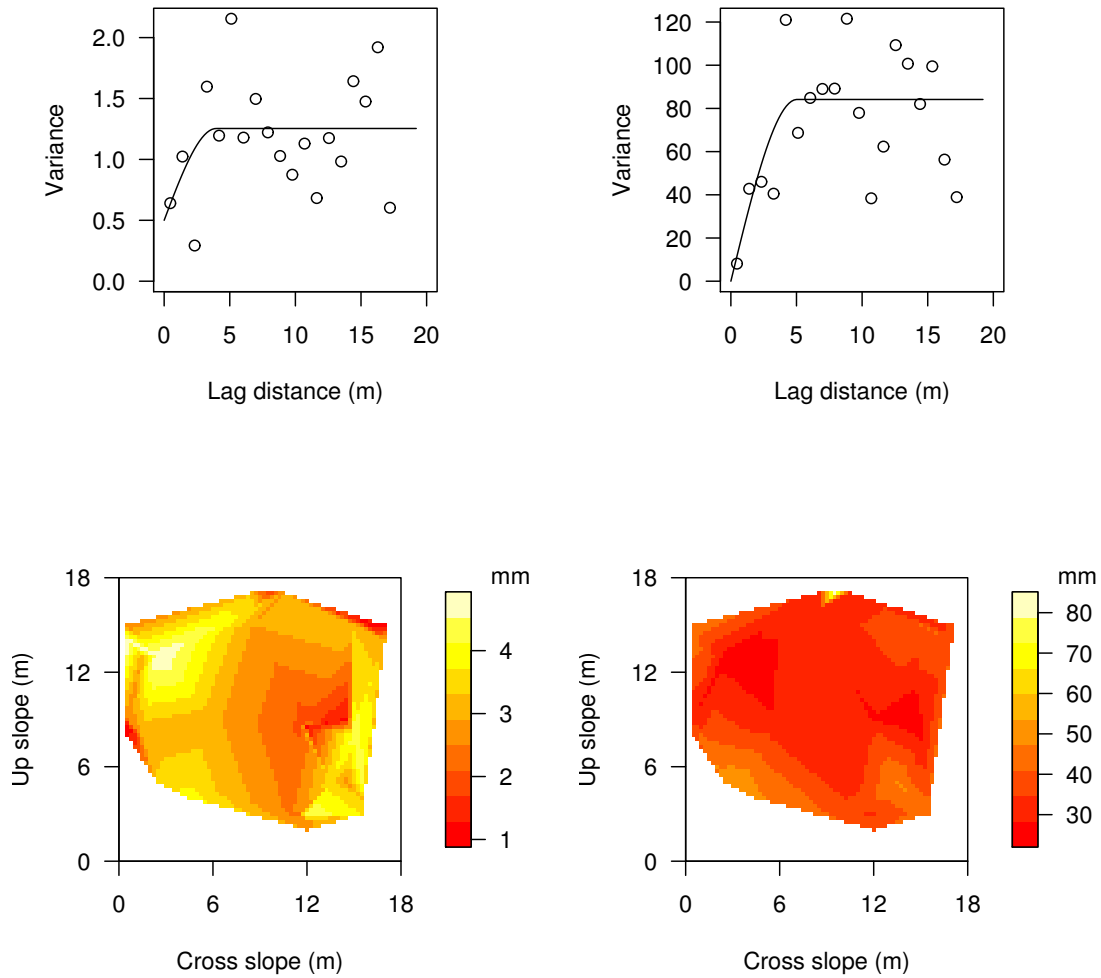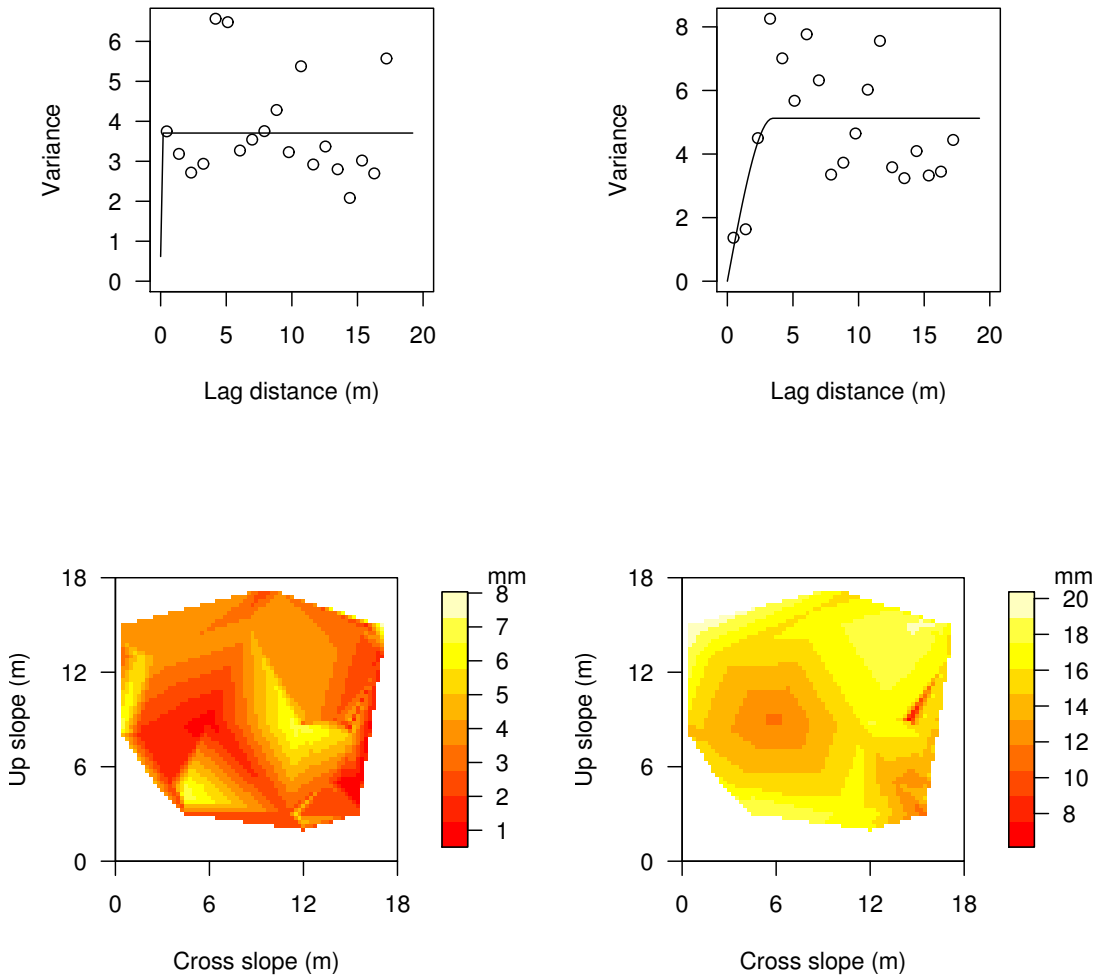
Figure E.15: Grid 4 winter 2008 - 2009. Experimental variogram (open circles) and modeled variogram of the the weak layer (top left) and the slab layers (top right) thickness D. Contour plots of the weak layer (bottom left) and the slab layer (bottom right) thickness D.

Figure E.16: Grid 6 winter 2008 - 2009. Experimental variogram (open circles) and modeled variogram of the the weak layer (top left) and the slab layers (top right) thickness D. Contour plots of the weak layer (bottom left) and the slab layer (bottom right) thickness D.
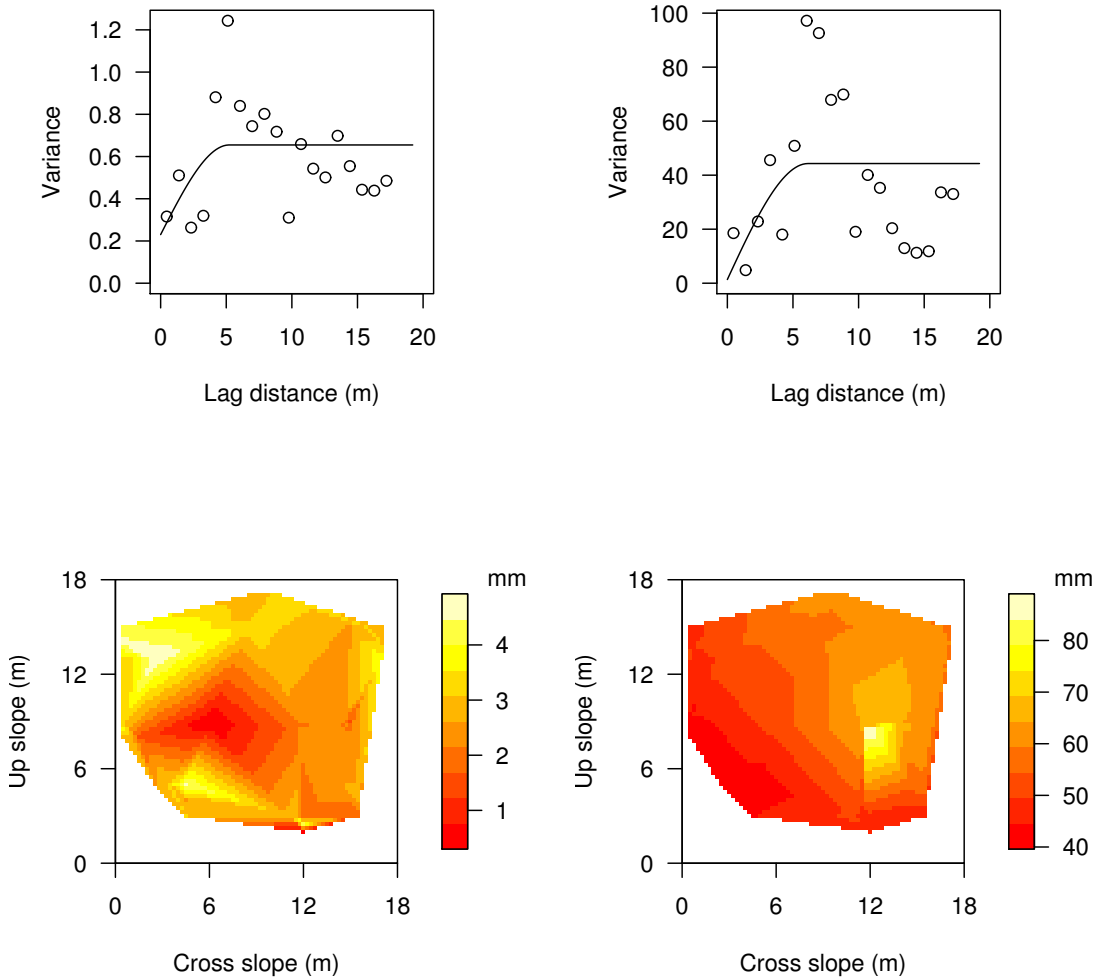
Figure E.17: Grid 7 winter 2008 - 2009. Experimental variogram (open circles) and modeled variogram of the the weak layer (top left) and the slab layers (top right) thickness D. Contour plots of the weak layer (bottom left) and the slab layer (bottom right) thickness D.
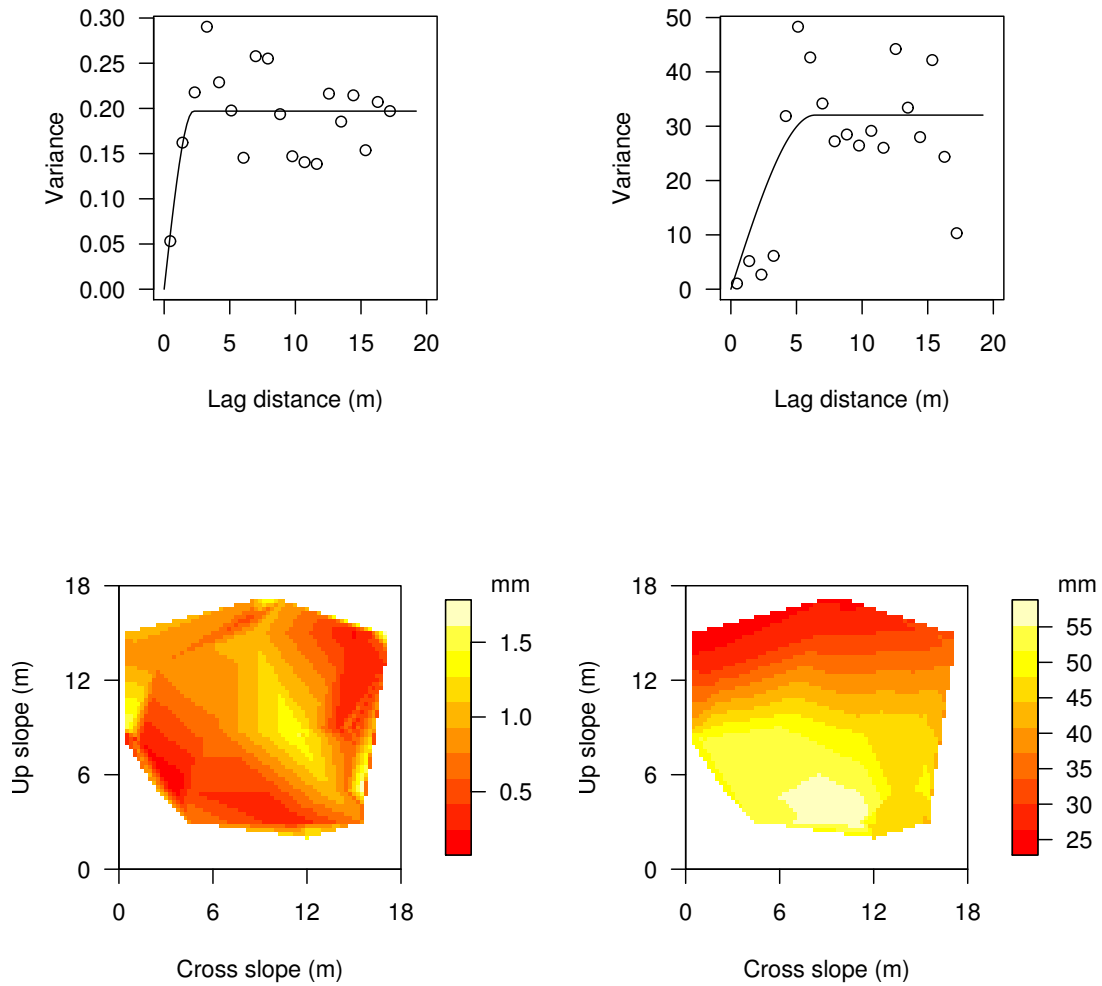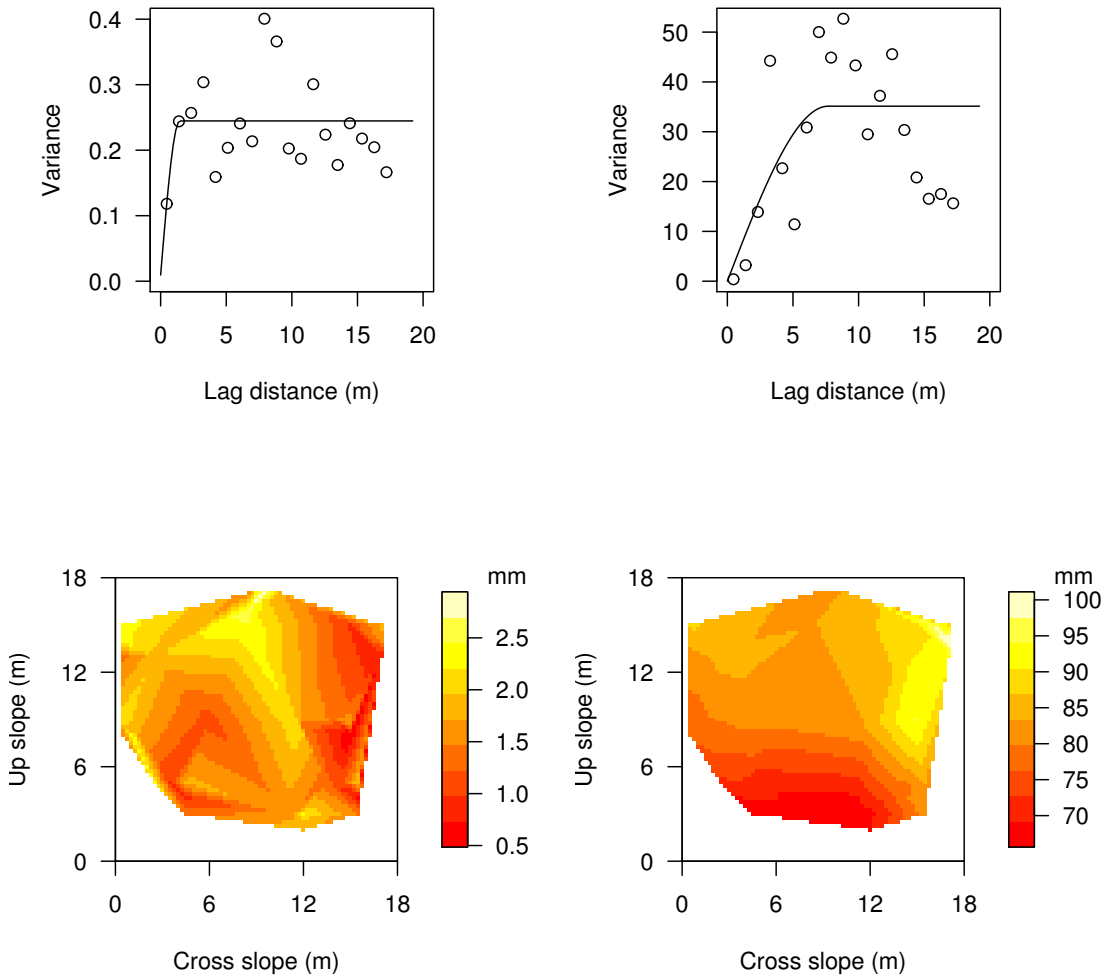
Appendix F

Table F.1: Summary of the 71 SMP profiles used for verification of the SMP stability algorithm. Given are the recording date (Date), the corresponding location (Europe, Eastern Swiss Alps) as well as the SMP-filename. In addition given are the snow height (HS), the slope angle, the rutschblock score (RB), the primary grain type (Fierz et al., 2009) as well as the depth of the weak layer top (Top) and bottom boundary (Bottom) as identified manually in the SMP signal. Aplpha = 0 indicates locations where a compression test was performed instead of a rutschblock test. The compression test score was converted into rutschblock scores according to Schweizer and Jamieson (2003).

No	Date	Location	Filename	HS cm	Alpha °	RB -	Type -	Top mm	Bottom mm
1	2003-02-14	Weissfluhjoch	00010008.pnt	222	0	3	DF	186.5	209.3
2	2003-04-16	Weissfluhjoch	00100061.pnt	215	0	3	FCxr	51.5	118.9
3	2003-11-25	Jatzhorn NW	00170004.pnt	55	35	6	FCxr	408.4	428.4
4	2003-11-25	Jatzhorn SW	00180007.pnt	55	30	3	FCxr	259.8	289.1
5	2003-11-29	Weissfluhjoch	00190014.pnt	122	0	3	FCxr	336.8	362.8
6	2003-12-13	Weissfluhjoch	00200007.pnt	106	0	7	FCxr	307.8	311.3
7	2003-12-17	Könighang	00210013.pnt	214	37	4	FCxr	483.8	504.4
8	2004-01-02	Weissfluhjoch	00230005.pnt	150	0	3	DF	128.8	155.6
9	2004-01-26	Gipfeli S	00260006.pnt	105	30	5	FCxr	538.6	576.8
10	2004-01-30	Weissfluhjoch	00280010.pnt	235	0	4	DF	181.7	198.0
11	2004-02-14	Weissfluhjoch	00320003.pnt	250	0	3	DF	240.5	252.6
12	2004-03-16	Weissfluhjoch	00450007.pnt	225.7	0	3	DF	117.5	123.3
13	2004-03-18	Schafberg	00460000.pnt	95	38	2	RG	277.9	307.9
14	2004-03-22	Seetäli	00520006.pnt	183	35	3	RG	257.7	262.7
15	2004-04-05	Könighang	00570004.pnt	174	30	3	PPgp	63.9	66.7
16	2004-05-04	Saentisch	00600003.pnt	253	29	4	MF	97.1	116.4
17	2004-12-01	WF Gipfel Ost	00620002.pnt	43	30	4	FCxr	324.8	358.8
18	2004-12-24	Könighang	00650003.pnt	55	36	2	DH	401.4	448.8
19	2004-12-31	Wetterloch, Gau	00670014.pnt	79	38	3	DH	392.0	460.8
20	2005-01-05	Könighang	00690001.pnt	84	36	2	DH	457.9	509.4
21	2005-03-02	Mittelgrat	00710017.pnt	127	43	4	FCxr	291.5	296.4
22	2005-04-13	Titlis	00740010.pnt	186.5	33	4	FCxr	463.9	473.0
23	2006-01-04	Rätschenjoch	00770004.pnt	161	32	2	SH	511.0	514.0
24	2006-01-16	Weissfluhjoch	00780003.pnt	83.5	0	4	FCxr	200.6	207.6
25	2006-01-27	Schönenboden, Strela	00790005.pnt	125	30	3	FCxr	257.4	265.3
26	2006-02-01	Weissfluhjoch	00800002.pnt	106.8	0	7	FCxr	316.3	336.1
27	2006-02-03	Steintälli, Strela	00810027.pnt	165	25	5	SH	281.9	295.2
28	2006-02-15	Weissfluhjoch	00830002.pnt	115	0	7	FCxr	465.6	499.1
29	2006-02-16	Pizol	00840011.pnt	210	38	2	PP	297.6	449.7
30	2006-02-21	Gfrornhorn W	00850014.pnt	91	40	3	RG	202.3	220.4
31	2006-02-27	Weissfluhjoch	00870003.pnt	147	0	2	SH	87.0	105.2
32	2006-03-18	RadünerRh NW	00890003.pnt	199	33	6	FCxr	255.0	274.6
33	2006-03-18	RadünerRH NNW	00900006.pnt	88	34	2	FC	335.8	363.1
34	2006-03-18	RadünerRH NE	00910010.pnt	108	36	4	FC	307.7	326.9
35	2007-11-16	Jakobshorn	File0004a.pnt	-	37	5	RG	332.6	333.3
36	2007-12-30	Äbirügg	File0006.pnt	-	37	6	FC	384.8	411.4
37	2008-01-10	Piz Darlux	File0006a.pnt	-	35	6	FC	398.3	464.9
38	2008-02-14	Sur Carungas	File0007.pnt	-	35	5	Fc	454.9	480.7

39	2008-03-13	Haupter Tälli Königshang	File0009.pnt	-	36	2	MF	361.8	375.2
40	2008-02-16	Nülli Berg	File0012.pnt	-	32	4	FC	245.9	325.8
41	2007-11-30	Bergstat. Totalp	File0014.pnt	-	36	5	FC	164.4	216.1
42	2008-01-16	Sur Eva	File0015.pnt	-	30	3	FC	401.7	418.9
43	2007-12-28	Verborgen Pischa	File0017.pnt	-	36	2	FC	102.9	109.0
44	2007-11-30	Weissfluhjoch	File0017a.pnt	-	39	4	DH	395.0	434.1
45	2008-01-10	Piz Darlux, Skibegiet Bergün	File0018.pnt	-	37	3	FC	153.8	186.3
46	2008-01-13	Totalphorn	File0020.pnt	-	41	2	DH	245.0	247.4
47	2008-01-13	Schwarzhorn Parsenn	File0024.pnt	-	40	2	FC	224.6	230.5
48	2008-02-16	Chessi Hubel	File0029.pnt	-	38	6	FC	295.5	372.7
49	2007-12-28	Pischa Flüelaberg	File0030.pnt	-	37	4	FC	239.5	274.4
50	2008-01-04	Pischa Verborgen Pischa	File0031.pnt	-	41	4	FC	238.7	297.7
51	2008-01-11	Flüela Tschuggen	File0034.pnt	-	34	4	FC	521.7	541.6
52	2008-02-11	Rätschenjoch	File0035.pnt	-	37	6	FC	390.8	396.1
53	2008-01-18	Murtel Corvatsch	File0035a.pnt	-	29	6	DH	580.5	604.6
54	2008-02-15	Podestatenalp	FILE0039.pnt	132	35	6	DH	291.5	342.5
55	2007-12-29	Büelen	File0042.pnt	-	38	5	FC	192.9	242.9
56	2008-01-18	Murtel Skitraverse	File0052.pnt	-	37	5	DH	352.2	375.4
57	2008-01-06	La Vedutta	File0055.pnt	-	32	2	FC	264.4	298.8
58	2007-01-25	Steintälli	File0021.pnt	97	19	4	RG	222.3	223.8
59	2007-02-16	Steintälli	GRID3021.pnt	160	30	5	FC	328.1	339.1
60	2007-03-08	Steintälli	DYID5048.pnt	116	23	5	FCxr	409.0	423.4
61	2007-03-15	Wannengrat	GRID6048.pnt	144	33	3	DH	370.8	386.7
62	2008-01-10	SW Hang WAN5	GRID1021.pnt	93	22	2	FC	164.2	167.5
63	2008-01-17	Steintälli	GRID2022.pnt	197	32	5	RG	268.3	287.9
64	2008-01-23	SW Hang WAN5	GRID3022.pnt	141	22	2	DH	268.0	279.1
65	2008-01-31	Steintälli	GRID0025.pnt	159	20	4	FCxr	424.0	438.7
66	2008-02-07	SW Hang WAN5	GRID5024.pnt	90	22	4	DH	289.1	289.3
67	2008-03-18	Steintälli	GRID9026.pnt	200	34	4	RG	168.4	175.6
68	2009-01-14	Steintälli	GRID2023.pnt	155	20	5	RG	337.2	351.8
69	2009-01-30	Steintälli	GRID4022.pnt	151	30	4	EG	326.6	332.7
70	2009-02-05	Steintälli	GRID5024a.pnt	207	20	5	SH	471.8	473.1
71	2009-02-19	SW Hang WAN5	GRID6024.pnt	186	20	5	FCxr	620.6	641.0

Curriculum Vitae

PERSONAL DETAILS

Name	Sascha Bellaire
Date of birth	February 26, 1979
Place of birth	Lippstadt, Germany
e-mail	S.Bellaire@gmx.de

EDUCATION

Since 2010	Post-doctoral fellow, ASARC - Applied Snow and Avalanche Research, University of Calgary, Canada.
2006 - 2010	PhD student, WSL Institute for Snow and Avalanche Research SLF, Davos, Switzerland. Student at the Meteorological Institute, Cluster of Excellence, 'KlimaCampus', University of Hamburg. Field/Specialization: Avalanche Formation / Spatial Variability on slope scale, SMP
1999 - 2006	Studies, Meteorological Institute, University of Hamburg. Degrees: Master of Atmospheric Science, Bachelor of Science 2004 - 2005: Master Thesis at the WSL Institute for Snow and Avalanche Research SLF, Davos, Switzerland.

RESEARCH AND PRACTICAL EXPERIENCE

Since 2006	Avalanche research on spatial variability using a high-resolution snow micro-penetrometer. Manual snow cover observations including a variety of stability tests. Snow cover modeling with the snow cover model SNOWPACK.

2003	Member of an arctic expedition on a finish research ship during the project ACSYS.
2001	Member of a research campaign. Central Baltic sea during the project BALTIMOS.
Since 2001	Mountain Instructor

PERSONAL INTERESTS

All kinds and all season mountaineering all over the world.